



International Committee for Future Accelerators

Sponsored by the Particles and Fields Commission of IUPAP

Beam Dynamics Newsletter

No. 64

Issue Editor:
Y. Zhang

Editor in Chief:
W. Chou

August 2014

Contents

1 FOREWORD.....	9
1.1 FROM THE CHAIR	9
1.2 FROM THE EDITOR	10
2 THEME: BEAM COOLING AND RELATED TOPICS (PART I).....	12
2.1 BRIEF HISTORY AND PRESENT STATUS OF COOLING METHODS IN EXPERIMENTAL PHYSICS	12
2.1.1 Introduction	12
2.1.2 Past	13
2.1.2.1 <i>Introduction</i>	13
2.1.2.2 <i>First Experiment</i>	13
2.1.2.3 <i>Cooling Beam</i>	14
2.1.2.4 <i>1990-2014: The Productive Years</i>	14
2.1.3 High Lights of Cooling Applications	15
2.1.3.1 <i>Particle Physics</i>	15
2.1.3.2 <i>Nuclear Physics</i>	16
2.1.3.3 <i>Atomic Physics</i>	16
2.1.3.4 <i>Particle Beam Physics</i>	17
2.1.4 Present	18
2.1.5 Conclusions	19
2.1.6 References	19
2.2 RECENT DEVELOPMENT IN STOCHASTIC COOLING APPLICATIONS.....	20
2.2.1 Introduction	21
2.2.2 FAIR Project.....	21
2.2.2.1 <i>Pre-Cooling of Antiproton Beam in the Collector Ring</i>	22
2.2.2.2 <i>Accumulation of Pre-Cooled Beam with Stochastic Stacking System</i>	22
2.2.2.3 <i>Antiproton Accumulation in HESR</i>	23
2.2.2.3.1 <i>Simulation Method</i>	23
2.2.2.3.2 <i>Moving Barrier Voltage Method</i>	24
2.2.2.3.3 <i>POP Experiment at the ESR</i>	26
2.2.2.4 <i>Low Energy Antiproton Beam Production at FAIR</i>	26
2.2.2.3 NICA Project	26
2.2.2.4 Stochastic Cooling at Electron Ion Collider Project.....	28
2.2.2.5 References	29
2.3 OVERVIEW OF THE COOLING PROGRAM AT CERN	29
2.3.1 Introduction to CERN.....	29
2.3.2 Stochastic Cooling	30
2.3.2.1 <i>First Ideas</i>	30
2.3.2.2 <i>The “ICE” Age</i>	31
2.3.2.3 <i>The Antiproton Accumulator and the Antiproton Accumulator Complex</i>	32

2.3.2.4 <i>Antiprotons in the Intersecting Storage Ring (ISR)</i>	33
2.3.2.5 <i>The Low Energy Antiproton Ring (LEAR)</i>	33
2.3.2.6 <i>The Antiproton Decelerator (AD)</i>	34
2.3.3 Electron Cooling.....	35
2.3.3.1 <i>First Experiments on ICE</i>	35
2.3.3.2 <i>Electron Cooling on LEAR</i>	35
2.3.3.3 <i>From LEAR to LEIR</i>	37
2.3.3.4 <i>Electron Cooling on the AD</i>	38
2.3.3.5 <i>ELENA, the Extra Low Energy Antiproton Ring</i>	39
2.3.4 References.....	40
2.4 DEVELOPMENT OF ELECTRON COOLERS IN NOVOSIBIRSK.....	41
2.4.1 Introduction.....	41
2.4.2 First Electron Cooler at NAP-M Storage Ring.....	41
2.4.3 Test Bench for Magnetized Cooling (MOSOL)	42
2.4.4 SIS-18 Cooler	42
2.4.5 CSRm and CSRe Coolers	43
2.4.6 LEIR Cooler.....	44
2.4.7 COSY Cooler.....	45
2.4.8 References.....	47
2.5 FERMILAB'S 4.3-MEV ELECTRON COOLER.....	48
2.5.1 Introduction.....	48
2.5.2 Recycler Electron Cooling (REC) System.....	49
2.5.3 Electron Cooling Formulae.....	50
2.5.4 Cooling Measurements	51
2.5.5 Conclusion	54
2.5.6 Acknowledgement	54
2.5.7 References.....	55
2.6 ELECTRON COOLING AT IMP	55
2.6.1 Introduction of CSR.....	55
2.6.2 Electron Cooling for CSR.....	55
2.6.2.1 <i>Functions of Electron Cooling</i>	56
2.6.3 Main Physics Goals at CSR	56
2.6.4 Operation Modes of HIRFL-CSR.....	57
2.6.5 Electron Dynamics in the Cooling Devices	57
2.6.5.1 <i>Adiabatic Expansion</i>	57
2.6.5.2 <i>Toroids</i>	57
2.6.5.3 <i>Parallelism of Magnetic Field in the Cooling Section</i>	58
2.6.5.4 <i>Collector</i>	59
2.6.6 Parameters Optimization of CSR	59
2.6.7 Commissioning and Operation of Electron Cooling in CSR	63
2.6.8 Electron Cooling Experiments at CSR	63
2.6.9 Physics Experiments Related Electron Cooling at CSR	63
2.6.10 Planned Experiments Related with Electron Cooling	63
2.6.10.1 <i>Longitudinal Stacking</i>	63
2.6.10.2 <i>Ion Beam Crystallization</i>	64
2.6.10.3 <i>High Energy Density Physics</i>	64

2.6.10.4	<i>Suppression of Instability of Ion Beam with Modulated Electron Beam</i>	64
2.6.11	Status of HIRFL-CSR	65
2.6.12	Research Activities of HIRFL-CSR in Near Future.....	65
2.6.13	Summary	65
2.6.14	References	65
2.7	NEW STOCHASTIC COOLING KICKERS FOR RHIC	67
2.7.1	Introduction	67
2.7.2	System Description and Requirement	67
2.7.2.1	<i>Bunched Beam and Narrowband Kickers</i>	67
2.7.2.2	<i>Goals of the Upgrade</i>	68
2.7.3	Cavity Design	69
2.7.3.1	<i>RF Structure</i>	69
2.7.3.2	<i>Fill and Decay Time</i>	69
2.7.3.3	<i>Opening of Cavities</i>	70
2.7.3.4	<i>Waveguide Power Feed</i>	70
2.7.4	Cavity Fabrication	72
2.7.4.1	<i>Matching</i>	72
2.7.4.2	<i>Frequency and Bandwidth Tuning</i>	72
2.7.5	Operation	72
2.7.5.1	<i>Temperature Control</i>	72
2.7.5.2	<i>Vacuum</i>	73
2.7.5.3	<i>Tune Up of the Cooling System</i>	73
2.7.6	Summary.....	74
2.7.7	References	74
2.8	2 MEV ELECTRON COOLER AT COSY JUELICH	75
2.8.1	Introduction	75
2.8.2	Basic Design Features	76
2.8.3	Diagnostics and Commissioning	79
2.8.4	First Experimental Results at COSY	81
2.8.4.1	<i>Cooling at 200 MeV</i>	81
2.8.4.2	<i>Cooling at 1670 MeV</i>	83
2.8.5	Conclusion	84
2.8.6	Outlook	85
2.8.7	References	85
2.9	BEAM COOLING AT GSI	86
2.9.1	Introduction	86
2.9.2	Beam Cooling in the ESR Storage Ring.....	86
2.9.2.1	<i>ESR Electron Cooling</i>	86
2.9.2.2	<i>ESR Stochastic Cooling</i>	89
2.9.2.3	<i>Latest Achievements of the ESR Cooling Systems</i>	91
2.9.3	Electron Cooling in the Heavy Ion Synchrotron SIS	91
2.9.4	References	93
2.10	NICA COOLING PROGRAM	94
2.10.1	Introduction	95

2.10.2	Operation of the Booster with Electron Cooling System Goals and Objectives	95
2.10.3	Low Energy Heavy Ion Collider: Requirements and Challenges for Luminosity, Region of Operation	97
2.10.4	Beam Stacking in Longitudinal Phase Space	99
2.10.5	Stochastic Cooling.....	100
2.10.6	Electron Cooling.....	101
2.10.7	R&D for Collider Stochastic Cooling System, Results at Nuclotron Complex.....	103
2.10.8	NICA Start-up Configuration	105
2.10.9	Acknowledgement	106
2.10.10	Reference	106
2.11	STOCHASTIC COOLING FOR FAIR	106
2.11.1	Introduction	107
2.11.2	The Stochastic Cooling System of the Collector Ring (CR)	108
	2.11.2.1 <i>Overview</i>	108
	2.11.2.2 <i>Hardware Design and Developments</i>	111
	2.11.2.2.1 Electrodes, Pick-ups and Kicker tanks	111
	2.11.2.2.2 RF Signal Processing.....	113
	2.11.2.3 <i>Simulations of Cooling Performance</i>	114
2.11.3	The Stochastic Cooling System of the HESR	115
	2.11.3.1 <i>Stochastic Cooling Tanks</i>	118
	2.11.3.2 <i>Signal Combination</i>	119
2.11.4	References	120
2.12	STOCHASTIC BEAM COOLING IN THE STORAGE RINGS COSY AND THE FUTURE HESR WITH INTERNAL TARGET OPERATION.....	121
2.12.1	Introduction	121
2.12.2	Brief Outline of Stochastic Momentum Cooling.....	121
2.12.3	Model Predictions and Experimental Results at COSY	122
	2.12.3.1 <i>Internal Target Experiments with Stochastic Cooling assisted by a Barrier Bucket Cavity</i>	123
	2.12.3.2 <i>Time-Of-Flight and Filter Cooling</i>	125
2.12.4	Stochastic Momentum Cooling Investigation for the HESR.....	127
	2.12.4.1 <i>The Antiproton Beam Mode in the HESR</i>	127
	2.12.4.2 <i>The Heavy Ion Beam Mode in the HESR</i>	129
2.12.5	Summary and Conclusions	131
2.12.6	Acknowledgement	131
2.12.7	References	131
3	ACTIVITY REPORTS.....	133
3.1	THE ADVANCED SUPERCONDUCTING TEST ACCELERATOR AT FERMILAB	133
	3.1.1 Introduction.....	133
	3.1.2 Facility Overview & Capabilities	134
	3.1.2.1 <i>Injector and Superconducting Radiofrequency (SRF) Linac</i>	135
	3.1.2.2 <i>Integrable-Optics Test Accelerator (IOTA) Ring</i>	137
	3.1.2.3 <i>Superconducting Radiofrequency (SRF) Infrastructure</i>	139

3.1.3 Planned Experiments & Opportunities	140
3.1.3.1 <i>IOTA-based Experiments</i>	140
3.1.3.1.1 Integrable-Optics	140
3.1.3.1.2 Optical-Stochastic Cooling	141
3.1.3.1.3 Space-Charge Compensation for High-Intensity Circular Accelerators.....	143
3.1.3.2 <i>Linac-based Experiments</i>	144
3.1.3.2.1 Accelerator R&D at the Energy and Intensity Frontiers	144
3.1.3.2.2 Accelerator R&D for Future SRF Accelerators	144
3.1.3.2.3 Accelerator R&D for Novel Radiation Sources	145
3.1.3.2.4 Accelerator R&D for Stewardship and Applications ...	146
3.1.4 Commissioning Status	147
3.1.4.1 <i>Photocathode Laser System</i>	148
3.1.4.2 <i>Radiofrequency Gun Characterization</i>	149
3.1.4.3 <i>Electron Beam Measurements</i>	150
3.1.4.4 <i>SRF Cavities Achieve ILC Specifications</i>	151
3.1.5 Upgrade Path	152
3.1.6 Acknowledgements	153
3.1.7 References	153
4 WORKSHOP AND CONFERENCE REPORTS	156
4.1 ICFA MINI-WORKSHOP “ELECTROMAGNETIC WAKE FIELDS AND IMPEDANCES IN PARTICLE ACCELERATORS”	156
5 RECENT DOCTORIAL THESES ABSTRACTS.....	157
5.1 OPTICS DESIGNS OF FINAL-FOCUS SYSTEMS FOR FUTURE LHC UPGRADES	157
5.2 ELECTRON CLOUD STUDIES FOR THE LHC AND FUTURE PROTON COLLIDERS	158
6 FORTHCOMING BEAM DYNAMICS EVENTS	160
6.1 4 TH LOW EMITTANCE RINGS WORKSHOP	160
6.2 INTERNATIONAL WORKSHOP ON BEAM COOLING AND RELATED TOPICS COOL’15	160
6.3 ICFA MINI-WORKSHOP ON BEAM COMMISSIONING FOR HIGH INTENSITY ACCELERATORS	161
7 ANNOUNCEMENTS OF THE BEAM DYNAMICS PANEL.....	161
7.1 ICFA BEAM DYNAMICS NEWSLETTER.....	161
7.1.1 Aim of the Newsletter.....	161
7.1.2 Categories of Articles	162
7.1.3 How to Prepare a Manuscript	162
7.1.4 Distribution.....	162
7.1.5 Regular Correspondents	163
7.2 ICFA BEAM DYNAMICS PANEL MEMBERS	164

1 Foreword

1.1 From the Chair

Weiren Chou, Fermilab
 Mail to: chou@fnal.gov

The International Committee for Future Accelerators (ICFA) met on July 6, 2014 at Valencia, Spain. Nigel Lockyer, Fermilab Director and ICFA Chair chaired the meeting. This meeting was preceded by a Linear Collider Board (LCB) meeting earlier on the same day in the same place.

The Funding Agencies for Large Colliders (FALC) gave a report. The LCC common fund MOU has been established, with an annex under study on contribution sharing. The next FALC Chair, for the period 2015 to 2017 will be from Europe, and the name will be announced soon.

Atsuto Suzuki, Director General of KEK, reported that an ILC preparatory office has been established in KEK. The Japanese funding agency MEXT has set up a 13-member “Wisemen” committee for advices on the decision about whether or not Japan will host the construction of the ILC. This committee has under it a Particle/Nuclear Physics working Group and a TDR Validation Working Group. A report is expected in March, 2016 or earlier.

Nigel noted that the P5 report has been delivered to and accepted by the DOE and NSF in the US, and is now at the beginning of the implementation stage. A new HEPAP subpanel on accelerator R&D has been set up and is co-chaired by Marty Breidenbach and Don Hartill.

ICFA discussed the global planning for HEP, including a 100 TeV pp collider. Rolf Heuer, Director General of CERN, said that over the next few years, Europe would look at a ~100 TeV pp collider, with an 80 – 100 km circumference; it could also be used for heavy ions and possibly electron-hadron collisions. There is a possibility of 350 GeV e+e- collisions in the tunnel, but pp is the primary goal. Yifang Wang, Director of IHEP, reported that China is considering an e+e- machine (CEPC) in a large tunnel; the tunnel could later contain a pp collider. Construction could start after 2020, with funding from government agencies other than those that so far have funded particle physics. The e+e- machine is complementary to the ILC, and would not be a competitor; China still supports the ILC. There will be a preliminary CEPC design and cost estimate by the end of 2014. After an extensive discussion, it was agreed to issue an ICFA Statement as follows: *“ICFA endorses the particle physics strategic plans produced in Europe, Asia and the United States and the globally aligned priorities contained therein. Here, ICFA reaffirms its support of the ILC, which is in a mature state of technical development and offers unprecedented opportunities for precision studies of the newly discovered Higgs boson. In addition, ICFA continues to encourage international studies of circular colliders, with an ultimate goal of proton-proton collisions at energies much higher than those of the LHC.”*

Yifang also reported on the organization of the ICFA Seminar, which will take place from October 27 to 30, 2014 at IHEP, Beijing, China. The participation is by invitation

only. There is a quota for each country. The invitees include funding agency representatives, lab directors and scientists all over the world. There will also be a significant media attendance.

Steinar Stapnes discussed the next three years of the Linear Collider School. The School in October/November 2015 will be hosted at TRIUMF; the School in 2016 will be in Japan, arranged by KEK; and the School in 2017 will be a specialized CERN School.

The ICFA HF2014 Workshop for a future circular Higgs factory will take place October 9-12, 2014 at Wanda Hotel, Beijing, China. The program is available online: (<http://indico.ihep.ac.cn/conferenceOtherViews.py?view=standard&confId=4221>)

The editor of this issue is Dr. Yuhong Zhang, the archivist of the ICFA Beam Dynamics Newsletter and a senior scientist at JLab, USA. The theme is “*Beam Cooling and Related Topics.*” He collected 25 well-written articles for a total of 250 pages. Since this is about twice the size of a normal theme section, we decided to publish them in two issues: 12 articles in this issue, and the remaining in No. 65 in December.

In this issue there is also an activity report (*ASTA at Frmilab*), a workshop report (*Wakefield and Impedance*), two recent PhD thesis abstracts (José Luis Abelleira Fernández, and César Octavio Dominguez Sanchez de la Blanca, both from École Polytechnique Fédérale de Lausanne), and three workshop announcements (*Low Emittance Rings, COOL'15, Beam Commissioning for High-Intensity Accelerators*). I want to thank Yuhong for editing a newsletter of substantial contents and good quality for our accelerator community.

1.2 From the Editor

Yuhong Zhang, Thomas Jefferson National Accelerator Facility
Mail to: yzhang@jlab.org

For this issue of the ICFA Beam Dynamics Newsletter, I selected beam cooling and related topics for the theme section. The importance of this technology to many accelerator-based scientific facilities is well established and its critical role in many great discoveries (including the discovery of W and Z particles) is well known. One Nobel Prize was awarded to the invention of stochastic cooling, one of two most successful flavors of beam cooling techniques. The first article of the theme section has a very nice and entertaining review of the history of the beam cooling field.

I have collected twenty-five well written review articles for covering activities in the most research areas and programs in the field of beam cooling. The theme section is organized in four groups as follows. The first two articles provide brief overviews in, respectively, general beam cooling and the recent developments of stochastic cooling. They are followed by summaries of developments as well as the present status of the individual existing or proposed cooling programs worldwide. These summary articles are loosely organized according to stages of these programs: existing; approved/in construction; and finally in the proposal stage. Laser cooling and ionization cooling of muons are also included in this group. In the next group, four articles are devoted to the new ideas of beam cooling including optical stochastic cooling, SASE-FEL based and micro-bunching instability based coherent electron cooling, and their experimental tests. In the last group, additional and related topics are covered, including cooling simulations and code development, and lastly beam crystallization, an interesting

subject with a potential for great applications as well as for fundamental beam physics studies.

While I have made a great effort to cover the entire field of beam cooling, nevertheless, there are several important topics missing from this issue. For example, development of the supporting accelerator technologies such as high bunch charge electron sources, high current energy-recovery linac (ERL) and advanced beam manipulation are not covered due to the space limit. I hope interested readers may find information of these missing topics in other sources.

I would like to thank all of the authors for contributing excellent overview articles to the theme section. Many of them had to overcome challenges in their normal work load and busy schedules to complete their contributions in relatively short notice. I want to particularly thank Drs. Yaroslav Derbenev, Takeshi Katayama, Igor Meshkov, Akira Noda, and Markus Steck for helping me to assemble a list of topics for the theme section and for suggesting contributors. Dr. Michael Palmer of Fermilab also helped in identifying authors for the topics of muon cooling.

After completion of this issue, Dr. Weiren Chou, chair of the ICFA Beam Dynamics Panel and the newsletter editor-in-chief, decided to publish the articles in the theme section in two issues. This decision was made for the purpose of maintaining the regular size of a single issue of the newsletter since the completed theme section has 239 pages. Following this two-issue plan, the first twelve articles are in this issue, the rest thirteen articles which cover the topics of laser cooling, muon cooling, future cooling facilities and programs, new cooling concepts, simulations and beam crystallization, will appear in the next issue (No. 65) of the newsletter scheduled to be published in December of this year.

Lastly, I also want to mention the COOL workshop series, the most important forum that experts and enthusiasts of beam cooling use for exchanging new ideas, concept and technology development. This very successful workshop series was started at Karlsruhe, Germany in 1983, more than 30 years ago. It became a bi-annual event since 1999 and adopted the present name since 2001. The figure (courtesy of Igor Meshkov) below shows the posters of all previous workshops. The next one, COOL'15, will be held at Jefferson Lab, from Sept. 28 to October 3, 2015 (see the workshop announcement in this issue). The workshops published proceedings, in recent years switched to electronic format which are archived in the JACoW web site.

The COOL workshop presents Dieter Möhl Medal, in memory of one of the pioneers in stochastic cooling who passed away recently, to reorganize the outstanding researches and contributions in the field of beam cooling. The recipients of the inauguration Dieter Möhl Medal at COOL'13 are Yaroslav Derbenev (Jefferson Lab), Igor Meshkov (Joint Institute of Nuclear Research at Dubna), Vasily Parkhomchuk (Budker Institute of Nuclear Research) and Lars Thorndahl (CERN).

In the section of activity report, I am pleased to have a special report on the newly established Advanced Superconducting Test Accelerator (ASTA) at Fermilab. The report provides a comprehensive overview of this test facility, its staging realization plan and the rich research programs it supports. Two annual user workshops were also held. I want to thank the authors of this special report.

In other sections of this issue of the newsletter, there are one workshop report, three future workshop announcements and abstracts of two recent Ph. D theses abstracts.



2 Theme: Beam Cooling and Related Topics (Part I)

2.1 Brief History and Present Status of Cooling Methods in Experimental Physics

Igor Meshkov, Joint Institute of Nuclear Research, 141980 Dubna, Russia

Mail to: meshkov@jinr.ru

2.1.1 Introduction

The truism saying “the history does not teach anything” has no relation to physics. The longstanding history of cooling method development is a fascinating “novel” of fighting with famous theorem formulated by Joseph Liouville in 1838: the theorem of phase space density conservation [1]. And very first significant step has been done by A. Kolomensky and A. Lebedev [2] more than one century later. They have described process of particle momentum spread decrease (“damping”) in electron beam subjected to synchrotron radiation (SR) and have derived the formula for characteristic time of the process. The development of the SR damping theory was continued by K.W. Robinson who deduced the theorem on sum of decrements, the rule of decrements redistribution,

etc. [3]. However, the synchrotron radiation is “a gift of nature” that does not work for heavy particles (SR intensity is inversely proportional to cube of particle mass for given particle energy value). Therefore we consider further the history of the cooling methods which allow to reduce phase space volume of heavy particle beams, i. e. enhance the beam phase space density. Beginning with description of the first proposals and methods development in the past we come to present status of this activity.

2.1.2 Past

2.1.2.1 *Introduction*

The very first step in creation of a cooling method for heavy particles has been done by A. Kolomensky in 1965. He proposed [4] to use particle ionization losses in a medium. However, the nature turned out to be merciless to strongly interacting particles -- the particle loss rate is higher of cooling rate by two orders of magnitude in relativistic energy range ($\varepsilon > m_p c^2$) where *ionization cooling* works. Nevertheless, it was a good start idea that has been reformulated later (see below, 1970). First really effective cooling method - *the electron cooling* - was invented at the same time by G. Budker [5]. Soon, together with A. Skrinsky, they proposed to apply this method to storage of antiprotons in an accelerator ring. In 1968 S. van der Meer has published the idea of *stochastic cooling* [6]. It is worth to quote his Nobel lecture [7]: “Such a system resembles Maxwell’s demon, which is supposed to reduce the entropy of a gas by going through a very similar routine, violating the second law of thermodynamics in the process. It has been shown by Szilard that the measurement performed by the demon implies an entropy increase that compensates any reduction of entropy in the gas. Moreover, in practical stochastic cooling systems, the kicker action is far from reversible; such systems are therefore even less devilish than the demon itself.” And two years later G. Budker and A. Skrinsky proposed to use ionization cooling method for cooling of muons which are devoid of strong interaction [8, 9]. This version of the method is known since that time as “*muon cooling*”. As Sasha Skrinsky wrote later to the author [10], “We began to elaborate muon collider based on ionization cooling in the end of the 60th... Andrey Mikhailovich [Budker nick name – I.M.] mentioned this idea in his talk at ICHEP’1969 (Kiev) and I described it, more or less, in detail at a conference at Morge in 1971 and at great length in my talk opening the ICHEP (“Rochester”) 1980 at Madison... The extended version of the talk has been published in “Physics-Uspekhi”... However, reaction was very weak... Then, in 1981 we published in Particle and Nuclei Physics Journal at JINR review on cooling method. It initiated an “explosion” of publications (D.J. Neuffer, R.B. Palmer and others)... I believe correct formulation of the priority would be «Initial proposal of muon collider based on ionization cooling was done by G. Budker and A. Skrinsky»”.

2.1.2.2 *First Experiment*

It has taken 8 years until first experiment on electron cooling of protons at NAP-M storage ring has been performed in 1974 in INP, Novosibirsk (Fig.1). Simultaneously first approximation of the method theory has been developed (see details in Ref. 11). One year later the first *stochastic cooling* has been demonstrated at ISR (CERN) [12]. Lars Thorndahl, one of the experiment leaders, remembers [13]: “The first experimental proof in the ISR was in 1976 (vertical betatron cooling) using movable Roman Pots to

hold the pickup electrodes (left over from a physics experiment) and it used the band 1–2 GHz. Later, to test dp/p cooling as a preparation for the AA machine, bands like 100–400 GHz were used in the ISR”. The method was significantly developed at LEAR (Fig.2), TSR, ISR and other cooler rings.

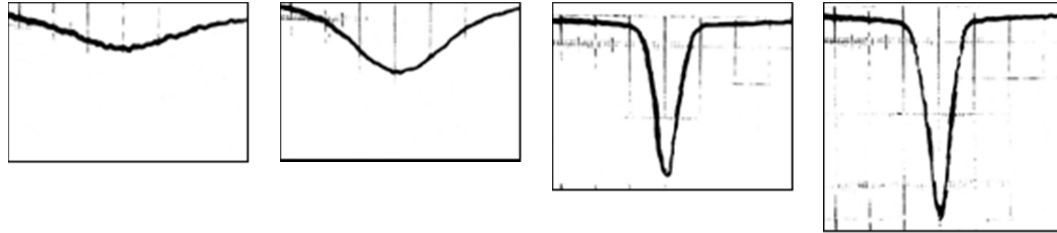


Figure 1: Dynamics of proton density distribution in NAP-M at electron cooling (BPM based on Mg vapor jet, 1975)

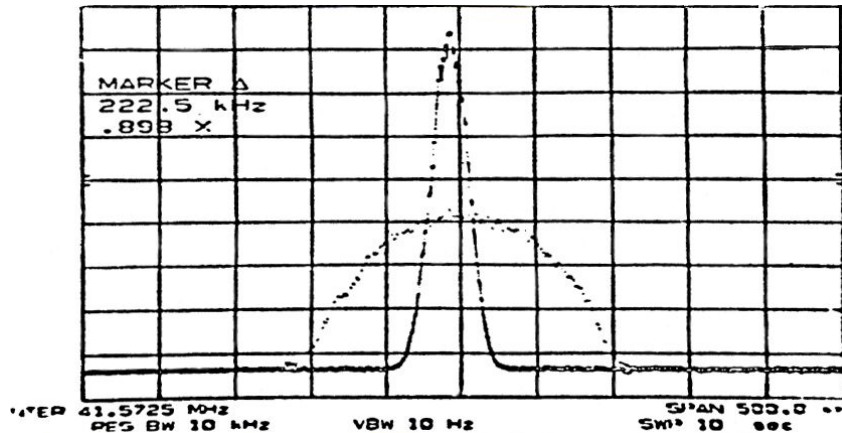


Figure 2: Momentum cooling of antiprotons in Low Energy Antiproton Ring (LEAR), CERN, 1988. Momentum distribution of 3×10^9 antiprotons at injection and after 3 min. cooling; $W=250$ MHz.

2.1.2.3 Cooling Beam

After first advance of the middle of the 70th in experimental corroboration of two cooling methods a cooling “boom” seized many accelerator laboratories around the World. Twelve laboratories constructed cooler rings and performed experiments on study of cooling physics during the 80s and beginning of the 90s (Table 1).

In 1984 by initiative of Helmut Poth the first workshop dedicated to electron cooling had been organized and performed in Karlsruhe Kernforschungszentrum. It is followed with biennial periodicity since then and until now.

2.1.2.4 1990-2014: The Productive Years

As result of following advance in cooling method development many remarkable results have been achieved. First the creation of laser cooling should be pointed out. These studies were performed at TSR (1990) [14] and ASTRID (1991) [15] cooler storage rings. Extremely low ion longitudinal temperature, of the order of a few meV, has been obtained.

Table 1: The first generation of cooler storage ring

Facility (Lab)	Operation years
1 NAP-M (Storage Ring for Antiprotons-Model, Budker INP)	1974–1984
2 ICE (Initial Cooling Experiment, CERN)	1979–1980
3 Test Ring (Fermilab)	1980–1982
4 MOSOL (MOdel of SOlenoid, BINP)	1986–1988
5 LEAR (Low Energy Antiproton Ring, CERN)	1988–1996
6 IUCF Cooler (Indiana Univ. Cyclotron Facility)	1988–2002
7 TSR (Test Storage Ring, MPI, Heidelberg)	1988–2012
8 TARN-II (Test Accumulation Ring for Numatron, Tokyo Univ.)	1985–2000
9 ASTRID (Aarhus STorage RIing in Denmark, Aarhus Univ.)	1989–2005
10 CELSIUS (Cooling with ELectrons and Storing of Ions from Uppsala Synchrocyclotron, Uppsala Univ.)	1989–2005
11 ESR (Experimental Storage Ring, GSI)	1990 ⇒
12 CRYRING (CRYebis connected to a small synchrotron RING, MSL, Stockholm Univ.)	1992–2009
13 COSY (COoler-SYnchrotron, FZJ)	1992 ⇒

During these years both electron and stochastic cooling systems became routine tools at cooler storage rings. The BETACOOL code for cooling processes simulation was developed by JINR group and experimentally tested at COSY, ESR, CELSIUS, S-LSR, LEAR, Fermilab Recycler, and others (see Ref. 16 and References there).

Several cooling facilities have been constructed and commissioned:

- SIS-18 (1998, Schwer Ionen Synchrotron, GSI), its electron cooler was constructed at BINP;
- HIMAC (2000, Heavy Ion Medical Accelerator in Chiba, Japan);
- AD (2000, Antiproton Decelerator, CERN);
- S-LSR (2005, Small Laser Equipped Storage Ring, Kyoto Univ.) commissioning with electron cooling;
- HIRFL (2008, Heavy Ion Research Facility at Lanzhou, IMP Lanzhou) [17]; two electron coolers have been constructed at BINP;
- In 2001 the International Muon Ionization Cooling Experiment (MICE) was started at RAL (Great Britain) and Fermilab [18];
- Significant advance in electron cooling method expansion into high energy range has occurred in 2005 with commissioning of “The Pelletron”, HV electron cooler of 4.3MeV electron energy and 1 A electron current at Fermilab [19];
- In 2006 with the bounds of LHC project (CERN), the Low Energy Ion Ring (LEIR) was commissioned with electron cooling of Pb ions; electron cooler has been constructed at BINP [20].

2.1.3 High Lights of Cooling Applications

2.1.3.1 *Particle Physics*

Most remarkable result in particle physics has been obtained in 1984 at Super Antiproton-Proton Synchrotron-collider (SP-barPS, CERN) in experiment on search for W^\pm and Z^0 bozons. The collider was operated with antiprotons provided by Antiproton

Generation Complex based on *stochastic cooling* application and included Antiproton Accumulator (AA) (constructed around 1978). Lars Thorndahl [13]: “The first fast precooling in the AA used bandwidth 150÷500 MHz. Soon a second ring, the Antiproton Collector, was built especially for precooling with a low eta value in order to use higher frequencies. The AC had 3 bands 0.7÷1.6, 1.6÷2.3, and 2.3÷3.1GHz. The 6D emittance (AC) was reduced by about a factor 200 in 4.5 seconds. For the stack in the AA: 1÷2, 2 ÷4 and 4÷8 GHz were installed, the latter was experimental only”. Owing to this technology collider had sufficient luminosity. The experiment resulted in the discovery of “Nobel level”.

Another significant achievement in particle physics occurred owing to both stochastic and electron cooling. At the end of the 80s proton-antiproton collider “Tevatron” with a chain of intermediate synchrotron storage rings was commissioned at Fermilab. Antiproton storage and antiproton beam formation was being accomplished at this facility with application of *stochastic cooling*. And in 1995 the CDF and DO collaborations at Tevatron announced discovery of the top quark. At the same year *electron cooler* “Pelletron” mentioned above was commissioned. Its application to antiproton storage in Recycler ring allowed to reach in Run IIA the luminosity of proton-antiproton collider “Tevatron” (2×900 GeV) of $L_{\max}=4 \cdot 10^{32} \text{ cm}^{-2} \cdot \text{s}^{-1}$ and provide during 2001–2011 the integrated luminosity of $11.87103 \text{ fb}^{-1} \approx 1.19 \cdot 10^{39} \text{ cm}^{-2}$. That led to “observation” of the Higgs boson of 126 GeV at 3σ CL (as announced 2 July 2012 at Fermilab seminar) and high precision measurement of the top quark mass.

The next physics result to be pointed out is H-bar generation in ALPHA Trap (CERN). Application of *stochastic and electron cooling* in AD ring allowed to store and decelerate sufficient number of antiprotons for 3 experiments—ALPHA, ASACUSA and ATRAP. The first of them Anti-hydrogen Laser PHysics Apparatus (ALPHA) succeeded in November 2010 first to capture and store 38 anti-hydrogen atoms for about 170 ms. Then, 26 April 2011 309 anti-hydrogen atoms were trapped and kept, some for as long as 1000 seconds. It really clears the way to experiments with antimatter (antiatoms).

Since November 2011 LHC operates in heavy ions' collision mode. An important and efficient element of the chain of injection accelerators in this mode is mentioned above electron cooler storage ring Low Energy Ion Ring (upgraded LEAR).

2.1.3.2 *Nuclear Physics*

Electron cooling application at ESR (GSI) allowed to develop, beginning since 1996, the high precision Schottky mass spectroscopy. During this period 194,000 Schottky peaks for different nuclei peaks have been identified, 500 different nuclei have been measured and about 200 of them of unknown mass. Mass measurement accuracy is of $2 \cdot 10^{-7}$. Later high precision Time-Resolved Schottky Mass Spectroscopy (TR SMS) was developed at GSI [21]. This method is a perfect tool to study nuclei decays in-flight. Another example of electron cooling unique application in nuclear physics studies is measurement of half-life of bare nuclei in-flight inside the cooler ring developed at ESR as well.

2.1.3.3 *Atomic Physics*

It is enough to present here one but remarkable example of unique experiment setting up in atomic physics that has been performed at cooler storage ring. Such an

experiment at ESR (1996) had a purpose of high precision measurement of U^{91+} 1S Lamb shift. The theory gave value of 463.4 ± 1 eV, and the experiment has given 459.8 ± 4.6 eV [22]. Such QED related studies will be continued at FAIR.

2.1.3.4 Particle Beam Physics

Crystalline beam is one of most bright phenomena discovered in particle beam physics with application of electron cooling method (See details in Ref. 23).

Antiproton electron cooling was first accomplished at LEAR at the end of 1988 — beginning of 1989 (Fig. 3). Since that time “era” of antiproton generation and cooling by electrons began at CERN and lasts to present days.

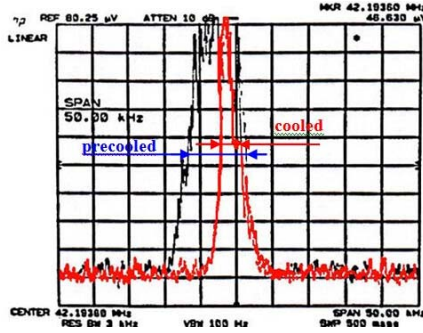


Figure 3: First Electron Cooling of Antiprotons in LEAR (CERN), $\Delta p/p = 6 \cdot 10^{-5}$, Dec. 14, 1988

Stability of intense cooled beams is obviously a problem of practical interest. An excitation of instability of a proton beam in presence of electron one has been observed first at CELSIUS (1993) and later at COSY (2001) and HIMAC (2003). The instability had coherent character, was accompanied with horizontal-vertical coupling and damped with an efficient feed-back system (see details in Ref. 24). Analyzing this problem V. Parkhomchuk derived a criterion for coherent instability threshold. He used an original transfer matrix approach [25]. Until now the criterion was not tested properly in experiments and the problem requires further investigation.

Laser cooling method being under development since 1990 is an outstanding achievement of particle beam physics that allows forming ultra-cold particle beams (Table 2). It is necessary for formation of both ordered beams and 3D crystalline ones. The first one can find application to creation of ion-ion colliders with the beams of rare and/or short-lived isotopes [26] and in the Schottky mass spectroscopy [27]. One should note also the recent progress in 3D laser cooling. The first *indirect transverse laser cooling* (ITLC) observed in 1995 by Heidelberg MPI group was based on longitudinal-transverse coupling via IBS in an intense ion beam [28]. Different methods of ITLC applicable to low intensity ion beams have been developed recently by S-LSR group [29].

Table 2: Minimum particle temperature in cooled beams

Cooling method	Particles/Ring	Energy	T_{\parallel}, K	T_{\perp}, K	Reference
Electron cooling	$^{40}\text{Ar}^{18+}$ / ESR	360 eV/u	10	2000	[30]
	protons / S-LSR	7 MeV	1.9	11	[23]
Laser cooling	$^9\text{Be}^+$ / TSR	7.3 MeV	$5 \cdot 10^{-3}$	—	[28]
	$^{24}\text{Mg}^+$ / S-LSR	40 keV	0.4	6.4 (hor.)/2.1 (ver.)	[29]

2.1.4 Present

We have now 9 cooler storage rings operated in the laboratories around the world (commissioning year is shown in brackets): TSR (MPI, Heidelberg, 1988), ESR (GSI, 1990), COSY (FZJ, 1992), SIS-18 (GSI, 1998), HIMAC (Chiba-Inage, 2000), AD (CERN, 2000), LEIR (CERN, 2006), S-LSR (Kyoto Univ., 2005), CSRe (HIRFL, IMP, Lanzhou, 2008). All they cover a wide range of physics problems and applications which are being studied or used at these facilities: particle, nuclear and atomic/molecular physics, fundamental (antimatter) physics, particle beam physics and formation of beams as intermediate accelerators of accelerator facilities, accelerator technology and cancer therapy.

Among considerable number of projects with cooling application under development at least 6 reached the stage of technical design, prototype development and elements fabrication. Those are, first of all, Nuclotron-based Ion Collider fAcility — NICA (JINR, Dubna) [31] and Facility for Antiproton and Ion Research — FAIR (Darmstadt) [32]. Both of them need for operation stochastic cooling systems and medium energy electron coolers. Particularly, the NICA collider will use two beam cooler of maximum electron energy of 2.5 MeV. The Energy Storage Ring (HESR) at FAIR is designed for application of 8 MeV electron cooler. The working prototype of such machines is electron cooler of 2 MeV electron energy constructed in Budker INP (Novosibirsk) and being under commissioning at COSY presently. The third project dedicated to development of stochastic cooling of a bunched ion beam in Relativistic Heavy Ion Collider (RHIC, BNL) has reached recently remarkable results demonstrating 6D cooling of U^{92+} bunched beam [34]. It promises to increase luminosity of RHIC and to be applied efficiently at NICA and FAIR.

The Muon Ionization Cooling Experiment (MICE) is being developed by wide collaboration under leadership of Rutherford-Appleton Lab (RAL, Great Britain) and Fermilab. The MICE is based on high intense proton beam delivered by 800 MeV proton synchrotron ISIS at RAL. The goal of MICE is to demonstrate in 2018 “ $a \approx 10\%$ reduction in the emittance of muon beams of various emittances and momenta...” [18]. The MICE project is of great interest not only for muon collider that is of rather far future, but also for today’s projects of muon neutrino fabrics.

Two other projects under development belong to low energy range. First of them, the Cryogenic Storage Ring (CSR) [35] is aimed to perform experiments on atomic physics of molecular ions. Typical ion energy in such experiments is of the order of several keV/u that correspond to energy of cooling electrons is of a few eV. Optimal focusing system at such low energy of heavy (molecular!) ions in a low charge state is designed with electrostatic focusing and bending fields. First cooler storage ring of such type was constructed and operated at KEK [36].

The second project, Low Energy Particle Toroidal Accumulator (LEPTA) is several years in commissioning stage suffering problems due to lack of positrons [37]. Upgrade of vacuum system of the positron trap done this year promises to resolve the problem.

Two shut-down cooler storage rings have been destined for a new life. The CRYRING will be coupled with ESR providing a deeper deceleration of high charge ions down to 4 MeV/u. The TSR will be transferred to CERN and used at Isotope Separator On-line (ISOLDE) facility. This will extend experimental potentialities of the facility enriching it with the methods developed at cooler storage rings.

One can point out also 5 projects which are for the present moment in the stage of conceptual design (“paperwork”).

Extra Low Energy ANtiproton storage ring (ELENA) aimed for antihydrogen physics has been approved at CERN after many years of unsuccessful attempts. It will decelerate antiprotons delivered by AD to 100 keV kinetic energy that expands significantly experimental possibilities of the facility [38].

The High Intensity heavy ion Accelerator Facility (HIAF) stands out among the projects of not so distant future because of its grandiosity. The project proposed and being developed by group from the Institute of Modern Physics (Lanzhou, China) is aimed for construction of accelerator complex comprising two superconducting linacs (ion and electron ones), two multipurpose cooling storage rings and electron-ion collider [39]. The project has the goal “to advance nuclear physics studies and applied research in the matter state unreachable before and provide conditions for experimental studies of this region at the most advanced level of experimental technology”. The ambitious project was approved in 2012 by the Central Government of China “in principle”, the commissioning is scheduled for 2022–2030 (at such an uncertainty!).

The Jefferson National Laboratory (USA) began the development of the project of Medium Energy Electron-Ion Collider based on CEBAF recirculating SRF linac (MEIC, JLab) [39, 40] with both DC electron cooler of 1.5 MeV electron energy and of 50 MeV one based on electron energy recovery linac (ERL).

Electron-Ion Collider (eRHIC) project of BNL is aimed for particle physics with polarized electron and ion beams. There are no definite plans for the project implementation.

An old idea — coherent electron cooling (CEC) experiences “the second birth” by efforts of BNL/JLab group [42]. The initial proposal made at Budker INP (Novosibirsk) suggested to use electron beam in a stochastic cooling system instead of electronic feedback with signal amplification. The authors of the new (advanced) version of CEC propose to use a wiggler as an amplifier of electron beam density fluctuation caused by interaction of an ion with electrons of the cooling beam. Creation of CEC promises further development of electron cooling with numerous possible applications.

2.1.5 Conclusions

By now cooling methods have been developed for cooling by synchrotron radiation (SRC), electrons (EC), high frequency stochastic signal (stochastic cooling, SC), laser radiation (laser cooling, LC). Cooling of muons by ionization in medium (muon cooling, MC) is not demonstrated yet but eagerly awaited. These methods allow to cool particle beams of electrons (SRC), protons and antiprotons (EC, SC), ions (EC, SC, LC), muons (MC). The particle energy range covered by different cooling methods stretches from several keV/u (ions) up to 8 GeV (p-bars).

The ideas and proposals stated recently (e. g., like coherent electron cooling, ERL-cooler, etc.) do show that development of cooling methods is in active state and did not reach yet its apogee.

Work supported by RFBR grant 12-02-00072-a

2.1.6 References

1. Joseph Liouville, J. De Math., **3** (1838) 349.

2. A. A. Kolomensky & A. N. Lebedev, Proc. of the USSR Academy of Sci., **106** (1956) 807.
3. Kenneth W. Robinson, Phys. Rev., **11** (1958) 373.
4. A. A. Kolomensky, Atomnaya energiya, **19** (1965) 534 (in Russian).
5. G. I. Budker, Proc. of the Intern. Symp. on Electron and Positron Storage Rings, Saclay, 1966, p. II-I-I; Atomnaya Energia, 22 (1967) 346 (in Russian).
6. S. van der Meer, Internal Report CERN/ISR-PO/72-31, 1972.
7. S. van der Meer, Nobel Lecture, 8 December, 1984, p. 2.
8. G. I. Budker, in Proc. of 15th Intern. Conf. on High Energy Physics, Kiev, 1970.
9. G. I. Budker and A. N. Skrinsky, Physics-Uspokhi, **124** (1978) 561.
10. A. Skrinsky, private communication (2010).
11. I. N. Meshkov, Part. and Nuclei Physics, **25** (1991) 1238.
12. S. van der Meer, Autobiography of Nobel Laureat.
13. L.Thorndahl, private communication (2014).
14. S. Schroeder et al., PRL, **64** (1990) 2901.
15. J. S. Hangst et al., PRL, **67** (1991) 1238.
16. A. Sidorin, A. Smirnov, Proc. RuPAC-2012, (2012), TUACH02.
17. X. Yang et al., Proc. of COOL'13 Workshop, WEAM1HA02.
18. D. Kaplan et al., ibid., MOAM2HA01.pdf
19. S. Nagaitsev et al., Proc. COOL'2005 Workshop, AIP Conf. Proc., **821** (2006) 39.
20. D. Manglunki et al., Proc. of COOL'13 Workshop, MOPM2HA01.
21. Yu. Litvinov, G. Münzenberg, M. Steck et al., NIM A **756** (2005) 3; B. Franzke, H. Geissel, G. Münzenberg, Mass Spectrometry Reviews, **27** (2008) 428-469.
22. A. Gumberidze et al., PRL, **94** (2005) 223001.
23. I.Meshkov, A. Noda & A.Smirnov, ICFA BD #64 (This issue); T. Shirai, A. Noda, I. Meshkov et al., PRL, **98** (2007) 204801.
24. J. Dietrich, I. Meshkov, J. Stein et al., Proc. COOL'2005 Workshop, ibid, p. 270.
25. V. Parhomchuk, Proc. Joint Acc. School (JAS'2000), p.53; Physics-Uspokhi, **170** (2000) 473.
26. I. Meshkov, D. Moehl, T. Katayama, A. Smirnov, et al., NIM A, **532** (2004), 19.
27. B.Franzke, K.Beckert, H.Eickhoff et al., Proc. EPAC'1998, p.256
28. H.-J. Miesner, R. Grimm, M. Grieser, et al., PRL, **77** (1996) 623
29. A.Noda et al., Proc. IPAC'2014, MOZA01
30. M. Steck et al., PRL. **77** (1996) 3803.
31. A. Smirnov et al., Proc. of COOL'13 Workshop, THPM2HA01.pdf.
32. M. Steck et al., ibid., MOPM1HA01.pdf.
33. D. Prasuhn et al., ibid., THPM2HA02.pdf.
34. M. Blashkewicz et al., ibid., MOAM1HA02.pdf.
35. A. Wolf et al., ibid., WEAM1HA01.pdf.
36. T. Tanabe, K. Noda, E. Syresin, NIM A 532 (2004) 105–110.
37. A. Kobets et al., Proc. COOL'13 Workshop, WEPP011.pdf.
38. P. Beloshitskii et al., ibid., THPM1HA02.pdf.
39. X. Yang et al., ibid., MOPM1HA04.pdf.
40. Y. S. Derbenev, ibid., MOPM1HA02.pdf.
41. Y. Zhang et al., ibid., TUPM1HA03.pdf.
42. V. Litvinenko et al., ibid., TUPM1HA03.pdf.

2.2 Recent Development in Stochastic Cooling Applications

Takeshi Katayama, Nihon Univ., 1-2-1, Izumi, Narashino, Chiba, Japan
 Mail to: tkatayama.vc@nifty.com

Abstract:

In this article the topics of stochastic cooling application to the major accelerator projects are described after the brief review of the achieved performance in the past three decades. Details of theoretical aspect or simulation results in each project will be given in the separate contributions from related laboratories in this letter and here just the summaries of topical subjects are presented.

2.2.1 Introduction

The beam cooling has been playing the key role for the experiment at the hadron storage ring and colliders in the past three decades. In the antiproton and proton collider at CERN, the antiproton beam was collected and accumulated in the small rings (kinetic energy=2.8 GeV) with stochastic cooling and stacking system to form the high dense antiproton beam and then transferred to the SPS collider. Thus attained high luminosity collision experiment was culminated in the discovery of weak boson W and Z in 1983. At the FNAL the similar way was followed (8 GeV) to perform the collision experiment at the TEVATRON. The stochastic cooling has been the excellent tool not only for the antiproton cooling but also for the low energy ion cooling. At the ESR GSI the rare isotope beam (0.4 GeV/u) was pre-cooled by stochastic cooling effectively prior to the further cooling by electron cooling system. At the COSY FZJ the proton and deuteron beams (1~2 GeV/u, polarized and un-polarized) are used for the internal target experiments where the stochastic cooling was used to compensate the target effects to keep the beam in the small momentum spread and transverse emittances.

The challenging program of production of low energy antiproton beam has been successfully attained at CERN AD (Antiproton Decelerator) where the 2.8 GeV antiproton beam is decelerated to 47 MeV with use of the stochastic cooling and further decelerated to 5 MeV with the electron cooling to compensate the anti-damping emittance increase through the deceleration. The lower energy ~0.1 MeV antiproton beam production is promoted at the ELENA project located downstream the AD.

The other remarkable result attained recently at BNL RHIC, for long years being tried at several laboratories but not succeeded, is the stochastic cooling of bunched beam. The Au beams of 100 GeV/u are collided in the RHIC where the luminosity is gradually reduced mainly due to the diffusion phenomena of Intra-Beam-Scattering (IBS) effects. The unique pickup and kicker system with the bandwidth of 4-8 GHz could successfully compensate the diffusion effects and the luminosity lifetime is remarkably improved.

In the following sections the stochastic cooling concept envisaged at the major projects are outlined emphasizing the unique performance of each project.

2.2.2 FAIR Project

The FAIR (Facility of Antiproton and Ion Research) accelerator is under construction at GSI aiming to complete it by 2019 where the stochastic cooling is planned to play the key role to attain the required beam quality of antiproton and heavy ion (rare isotope) beams. The storage ring complex of Modularized Start Version of the FAIR project consists of Collector Ring (CR) and High Energy Storage Ring (HESR) while the original version included the antiproton accumulator ring (RESR) and experimental rings (NESR) which are postponed to the next construction phase.

2.2.2.1 *Pre-Cooling of Antiproton Beam in the Collector Ring*

A proton beam is accelerated in the SIS100 synchrotron up to the energy of 29 GeV with an intensity of 2×10^{13} with cycle time of 10 sec. A single proton bunch, formed with RF manipulation after the acceleration in SIS100 is fast extracted and hits the production target of nickel. An antiproton flux of 4×10^8 is produced within the transverse emittance of $240 \pi \text{ mm.mrad}$ (6 times the rms value) and the momentum spread of +/- 3% (uniform spectra). The bunch length from the SIS100 is +/- 25 n sec. Thus produced antiproton beam is transferred and injected into the CR where the injected bunch is rotated in the longitudinal phase space to reduce the momentum spread from +/- 3 % to 2.45×10^{-3} (rms) by the harmonic $h=1$ RF of an amplitude of 100 kV. Subsequently the stochastic cooling is applied to further reduce the momentum spread to 5.0×10^{-4} (rms) with the Notch Filter cooling system. The bandwidth of stochastic cooling system is 1-2 GHz. In order to have a fast extraction from the CR, the cooled coasting is adiabatically bunched to make the beam free gap of 300 nsec as the full aperture fast kicker magnet in CR needs such a long rising time of magnetic field. The RF voltage of 450 Volt of harmonic number=1 is adiabatically applied and resultantly the $\Delta p/p$ is increased to 8×10^{-4} (rms). A transverse stochastic cooling system is designed to reduce the emittance from $60 \pi \text{ mm.mrad}$ to $1.25 \pi \text{ mm.mrad}$ (ε_{rms}).

This procedure is essentially the same as the antiproton pre-cooling process at CERN AAC (cycle time=5 sec) and FNAL (cycle time=2 sec).

2.2.2.2 *Accumulation of Pre-Cooled Beam with Stochastic Stacking System*

The subsequent accumulator ring, named RESR was conceived to accumulate the 1×10^{11} antiprotons by the stochastic stacking method with an injected particle number of 1×10^8 from the CR every 10 sec. While the cycle time is planned as 10 sec in the 1st phase of the FAIR project, it can be shortened to 5 sec after an upgrade. Then all the stacking system is designed to support this final goal.

The stochastic stacking system of RESR is similar to the one at CERN AAC conceived by S. van der Meer. [1]

The antiproton beam is single turn injected on the orbit of the RESR, and is accelerated to the deposit orbit which is apart from the injection orbit by around $\Delta p/p=1.0$ % where is prepared a stochastic stacking system, being composed of radial aligned two Tails and Core cooling system.

The frequency bands of two Tail's system are chosen as 1-2 GHz while for the Core system the wider bandwidth of 2-4 GHz is selected. The positioning of PU and kicker are determined from the results of numerical calculation.

The essential point of designing the Tail system is to prepare the profile of exponential decaying cooling force along the radial direction. The Core system, being composed of two PUs and operated with push-pull mode, provides the edge of stacking beam profile. In Fig. 2.1 the positioning of two Tails and Core system are illustrated as a function of radial position. The cooling force is given in green line which shows the exponential decreasing as a function of radial distance. The high gain, more than 145 dB is necessary to move the deposited beam into the stack region by the next injection cycle and then the Beam Feedback Effect becomes noticeable for the deposited beam.

The profiles of the deposited and 1000 times stacked beams are given in red lines [2] where we include the diffusion process by the Intra Beam Scattering (IBS) effects formulated by M. Martini [3].

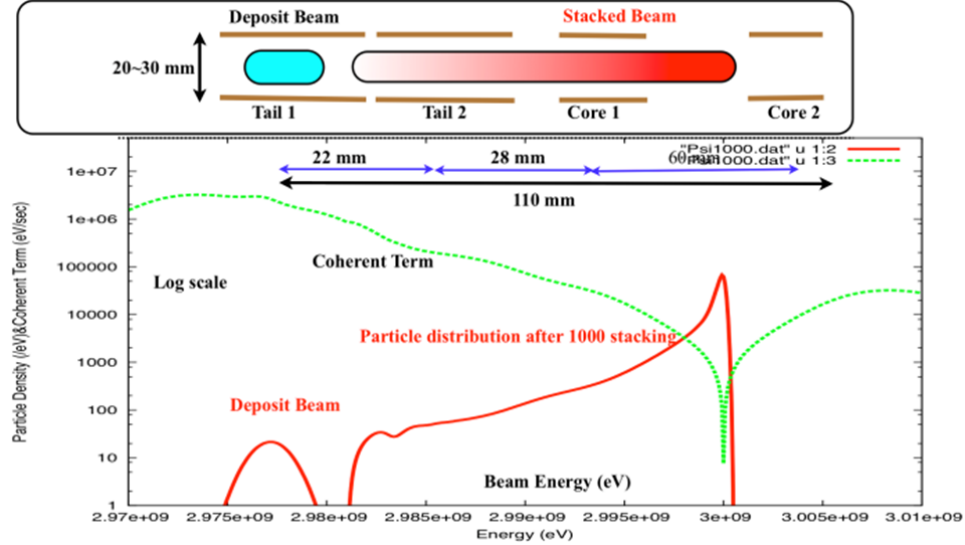


Figure 2.1: The schematic layout of the stochastic stacking system of RESR. The injection orbit (not illustrated in the figure) is around 1 % ($\Delta p/p$) left from the deposit position. Two Tails system and the Core system (push-pull mode) produce the required cooling force profile (green line). The profiles of the deposited and 1000 times stacked beam are given in red lines.

The advanced cooling stacking method is envisaged to use the pre-cooling of the injected beam before shifting it to the deposited orbit. In this case the pre-cooling at the injection orbit is performed in parallel with the cooling stacking process in the stacking area. In the design of RESR it is found that the pre-cooling can be performed within 5 sec which reduces the momentum spread (rms) from 5×10^{-4} to 1×10^{-4} .

2.2.2.3 Antiproton Accumulation in HESR

As is postponed the construction of RESR ring to the second phase, it is inevitable to prepare the accumulation function of 3 GeV antiproton beam in the HESR, with the circumference of ~ 500 m where the antiproton is decelerated to 1 GeV or accelerated to 14 GeV after the accumulation.

Investigated are three methods of beam accumulation in the longitudinal phase space assisted with the stochastic cooling. The first one is the moving barrier voltage method, the 2nd one is the fixed barrier voltage method and the 3rd one is to use the harmonic=1 RF voltage. Details of the simulation results for each accumulation methods are described elsewhere. Among these three methods, we have a conclusion to use the moving barrier method as it gives the most high accumulation efficiency and has several advantages over others. [4]

2.2.2.3.1 Simulation Method

The accumulation process are simulated with the particle tracking code which includes the effects of RF field by barrier voltages, stochastic cooling force, diffusion forces such as Schottky diffusion, thermal diffusion and Intra-Beam-Scattering effects. If necessary other effects associated with internal target, mean energy loss and multiple scattering could be included. The basic algorithm of the code is as follows.

First the stochastic cooling force is calculated as a function of energy. If the gain of the cooling system is varied with time, the cooling force is re-calculated at each

computing cycle. The thermal diffusion force is simply calculated with given cooling parameters. On the other hand the Schottky diffusion term requires the energy spectrum of the particles, and then at each computing cycle the energy spectrum is calculated and the Schottky diffusion term is obtained. The IBS heating term is calculated with use of Martini formula with use of lattice Twiss functions of the HESR ring including the change of bunch length. The transverse emittance is assumed as constant during the accumulation as only the momentum cooling is used in this process.

Once the cooling force and diffusion force are obtained it is straightforward to calculate the energy decrease by the cooling force and the increase by the diffusion force as a random kick to each particle. The longitudinal equations of motion to be solved are as follows.

$$\frac{d\Delta E}{dt} = \frac{q\omega_0}{2\pi} V(\tau) + F(\Delta E) + \xi_s(\Delta E, t) + \xi_t(\Delta E) + \xi_{IBS}(t) \quad (1)$$

$$\frac{d\tau}{dt} = -\frac{\eta}{\beta^2 \gamma E_0} \Delta E \quad (2)$$

where V represents the barrier voltage, F the cooling force, ξ_s , ξ_t , ξ_{IBS} the diffusion terms associated with Schottky, thermal and IBS diffusion. q is a charge state of ion and η is the momentum slipping factor.

2.2.2.3.2 Moving Barrier Voltage Method

The process of beam accumulation with moving barrier method is illustrated in Fig. 2.2 where the particle distribution (red dots) in the longitudinal phase space is shown as well as the barrier voltage (blue lines). The horizontal scale is the time and the full range is corresponding to the one revolution period. The left scale is the energy and the right scale is the barrier voltage. After the 1st beam injection (time=0 sec), the barrier voltage is switched off within 0.2 sec and the beam becomes coasting one. Until time=9.5 sec, the coasting beam is well cooled by stochastic cooling system. At time=9.5 sec, the barrier voltage is adiabatically increased again to 2 kV and the right hand side pulse starts to push the beam to prepare the empty space for the next beam injection. At the time=10 sec, the 2nd injected particles are found in the central part whereas the 1st injected ones are shifted in the accumulation area.

The accumulation has been accomplished with the repetition of this process until the accumulated particle number reaches to the desired particle number. In Fig. 2.3 the accumulated particle number and the accumulation efficiency is given up to the 100 times stacking where the accumulation efficiency is defined as the ratio of accumulated particle number divided by the total injected particle number. The accumulated particle number up to the 100 stacking are almost linearly increased with stacking number and the accumulation efficiency is around 98.5% after the 100 stacking.

The cooling gain is reduced according to the increase of the particle number. This reduction of gain is essential to assure the high accumulation efficiency as the Schottky diffusion term is proportional to the density of particle and the square of the cooling gain.

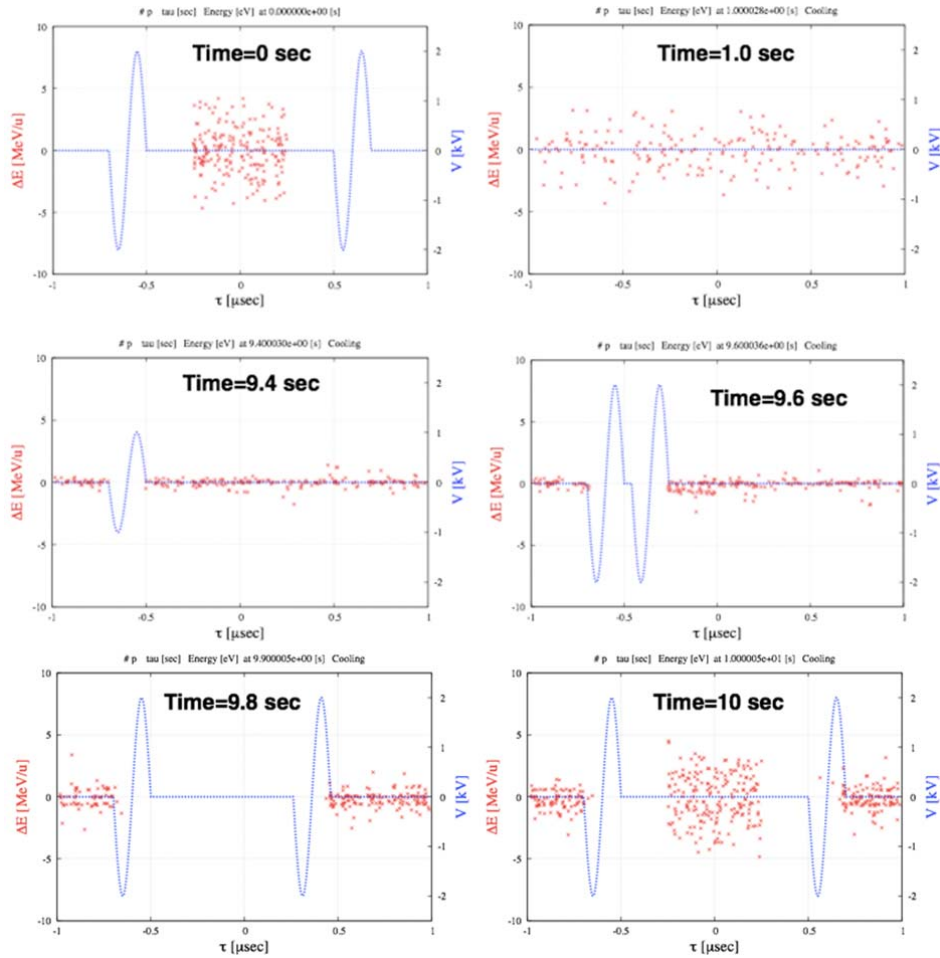


Figure 2.2: Particle distribution (red dot, energy is given left scale) in the longitudinal phase space during the one cycle, 10 sec as well as the barrier voltages (blue line, right scale) for the moving barrier voltage case.

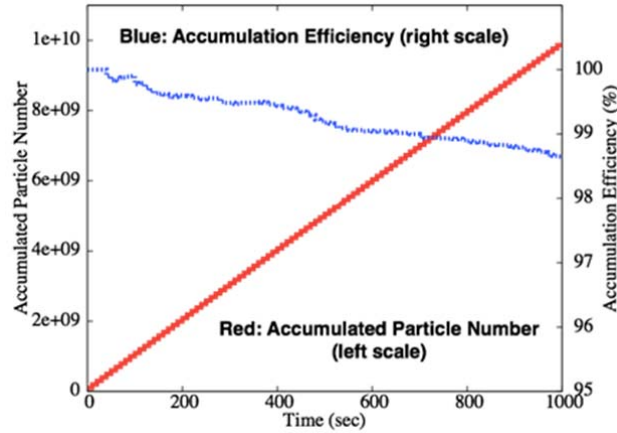


Figure 2.3: The increase of accumulated particle number (red line, left scale) and the accumulation efficiency (blue line, right scale).

2.2.2.3.3 POP Experiment at the ESR

To check the validity of the simulation code and the basic concept of the barrier bucket accumulation, moving and fixed barrier method, the POP (Proof of Principle) experiment was performed at the ESR using the $^{40}\text{Ar}^{18+}$, 0.4 GeV/u beam from SIS18 synchrotron. The results are quite satisfactory and show that the simulation results are close in agreement with experimental results. [5] The barrier voltage was as low as 120 V because the ferrite loaded cavity for harmonic=1 RF was used for the experiment with the cavity gap just terminated by 50 Ohm register. To overcome the problem of this too low barrier voltage, the electron cooling was simultaneously used with stochastic cooling.

The experimental results of the accumulation of the moving barrier operation with simultaneous use of the stochastic cooling and electron cooling are given in Figure 2. 4. The left figure shows the simulation result and the right figure is the experimental result.

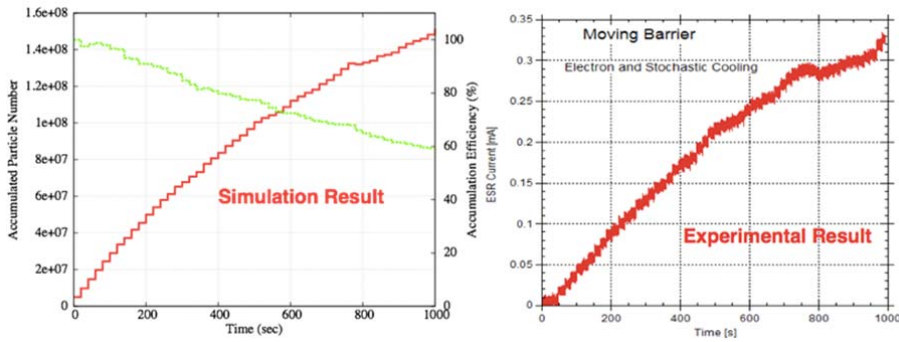


Figure 2.4: The simulation (left) and the experimental (right) results of the moving barrier operation. The red line in the left figure shows the accumulated particle number and the green line the accumulation efficiency.

2.2.2.4 Low Energy Antiproton Beam Production at FAIR

The low energy antiproton beam has been used for the unique experiment such as the production of anti-hydrogen, at CERN AD which is the all-in-one storage ring served for the bunch rotation, the stochastic cooling of longitudinal and transverse phase spaces, the deceleration with stochastic cooling and electron cooling. Presently available beam intensity is $2\sim 5\text{e}7$ per 120 sec cycle time. On the other hand at the FAIR the 3 GeV antiproton beam is planned to accumulate in the HESR up to 10 batches, namely $1\text{e}9$ with cycle time 100 sec, and then it is decelerated to 1 GeV in the HESR with the stochastic cooling at 2 GeV, and transferred to ESR (presently operating machine at GSI) to further decelerate to 30 MeV. The beam is transferred to CRYRING (now connected to ESR) to decelerate to 0.3 MeV. The available beam intensity is estimated at $8\text{e}8/220$ sec. One of serious points in this scenario is the space charge tune shift at the lowest energy in CRYRING. The possibility of this low energy antiproton beam scenario is extensively discussed. [6]

2.2.3 NICA Project

The heavy ion collider proposed at the Joint Institute for Nuclear Research, JINR Dubna, Russia aims to achieve the head-on collision of 1-4.5 GeV/u, $^{197}\text{Au}^{79+}$ ion beam

with the luminosity of $\sim 1e27/cm^2/sec$. [7] The number of bunches in the collider is 20 ~ 24 and each bunch contains the ion number of $\sim 1e9$, depending upon the operation energy. Thus totally around $\sim 2.4e10$ ions should be accumulated in the collider ring. The injector for the collider is the existing superconducting synchrotron, Nuclotron, which could provide the beam of 1-4.5 GeV/u with the intensity of 10^8 - 10^9 /cycle of the cycle time 5 sec. The bunch length of the beam from the Nuclotron is around 1/3 of the circumference, 300 nsec.

In this scenario, the bunch is transferred to the collider without any manipulation for the short bunch formation in the Nuclotron which allows much easier operation of the Nuclotron. The long bunch is transferred in the longitudinal injection area which is provided by the barrier voltages, and is accumulated with the assistance of stochastic cooling for the high energy and the electron cooling for the low energy below 2.5 GeV/u.

Thus accumulated and well cooled heavy ion beam is the coasting beam condition, and then the large RF voltage is applied adiabatically as well as the beam cooling. The beam is gradually bunched to the required rms bunch length for the collision experiment ~ 2 ns (rms). The bunch length is the equilibrium state of RF field, beam cooling, Intra Beam Scattering and space charge repulsion force. Especially at low energy, the IBS diffusion and space charge force could affect the beam motion at the short bunch condition.

The typical specifications of the stochastic cooling with the Palmer method are as follows: beam energy= 3.5 GeV/u, ring slipping factor=0.0232, TOF from pickup to kicker=400 nsec, number of pickup and kicker loop couplers=128, band width=2-4 GHz, coupling impedance=50 Ohm, atmospheric temperature=300 K, barrier voltage=5 kV and frequency=5 MHz. The electronic gain of the cooling system is 90 dB and the required maximal microwave power is 50 W. The barrier voltage is assumed as 2 kV with T=200 nsec. The fixed barrier accumulation method is used. In Fig. 3.1 the accumulated particles and barrier voltage are illustrated at 1st injection and after 30 stacking.

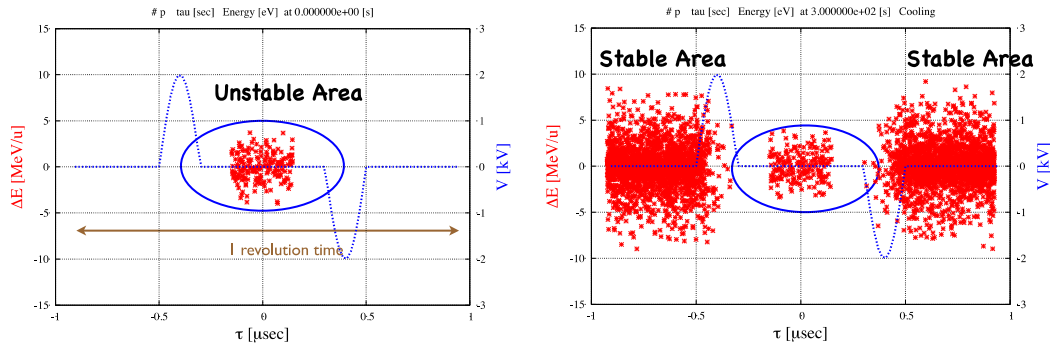


Figure 3.1: Phase space mapping of particles at the 1st injection (left) and after 30 stacking (right). The particles are represented with red dots and the barrier voltages are blue line. The injected beam is located in the central unstable area. Ion energy is 3.5 GeV/u.

In Fig. 3.2 (left) the calculated accumulated particle number and the accumulation efficiency, (defined as the ratio of accumulated particle number to the total injected particle number) are illustrated.

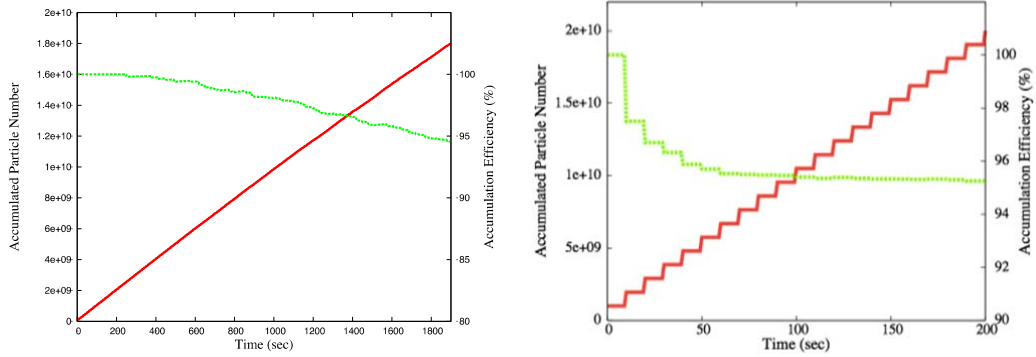


Figure 3.2: (Left figure) Accumulated particle number (red, left scale) and accumulation efficiency (green, right scale) for the NICA collider with stochastic cooling. Ion energy=3.5 GeV/u. (right figure) The accumulated particle number (red) and the accumulation efficiency (green) up to 20 times injection with electron cooling including the space charge effects. Ion energy is 1.5 GeV/u.

At the lower energy the stochastic cooling system does not work as the momentum slipping factor becomes large and resultantly the mixing factor from PU to kicker is un-tolerably large. In that case the electron cooling can be used effectively. In Fig. 3.2 (right) the accumulation efficiency of 1.5 GeV/u Au is illustrated where the space charge repulsion force and the IBS effects are included as the ion energy is as low as 1.5 GeV/u.

It is found that the stochastic cooling well works at the energy beyond 2.5 GeV/u while at the less energy the momentum acceptance of stochastic cooling system becomes too narrow due to the large slipping factor. On the other hand below 2.5 GeV/u the electron cooling could work to accumulate the beam as well as the short bunch formation. In this sense, both cooling method are perfectly complimentary each other. [8]

The space charge effects during the barrier bucket accumulation and the short bunch formation was investigated with Particle In Cell method. The space charge potential becomes around +/- 20 kV at 1.5 GeV/u at the bunch length of +/- 3 nsec while at the higher energy the space charge potential becomes small value. Considering the external RF voltage, 500 kV, this space charge problem could be minor effects to the short bunch formation.

2.2.4 Stochastic Cooling at Electron Ion Collider Project

Several proposals of electron-ion-collider are under conceptual design stage, at Jlab, BNL, CERN, FAIR and IMP. The design goals are typically (JLab case), 40 GeV/u, $^{208}\text{Pb}^{82+}$ ion beam collision with 12 GeV electron beam with the maximal luminosity $\sim 10^{34} \text{ cm}^{-2}\text{sec}^{-1}$.[9] It is evident that the beam cooling is essential to compensate the IBS diffusion process at the collision experiment as well as the ion beam accumulation and the formation of short bunches like the NICA project case. The IBS diffusion time is estimated at a few tens second for the nominal operation and then presently the main effort has been focused to attain the electron cooling with Recirculating Electron Linac (ultimately Coherent Electron Cooling) to attain the strong and fast electron cooling.

The stochastic cooling could be used for the reduction of emittance of coasting beam before the short bunch formation in the collider ring. If the start operation is

planned at the less luminosity, the IBS diffusion time is a few thousand sec, and the stochastic cooling of bunched beam can be used for the compensation of IBS effects. Presently the possibility of stochastic cooling for the short bunched beam is being carefully investigated taking account the mixing problem between Kicker to Pickup.

2.2.5 References

1. S. van der Meer, "Stochastic Stacking in the Antiproton Accumulator", CERN/PS/AA/78-22, 1978.
2. T. Katayama, O. Dolinskyy, B. Franzke, S. Litvinov, F. Nolden, M. Steck, D. Moehl and L. Thorndahl, "Numerical Design Study of Stochastic Stacking of 3 GeV Antiproton Beam in the RESR for the FAIR Project", MOA2MCIO02, Proc.of COOL09 at IMP, Lanzhou China.
3. M. Martini "Intra-beam Scattering in the ACOL-AA Machines", CERN PS/84-9, 1984.
4. T. Katayama, M. Steck, R. Maier, D. Prasuhn, R. Stassen, H. Stockhorst, I. Meshkov and T. Kikuchi, "Beam Accumulation with Barrier Voltage and Stochastic Cooling", MOPD065, Proc. of IPAC 2000, Kyoto, Japan.
5. M. Steck, C. Dimopoulou, B. Franzke, O. Gorda, T. Katayama, F. Nolden, G.Schreiber, D. Moehl, R. Stassen, H. Stockhorst, I. Meshkov, A. Sidorin and G.Turbinikov, "Demonstration of Longitudinal Stacking in the ESR with Barrier Buckets and Stochastic Cooling", TUPS20, Proc. of COOL11, Alushta, Ukraine.
6. M. Steck, F. Herfurth, M. Lestinsky, Y. Litvinov, Th. Stöhlker, T. Katayama, R. Maier and D. Prasuhn, "Deceleration of Antiprotons in the Modularized Start Version of FAIR Employing the ESR Storage Ring", FLAIR workshop, May 2014, MPI, Heidelberg.
7. N. Agapov, V. Kekelidze, R. Lednicky, V. Matveev, I. Meshkov, A. Sorin, G. Trubnikov, "NICA Project at JINR", RuPAC12, St. Petersburg, 2012.
8. T. Katayama, I. Meshkov, A. Sidorin and G. Trubnikov, "Beam Cooling at NICA Collider", RuPAC12, St. Petersburg, 2012.
9. Y. Zhang and J. Bisognano (Editors), "Science Requirements and Conceptual Design for a Polarized Medium Energy Electron-Ion Collider at Jefferson Lab", 2012.

2.3 Overview of the Cooling Program at CERN

Gerard Tranquille, BE Department, CERN
 Mail to: gerard.tranquille@cern.ch

2.3.1 Introduction to CERN

CERN, the European Organization for Nuclear Research, is an intergovernmental organization with 21 Member States.

The accelerator complex at CERN is a succession of machines with increasingly higher energies. Each machine injects the beam into the next one, which takes over to bring the beam to an even higher energy, and so on. The flagship of this complex is the Large Hadron Collider (LHC). There are several additional facilities where beams of different energies are provided to experiments. The whole CERN complex is depicted below:

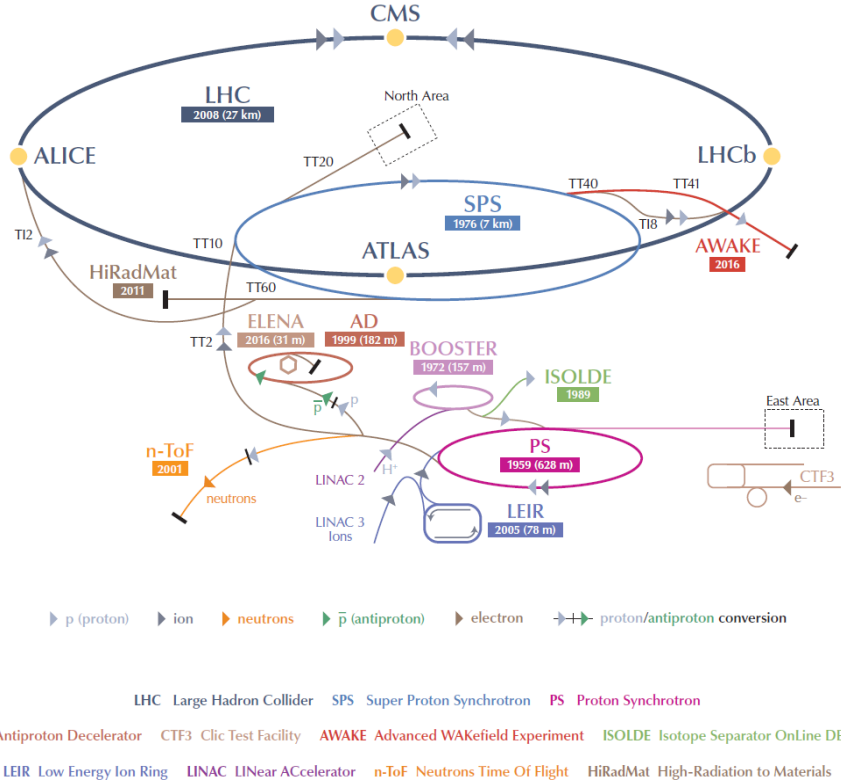


Figure 1: The CERN accelerator complex.

At CERN the technique of beam cooling has made many varied and ambitious physics programs possible. The observation of the intermediate vector bosons predicted by the unifying electro-weak theory and the trapping of anti-hydrogen atoms are just two examples of such achievements. More recently lead-lead and proton-lead ion collisions in the LHC have been made possible thanks to the cooling and accumulation of lead ions in the low energy ion ring LEIR.

Stochastic and electron cooling have been used extensively on all the storage rings of the CERN accelerator complex primarily for the accumulation of rare particles (e.g. antiprotons) or for the improvement of beam quality for precision experiments.

2.3.2 Stochastic Cooling

2.3.2.1 First Ideas

The first ideas on stochastic cooling were formulated at CERN in the late 60's when Simon van der Meer [1] noted that if one could detect statistical fluctuations in a beam, then the oscillations that happened to be coherent at any time because of their statistical nature could be damped very much like the feedback systems known as "dampers" that were commonly used to counteract coherent beam instabilities. At the time this idea seemed farfetched, but when, in 1971, the noise of a coasting beam in the ISR (Intersecting Storage Ring) was observed on very sensitive pick-up electrodes the basis for stochastic cooling became a reality.

The first experimental demonstration of stochastic cooling was made in the ISR in 1974 with one ring fitted with a simple vertical cooling system. This system had a

bandwidth from 0.8 to 1.5 GHz and an amplification of 95 dB, and when applied to the 2×10^{13} protons at 26 GeV in the ring the height of the Schottky side-bands slowly decreased indicating beam cooling. The measured rate, about 2% per hour, was in excellent agreement with expectation for the experiment.

2.3.2.2 *The “ICE” Age*

At about the same time Carlo Rubbia et al. [2] were exploring possibilities to collide counter rotating beam of protons and antiprotons in one and same ring. In order to reach high luminosities Budker had proposed to use the technique of electron cooling to accumulate a sufficient number of antiprotons in an accumulator ring. To test the different cooling systems, the ICE (Initial Cooling Experiment) ring was built at CERN in 1977 using components from the g-2 storage ring previously used to measure the magnetic moment of the muon.

Thorndahl and Carron set about designing and installing the hardware for a system used to investigate all aspects of stochastic cooling. A 2 GeV beam of about 10^9 protons injected from the CPS was successfully cooled not only in the transverse planes but also longitudinally using the newly invented filter technique [3]. Even first attempts of bunched beam cooling gave encouraging results and by mid-1978 all systems worked to expectation. Cooling not only increased the 3-dimensional density of the circulating beam but also significantly increased the lifetime by counteracting the blow-up due to scattering on the residual gas molecules. When the few hundred antiprotons produced by the CPS protons were stored and cooled in ICE, their lifetime made a jump from $120\mu\text{s}$ to 80 hours thanks to stochastic cooling.

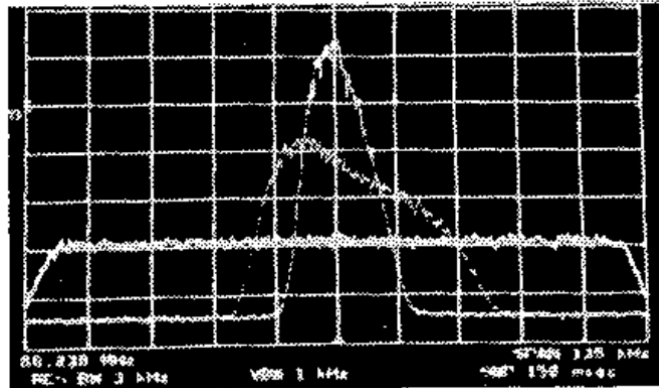


Figure 2: Momentum Stochastic cooling of 7×10^7 protons in ICE. The three traces represent the initial density distribution and the density distribution after four and eight minutes.

During 1978, theoretical work started on the stochastic stacking of particles in momentum space [4] in which each new batch of antiprotons (containing a few 10^7) is deposited at the edge of the stack tail and displaced towards the core by the cooling system to make place for the subsequent batch arriving 2.4 s later. This is repeated nearly 10^5 times until sufficient antiprotons are accumulated. For this to work two “stack tail” and “stack core” cooling systems are needed. Their pick-ups are centred at different radial positions (corresponding to different momenta) in a region of “large dispersion” where the orbits strongly displace with momentum. This idea formed the basis of the CERN Antiproton Accumulator (AA).

2.3.2.3 *The Antiproton Accumulator and the Antiproton Accumulator Complex*

The antiproton accumulator [5] proposed in 1978 had a circumference of 157 m and stored the beam at a fixed momentum of 3.5 GeV/c, close to the production maximum of antiprotons by 26 GeV/c protons from the CPS.

Construction of the AA began in 1979, running-in started in the summer of 1980, and as of 1981 stacks of several 10^{11} antiprotons per day were routinely accumulated from batches of a few 10^6 pbars per second. Already in this early period the increase of the three dimensional beam density was almost 10^8 . In April 1981 the ISR first took an antiproton beam from the AA followed by the SPS on 10 July 1981. The first W data were taken in 1982 and the discovery of the W and Z was announced in 1983. In order to satisfy the ever-increasing appetite of antiproton users, the Antiproton Collector (AC) was built around the AA in 1986. From 1987 on, it boosted the accumulation rate, eventually by an order of magnitude.

In the original AA, a fresh burst of antiprotons remained on the injection orbit for at least 2.4 s for stochastic pre-cooling of the momentum spread using the filter method. The radiofrequency system then trapped and moved them to the stacking region where a first stack-tail momentum cooling system took over. The injection region was now free for the next burst of antiprotons, arriving 2.4 or 4.8 s later. This sequence was repeated during the whole accumulation period of typically 24 h.

In the AC, a powerful “bunch rotation” RF system (1.5 MV, 9.5 MHz) reduced the momentum spread by turning the incoming 5 antiproton bunches into a nearly continuous beam of lesser momentum spread [6]. Stochastic cooling in all three planes then reduced the beam size and energy spread by large factors. Another RF system (3.5 kV, 1.6 MHz) re-bunched the antiprotons, for ejection and transfer into a matched bucket on the AA injection orbit. Over a day, a stack with a dense core of several 10^{11} antiprotons was accumulated.

The AA, and later the AC, had a large number of stochastic cooling systems: in total 7 in the original AA, 5 in the modified AA and 9 in the AC. As each had to be optimised for a specific task, their characteristics (including pick-up/kicker technology, bandwidth, gain and power, etc.) differed vastly.

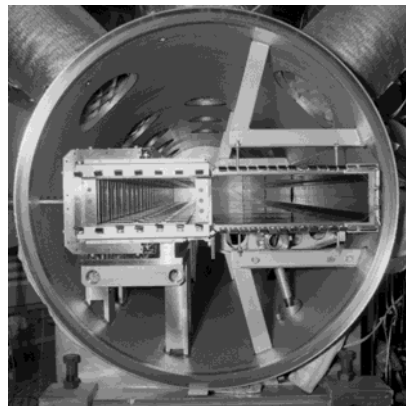


Figure 3: AA stochastic pre-cooling pickup in its tank with the fast shutters in the closed position.

The pre-cooling systems, acting on the newly injected beam (less than 10^8 pbars) and with time constants of a second, needed high-gain, high-power amplifiers. In the

AA, pre-cooling only acted on the momentum spread and the band used was 150–500 MHz using a 5 kW amplifier. For the AC, pre-cooling was applied in all three planes. Pick-ups and kickers consisted of loop couplers, with electrodes left and right, or above and below the beam. The difference signal served for transverse cooling and the sum signal for momentum cooling. The electrodes moved inwards, to follow the shrinking beam size during cooling, thus maximising pick-up sensitivity and minimising kicker power. The low-level components (pick-ups, terminations and preamplifiers) were cryogenically cooled to reduce their noise. Three bands (1–1.65, 1.65–2.4 and 2.4–3 GHz) were used, with three combined horizontal momentum and three vertical momentum systems a total of 6 pick-up tanks and 6 kicker tanks. Amplifier ratings were 4.5 kW for the lower band and 2.6 kW for each of the higher bands.

After the commissioning of the AC, simplifications in the AA cooling systems became possible. In particular, shutters on the injection kicker and on the cooling devices at the injection orbit were no longer needed. Transverse cooling was less demanding, as beams were already pre-cooled in the AC. On the other hand the higher intensity and density put greater demands on stack cooling. The performance was improved by further momentum pre-cooling on the AA injection orbit and by a powerful transverse stack-core cooling system using partly the difference signal from the momentum systems. All cooling systems of the original AA were replaced by higher frequency ones.

From 1990 onwards up to 10^{12} pbars/day could be stacked from pulses of 7×10^7 with an increase of the three-dimensional phase-space density of several 10^9 .

2.3.2.4 *Antiprotons in the Intersecting Storage Ring (ISR)*

From 1981 to 1984 the ISR facility was also included in CERN's antiproton program [7]. When operating as a p-pbar collider, a dense antiproton beam would be transferred from the AA through the CPS and along a new transfer line before injection into the ISR. The low-intensity antiproton beam in ring 2 (R2) was brought into collision with a much higher intensity proton beam in R1 for periods of up to two weeks with one single fill. The luminosity lifetime was increased with a vertical stochastic cooling system in R1 designed for currents up to 10 A ($\approx 5 \times 10^{13}$ protons) with a band of 0.85–2.5 GHz. The antiprotons in R2 were cooled vertically with a 100–600 MHz system which decreased the initial beam height by up to a factor of 7. A momentum cooling system in R2 (frequency range: 55–155 MHz) created space within the stacking aperture. This allowed several stacks from the AA to be stored in the ISR.

2.3.2.5 *The Low Energy Antiproton Ring (LEAR)*

In parallel to the proposal to collide protons and antiprotons in the SPS, Kilian et al. [8] realised in 1977 that cooling and deceleration of antiprotons would provide beams of unprecedented intensity and purity for low-energy physics. This led to the proposal to add to the antiproton project a small facility for experiments with cooled pbar beams in the energy range of 5–1200 MeV. The proposal received enthusiastic support and, in 1980, the LEAR project was launched.

The 78 m ring was housed in the South Hall of the CPS complex which also served as its experimental area. LEAR worked with a single bunch, of usually a few 10^9 antiprotons. This bunch was skimmed off the AA stack at intervals ranging from 15 min to several hours. The bunch was decelerated in the CPS to 609 MeV/c and transferred to

LEAR, where it could either be decelerated to momenta as low as 100 MeV/c (5.3 MeV kinetic energy), or accelerated, up to nominally 2000 MeV/c (1270 MeV).

Stochastic cooling in all three planes was optimised for several strategic momenta: 609 (injection), 300, 200 and 100 MeV/c, and 1000, 1500 and 1940 MeV/c on the high energy cycle. Cooling compensated the adiabatic beam growth during deceleration and counteracted various heating mechanisms, such as multiple Coulomb scattering, notably on the internal targets of the JETSET experiment. Final cooling was applied at the momentum at which the beam was delivered to the users, to provide a highly monochromatic and small-sized beam. A complex cooling system with a great number of different pick-ups and kickers and containing a plethora of switchable delays was necessary to permit cooling at all momenta.

2.3.2.6 *The Antiproton Decelerator (AD)*

By 1994 it had become evident that one could not afford for much longer the complex and costly operation for low-energy antiprotons (involving CPS, AC and AA again CPS, and LEAR). The desire of the users' community to continue the highly interesting physics with low-energy antiprotons initiated a search for a substitute facility, which would satisfy at least part of the program, such as the production of anti-hydrogen.

A scheme was studied in which the AA would be removed, the AC would be modified to be ramped from the injection momentum of 3.5 GeV/c down to 100 MeV/c, and only fast ejection of antiprotons in a single bunch of about 10^7 pbars approximately every minute would be provided [9].

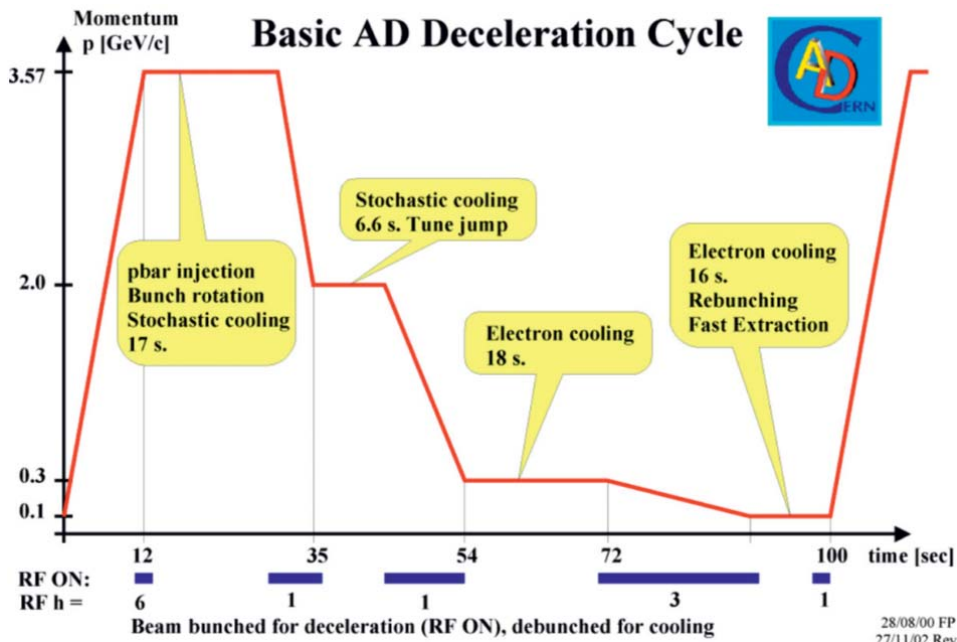


Figure 3: The AD deceleration cycle

Conversion of the AC to the AD began in 1997 and by 2000 the new machine had been commissioned and was ready to provide antiproton beams to the experiments. Apart from the magnetic aspects, it is the adiabatic increase of beam size during

deceleration that posed the greatest challenge. The beam has to be cooled, not only immediately after injection, but also on intermediate plateaus. The AC stochastic cooling system was therefore adapted for additional use at 2 GeV/c and electron cooling had to supplement it at lower energies.

A typical cycle is shown in the figure above. After injection, the antiprotons fill the acceptances and the bunch rotation system is used to reduce the momentum spread and lengthen the bunches. The beam is then de-bunched whereupon stochastic cooling in all 3 phase spaces reduces the transverse beam size and the momentum spread. This now permits deceleration to 2.0 GeV/c, where further stochastic cooling is applied, allowing the next deceleration to 300 MeV/c. Now electron cooling is called upon before the last deceleration to 100 MeV/c where final electron cooling contracts the beam to high density. The particles are then re-bunched and rotated in longitudinal phase space by RF, whilst cooling continues, to provide a bunch of only 90–200 ns length as required by the trap experiments, still with a $\Delta p/p$ of a few 10^{-4} . In this way, some 10^7 antiprotons are provided for the experiments every 90 seconds.

2.3.3 Electron Cooling

2.3.3.1 *First Experiments on ICE*

A few years after the first successful demonstration of electron cooling in 1974 on the proton storage ring NAP-M in Novosibirsk, CERN decided to build a dedicated facility, ICE (see 2.4.2.2) to study in more detail the cooling of particle beams.

Electron cooling was used to cool 46 MeV protons with a 1.3 A, 26 kV electron beam of 5 cm diameter over a cooling length of 3 m. The electron gun used a resonant optics scheme with five accelerating anodes in order to ensure that electron beam did not experience any additional transverse kicks which would be detrimental for cooling. The collector was equally elaborate, consisting of multiple shaped electrodes designed to efficiently recuperate the main beam and prevent secondary electrons escaping back towards the cooling section and the gun. The complete system was immersed in a longitudinal guiding field of 500 gauss.

Cooling effects in all three planes were observed immediately after the electron and proton beams were aligned and their velocities matched. In the first experiments, cooling was so strong that the beam was bunched longitudinally. By modifying the betatron frequencies to move the transition energy above the operating energy, the bunching effect disappeared and the best cooling was achieved.

2.3.3.2 *Electron Cooling on LEAR*

Even though stochastic cooling was retained for the Antiproton Accumulator project, the request by physicists for a program with low energy antiprotons gave a new lease of life to the ICE electron cooler.

To complement the stochastic cooling system and to improve the duty cycle of the LEAR ring, the original ICE cooler went through a number of modifications between 1981 and 1986 in order for it to be integrated in LEAR.

Operation in LEAR required a static vacuum level less than 10^{-11} torr which meant that the cooler needed a major upgrade of its vacuum system. The high gas load coming from the cathode and collector regions had made the operation on ICE very problematic and the best obtainable vacuum was in the order of 10^{-10} torr. Higher pumping speeds

and a careful choice of materials were needed if any significant reduction in the vacuum level was to be obtained. The complete vacuum envelope was re-designed and built using high quality AISI 316LN stainless steel and the whole system was designed to be bakeable at 300°C in situ for 24 hours, thus requiring permanently installed jackets providing the necessary thermal insulation. The use of NEG (non-evaporable getter) strips developed for the LEP project provided the increase in pumping speed and three such modules were initially installed on the cooler.

To fit into one of the eight metre-long straight sections, the interaction length of the cooler had to be reduced by half. Luckily the drift solenoid had been designed in two equal parts so removing one half was not a problem. The high voltage and the control systems of the device were also completely refurbished and a dedicated equipment building was erected close to the LEAR ring. The actual installation of the cooler took place during the summer of 1987 followed by the conditioning of the cathode and further tests to monitor the evolution of the LEAR vacuum in the presence of the electron beam. By the autumn of 1987 the cooler was ready to cool its first beam. The first cooling tests were made on a 50 MeV proton beam injected directly from the Linac 1 and the initial results confirmed all expectations from this device.

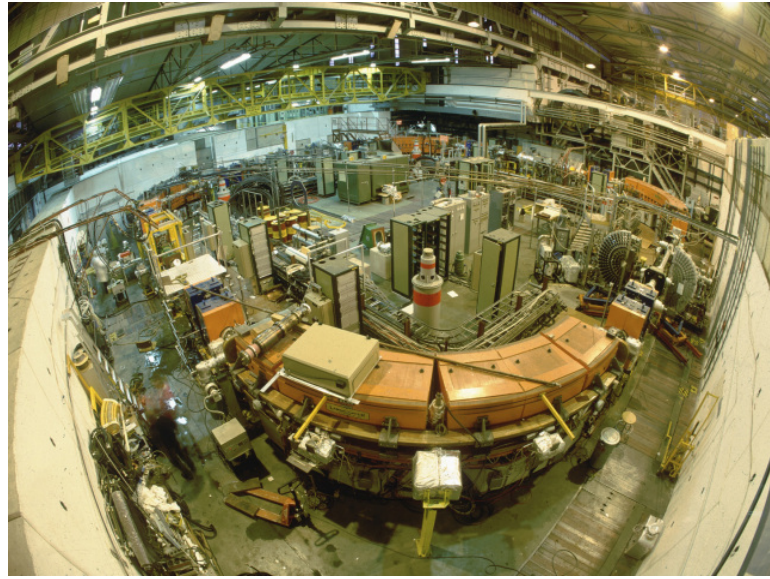


Figure 4: The LEAR ring just before its conversion to LEIR. The electron cooler can be seen on the left and the JETSET experiment to the right.

After protons the attention turned to antiprotons and the use of electron cooling for improving the duty cycle of the LEAR deceleration. Around 15 minutes would normally be necessary to obtain a “cold” beam at 100 MeV/c, the lowest momentum in LEAR. With electron cooling this duration was decreased to 5 minutes as cooling was only needed for 10 seconds on each of the intermediate plateaus compared to 5 minutes per plateau with stochastic cooling. The necessary hardware modifications needed to render the cooler operation as reliable and effective as possible included the replacement of the collector with one having a better collection efficiency (>99.99%), a new control system to synchronise the cooler power supplies with the LEAR magnetic cycle, and the implementation of a transverse feedback system (or “damper”) needed to counteract the coherent instabilities observed with such dense particle beams [10].

Another important modification to the cooler was the development, with CAPT in Lipetsk, of a variable current electron gun. The gun inherited from ICE offered little operational flexibility. The new gun was of the adiabatic type with the peculiarity that it had been designed to operate in a relatively low magnetic field, a prerequisite for its integration in LEAR. Online control of the electron beam intensity was possible by simply varying the voltage difference between the cathode and the “grid” electrode.

Apart from being the first cooler to be used routinely for accelerator operations, the apparatus was also the first to demonstrate the cooling and stacking of ions. In 1989 a machine experiment was devoted to studies on O^{6+} and O^{8+} ions coming from the Linac 1. An increase by a factor of 20 in intensity was achieved by applying electron cooling during the longitudinal stacking process. Later these ions were accelerated to an energy of 408 MeV/u and extracted to an experiment measuring the depth dose distribution in tissue equivalent types of plastic.

In a separate study, also performed in collaboration with CAPT Lipetsk, the electron beam was neutralised by accumulating positively charged ions using electrostatic traps placed at either end of the cooling section and the cooling performance was monitored. By neutralizing the electron beam space charge, the induced drift velocity of the electrons would become negligible and hence the equilibrium emittances of the ion beam further reduced. Even though a neutralisation factor of over 90% could readily be obtained, it proved to be very difficult to stabilise this very high level of neutralisation. Secondary electrons produced in the collector would be accelerated out of the collector region and oscillate back and forth between the collector and the gun. At each passage through the cooling section they would excite the trapped ions causing an abrupt de-neutralisation.

2.3.3.3 *From LEAR to LEIR*

The experienced gain with the upgraded ICE cooler on LEAR provided the stepping stones for the design of a new state-of-the-art cooler for the I-LHC project (ions for LHC). This is the first of a new generation of coolers incorporating all the recent developments in electron cooling technology (adiabatic expansion, electrostatic bend, variable density electron beam, high perveance, “pancake” solenoid structure) for the cooling and accumulation of heavy ion beams. High perveance, or intensity, is required to rapidly reduce the phase-space dimensions of a newly injected “hot” beam whilst the variable density helps to efficiently cool particles with large betatron oscillations and at the same time improve the lifetime of the cooled stack. The adiabatic expansion also enhances the cooling rate as the transverse temperature of the electron beam is reduced by a factor proportional to the ratio of the longitudinal magnetic field between the gun and the cooling section.

The cooler was built in collaboration with BINP in Novosibirsk and was commissioned at the end of 2005. It has since been routinely used to provide high brightness Pb ion beams required for the LHC ion runs. In parallel, studies have been made to determine the influence of the cooler parameters [11] (electron beam intensity, density distribution, size) on the lifetime and maximum accumulated current of the ions.

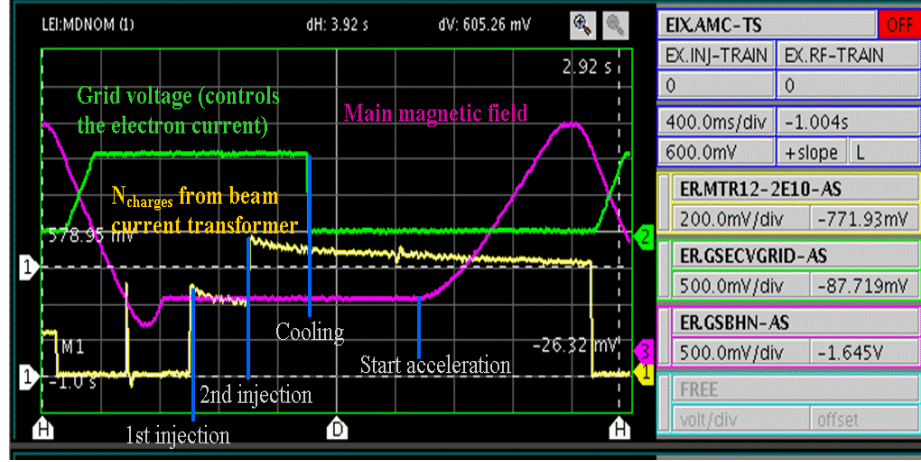


Figure 5: A standard 3.6s LEIR cycle during which 2 LINAC pulses are cooled-stacked in 800ms at an energy of 4.2 MeV/n. After bunching the Pb ions are accelerated to 72 MeV/n for extraction and transfer to the PS.

2.3.3.4 Electron Cooling on the AD

After 10 years on LEAR, the cooler was moved to the AD [9] in 1998 where it continues to provide cold antiprotons for the trap experiments in their quest to produce large quantities of antimatter. A novel deceleration technique using electron cooling was attempted at the AD where the cooler and the main magnetic field of the AD are ramped simultaneously to a lower energy plateau. In so doing the antiproton beam is kept cold throughout the deceleration process avoiding the adiabatic blow-up that all beams experience when their energy is reduced. The first tests were very modest decelerating 3.5×10^7 antiprotons from 46.5 MeV to 43.4 MeV whilst keeping the transverse emittances below $1 \pi \text{ mm mrad}$ during the whole deceleration. Experiments to go below 5.3 MeV have been made with the beam successfully decelerated to 4.8 MeV (95.37 MeV/c) in 33 seconds as expected from the measurements made in 2008. The control of the closed orbit, and more specifically the alignment of the antiproton beam with the electrons, proved to be more delicate than expected and hindered the progression of the experiments.

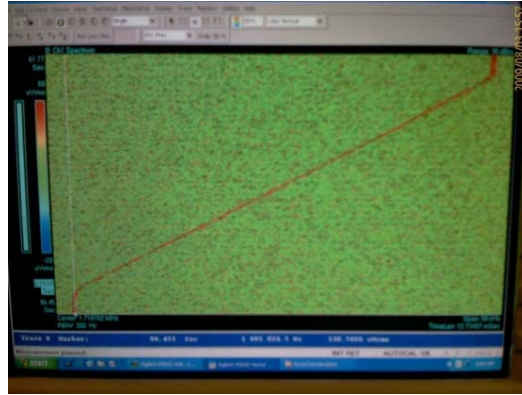


Figure 6: Longitudinal Schootky signal showing the deceleration of antiprotons from 5.3 MeV to 4.8 MeV in the AD using the technique of “ecool deceleration”.

After more than 30 years' of service and two reincarnations, it is planned to replace the AD electron cooler with a more modern device [12]. The new cooler will benefit from recent advances in cooler design and will be able to cool antiprotons at a higher energy in order to cool the antiprotons on an intermediate plateau between 2 GeV/c and 300 MeV/c.

2.3.3.5 *ELENA, the Extra Low Energy Antiproton Ring*

Deceleration of antiprotons in the AD goes a long way towards the needs of the experimenters, but the 5.3 MeV energy of the extracted beam is still far above what the experiments, accumulating antiprotons in stationary traps, require. The further deceleration in a degrader foil, still in use for two of the AD experiments, is accompanied by a big loss of density.

ELENA is a 30 m circumference ring for cooling and further deceleration of the 5.3 MeV antiprotons delivered by the AD down to 100 keV [13]. By deceleration using a ring equipped with beam cooling, an important increase in phase-space density and a high experiment injection efficiency can be obtained, resulting in an increased number of trapped antiprotons. With the construction of the ELENA ring, the AD experiments expect improvements of up to two orders of magnitude. In addition, ELENA will be able to deliver beams almost simultaneously to up to four experiments resulting in an essential gain in total beam time for each experiment.

The antiprotons will be decelerated in ELENA in two stages: first to a momentum of 35 MeV/c (corresponding to a kinetic energy of 650 keV) and then to 13.7 MeV/c (corresponding to a kinetic energy of 100 keV). Electron cooling will be essential at these two momenta in order to obtain the small emittance beams needed for either further deceleration or extraction to the experiments.

The electron cooler will be installed in one of the six straight sections of ELENA [14]. The rest of this section will accommodate the orbit correctors and compensation solenoids of the cooler.

An electron gun will produce a cold ($T_{\perp} < 0.1$ eV, $T_{\parallel} < 1$ meV) and relatively intense electron beam ($n_e \approx 3 \times 10^{12}$ m⁻³). The use of a photocathode cannot be considered as it is complicated to operate and has a short lifetime. Instead a conventional thermionic cathode will be used and the electrodes will be designed to minimize the transverse temperature after acceleration to the desired energy. For nominal operation the electron gun is immersed in a longitudinal field of 1000 gauss which is adiabatically reduced to 100 gauss in the transition between the expansion solenoid and the gun solenoid. In this manner the transverse temperature is reduced further through an adiabatic beam expansion. The lower field in the toroids and cooling section also minimizes the perturbations (closed orbit distortion and coupling) induced by the electron cooler to the circulating antiprotons. After the gun, the electrons are bent by 90° in a toroid and merged with the circulating antiprotons over a distance of 1 m in the drift solenoid. At the exit of this cooling section, the electrons are bent away from the antiprotons by a second 90° toroid and are dumped in a collector.

A crucial point of the design of the electron cooler is the quality of the longitudinal magnetic field guiding the electrons from the gun to the collector and in particular the quality of the magnetic field in the interaction region of the drift solenoid. The transverse components of the longitudinal field in the drift solenoid must be kept small ($B_{\perp}/B_{\parallel} < 5 \times 10^{-4}$ at 100 gauss) to ensure a minimal perturbation to the electron beam transverse temperature.

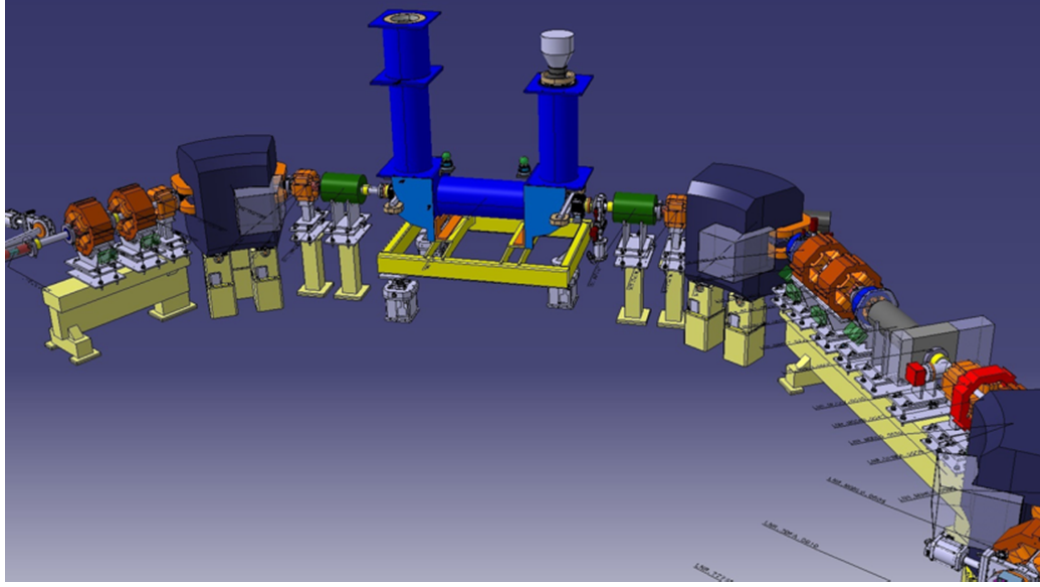


Figure 7: The ELENA electron cooler integrated in straight section 4 of the ring.

Table 1: Selected parameters for the ELENA electron cooler for nominal operation.

momentum	MeV/c	35	13.7
relativistic β		0.037	0.015
electron beam energy	eV	355	55
electron beam current	mA	10	2
electron beam density, n_e	m^{-3}	2.8×10^{12}	1.4×10^{12}
magnetic field at gun	gauss	1000	
magnetic field in cooling section	gauss	100	
expansion factor		10	
cathode radius	mm	8	
electron beam radius	mm	25	

2.3.4 References

1. S. van der Meer, "Stochastic Damping of Betatron Oscillations", CERN ISR-PO 72/31 1972.
2. C. Rubbia, P. McIntyre, "Producing Massive Neutral Intermediate Vector Bosons with Existing Accelerators", Proc. Int. Neutrino Conf., Aachen (1976).
3. G. Carron, L. Thorndahl, "Stochastic Cooling of Momentum Spread with Filter Techniques", CERN/ISR-RF/78-12 and ISR-RF/Note LT/ps.
4. S. van der Meer, "Stochastic Stacking in the Antiproton Accumulator", CERN/PS-AA 78-22.
5. "Design Study of a Proton Antiproton Collider Facility", CERN/PS-AA 78-3
6. "Design Study of an Antiproton Collector for the Antiproton Accumulator", edited by E.J.N. Willson, CERN Yellow Report 83-10.
7. E. Peschardt, M. Studer, "Stochastic Cooling in the ISR During p-pbar Colliding Beam Physics", Proc. PAC 1983, IEEE Trans. Nucl. Sci. NS-30, 2584 (1982).
8. K. Kilian et al., "Deceleration of Antiprotons for Physics Experiments at Low Energy: a Low Energy Antiproton Factory", CERN/PS/DL 77-19.

9. S. Maury et al., "Design Study of the Antiproton Decelerator AD", CERN-PS 96-42(AR).
10. J. Bosser et al., "Operational Aspects of Electron Cooling in LEAR", Proc. 14th IEEE Particle Accelerator Conference, San Francisco (1991).
11. G. Tranquille, "Electron Cooling Experiments at LEIR", Proc. 11th European Particle Accelerator Conference, Genoa (2008).
12. T. Eriksson et al., "AD Status and Consolidation Plans", International Workshop on Beam Cooling and Related Topics, Murren (2013).
13. W. Bartmann et al., "Extra Low Energy Antiproton ring ELENA: from the Conception to the Implementation Phase", CERN-ACC-2014-0144.
14. G. Tranquille et al., "The ELENA Electron Cooler: Parameter Choice and Expected Performance", International Workshop on Beam Cooling and Related Topics, Murren (2013).

2.4 Development of Electron Coolers in Novosibirsk

V.V. Parkhomchuk and V.B. Reva, BINP, Novosibirsk, Russia
 Mail to: V.V.Parkhomchuk@inp.nsk.su

2.4.1 Introduction

An electron cooling method was proposed by G. Budker almost 50 years ago. Since the first demonstrations of strong cooling in 1972, electron cooling has became important in advancing elementary particle and nuclear physics and even for atomic physics. Novosibirsk Institute of Nuclear Physics has continued to develop this technique for various machines with different energy of electron beams. BINP produces the electron cooler for following storage rings: SIS-18 (Germany), CSRm, CSRe (China), LEIR (CERN), COSY (Germany). In the present time BINP team designs the electron cooler for FAIR project with energy 4-8 MeV.

2.4.2 First Electron Cooler at NAP-M Storage Ring

The first electron cooler have all features of design that was named classical design. An electron gun was put into a solenoid producing the longitudinal magnetic field. The magnetic field guides the electron beam from the gun to the collector [1]. The longitudinal magnetic field enabled to transport an electron beam to a long distance (a few meters) without degradation of the beam quality. The focusing by the longitudinal magnetic field preserves degradation of electron beam parameters. Sections with a toroidal magnetic field were used for merging the proton and electron beams. For compensation of centrifugal drift the horizontal magnetic field was used. After the cooling section, the electron beam was decelerated and absorbed by the electron collector. In order to provide high vacuum, ion pumps were installed in all accessible places. These first experiments with electron cooling carried out in Novosibirsk in 1974 have demonstrated the possibility of obtaining high cooling rates and low equilibrium temperatures[1,2].

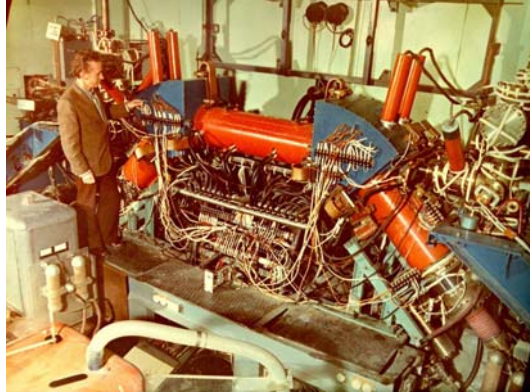


Figure 1: First electron cooling installation in the NAP-M storage ring.

2.4.3 Test Bench for Magnetized Cooling (MOSOL)

The high rate of cooling process at NAP-M stimulated to design a test bench with high magnet field in cooling section. Solenoid with magnetic field up to 4 kG and Van-De-Graff electrostatic accelerator with 1 MeV ion beam was used for verification of model of magnetized electron cooling. The electron beam with energy 500 eV was generated directly inside solenoid. Figure 3 shows cooling force [2] measured by A. Sery. One can see (Fig.2) that the optimal electron current and the electron friction force increase with growth of the value of the magnetic field. These results proved that obtaining of maximal high cooling is possible with high magnetic field. At next cooler BINP team try to use the maximal magnetized electron beam for the electron cooling.

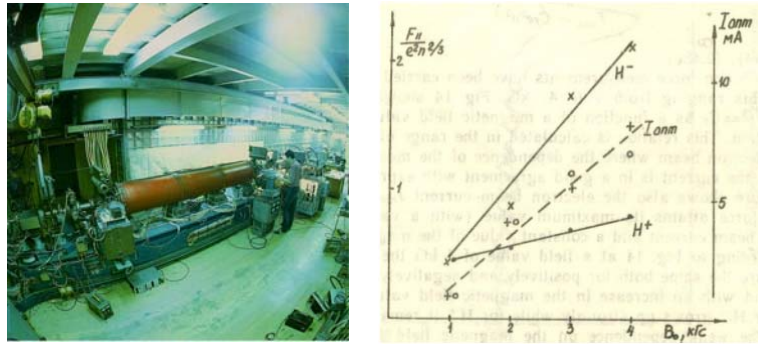


Figure 2: Test bench for direct measuring cooling force (left picture) and cooling force for H^+ and H^- versus magnet field at cooling section (right picture).

2.4.4 SIS-18 Cooler

At 1998 the new cooler for GSI synchrotron SIS-18 was designed and produced at BINP (see Fig.3). The cooling rate increases for highly charged ions and it is attractive for fast beam accumulation especially for rear ions that can not produced with high intensity at ion source. The design of this cooler had aim to made cooler for existing synchrotron SIS-18. Requirement for the cooler was high level reliability for cooler operation during long life-time (about 20 years). For obtain high cooling rate the straightness of magnet lines at cooling section should be as high as possible. The pancake coils for cooling section with the individual spacers for the adjust position of

coils was used at this cooler. The length of all spacers was calculated after magnetic line measurements. High efficiency beam accumulation was demonstrated SIS-18 cooler [3]. But the high intensity and high brightness of cooled ion beams open possibility to development of an instability. The experiments with ion beams at CELSIUS and SIS-18 show that the increase of electron beam density leads to problems interaction of the high dense of ion beam with electrons. As results the idea of decreasing the electron beam density at centre of beam was proposed. The high density of the electron beam at zone of fresh injected ion beam provides high cooling rate but the centre of the electron beam (where the density ion beam is high) doesn't provide overcooling. For realization of this idea a new electron gun with variable electron beam profile was designed [4]. This electron gun enables to optimise the cooling rate across the radius of the ion beam.



Figure 3: Electron cooler for SIS-18.

2.4.5 CSRm and CSRe Coolers

China Institute of Modern Physics at Lanzhou started the physics program of the investigation of ion beam at the end of XX century. The CSR team decided to use the electron cooling for accumulation of the ion at injection energy (CSRm ring) and experiment energy (CSRe ring). The BINP team designed two coolers on 30 kV CSRm and 300 kV CSRe [5]. The new features of these coolers were variable profile of electron beam [4] and the electrostatic bending for decreasing losses of electron current to vacuum chamber. Minimization of desorption coefficient helps to improve the vacuum condition that is extremely important for obtaining long life time of the high charge ions beam.

The electron gun with special electrode for changing profile demonstrated good performance for modification profile of electron beam. The profile was changed from narrow parabolic shape to hollow electron beam with almost empty central part (see fig. 4). The CSRe (300kV) cooler was equipped the special high voltage generator installing at vessel with SF₆ gas isolation. The connections of high voltage terminal to the electron gun cathode and collector was made with the concentric transmission line filled SF₆ (see fig. 5). The electron cooling rate was sufficient high for repetition injection with period 0.5 second for ion C⁺⁶ with energy 7 MeV/u. Figure 4 shows an example of cycle accumulation and acceleration beam up to 600 M/u.

Successfully using the high quality beams of carbon ions for the hadrons therapy at IMP stimulated BINP team on development the special synchrotron with electron cooling system for cancer therapy [6].

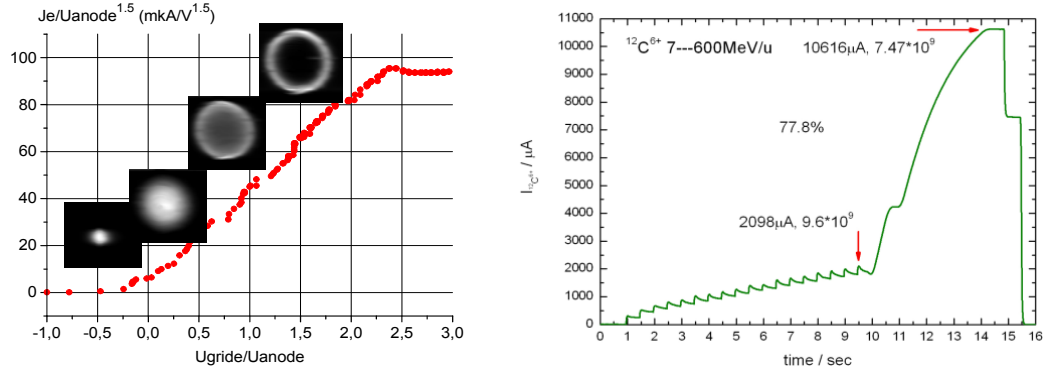


Figure 4: Beam profile and permeance of electron gun with variable profile (left picture). CSRm accumulation of carbon beam and acceleration to energy 600 MeV/u (right picture).



Figure 5: CSRe cooler after finishing commissioning at BINP.

2.4.6 LEIR Cooler

The low energy cooler for LEIR [7] (see fig. 6) was designed after commissioning CSRm and CSRe coolers and its design contains main features of CSR coolers: electrostatic bending, electron gun with variable profile and adjusting of pancake coils in vertical and horizontal directions for good magnet lines straightness. Additional improvement of vacuum condition was made with NEG pumping technology. The NEG cassettes were installed near gun and collector and NEG coating of the vacuum chamber was made on the surface of the cooling section. The good vacuum was very critical point for using cooler with Pb^{+54} ions. The ions have high cross-section of electron capture from the atoms of residual gas. Figure 7 shows the variation of horizontal profile of Pb ions beam during injection process, electron cooling and acceleration of ion beam. At top side of figure the profile of electron beam is shown (red curve) that was used at these experiments. One can see shrinking the ion beam with electron cooling. After second injection and switching off electron current the size of the ion beam increases due to IBS effect. In finish the size of the ion beam decreases because of adiabatic “cooling” at acceleration. The electron cooling at LEIR help to prepare good bunches for operation LHC at ion*ion collision.



Figure 6: LEIR cooler in CERN.

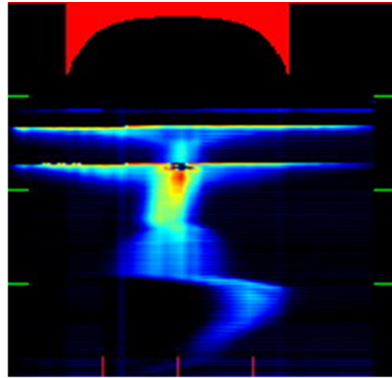


Figure 7: LEIR cycle- two pulse of injection with electron cooling and them acceleration.

2.4.7 COSY Cooler

The electron cooler of a 2 MEV for COSY [8] storage ring was constructed and manufactured in BINP (see Fig.8). The electron cooler is designed on the classic scheme of low energy coolers like cooler CSRe, LEIR that was produced in BINP before. The electron beam is transported inside the longitudinal magnetic field along whole trajectory from an electron gun to a collector. This optic scheme is stimulated by the wide range of the working energies 0.1(0.025)-2 MeV. The electrostatic accelerator consists of 34 individual unify section. Each section contains two HV power supply (plus/minus 30 kV) and power supply of the magnetic coils. The electrical power to each section is provided by the cascade transformer. The cascade transformer is the set of the transformer connected in series with isolating winding. The high voltage testing was made up to 1.5 MV voltage and the electron beam transport line with electron beam was tuned for different energy.

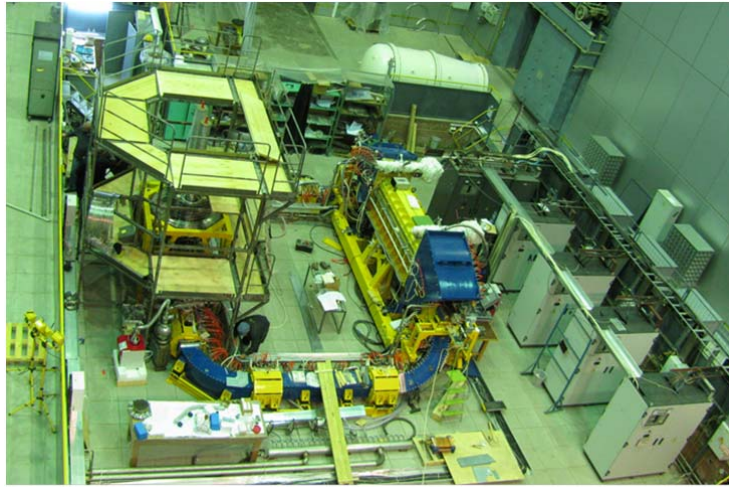


Figure 8: COSY cooler under commissioning at BINP.

The collector of this cooler consists of the usual collector and special filter. The filter contains the crossing magnetic and electric fields for suppressing back moving electron beam. The efficiency of the pure collector is near $3 \cdot 10^{-3}$. The filter adds the suppression of the secondary electron flux with factor about 100. So, the result efficiency of collector is about $3 \cdot 10^{-5}$. The radiation level near cooler is 0.01 Sv/hour at 1 MV and 0.2 mA electron beam.

The first electron cooling experiments was done with electron energy 109 kV and the proton energy 200 MeV. The longitudinal magnetic field in the cooling section was 530 G. The choice of such energy is avoidance of the problem with electron beam tracing. Such electron energy is small enough for the strong adiabatic motion of the electron along its trajectory, but the proton beam life is higher as compared with the injection energy. Observing of the electron cooling effects is easy at small value of the electron friction force when all parameters are not in optimum. After obtaining first cooling the adjustment of the electron cooling process is easy process.

Figure 9 shows the parameters of the proton beam versus time. One can see that the sizes of the proton beam decrease from 5÷7 mm to 1 mm. The losses of the proton beam are small enough.

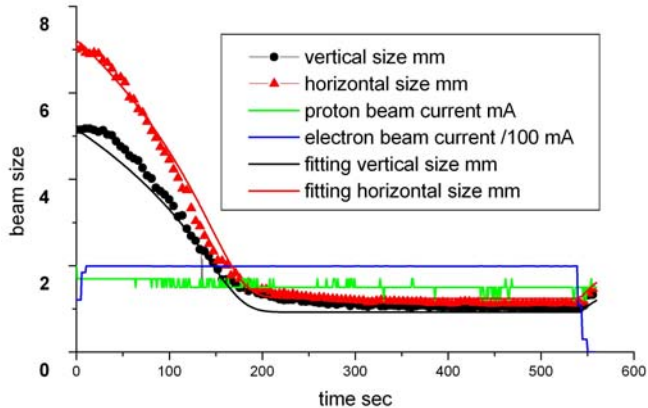


Figure 9: Parameters of the proton beam versus time during the electron cooling process

The storage ring COSY is equipped by the system of the stochastic cooling. In time of the electron cooling experiments the stochastic system was tuned on the energy corresponding to the energy of the electron beam 908 kV and it was operated in the vertical direction only. The experiment with joint action of the different cooling systems was done at this energy. Figure 10 shows the dynamics of the proton beam in machine cycle with action of both cooling systems. In first moment the stochastic cooling was used only. In the middle of cycle the electron cooling was added. The rate of the cooling in the transverse direction became higher.

The experiments with joint action of the electron and stochastic cooling is very important because the stochastic cooling is very effective at large amplitude of the betatron oscillation, but the electron cooling is effective at small betatron amplitudes.

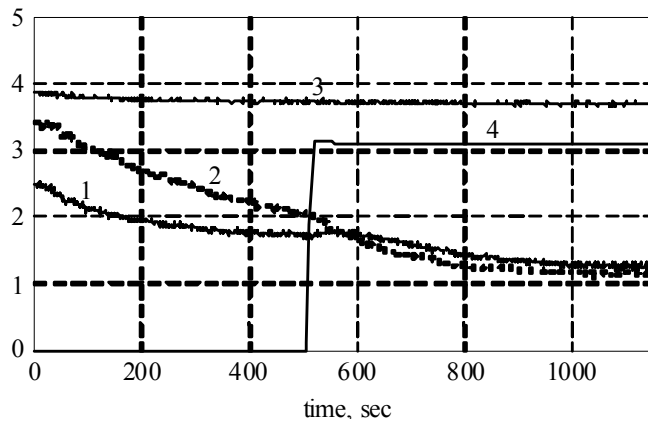


Figure 10: Parameters of the proton beam versus time. The electron energy is 908 kV. The vertical size is 1, the horizontal size is 2, the proton current is 3 (in unit 100 uA), the electron current is 4 (in unit 100 mA).

2.4.8 References

1. G.I. Budker, N.S. Dikansky, V.I. Kudelainen, I.N. Meshkov, V.V. Parkhomchuk, A.N. Skrinsky, B.N. Sukhina, First experiments on electron cooling, IEEE Trans. Nucl. Sci. 22, 2003-7, 1975.
2. Parkhomchuk V.V., Skrinsky A.N., Electron cooling: physics and prospective applications, Rep. Prog. Phys. 54 (1991), p.919-947.
3. M.Steck, L.Groening, K.Blahe, B.Franczak, B. Frannzke, T.Winkler, V.V.Parkhomchuk, Beam accumulation with the SIS electron cooler, NIM in Phys. Res. A441 (2000) p. 175-182.
4. A.V. Ivanov, A.V. Buble, A.D. Goncharov, E.S. Konstantinov, S.G. Konstantinov, A.M. Kryuchkov, V.M. Panasyuk, V.V. Parkhomchuk, V.B. Reva, B.A. Skarbo, B.M. Smirnov, B.N. Sukhina, M.A. Tiunov, M.N. Zakhvatkin, BINP, Novosibirsk; X.D. Yang, IMP, Lanzhou The Electron Gun with Variable Beam Profile for Optimization of Electron Cooling. Proceeding of EPAC 2002, Paris, France, p.1357 - 1358.
5. XiaoDong Yang Electron cooling performance of at IMP facility, COOL11 report, Alushta, Ukraine,
6. V.Vostrikov, B.Grishanov, Vasily V.Parkhomchuk, S.Rastigeev, V.Reva (BINP SB RAS, Novosibirsk), Masayuki Kumada (NIRS, Chiba-shi). Electron Cooling for Cold Beam Synchrotron for Cancer Therapy. Proceedings of COOL 05, FNAL, USA, September 18-23, 2005, p.365-369.

7. A.Bublej, V.Bocharov, M.Brizgunov, V. Ershov, A.Goncharov, S.Konstantinov, A.Lomakin, V.Panasyuk, V. Parkhomchuk, V. Polukhin, V.Reva, B.Skarbo, B.Sukhina, M.Vedenev, M.Zakhvatkin, N.Zapiatkin. First test of the LEIR-cooler at BINP. Proceedings of COOL 05, FNAL, USA, September 18-23, 2005, AIP Conf. Proc 821, March 2006, p.355-359. COSY
8. V. Kamerdzhev, U. Bechstedt, F.M. Esser, O. Felden, R. Gebel, A.J. Halama, F. Klehr, G. Langenberg, A. Lehrach, B. Lorentz, R. Maier, D. Prasuhn, K. Reimers, M. Retzlaff, R. Stassen, H. Stockhorst, R. Tölle (FZJ, Jülich, Germany), N. Alinovskiy, T.V. Bedareva, E.A. Bekhtenev, O.V. Belikov, V.N. Bocharov, V.V. Borodich, M.I. Bryzgunov, A.V. Bublej, V.A. Chekavinskiy, V.G. Cheskivod, B.A. Dovzhenko, A.I. Erokhin, M.G. Fedotov, A.D. Goncharov, K. Gorchakov, V.K. Gosteev, I.A. Gusev, G.V. Karpov, Y.I. Koisin, M.N. Kondaurov, V.R. Kozak, A.M. Kruchkov, A.D. Lisitsyn, I.A. Lopatkin, V.R. Mamkin, A.S. Medvedko, V.M. Panasyuk, V.V. Parkhomchuk, I.V. Poletaev, V.A. Polukhin, A.Yu. Protopopov, D.N. Pureskin, A.A. Putmakov, V.B. Reva, P.A. Selivanov, E.P. Semenov, D.V. Senkov, D.N. Skorobogatov, N.P. Zapiatkin (BINP SB RAS, Novosibirsk, Russia) J. Dietrich (HIM, Mainz, Germany) T. Katayama (Nihon University, Narashino, Chiba, Japan) L.J. Mao (IMP, Lanzhou, People's Republic of China). "2 MeV Electron Cooler for COSY and HESR – First Results" Proceedings of IPAC 2014 (5th International Particle Accelerator Conference), Dresden, Germany, June 15-20 2014, MOPRI070, p. 765-767.

2.5 Fermilab's 4.3-MeV Electron Cooler

Sergei Nagaitsev, Lionel Prost, and Alexander Shemyakin
 Fermilab, Batavia, IL 60510, USA
 Mail to: shemyakin@fnal.gov

2.5.1 Introduction

The antiproton source for a proton-antiproton collider at Fermilab was proposed in 1976 [1]. The proposal argued that the requisite luminosity ($\sim 10^{29} \text{ cm}^{-2}\text{s}^{-1}$) could be achieved with a facility that would produce and cool approximately 10^{11} antiprotons per day. At the end of its operation in 2011, the Fermilab antiproton production complex consisted of a sophisticated target system, three 8-GeV storage rings (namely the Debuncher, Accumulator and Recycler), 25 independent multi-GHz stochastic cooling systems and the world's only relativistic electron cooling system. Sustained accumulation of antiprotons was possible at the rate of greater than 2.5×10^{11} per hour.

The production of antiprotons started with a 120 GeV proton beam from the Main Injector striking an Inconel target every 2-3 seconds. From all the particles thus created, 8.9-GeV/c antiprotons were collected in the Debuncher and stored in the Accumulator (the process known as stacking). The Recycler [2] is a permanent-magnet, fixed momentum (8.9 GeV/c) storage ring located in the Main Injector tunnel. As conceived, the Recycler would provide storage for very large numbers of antiprotons (up to 6×10^{12}) and would increase the effective production rate by recapturing unused antiprotons at the end of collider stores (hence the name Recycler). Recycling of antiprotons was determined to be ineffective and was never implemented. However, the Recycler was used as a final antiproton cooling and storage ring. The Accumulator antiproton stack was periodically transferred to the Recycler where electron cooling allowed for a much larger antiproton intensity to be accumulated with smaller emittances. Typically 22-

25×10^{10} antiprotons were transferred to the Recycler every ~ 60 minutes. Prior to electron cooling in the Recycler, antiprotons destined for the Tevatron were extracted from the Accumulator only. Since late 2005, all Tevatron antiprotons were extracted from the Recycler only. Figure 1 illustrates the flow of antiprotons between the Accumulator, Recycler and Tevatron over a one-week period.

The Recycler had a number of stochastic cooling systems in operation from day one; the electron cooling system was envisioned as an upgrade [2] to complement the stochastic cooling system (in particular the longitudinal one because of the longitudinal injection scheme in the Recycler) and was placed into operation within days of its first successful demonstration in July 2005 [3]. Electron cooling in the Recycler directly allowed for significant improvements in Tevatron luminosity. With it, the Recycler has been able to store up to 6×10^{12} antiprotons. In routine operations, the Recycler accumulated $3.5\text{--}4.0 \times 10^{12}$ antiprotons with a $\sim 200\text{-hr}$ lifetime before injection into the Tevatron [4].

In this paper we will describe the electron cooling system installed in the Recycler, its physics principles, and the electron cooling measurements.

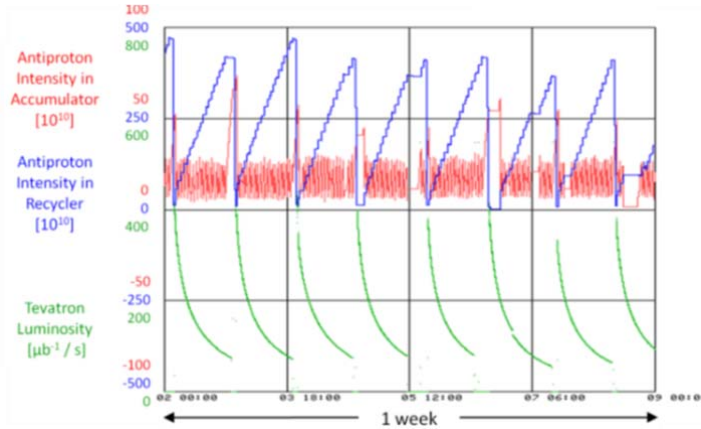


Figure 1: Production and transfers of antiprotons between the Accumulator and Recycler over a period of one week. While the Tevatron had a colliding beam store, small stacks of antiprotons were produced and stored in the Accumulator, and then periodically transferred to the Recycler in preparation for the subsequent Tevatron fill.

2.5.2 Recycler Electron Cooling (REC) System

Electron cooling is a method of increasing the phase-space density of “hot” heavy charged particles, ions or antiprotons, through Coulomb interactions with a “cold” electron beam, co-propagating with the same average speed in a small section of the ring. The method was proposed by G. Budker in 1967 [5], successfully tested in 1974 with low-energy protons [6], and later implemented at a dozen of storage rings (see, for example, a review [7]) at non-relativistic electron energies, $E_e < 300$ keV.

Figure 2 shows the schematic layout of the Fermilab electron cooling system. The Pelletron (an electrostatic accelerator manufactured by the National Electrostatics Corp.) provided a 4.3 MeV (kinetic) electron beam (up to 500 mA, DC) which overlapped the 8-GeV antiprotons circulating in the Recycler in a 20-m long section and cooled the antiprotons both transversely and longitudinally. The dc electron beam was generated by a thermionic gun, located in the high-voltage terminal of the electrostatic

accelerator. This accelerator was incapable of sustaining dc beam currents to ground in excess of about 100 μA . Hence, to attain the electron dc current of 500 mA, a recirculation scheme was employed, in which the electron beam that has interacted with the antiprotons is decelerated to 3.5 keV and accepted into the collector, located in the high-voltage terminal of the Pelletron. The typical relative beam current loss in the system was 2×10^{-5} [8].

The Fermilab cooler employed a unique beam transport scheme [9]. The electron gun was immersed in a solenoidal magnetic field, which created a beam with large angular momentum. After the beam was extracted from the magnetic field and accelerated to 4.3 MeV, it was transported to the 20-m long cooling section solenoid using lumped focusing elements (as opposed to low-energy electron coolers where the beam remains immersed in a strong magnetic field at all times). The cooling section solenoid removed this angular momentum, and the beam was made round and parallel such that the beam radius, a , resulted in the same magnetic flux, Ba^2 , as at the cathode. The magnetic field in the cooling section was low, ~ 100 G, therefore the kinetics of the electron-antiproton scattering was weakly affected by the magnetic field.

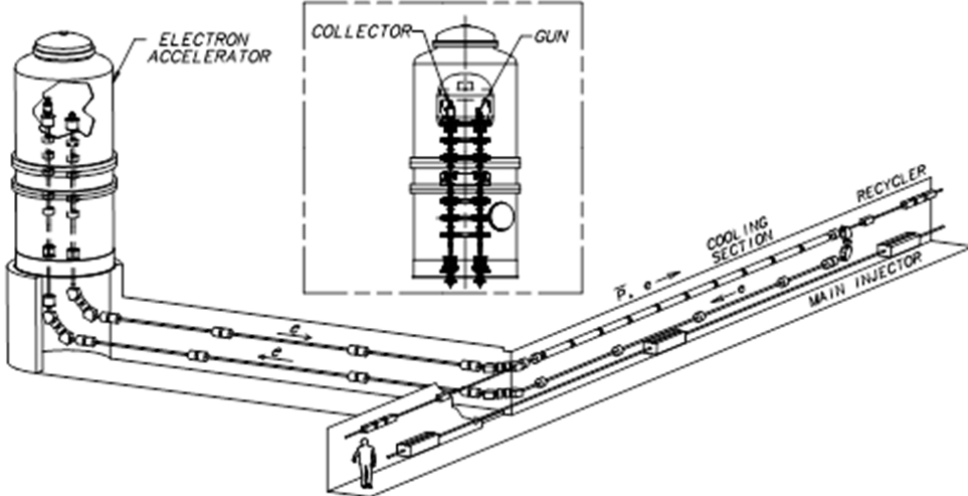


Figure 2: Schematic layout of the Recycler electron cooling system and the accelerator cross-section (inset).

2.5.3 Electron Cooling Formulae

A heavy charged particle moving in a free electron gas with a velocity distribution $f_e(\vec{v}_e)$ experiences a friction force that in a model of binary collisions can be written following Ref. [6]:

$$\overline{F}_b(\overline{V}_p) = -\frac{4\pi e^4 n_{eb}}{m_e} \eta \int L_c \frac{f_e(\vec{v}_e)}{(\overline{V}_p - \vec{v}_e)^2} \frac{\overline{V}_p - \vec{v}_e}{|\overline{V}_p - \vec{v}_e|} d^3 v_e, \quad (1)$$

where n_{eb} is the electron density in the beam rest frame, m_e the electron mass, e the elementary charge, \overline{V}_p the velocity of the heavy particle, and $\eta = L_{cs}/C$ indicates the portion of the ring circumference C occupied by the cooling section of length L_{cs} , L_c is the Coulomb logarithm

$$L_C = \ln\left(\frac{\rho_{\max}}{\rho_{\min}}\right) \quad (2)$$

with the minimum and maximum impact parameters, ρ_{\min} and ρ_{\max} , in the Coulomb logarithm defined as

$$\rho_{\min} = \frac{e^2}{m_e (\vec{V}_p - \vec{v}_e)^2}, \quad \rho_{\max} = \min\left\{R_D, R_e, |\vec{V}_p - \vec{v}_e| \cdot \tau_f\right\}. \quad (3)$$

The maximum impact parameter is determined by the electron beam radius R_e , (typically the case in the Fermilab cooler), the Debye radius R_D , or the relative displacement of the particles during the flight time through the cooling section $\tau_f = L_{cs}/\gamma\beta c$, where γ and β are the relativistic factors of co-propagating particles in the lab frame, whichever is the smallest. In this paper, the electron velocity distribution is assumed to be Gaussian in each plane. Note that if the variations of the Coulomb logarithm in the integrand of Eq. (1) can be neglected, L_c can be taken out of the integral and instantaneous cooling rates of an antiproton beam with a Gaussian velocity distribution can be expressed with elementary functions [8].

2.5.4 Cooling Measurements

Analysis of the cooling properties of the electron beam was made primarily with ‘drag rate’ measurements obtained via a voltage jump method similar to the one used in the early age of electron cooling [10]: a “pencil” coasting antiproton beam is cooled to an equilibrium; then, the electron energy is changed by a jump, and the rate of change of the mean value of the antiprotons momentum distribution is recorded while the antiprotons are dragged toward the new equilibrium. If the momentum spread remains small in comparison with the difference between the two equilibria, this ‘drag rate’ is equal to the longitudinal *cooling* force. Results of the drag force as a function of the voltage jump amplitude (expressed in units of the antiproton momentum offset) are presented in Fig. 3. For these data, the electron and antiproton beams are concentric and collinear, which was defined as the electron beam being ‘on-axis’.

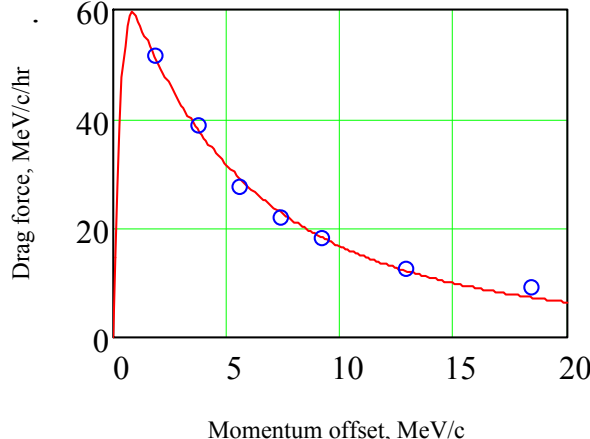


Figure 3: Drag rate on-axis as a function of momentum offset. Electron beam current $I_e = 0.1\text{A}$. The circles are data, and the solid line is a calculation using Eq.(1) with the rms electron angle of $\theta_e = 80 \mu\text{rad}$ and energy spread of $\delta W_e = 200\text{eV}$, $L_c = 9$.

For the case of the Fermilab cooler, the main contribution to the cooling force comes from collisions with low impact parameters. Therefore, the drag rate depends primarily on the electron beam properties in the vicinity of the probing antiproton beam. In turn, information about the transverse distribution of the electron density and angles can be obtained with drag rate data taken at several spatial offsets (parallel shifts) between the two beams in the cooling section. Fig. 4 shows an example of such measurements along with a fit to a simplified formulation of the drag rate as a function of the transverse distance between the two beams (or equivalently, the radius of the electron beam) written as

$$F_z(x) = F_0(\Delta p_p) \cdot \begin{cases} 1 - \left(\frac{x}{a_e} \right)^2 & x \leq a_e, \\ \frac{1 - \left(\frac{x}{a_e} \right)^2}{1 + \left(\frac{x}{b} \right)^2} & x > a_e \end{cases} \quad (4)$$

where a_e is the electron beam radius and F_0 , the maximum drag rate (by definition at the center of the electron beam current density transverse distribution) for a given momentum offset. In the fraction, the numerator approximates the electron current density profile determined from electron gun simulations, while in the denominator, b describes an increase of the electron angles with the radial offset. For such a profile, the finite size of the probe antiproton beam results in a decrease of the measured drag rate in comparison with the cooling force experienced by the antiprotons at the center. The red curve on Figure 4 shows the corresponding correction.

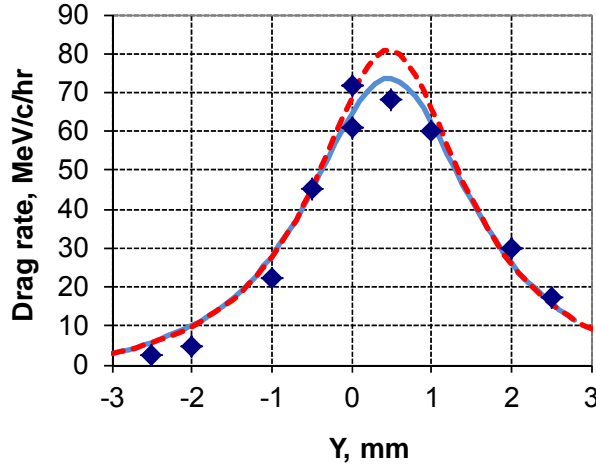


Figure 4: Drag rate as a function of the electron beam offset with respect to the co-propagating antiprotons. The voltage jump was 2 kV, $I_e = 0.3$ A, number of antiprotons $N_p = 1.3 \cdot 10^{10}$. The blue curve is the best fit to the model described with $a_e = 4.3$ mm, and fitting parameters $F_0 = 80$ MeV/c/hr and $b = 1.2$ mm. During the measurement, the rms size of the antiproton beam was estimated to be ~ 0.25 mm. The red dashed curve shows the fitted cooling force after correcting for the finite size of the antiproton beam.

If the electron angles remain the same, the cooling force should increase proportionally to the current density. Drag rates measured at different beam currents during the entire span of the cooler's operation are shown in Fig. 5 together with the simulated current density at the beam center.

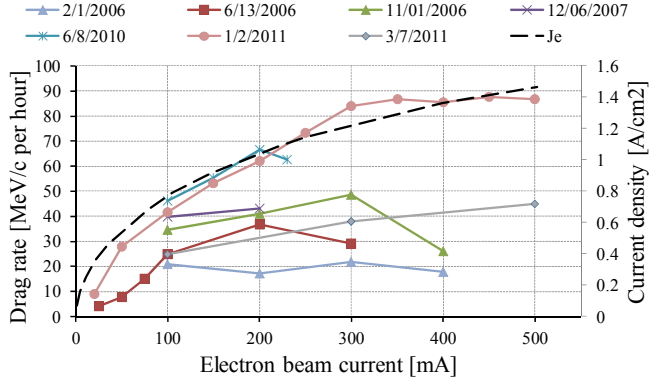


Figure 5: Drag rate measured on axis as a function of the beam current at various dates with a 2 kV voltage jump. The current density calculated at the beam center (dashed curve) is shown for comparison.

The large scatter in the measured drag rates is related to important variations of the electron angles in the cooling section. Until the end of the collider operation, significant efforts were devoted to understanding what determined these angles and how they could be reduced. Best estimates of the various contributions to the total rms electron angle are presented in Table 1.

Table 1: Contributions to the total electron angle in the cooling section. Shown values are 1D, rms, obtained from averaging the angles over the cross section of a 0.1A beam in the best scenario.

Effect	Angle, μrad	Method of evaluation
Thermal velocities	57	Calculated from the cathode temperature
Envelope mismatch	~ 50	Resolution of tuning + optics simulations
Dipole motion (above 0.1 Hz)	~ 35	Spectra of BPMs in the cooling section
Dipole motion caused by field imperfections	~ 50	Simulation of electron trajectory in the measured magnetic field
Non-linearity of lenses	~ 20	Trajectory response measurements
Ion background	< 10	Cooling measurements
Total	~ 100	Summed in quadratures

With a detailed description of improvements and measurements given in Ref. [8], here we would like only to highlight several important milestones in the evolution of the electron beam angles:

- Quadrupole correctors allowed to significantly decrease the beam envelope angles at low beam currents.
- Development of a beam-based procedure for aligning the magnetic field in the cooling section alleviated the effect of mechanical drifts of the cooling section's solenoids.
- Clearing the background ions to <1% of the electron density by interrupting the electron beam for 2 μs at 100 Hz improved cooling at higher beam currents.

While the drag rate measurements were the instrument to estimate and improve the electron beam properties, cooling efficiency for operation was described by the cooling rates. To measure cooling rates, the antiproton beam, confined by rectangular RF

barriers, was first let diffuse for 15 minutes with no cooling (including stochastic cooling) and then the electron beam was turned on and cooled the antiprotons for 15 minutes. The cooling rate was calculated as the difference between the time derivatives of the momentum spread (or transverse emittances) before and after turning on the electron beam.

Typically, in this case the rms antiproton beam radius exceeded the size of the electron beam area with good cooling properties, and a model of cooling in an infinite homogenous electron gas predicted much higher cooling rates than were actually measured. One still can examine consistency between drag rates and cooling rates in a simple model assuming that measurements of the drag rates at various electron beam offsets (e.g. as in Fig. 4) represent the cooling force experienced by an antiproton at that given radius. Results of such comparisons are shown in Fig. 5, where cooling rates measured with similar electron beam conditions are plotted for different initial antiproton beam transverse emittances. The dash-dotted curve is the result of the integration of the cooling force, reconstructed from drag rate measurements for the same electron beam parameters at various offsets over a Gaussian spatial distribution of antiprotons with the rms size calculated from their measured emittance. Note that integration does not involve any additional fitting parameters. Taking into account the approximate nature of this model, the agreement is reasonable.

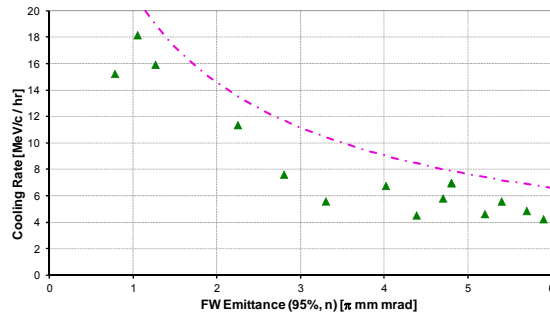


Figure 5: Longitudinal cooling rate (negated) as a function of the antiproton emittance for $I_e=0.1$ A.

2.5.5 Conclusion

The Recycler Electron Cooler at Fermilab made an important contribution to the success of the Tevatron Run II by increasing the antiproton flux and brightness. It also marked a significant step in the development of accelerator technology and accelerator physics, demonstrating for the first time relativistic cooling as well as beam transport of a magnetized beam with lumped focusing.

Drag rate measurements proved to be the main tool for analyzing and improving cooling properties of the electron beam. Various types of cooling measurements were eventually found to be mutually consistent and in a reasonable agreement with a non-magnetized description of electron cooling.

2.5.6 Acknowledgement

Fermilab is operated by Fermi Research Alliance, LLC under Contract No. DE-AC02-07CH11359 with the United States Department of Energy.

2.5.7 References

1. D. Cline et al., “Proposal to construct an antiproton source for the Fermilab accelerators”, proposal 492, in Proceedings of 1976 NAL Summer Study on Utilization of the Energy Doubler/Saver, Fermilab, Batavia U.S.A. (1976), pg. 309.
2. Fermilab Recycler Ring Technical Design Report, Ed. G. Jackson, Fermilab Preprint TM-1991 (1997).
3. S. Nagaitsev et al., “Experimental Demonstration of Relativistic Electron Cooling”, Phys. Rev. Lett. 96, 044801 (2006).
4. A. Shemyakin and L.R. Prost, “Ultimate performance of relativistic electron cooling at Fermilab”, in Proceedings of COOL11, THIOA01, Alushta, Ukraine (2011).
5. G. Budker, Sov. Atomic Energy, vol. 22, p. 346, 1967.
6. G. I. Budker et al., IEEE Trans. Nucl. Sci., Vols. NS-22, p. 2093, 1975.
7. I. N. Meshkov, Phys. Part. Nucl., vol. 25, no. 6, p. 631, 1994.
8. A. Shemyakin and L. Prost, “The Recycler Electron Cooler”, FERMILAB-FN-0956-AD (2013), arXiv:1306.3175.
9. A. Burov et al., “Optical principles of beam transport for relativistic electron cooling”, Phys. Rev. ST, Accel. Beams 3, 094002 (2000).
10. G.I. Budker et al., Preprint IYaf 76-32 (1976),
<http://cdsweb.cern.ch/record/118046/files/CM-P00100706.pdf>

2.6 Electron Cooling at IMP

Xiaodong Yang, Institute of Modern Physics, CAS, Lanzhou, China

Mail to: yangxd@impcas.ac.cn

2.6.1 Introduction of CSR

HIRFL-CSR (Heavy Ion Research Facility at Lanzhou---Cooling Storage Ring) is multi-purpose accelerator complex [1], it is consisted two storage ring, the heavy ion beam with energy range 8-50 MeV/u from HIRFL—composed two existing cyclotron SFC(K=69) and SSC (K=450) is used as injector, will be accumulated, cooled and accelerated to the high energy range of 100—400 MeV/u in the main ring(CSRm), then extracted fast to produce RIB or highly charged heavy ions. The secondary beams will be accepted and stored by experimental ring (CSRe) for many internal target experiments or high precision spectroscopy with beam cooling, On the other hand, the beam with energy range of 100-900 MeV/u will also be extracted from CSRe with slow and fast extraction mode for many external target experiments. Each ring was equipped an electron cooling device, the electron energy in the main ring is 35 keV and 300 keV for the experimental ring.

2.6.2 Electron Cooling for CSR

CSRm is a 161m circumference cooler storage ring with sixteen 22.5 degree H-type bending dipole magnets. The maximum betatron functions are 15.3 m and 30.5 m in horizontal and vertical respectively. The maximum dispersion is 5.4 m, and the dispersion at injection point is 4m. The betatron functions at electron cooler are 10m and 17m in the two transverse directions respectively, the dispersion is zero here. The

emittance of ion beam from SFC and SSC is about $20\pi\text{ mm mrad}$ and $10\pi\text{ mm mrad}$, and the acceptance of CSRm is about $150\pi\text{ mm mrad}$.

Two modes of injection are used in CSRm, stripping for lighter ions and repeated multитurn for heavier ones. The accumulation duration of CSRm is about 10s, and the acceleration time of CSRm is nearly 3s, and the one whole cycle period is about 17s.

In CSRm, the electron cooling device plays an important role in the heavy ion beam accumulation at injection energy. The new state-of-the-art electron cooling device was designed and manufactured in the collaboration between BINP and IMP, it has three distinctive characteristics, namely high magnetic field parallelism in cooling section, variable electron beam profile and electrostatic bending in toroids.

CSRe is a 128.8m circumference cooler storage ring with sixteen 22.5 degree C-type bending dipole magnets. The maximum Betatron functions are 30.9m and 22.3m in horizontal and vertical respectively. The maximum dispersion is 7.8m, and the dispersion at injection point is zero, the Betatron function is 30.4m in the Septum. The Betatron functions at electron cooler are 12.5m and 16m in the two transverse directions respectively, the dispersion is near zero here. The tunes are about 2.53 and 2.57, the transition gamma is 2.629, and the transverse acceptance of CSRe is about $150\pi\text{ mm mrad}$, and the longitudinal one is $\pm 5 \times 10^{-3}$.

Accelerated ion beam from the CSRm through the radioactive beam separator line with the length of 100m was injected into the CSRe. Generally the CSRe operated with the DC mode. A gas jet internal target was installed in the opposite side of electron cooler.

The electron cooling device plays an important role in HIRFL-CSR experimental ring for the heavy ion beam. Continuous electron cooling is applied to the stored ion beam for the compensation of the heating by various scattering. The most important is the ability to cool ion beams to highest quality for physics experiments with stored highly charged ions.

2.6.2.1 *Functions of Electron Cooling*

CSR

- Accumulation of heavy ion (Increase the phase space intensity)
- Provide high precision, high resolution heavy ion beam
- Improve the quality of ion beam
- Counteract scattering due to gas target and residual gas

2.6.3 Main Physics Goals at CSR

Radioactive Ion Beam Physics

Nuclear structure of unstable nuclei

Isospin dependence nuclear matter

Meson-Nucleon Physics in Energy $<1.1\text{ GeV/u HI & } <2.88\text{ GeV (3.7 GeV/c) Proton}$

High Charge State of Atomic Physics

High Energy Density Matter

Applications

Astrophysics

Irradiative Biology (Cancer Therapy)

2.6.4 Operation Modes of HIRFL-CSR

- CSRm + external target
- CSRm+RIBLL-II + external target
- CSRm+CSRe + internal target (high accuracy)
- CSRm+RIBLL-II+CSRe + internal target (high accuracy)
- CSRm+CSRe+E_Cooler + laser (high accuracy)

2.6.5 Electron Dynamics in the Cooling Devices

Electron cooling devices for HIRFL-CSR were under construction through collaboration between BINP and IMP. The main parameters, design points and progress of the cooler devices were presented in reference [2,3]. The electron motions in the gun region, adiabatic expansion region, toroid region and collector region were simulated with the help of numerical calculation. Cooling times of the typical heavy ions with injection energy were calculated with aid of the code. The prototypes of solenoid coils at the cooling section were fabricated and measured, the results show that the transverse components of the magnetic field for single coil is less than 2×10^{-4} .

2.6.5.1 Adiabatic Expansion

The temperature of electron beam is an important parameter in electron cooling device. Transverse temperature could be reduced when an electron beam passes through a magnetic field with negative gradient. Adiabatic expansion of electron beam moving in different magnetic fields with different energy and current was studied by computer simulation [4]. The result shows that in the adiabatic expansion region the transverse temperature of electron beam is reduced by a factor equal to the ratio between the initial and final magnetic field strengths, provided that the field change is adiabatic with respect to the cyclotron motion of the electrons.

2.6.5.2 Toroids

The electron beam is deflected into and out interaction region by toroid in the electron cooling device. The magnetic field distribution in toroid and at the interface among toroid and solenoids is very complicated. The properties of the magnetic field in the toroid give rise to a change in the transverse energy of the electron.

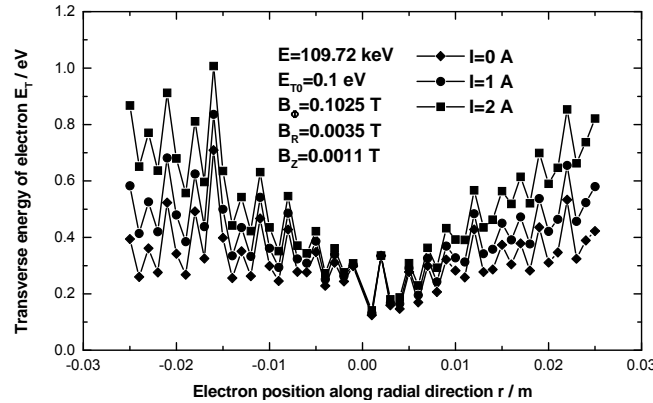


Figure 1: Electron transverse energy distribution along radii at different beam current

A code was developed to study the spatial distribution of electron transverse energy in the beam as it moves through the toroid [5]. The space charge effect was taken into account in the code. The simulation results show that the increase of the transverse energy could be minimized when the ratio between the central length of the toroid and the electron cyclotron wavelength is an integer. Figure.1 and Figure.2 demonstrate the electron transverse energy distributions along the radial and azimuth direction after pass through the toroid.

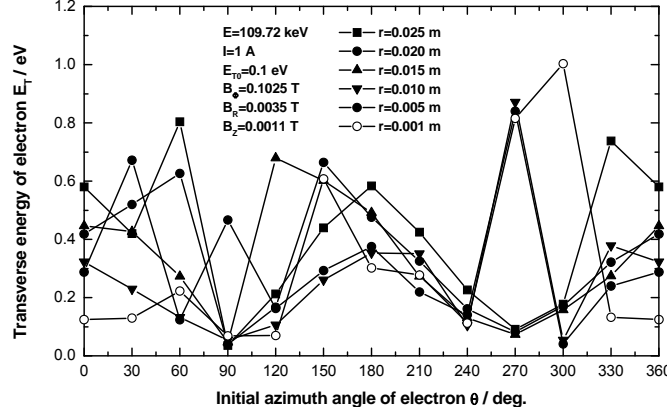


Figure 2: Electron transverse energy azimuth distribution.

2.6.5.3 Parallelism of Magnetic Field in the Cooling Section

In order to obtain the tolerance requirement of magnetic field homogeneity of solenoids in electron cooling devices, the source of the magnetic imperfection and its influence on the transverse temperature of electron beam was investigated by means of numerical simulation, and the space charge effect of electron beam was taken into account [6]. The calculated result shows that the influence of imperfection of magnetic field will be negligible when the relative magnetic field perturbation is less than 1×10^{-3} . The electron transverse energy as a function of relative perturbation amplitude at different beam current are illustrated in Figure.3.

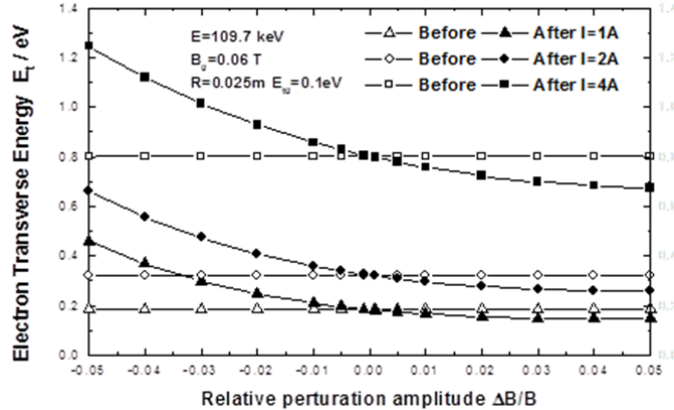


Figure 3: Electron transverse energy as a function of relative perturbation amplitude at different beam current.

2.6.5.4 Collector

High efficiency collector is favorable for stable operation of an electron cooling device and regulation of high voltage power supply. The dependences of collector efficiency on the geometric, electrical and magnetic factors are investigated [7]. The result shows that high efficiency can be obtained under appropriate parameter setup. The loss current with respect to primary beam current is less than 1×10^{-4} , the efficiency is higher than 99.99%. The relative loss current of collector as a function of magnetic field ratio is presented in Figure.4.

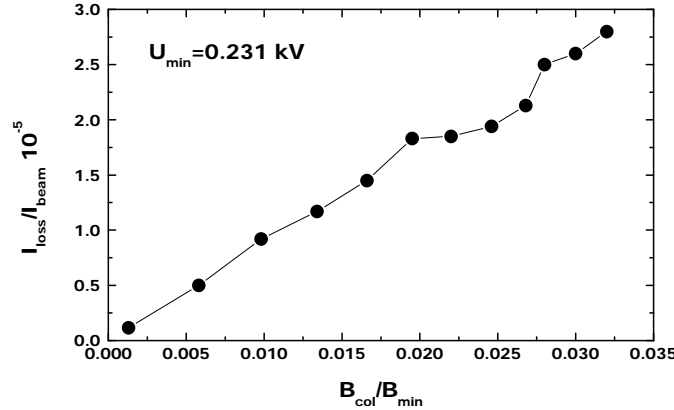


Figure 4: Relative loss current of collector as a function of magnetic field ratio.

2.6.6 Parameters Optimization of CSR

With the help of electron cooling code, the cooling time of ion beam were extensive simulated in various parameters of the ion beam in the HIRFL-CSR electron cooling storage rings respectively [8].

The cooling rate depends on not only the storage ring lattice parameters, the Betatron function, dispersion of the cooling section, initial emittance and momentum spread of ion, energy and charge state of ion beam, but also on the construction of electron cooling device, the strength of magnetic field, the parallelism of magnetic field in the cooling section, the effective cooling length, and the parameters of electron beam, such as radius, density and transverse temperature of electron beam. These parameters are determined by the storage ring and the technology limitation, on the other hand, they are influenced and restricted each other.

For the ion beam given initial emittance and momentum spread, the Betatron function and dispersion of the storage ring determine the size and angle spread of ion beam in the cooling section. According to the cooling formula, when the angle spread of ion is bigger than electron, the ion will be cooled faster if the Betatron function is bigger, at the same time, the size of ion beam will approach the size of electron beam, the cooling action will be weakened due to the space charge effect. On the other hand, Betatron function decide the size of ion beam, dispersion determines the displacement of ion beam. In order to cool ion beam down fast, one should compromise among these parameters.

Figure 5 gives the dependence of cooling time of the transverse direction on the transverse Betatron function, the cooling time denotes the time that the emittances

change from initial to the $30 \pi \text{mm mrad}$, other parameters appear in the figure. Only the x-coordinate value changes, the other was fixed. Intermediate Betatron function yields shorter cooling time than large ones. The optimal Betatron function is about 10—20 M.

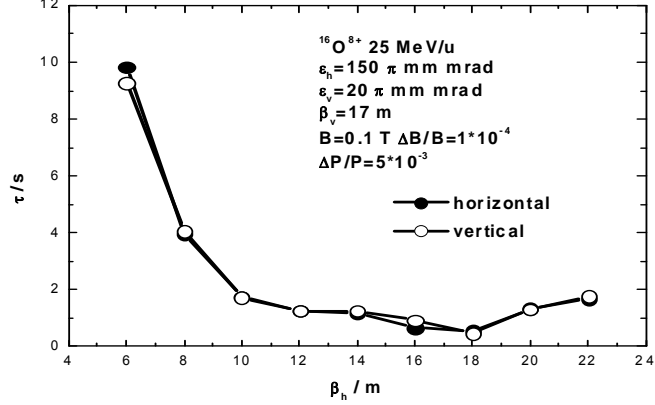


Figure 5: Cooling time as a function of horizontal Betatron function.

In order to get fast cooling, the electron cooling device generally was located in the straight section of storage ring where the dispersion is zero, but if the dispersion is not zero in the cooler location, an additional angle was introduced, it will be helpful for cooling, it was dispersive cooling. Figure 6 presents the cooling time as a function of dispersion. If the dispersion in the cooler position is positive, the cooling time becomes shorter than zero dispersion.

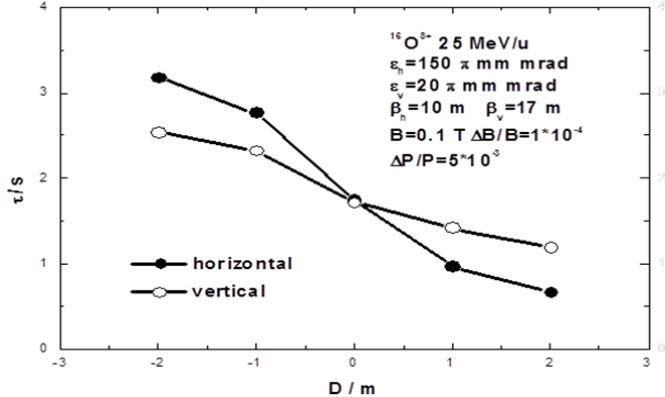


Figure 6: Cooling time as a function of dispersion.

The cooling time depends on the average longitudinal velocity of ion and electron, it will be longer in the case of higher energy for the same ion. From the view of electron density, this velocity decides the density of electron and time that ion passes through the cooling device in the case of fixed cooling length, the probability of interaction between ion and electron will increase if the velocity is small.

The cooling time is directly proportional to the ion mass, and inversely proportional to the square of ion charge state from the formula. Figure 7 presents the cooling time as a function of ion energy, and figure 8 shows the cooling time as a function of ion charge state, the lower energy and higher charge state is helpful to cooling.

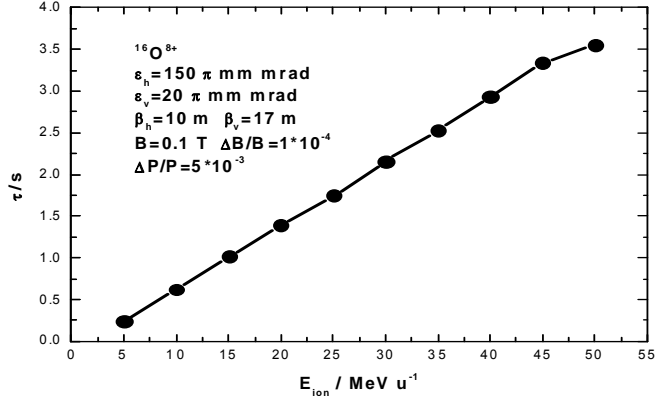


Figure 7: Cooling time as a function of ion energy.

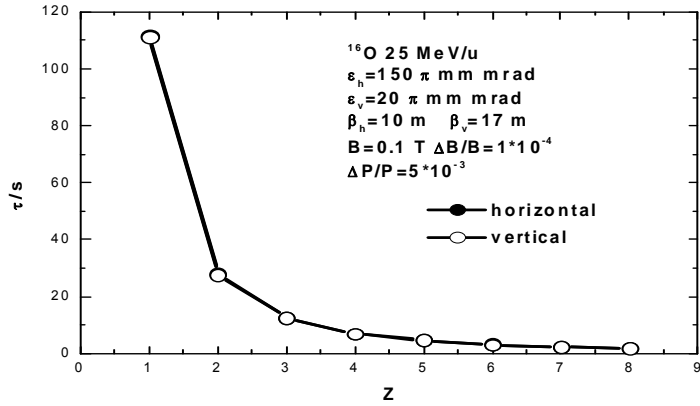


Figure 8: Cooling time as a function of ion charge state.

The effective transverse velocity is only determined by the magnetic field in the cooler and space charge of electron beam if there is not other factor. The electron density is not same for different energy. Figure 9 presents the cooling time as a function of magnetic inductive strength in cooling section. The influence of magnetic field parallelism on cooling time is demonstrated in Figure 10. The cooling time becomes shorter when the magnetic field strength and its parallelism is higher in the cooling section.

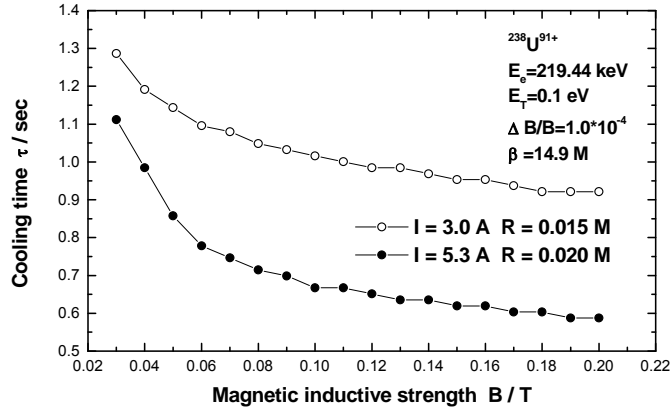


Figure 9: Cooling time as a function of the magnetic inductive strength in cooling section.

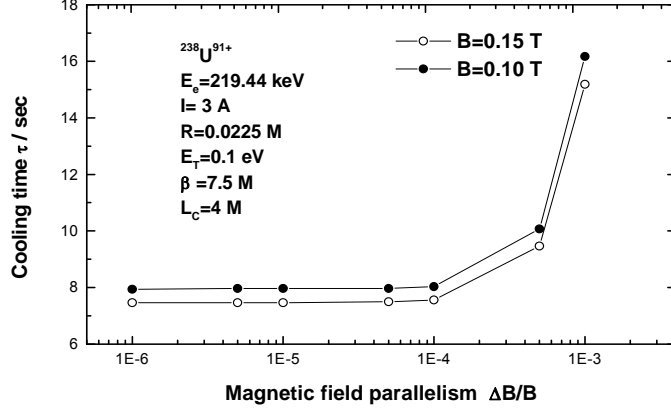


Figure 10: Cooling time as a function of the magnetic field parallelism in cooling section.

The magnetic field strength and its parallelism in the cooling section influence the electron transverse temperature, specially in case of high energy, the effective velocity caused by transverse components of magnetic field will be comparable with initial electron temperature, if the ion energy is $400 \text{ MeV}/\mu$, and $\Delta B/B=10^{-4}$, then corresponding temperature is near 50 K.

For fixed electron density, the radius of electron decides the region of interaction between ion and electron, if the radius of electron beam is smaller, the outside ion will not be cooled well by electron, the cooling time will become longer, as shown in Figure 11. The electron temperature before the cooling section is determined by the electron gun construction, expansion factor and additional energy caused by through the toroid region, Figure 12 presents the influence of electron transverse temperature.

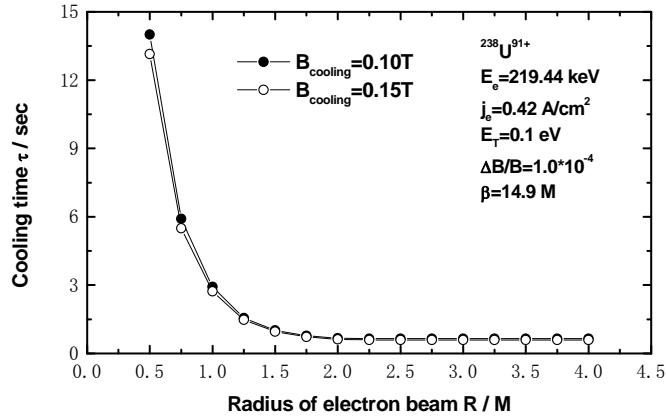


Figure 11: Cooling time as a function of the radius of electron beam.

From the simulation of electron cooling, it turns out that the lattice parameters of HIRFL---CSR lie in the optimal range for electron cooling. In the CSRm, the ion with higher charge state and lower energy should be chose as injection so that the ion beam will be cooled to required emittance in the shorter time, Electron cooling is more powerful when the injected ion beam has smaller initial emittance and momentum spread . If introduce positive dispersion in the cooling section, the cooling time will become shorter than zero dispersion. For electron beam, its density should approach optimal value in the case of low energy, and as big as possible in the case of high

energy. The magnetic field should be strong enough and parallelism is better than 1×10^{-4} .

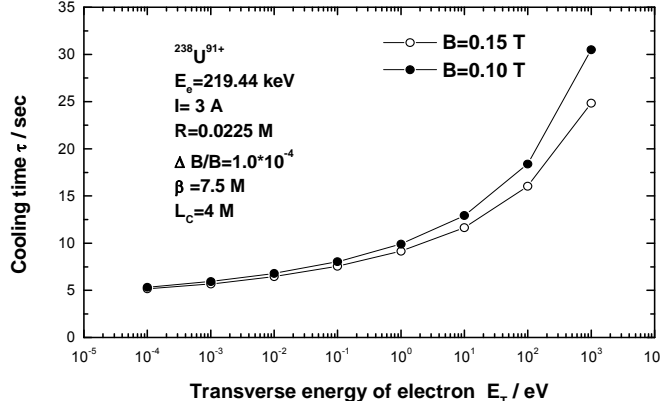


Figure 12: Cooling time as a function of the transverse temperature of electron.

2.6.7 Commissioning and Operation of Electron Cooling in CSR

About kind of ion beam was accumulated with the help of electron cooling in CSRM. The ion species from H to Uranium, and the energy range from to 1.2MeV/u to 21.7MeV/u. The experiments and operation results were reported in the workshop on the beam cooling and related topics from 2005 to 2013 [12, 13, 14, 18, 23] and RuPAC 2010 [17], RuPAC 2012 [20]. One can find the related papers in the references [15, 16, 19, 21, 22].

2.6.8 Electron Cooling Experiments at CSR

Some investigation and optimization experiments were completed in CSR, such as,

- Accumulation experiments in CSRM
- Cooling force measurement
- Optimization of electron cooling
- Bunch length measurement

2.6.9 Physics Experiments Related Electron Cooling at CSR

- Recombination of ion with the free electron of cooler
- Mass measurement in the isochronous mode
- Internal target experiment
- Schottky mass measurement

2.6.10 Planned Experiments Related with Electron Cooling

2.6.10.1 *Longitudinal Stacking*

From the experience of operation in the past several years, the ion beam accumulation in the transverse phase performed well. The higher ion beam density and stored particle number was asked by the physics experiments. The longitudinal stacking

methods will be taken into account in the developing and improvement scheme of HIRFL-CSR. The RF stacking and the barrier bucket methods will be tested in the near future.

2.6.10.2 *Ion Beam Crystallization*

In the case of smaller stored particle number in the heavy ion storage ring, the momentum spread of the electron-cooled highly charged ion beam observed in the Schottky spectrum presented sudden drop. This sudden change has been interpreted as a transition to an ordered state in longitudinal direction. This phenomenon was studied in the many storage ring. On the one hand, this investigation is helpful to the understanding the condition and situation of the ordered beam, on the other hand, the stability and reliability of the storage ring were required for this study. The requirement of high performance of machine and high precision of ion beam will push the improvement and upgrade of facility. It will become understandable for the specifications of different aspects of the storage ring.

2.6.10.3 *High Energy Density Physics*

High Energy Density Physics is one of the most active areas of research, it is helpful and useful for astrophysics, planetary physics, geophysics inertial fusion and many others. It is necessary to develop the investigation on the application of storage ring to generate the high energy density heavy ion beam. In base on the techniques of the beam accumulation, electron cooling in the transverse and longitudinal directions, with the help of the bun rotation, primary investigation of high energy density ion beam in the heavy ion storage ring is an interesting topics. The ion beam with big mass, low energy, and low density was prepared in the storage ring, and then cooling, accumulating, bunching, bunch compressing, and accelerating will act on this pulse beam, as a result, a shorter bunch with high density and high energy was expected to form in the storage ring.

2.6.10.4 *Suppression of Instability of Ion Beam with Modulated Electron Beam*

From the experience of commissioning and operation in the past several years, The most serious factor of the influence on the ion beam maximum accumulated ion beam intensity and the minimum momentum spread in the Cooler Storage Ring of Heavy Ion Research Facility in Lanzhou was the beam instability, and it brought on the shortening of beam lifetime and beam loss. It became the bottleneck of improvement on the beam quality and upgrade of the performance. The more intense, the more high precision and the more stable ion beam were asked by the physics experiments users on the storage ring. The systematic investigation on the mechanism and principle of the beam instability in detail were planned with help of the simulation and compared with the experiments. On the base of the results of simulation, some effective and helpful methods were proposed to suppress the ion beam instability. The electrostatic field produced by the space charge of electron beam in the cooler by means of modulation on the voltage of control electrode in the electron gun will act as a traveling wave in the cooling section. This new way will be attempted to suppress the ion beam instability in the presence of electron cooling device. Two functions were combined in the one electron beam. The more stable, the more intense and more precise heavy ion beam was expected in HIRFL-CSR. The constructive proposal for upgrade was suggested based

on these results. These results will be helpful for the upgrade and improvement of CSR in the near future and provide basis for further development.

2.6.11 Status of HIRFL-CSR

In the past several years, more than 7000 operational hours was scheduled yearly for HIRFL-CSR, half of them were provided by the storage ring. Most beamtime was dedicated to the mass measurement experiments, recombination of ion with the free electron of cooler and the internal target experiments. The other beamtime was devoted to the cancer therapy and related experiments. More than 100 patients were treated in CSRM with the carbon beam.

However, the extremely heavy ion beam like Bi and U were successfully cooled and accumulated with very low injection energy and weak intensity. A few times commission for accumulation of proton with the help of electron cooling were performed in CSRM, including instead of proton with H_2^+ , these commission were not successfully completed carried out up to now due to the mismatching parameters between injector and storage ring.

2.6.12 Research Activities of HIRFL-CSR in Near Future

1. Synthesis and study of new nuclides
2. Nuclear physics with research of radioactive ion beams
3. Research on heavy ion collisions at low and intermediate energies and the properties of hot nuclei
4. High spin nuclear structure studies
5. Theoretical nuclear physics
6. Atomic Physics of Highly Charged Ions
7. Study of SHIM (Swift Heavy Ion in Matters) physics
8. Research biological effects of heavy ion irradiation and heavy ion therapy

2.6.13 Summary

From 2006, the electron cooler have operated well for ten years. Electron cooling, ion beam accumulation and electron cooling were performed in HIRFL-CSR. Several physics experiments were completed with the help of electron cooling in CSR. The results show the electron cooling had well performance in the commission. In the future, the application of electron cooling should be extended according to the physics experiments. The performance of electron cooling should be improved carefully, and the reliability and stability of electron cooling should be upgraded in the future.

2.6.14 References

1. <http://english.imp.cas.cn/rh/>
2. X.D. Yang, H.W. Zhao, J.W. Xia, W.L. Zhan, B.W. Wei, V. V. Parkhomchuk, “HIRFL-CSR Electron cooling devices”, Cyclotrons and their Applications 2001, Sixteenth International Conference, East Lansing, Michigan 2001, 186-188.
3. X.D. Yang, H.W. Zhao, J.W. Xia, W.L. Zhan, B.W. Wei, V.V. Parkhomchuk, “HIRFL-CSR Electron cooling devices”, Proceedings of the Second Asian Particle Accelerator Conference, Beijing, China 2001, 777-779.

4. X. D. Yang, M. T. Song, J. W. Xia et al, "Adiabatic Expansion of Electron Beam", High Energy Physics and Nuclear Physics (in Chinese) Vol.24, No.12, (2000) 1179-1184.
5. X. D. Yang, M. T. Song, J. W. Xia et al, "The Motion of Electron Beam in Toroid", High Power Laser and Particle Beam (in Chinese) Vol.13, No.2, (2001) 223-227.
6. X. D. Yang, M. T. Song, J. W. Xia et al, "Influence of the magnetic Imperfection on the Transverse Temperature of Electron Beam", Nuclear Physics Review (in Chinese) Vol.18, No.2, (2001) 219-223.
7. X. D. Yang, M. T. Song, J. W. Xia et al, "Collection of Electron Beam, High Power Laser and Particle Beam "(in Chinese) Vol.12, No.2, (2000) 245-248.
8. X. D. Yang, V. V. Parkhomchuk, Parameters "Optimization of HIRFL-CSR Experiment Ring Electron Cooling Device", High Power Laser and Particle Beam (in Chinese) Vol.12, No.6, (2000) 771-775.
9. X. D. Yang, Y. He, H. W. Zhao, et al "Manufacture and Magnetic Field Measurement of High Precision Solenoid Coils for HIRFL-CSR Electron Cooling Device", High Power Laser and Particle Beam (in Chinese), Vol.13, No.5, (2001) 649-653.
10. YANG Xiao-Dong, PARKHOMCHUK V. V, ZHAO Hong-Wei, et al, "Test results of HIRFL-CSR main ring electron cooling device", Vol.27, No.8, (2003) 726-730.
11. YANG Xiao-Dong, PARKHOMCHUK V. V, ZHAO Hong-Wei, et al, "Electron cooling simulation in HIRFL-CSR main ring", High Energy Physics and Nuclear Physics (in Chinese) Vol.27, No.9, (2003) 824-827.
12. Xiaodong Yang, Vasily Parkhomchuk, Wenlong Zhan, Jiawen Xia, Hongwei Zhao, Youjin Yuan, Mingtao Song, Jie Li, Lijun Mao, Wang Lu, Zhixue Wang, BINP Electron Cooler Group, "Commissioning of HIRFL-CSR and its electron coolers", «AIP conference proceedings 821» ,2006,65-74.
13. X.D. Yang, V.V. Parkhomchuk, W.L. Zhan, J.W. Xia, H.W. Zhao, G.Q Xiao, Y.J. Yuan, M.T. Song, Y. Liu, J.C. Yang, L.J. Mao, J. Li, G.H. Li, D.Q. Gao, Z.Z. Zhou, Y. He, W. Zhang , X. T. Yang, J.H. Zheng, R.S. Mao, T.C. Zhao " Commissioning of electron cooling in CSRm", Proceedings of COOL2007, 59-63.
14. X.D. Yang, L.J. Mao, G.H. Li, J. Li, X.M. Ma, T.L. Yan, Y.J. Yuan, M.T. Song, J.C. Yang, Y. Liu,T.C. Zhao, J.W. Xia, W. Zhang, D.Q. Gao, Z.Z. Zhou, H.B. Yan, R.S. Mao, Y. He, S.F. Han, J.H. Zheng, X. T. Yang, H.W. Zhao, G.Q Xiao, C. Xiao, D.Y. Yin, P. Li, H. Jia, "Commissioning of electron cooling in CSRe", Proceedings of COOL 2009, Lanzhou, China, FRM1MCIO02, 173-177.
15. YANG Xiao-Dong, LI Jie, MAO Li-Jun, LI Guo-Hong, ZHAN Wen-Long, XIA Jia-Wen, ZHAO Hong-Wei, XIAO Guo-Qing, YUAN You-Jin, SONG Ming-Tao, LIU Yong, YANG Jian-Cheng, GAO Da-Qing, ZHOU Zhong-Zu, HE Yuan, ZHANG Wei, ZHANG Jian-Hua, MAO Rui-Shi, ZHAO Tie-Cheng, Parkhomchuk Vasily, "Commissioning of electron cooling in CSRm", Chinese Physics C (HEP & NP) Vol.33 No. SII 2009 18-21.
16. Yang Xiao-Dong, MAO Li-Jun, LI Guo-Hong,LI Jie, MA Xiao-Ming, YAN Tai-Lai, YUAN You-Jin, SONG Ming-Tao, YANG Jian-Cheng, LIU Yong, ZHAO Tie-Cheng, XIA Jia-Wen, ZHANG Wei, GAO Da-Qing, ZHOU Zhong-Zu, YAN Hong-Bin, MAO Rui-Shi, HE Yuan,HAN Shao-Fei, ZHENG Jian-Hua,YANG Xiao-Tian, ZHAO Hong-Wei,XIAO Guo-Qing,YIN Da-Yu, LI Peng, JIA Huan, PARKHOMCHUK Vasily, REVA Vladimir, SKOROBOGATOV Dmitry, "Commissioning of electron cooling in CSRe", Chinese Physics C (HEP & NP), 2010, 34 (7) , 998-1004.
17. Xiaodong Yang, Guohong Li, Jie Li, Xiaoming Ma, Lijun Mao, Ruishi Mao, Tailai Yan, Jiancheng Yang, Youjin Yuan, Vasily V. Parkhomchuk, Vladimir B. Reva,"Electron Cooling Experiments in CSR", Proceedings of RuPAC-2010, Protvino, Russia, WECHZ05, 161-165.

18. Xiaodong Yang, Jie Li, Lijun Mao, Guohong Li, Xiaoming Ma, Tailai Yan, Mingtao Song, Youjin Yuan, Jiancheng Yang, Ruishi Mao, Tiecheng Zhao, Peng Li, Wei Zhang, Dayu Yin, Weiping Chai, Huan Jia, Wenheng Zheng, Xiaohu Zhang, "Electron cooling performance at IMP facility", Proceedings of COOL'11, Alushta, Ukraine, MOIO01, 1-5.
19. YANG XiaoDong, LI Jie, MAO LiJun, LI GuoHong, MA XiaoMing, YAN TaiLai, MAO RuiShi, YANG JianCheng, YUAN YouJin, PARKHOMCHUK Vasily & REVA Vladimir. "Electron cooling experiments in CSR", SCIENCE CHINA, Physics, Mechanics & Astronomy, December 2011 Vol.54 Suppl.2. s274-s278.
20. Xiaodong Yang, Jie Li, Lijun Mao, Guohong Li, Xiaoming Ma, Tailai Yan, Ruishi Mao, Tiecheng Zhao, Junxia Wu, Youjin Yuan, Jiancheng Yang, Peng Li, "Beam instability phenomena observed at HIRFL-CSR in the presence of electron cooler", Proceedings of RuPAC-2012, St. Petersburg, Sept. 24-28 2012, MOZCH01.
21. YANG XiaoDong, LI Jie, MAO LiJun, et al, Electron Cooling Performance at HIRFL-CSR, High Power Laser and Particle Beam (in Chinese), Vol.24, No.10, (2012) 2435-2440.
22. YANG XiaoDong, LI Jie, MAO LiJun, LI GuoHong, MA XiaoMing, YAN TaiLai, MAO RuiShi, ZHAO TieCheng, WU JunXia, YUAN YouJin, YANG JianCheng, LI Peng. Beam instability phenomena observed at HIRFL-CSR in the presence of electron cooler. Sci Sin-Phys Mech Astron, 2013, 43(1): 76-84.
23. Xiaodong Yang, Jie Li, Lijun Mao, Guohong Li, Xiaoming Ma, Tailai Yan, Dayu Yin, Proceedings of COOL2013, Murren, Switzerland, WEAM1HA02 Proceedings, 84-88.

2.7 New Stochastic Cooling Kickers for RHIC

J. M. Brennan, M. Blaskiewicz, K. Mernick
 Brookhaven National Laboratory, Upton NY 11973
 Mail to: Brennan@bnl.gov

2.7.1 Introduction

Stochastic cooling increases the luminosity of RHIC by combating Intra-Beam Scattering and compressing the 6-dimentional phase space of the bunched beam during collisions at 100 GeV/nucleon.[1] Because IBS is strong for highly charged (bare) ions it is essential to simultaneously cool in all three phase space planes because increased density in one plane enhances the IBS-driven emittance growth rate in the others. Implementation of cooling for RHIC has progressed in stages by installing cooling systems plane by plane over several runs.[2,3,4] The first plane was longitudinal. The kickers of that system employed de-commissioned hardware from the Tevatron[5] retrofitted for the narrowband kicker concept of the RHIC cooling system. This report describes the new kickers that replaced the originals. The upgrade follows design concepts developed for the RHIC transverse systems. Some new features are employed to increase reliability, vacuum performance, and kicker voltage.

2.7.2 System Description and Requirement

2.7.2.1 *Bunched Beam and Narrowband Kickers*

A unique feature of cooling in the collider is that the beam is bunched. This implies that; 1. The local particle density is high so that a large system bandwidth is required for

practical cooling rate, and 2. The beam effective frequency spectrum is sparse, only harmonics of $1/(bunch\ length)$ (10 ns) being non-redundant[6]. The RHIC system exploits this situation by employing narrowband kickers whose resonant frequencies match these harmonics. This approach energy averages the drive power needed to excite the kickers, thereby reducing the power amplifier size requirement by an order of magnitude. The kickers' bandwidth is adjusted such that they fill and empty in the time between bunches. In this way the effective system bandwidth is 3 GHz while the kicker resonant frequencies range between 6 to 9 GHz in 200 MHz intervals.



Figure 1: Prototype of 6 GHz 6-cell kicker cavity. One half of the cavity is shown. Waveguide splits to feed the two 3-cells in phase.

Figure 1 shows a prototype kicker cavity. It is essentially six TM_{010} rectangular cells, tuned to one of 16 frequencies, 6.0, 6.2...8.8, 9.0 GHz. It is split into two sections on the vertical median plane. The symmetry of fields in the TM_{010} ensures that no currents cross the median plane. Therefore no ohmic contact between the two halves is necessary. The beam bore diameter is 20 mm when in operation but the two halves separate by ~ 70 mm during filling and ramping of the collider. Each cavity is driven with a 40 W solid state amplifier and develops ~ 3 kV of kick. More details below. The low-level electronics produces a drive signal that begins 80 ns before the beam arrives. The circuitry is described elsewhere [3] and was not part of this upgrade program.

2.7.2.2 *Goals of the Upgrade*

The prototype kickers provided barely enough kick as judged by maxim signal suppression being typically less than 6 dB and power level from drive amplifiers running near maximum output. These kickers were 4-cell cavities with R/Q of ~ 200 Ohms. The new kickers are 6-cell cavities giving 50% more voltage. The voltage can also be limited by precision of frequency of the cavities. The new design improves the precision by better mechanical tolerances and temperature stability. The vacuum performance is improved by eliminating coaxial cables and Teflon connectors from the vacuum vessel. Leaks occurred in the water cooling channels of original kickers. The new design has no cooling channels in the vacuum. Mechanical motion inside the vacuum is necessary to increase cavity's clear aperture for injection and ramping.

Metal-to-metal friction is always a problem in high vacuum. The new design provides motion with no sliding parts which improves precision and reliability.

2.7.3 Cavity Design

2.7.3.1 RF Structure

The 6-cell cavities are actually two 3-cells operating in π -mode and the two 3-cells are separated by one wavelength. They are fed by a TE₁₀ waveguide with a 3 dB H-field split. This drives the two innermost cells in phase. See figure 1. The rectangular shape of the cells facilitates the machining. CST Microwave Studio is used to find the dimensions of the cells with the Eigenmode solver. The cells are coupled via the beam bore. Adjustments are made to individual cell dimensions in order to equalize the field strength and thereby maximize the shunt impedance. A typical value for the 6-cell structure is R/Q = 300 Ω . The mode spectrum is generated with the Frequency Domain solver. The operating mode is the highest frequency. See figure 2. Each cell has two fine tuners to achieve frequency accuracy of 1 MHz. Tuners are silver plated 1/4-28 screws. The two 3-cells have the same frequencies. The material is copper-plated aluminum. The purpose of copper plating is to reduce the secondary electron yield. The benefit for reduced power dissipation is insignificant.

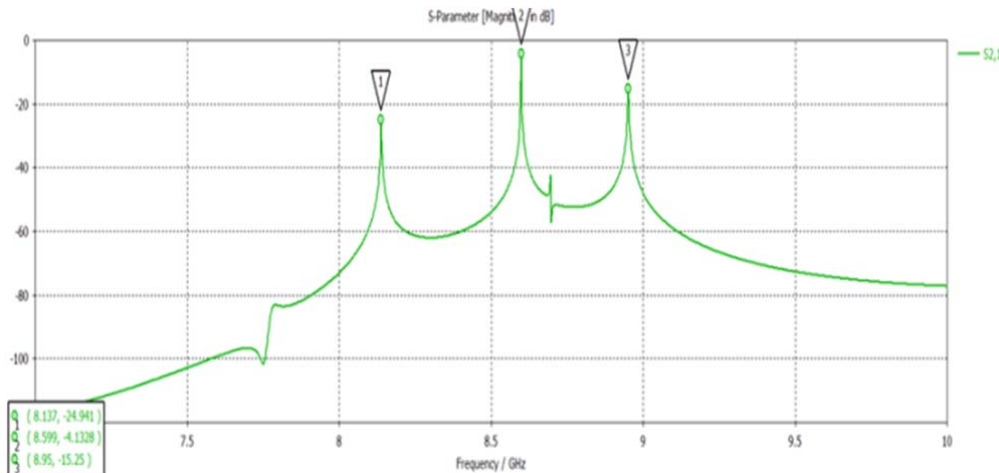


Figure 2: Mode spectrum of 9 GHz 3-cell substructure.

2.7.3.2 Fill and Decay Time

Coupling strength to the waveguide sets the Q_{external} to obtain a loaded bandwidth of 10 MHz, matching the cavity fill/decay time to the bunch repetition period. Coupling is determined by the size of the aperture between inner cells and the end of the waveguide where the magnetic fields are parallel. Coupling reduces the resonant frequency of the inner cells which is compensated by refinements to the cell dimensions.

2.7.3.3 *Opening of Cavities*

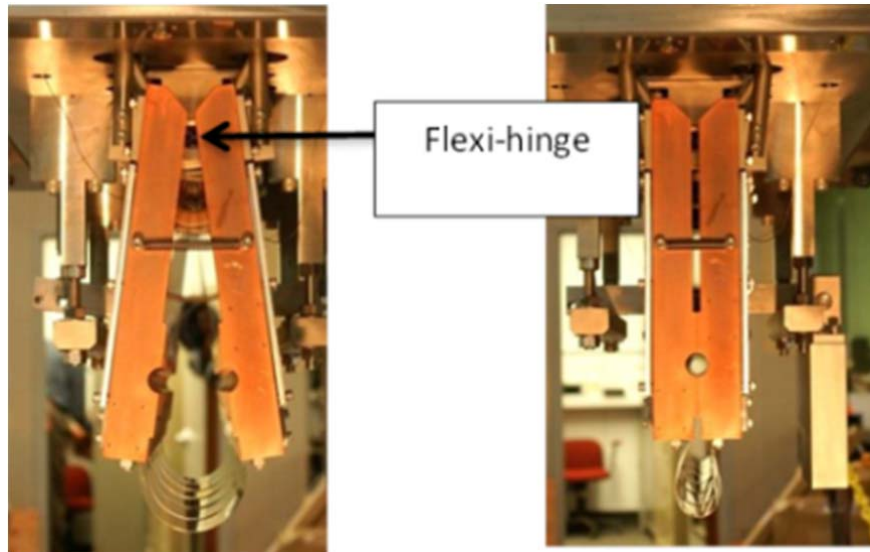


Figure 3: The cavities split on the vertical median plane and open, left, for filling and ramping then close, right, for operation during store.

Figure 3 shows how the cavities open. The two halves of cavities are suspended from the top by a “Flexi-hinge”[7]. This allows for rotation of 10 degrees, by elastic deformation only, of a stainless web structure within the hinge. No sliding metal-to-metal surfaces are employed and therefore problems of binding and galling in vacuum are eliminated. The mechanism achieves the 10^{-4} inch reproducibility needed for 1 MHz frequency precision. The two halves of the cavity are coupled in a master-slave arrangement. The master determines the location of the beam hole with respect to the beam axis and the slave is pulled to the master to ensure reproducibility of the cell dimensions and resonant frequency. The beam hole is referenced to survey targets outside the vacuum with a laser tracker and is not adjustable once the vacuum vessel is closed. Thin (0.010 inch) stainless straps at the bottom of cavity structures make an electrical connection between the two halves to prevent low frequency resonances from being excited by the beam when open. Actuators connect to the internal mechanism via welded bellows. Thin flexible straps of copper-beryllium connect the ends of the cavities to inside wall of the vacuum tank to pass beam image current.

2.7.3.4 *Waveguide Power Feed*

Each cavity assembly comprises five or six 6-cell cavities, figure 4. RF power is fed to the cavities via waveguides that are rigidly fixed to the top to the vacuum tank. The waveguide dimensions are 1.300 by 0.325 inches for all frequencies. They do not touch the cavity structures which move. A 1 mm gap allows for mechanical tolerance and accommodates relative motion between the aluminum cavities the stainless steel tank when the temperature changes. The largest motion occurs when the assembly is baked at 150 C for vacuum improvement. At the interface between the moving and fix parts a choke joint blocks power from escaping. Two sections of the joint provide coverage over the 6 to 9 GHz range with the same dimensions making the waveguides interchangeable.

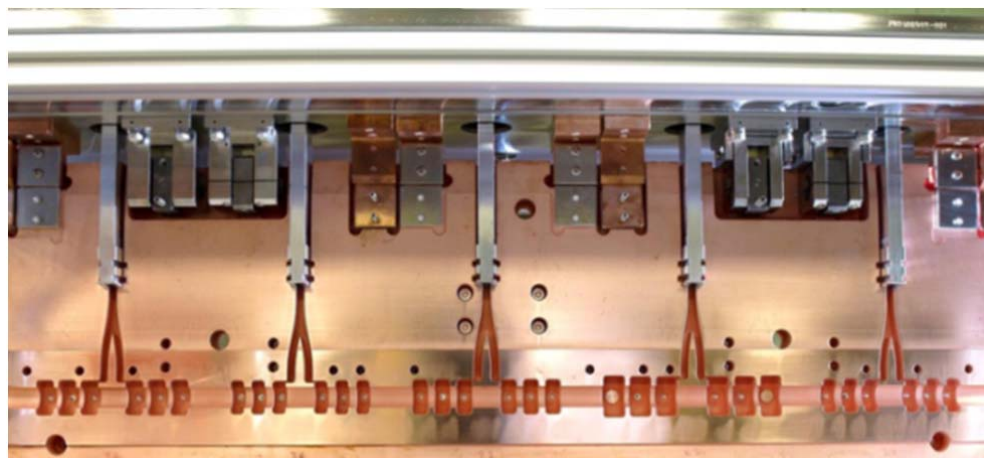


Figure 4: An assembly of 5 6-cell cavities. Waveguides fixed to the top deliver power to the movable assemblies. Flexible copper-beryllium straps conduct heat to the top plate.

At the top of waveguide there is a custom design of coax to waveguide transition and vacuum feedthrough. A loop couples the TEM coax to the dominant TE waveguide mode over the full frequency band. Loop coupling is preferable to probe coupling because the loop is well thermally anchored to the wall. Figure 5, right. In vacuum even a small amount of power can lead to high temperature unless the thermal conduction path is short. The shorted end of the waveguide is roughly $\frac{1}{2}$ guide wavelength from the loop. A short section of 66Ω coax matched the loop to 50Ω . At the coax end the hermetic seal is realized with an alumina-to-kovar braze assembly. Figure 5, right. The pin is 0.030 inch and the alumina dielectric seal is 0.400×0.200 inches. The mini-conflat knife edge is a solid kovar piece. The pin integrates into a 3.5 mm coax connector on the air side. A circulator separates the forward and reflected power. The reflected power is always high because the cavity is over coupled. The circulator improves the reliability of the power amplifiers and also provides a means to observe the emitted power from the cavities. The emitted power can be used to measure the resonant frequency of a cavity. It is sometimes used to see the beam induced signal from a cavity. This is useful for adjusting the pickup to kicker timing of the cooling system.

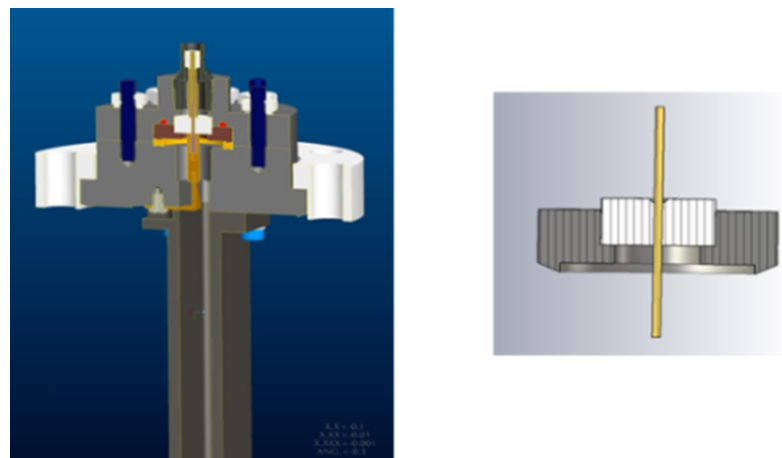


Figure 5: The coax to waveguide transition, left, and vacuum feedthru, right.

2.7.4 Cavity Fabrication

2.7.4.1 *Matching*

Cavity assemblies are CNC cut from 6061-T6 aluminum. STEP files containing the cells and the waveguide structures are generated by Microwave Studio and are integrated into assemblies with features for attaching the flexi-hinges and actuator brackets. The arrangement of 6-cell structures is sorted so as to prevent the lower frequency modes of one cavity from overlapping the operating mode of an adjacent cavity. In addition the beam tubes between 6-cells are always a least two diameters in length for further decoupling. A complete kicker consists of three pairs of the assembly shown in figure 4 in three vacuum tanks. The machining of the cavities is done in two stages. The first stage leaves 0.05 inch of material on all the critical dimensions. The piece is then heat treated to relax internal stresses before the finish stage. The plane where the right and left halves meet is flat to ± 0.001 inch over the 39 inch length.

2.7.4.2 *Frequency and Bandwidth Tuning*

The cavity fields are measured with the bead pull technique in the transmission mode. A small loop at the end of 0.085 inch semi-rigid coax is inserted through a hole in one of the tuning screws serves as a pickup for S21 measurement. Each 3-cell is measured independently of the other by either inserting a microwave absorber into the other's waveguide branch or by decoupling the two 3-cells by separating their frequencies with the tuning screws. First, the fields in the three cells are balanced by adjusting the tuners. The bandwidth is measured and corrected by making trim cuts to the size of waveguide-to-cavity aperture. This affects the frequency of the inner cells so the fields need to be balanced again with the tuners. Next, trim cuts are applied to the size of each cell to set the operating frequency. The target frequency anticipates the air-to-vacuum ($\Delta f/f = +2.8 \times 10^{-4}$) and ambient-to-operating temperature frequency ($\Delta f/f = -2.5 \times 10^{-5}/C$) shifts. The assembly is then copper plated, cleaned in a 10% solution of Citronox at 60 C, and vacuum baked at 150 C for 48 hours. The tuners adjustment is repeated before installing the cavity into the vacuum tank.

2.7.5 Operation

2.7.5.1 *Temperature Control*

In operation the cavities are cooled by conduction through flexible copper-beryllium straps between the cavity body and top of the vacuum tank. See figure 4. The straps are 0.010 inches thick by 1 inch wide and flex 10 degrees over a length of $\frac{1}{4}$ inch. This length is kept small by locating the straps on the axis of rotation of the hinge pivot. There are four stacks of the three strips per cavity half. The thermal conduction of each stack is ~ 0.7 Watt/C. The vacuum tanks are kept at ambient temperature by heat sinks and fans. The cavities are kept at an elevated temperature of 50 C so that power always flows through the straps. When not in operation all the power is delivered by thermal radiation through glass windows on the vacuum tank. The thermal radiation comes from ordinary 60 W halogen spot lights. Black targets are mounted on the cavities to absorb the power. Black porcelain enamel was chosen for the absorber because of its high emissivity and very low outgassing. Four bulbs per half cavity can deliver ~ 80 W, which is more than the RF dissipation. When in operation power comes from RF

dissipation in the cavities and the lights. The temperature of the cavity is monitored and the power of the bulbs is regulated to maintain a constant temperature of 50 C. See figure 6.



Figure 6: The three vacuum tanks of the new longitudinal kickers for the blue ring.
Spot lights shine through glass windows to keep the cavities at 50 C.

2.7.5.2 Vacuum

The vacuum tanks have a rectangular shape. This makes it difficult to make a reliable metal-to-metal demountable seal. Instead the top plates of the tanks are welded to tank bodies. Circular ports with standard conflat flanges at the windows allow access to the tuners if necessary. Major access would require cutting the weld so the joint was designed to accommodate rewelding. The tanks are baked at 150 C for 48 hours after installation. Vacuum levels are $\sim 6e-11$ Torr at 50 C and $<1e-11$ Torr at room temperature.

2.7.5.3 Tune Up of the Cooling System

The first step in switching on the cooling system is to make system transfer function measurement with a network analyzer. A transfer switch in the low-level electronics allows interjection of a test signal and connection to the return signal around the entire path of the cooling loop. That includes kicker, beam response, pickup output, signal transmission via the microwave link, revolution frequency notch filter, and low-level gain and phase control. Figure 7 is a polar plot of a typical transfer function measurement over one revolution harmonic. The response shows zero amplitude at the revolution frequency because of the notch filter. The plot is normalized such that full scale corresponds to optimal system gain and the phase shown is approximately correct. With these setting the cooling loop is closed and signal suppression is checked with the spectrum analyzer. Small corrections are usually made to the phase to balance the signal suppression between the high and low frequency sides of the revolution harmonic. The need for corrections comes from the difference in phase of the kickers when excited by the CW signal from the network analyzer and the pulsed signal from the bunched beam. The transfer function is measured again and saved as the “reference transfer function”. When cooling is in operation the transfer function is periodically re-

measured and gain and phase setting are updated to replicate the “reference transfer function”. The main need for corrections are drifts in cable delays, temperature variation of kickers, and changing emittance of the cooled beam.

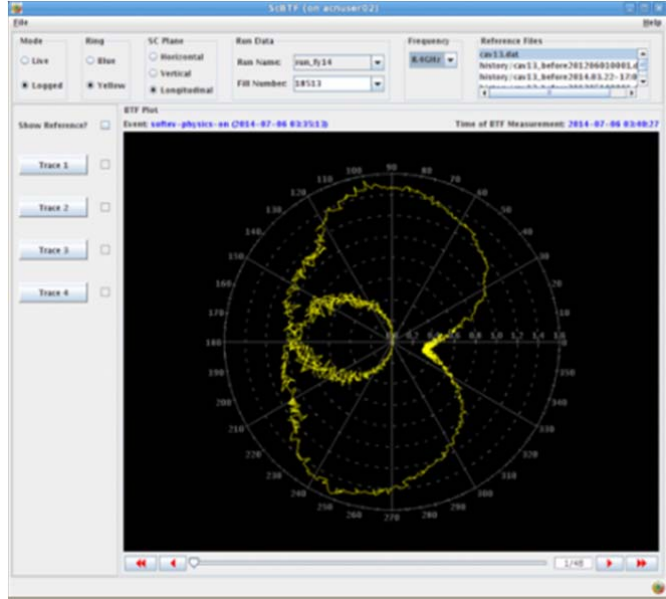


Figure 7: Longitudinal cooling system transfer function at 8.4 GHz. The amplitude is very close to zero at the revolution because of the notch filter. Full scale corresponds to unity gain for optimal cooling

2.7.6 Summary

New kickers have been built and commissioned for the longitudinal stochastic cooling system for RHIC. The new kickers improve reliability, vacuum performance, and provide more kick voltage. Key features of the new design are increased kick voltage from 6-cell cavities, improved vacuum performance by eliminating coaxial cables and cooling pipes in the vacuum and better reliability because of frictionless mechanical design of moving parts. The new kickers were commissioned and operated in the highly successful FY2014 RHIC.

2.7.7 References

1. Burn-off Dominated uranium and asymmetric copper-gold operation in RHIC, Y. Luo, W. Fischer, M. Blaskiewicz, J. M. Brennan, N. Kling, K. Mernick, and T. Roser, *Phus. Rev. ST Accel. Beams*, July 2014
2. Three-Dimensional Stochastic Cooling in the Relativistic Heavy Ion Collider, M. Blaskiewicz, J.M. Brennan, and K. Mernick, *Phys. Rev. Lett.* 105, 094801, 2010
3. Full 3D Stochastic Cooling at RHIC, K. Mernick, M. Blaskiewicz, J.M. Brennan, *Proceedings of PAC2013, Pasadena CA USA*.
4. Stochastic Cooling in RHIC, J.M. Brennan, M. Blaskiewicz, K. Mernick, *Proceeding of IPAC2012, New Orleans, USA*
5. Bunched Beam Cooling for the Tevatron, R. Pasquinelli, *PAC 1995*, p2379
6. D. Boussard, *CERN Accelerator School*, 87-03, Vol II, p423
7. C-Flex Bearing Co. www.c-flex.com

2.8 2 MeV Electron Cooler at COSY Juelich

J. Dietrich¹, V. Kamerdzhev², V.V. Parkhomchuk³, V.B. Reva³, M.I. Bryzgunov³

¹ Technische Universität Dortmund, Germany

² Forschungszentrum Juelich GmbH, Germany

³BINP, Novosibirsk, Russia

Mail to: juergen.dietrich@tu-dortmund.de

2.8.1 Introduction

Electron cooling is a very useful technique for obtaining high-intensity ion beams with low emittance and low momentum spread [1]. This method allows, increasing the phase-space density of an ion beam by means of Coulomb interaction of a “hot” ion beam with a “cold” electron beam. The ion beam repeatedly transfers its thermal energy to the electron beam moving with the same velocity. The electron cooling can be described by the simple plasma ion-electron model of the temperature relaxation. The first experimental results confirmed this fact. After modernization of the experimental setup the cooling time was decreased significantly [2]. The homogeneity of the magnetic-field in the cooling section was improved to 10^{-4} and the stability of the electron energy was improved to 10^{-5} . The theoretical and experimental investigations have shown a significant effect of a strong longitudinal magnetic field on the collision dynamics of electrons and ions. This effect distinguishes the electron cooling from the usual relaxation of a two-component plasma [3]. If the path length of the ion inside the electron beam is many times larger than the electron Larmor radius, the interaction can be described as Coulomb interaction with the electrons slowly moving along the magnetic field. The ion does not interact with a single electron but with a blur Larmor circle.

There are many experiments and theoretical calculations that show the usefulness of the magnetized cooling. This work was done in the different scientific centres in the world. The MOSOL experiments [4] and VORPAL calculations [6] show a slight growth of the friction force with growth of the value of the longitudinal magnetic field. The articles [7, 8] show the decreasing influence of the transverse velocity on the cooling rate. The transverse velocity was induced by a kick introduced by the electrostatic plates. The kick effect was observed in the recombination rate but the measured cooling rate did not change significantly. The work [9] deals with the investigation of the cooling force in the S-LSR device. A comparison of the experimental facts with the different theory models was done. The rate calculated according to Parkhomchuk’s equation [5] was the closest to the experimental data.

The basic idea of the new 2 MeV electron cooler at the Cooler Synchrotron COSY in Juelich is to use high magnetic field along the orbit of the electron beam from the electron gun to the electron collector. In this case sufficiently high electron beam density at the cooling section can be achieved with low effective temperature.

The 2 MeV cooler at COSY is the first device utilizing the idea of magnetized cooling in this energy range, being an important step towards relativistic electron cooling required for the HESR at FAIR [10, 11]. Furthermore, it has been shown, that the 2 MeV cooler, if installed in the HESR, can be used for the heavy ion operation modes [12, 13].

First ideas on the 2 MeV cooler were formulated in 2003. The first report was published in 2005 [14]. The construction of the 2 MeV electron cooler for COSY began at the Budker Institute of Nuclear Physics (BINP) in 2009 and ended 2012. In spring 2013 the cooler was installed in the COSY ring. First beam cooling results were obtained in October 2013 by the joint BINP-COSY team. Further beam cooling experiments followed during a two-week period of dedicated beam time in the beginning of 2014. At that time a first attempt to use electron and stochastic cooling in the same machine cycle was made. Furthermore, electron cooling of proton/deuteron beam into a barrier bucket was demonstrated. The design of the cooler and its main parameters are described in [15, 16].

2.8.2 Basic Design Features

The basic parameters of the COSY cooler are listed in Table 1 [15]. The length of the cooling section is given by the space available in the COSY ring.

Table 1: Basic Parameters and Requirements

COSY 2 MeV Electron Cooler	Parameter
Energy Range	0.025 ... 2 MeV
High Voltage Stability	$< 10^{-4}$
Electron Current	0.1 ... 3 A
Electron Beam Diameter	10 ... 30 mm
Length of Cooling Section	2.69 m
Toroid Radius	1.00 m
Magnetic Field (cooling section)	0.5 ... 2 kG
Vacuum at Cooler	$10^{-9} \dots 10^{-10}$ mbar
Available Overall Length	6.39 m
Maximum Height	5.7 m
COSY Beam Axis above Ground	1.8 m

The schematic design of the electron cooler is shown in Fig. 1. The electron beam is generated in an electron gun immersed into the longitudinal magnetic field. An electrostatic generator consisting of 33 individual sections connected in series provides the accelerating voltage. After acceleration the electron beam moves into the transport line to the cooling section where it interacts with protons of the COSY storage ring. After interaction the electron beam returns to the electrostatic generator where it is decelerated and absorbed in the collector.

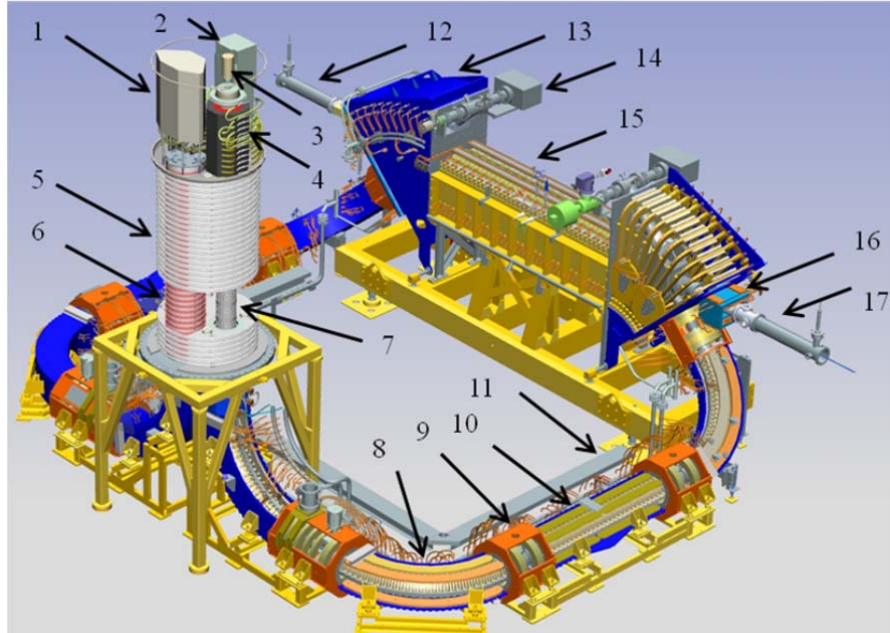


Figure 1: Design of the 2 MeV cooler. 1- collector power supply, 2 – electronics rack housing the power supplies of the electron gun, Wien filter, suppressor electrode and the coils, 3 - ion pump of the collector, 4 - collector with its magnetic system , 5 - HV section, 6 - cascade transformer, 7 - acceleration tube , 8 - 90 degrees bend, 9 - straight section, 10 - line section, 11 - cable tray, 12 - proton beam entry, 13 – 45 degrees toroid, 14 - vacuum pump, 15 - cooling section, 16 - ion dipole, 17 - ion beam exit.

The electron gun (see Fig. 3) and the collector are located in the high-voltage terminal (HVT) on top of the accelerating column. In addition the HVT contains electronics blocks providing control for the elements of the electron gun (filament, four control electrodes, anode), collector (collector rectifier, Wien filter electrodes, suppressor), power supplies of the coils, ion pumps and diagnostics.

The most power is consumed by the collector power supply, with up to 15 kW output power. Therefore it was designed as a standalone unit equipped with an oil cooling system. The power supplies of the magnet coils and the power supplies of the remaining electrodes are located in a separate electronics rack.

Each HV section of the HV generator contains two high-voltage power supplies providing voltage up to 30 kV and current up to 1 mA, two coils forming the magnetic field in the acceleration tubes, the section of the cascade transformer providing primary power to the electronics, the electronics module and oil pipes in order to remove the heat (see Fig.2). The electronic module of the section is located in a metal box to prevent sparking from effecting the electronics. Each section is installed on the polyamide isolators. The hight of one section is 40 mm. The distance between sections is 20 mm. Each section is surrounded by a guard ring. The electrostatic accelerator is located in a pressure vessel filled with SF₆ gas at 6 bar. The energy for the HV sections is provided by the corresponding section of the cascade transformer (see Fig.2). In the transformer the electrical energy is transmitted from section to section from the ground to high-voltage terminal. Along this way the energy is also consumed by the regular high-voltage sections. The transformer is put inside the vessel filled with oil for HV isolation and cooling.

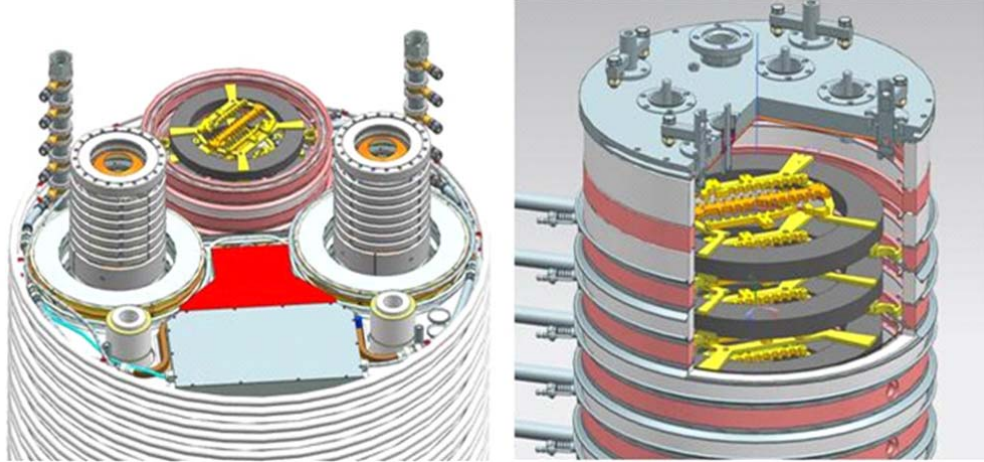


Figure 2: Design of the HV section (left picture) and cascade transformer (right picture).

The main problem of this design is the leakage magnetic field from the transformer core. This problem can be solved by adding compensative capacitance. The transformer column has its own spark-gap system for safety in case of gas breakdown.

The requirement to operate in the wide energy range from 25 keV to 2 MeV leads to the necessity of strong longitudinal magnetic field along the whole trajectory from the gun to the collector. So, the bending magnets and linear magnets contain solenoid coils. The sections made of large coils are intended to house the BPMs (beam position monitor), vacuum pumps. They also provide the required access to the beam pipe during assembling. The length of the linear magnets is defined by the necessity to locate the electrostatic generator outside the shielded area of the storage ring.

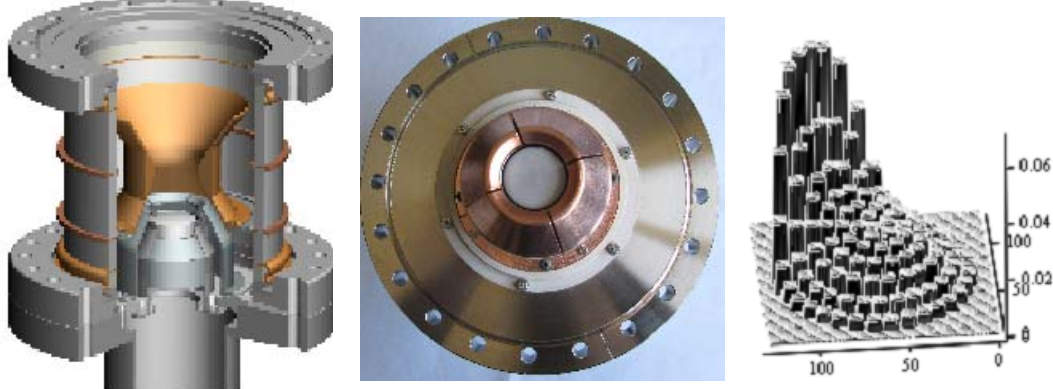


Figure 3: Design of the electron gun including the 4-sector control electrode. The right picture shows the distribution of the electron current when the control voltage is applied to a single sector.

A unique feature of this cooler is the possibility to perform *in situ* measurements of the transverse components of the magnetic field in the cooling section. This is done without breaking vacuum by a probe similar to the one described in [17]. The probe consists of a ferromagnetic rod and a mirror attached to it whose plane is perpendicular to the solenoidal field. This unit is installed into a gimbal that allows the magnetic body to align itself along the magnetic field lines. The sensor is mounted on a cart that can be

moved along the solenoid axis. A laser beam directed along the axis of the vacuum chamber is reflected by the mirror to a position sensitive photo detector. A signal proportional to the displacement of the laser spot controls the current in the corrector coils surrounding the vacuum chamber. These currents produce magnetic fields compensating the transverse components of the magnetic field. As a result the laser spot moves to the detector center and values of the transverse field components are determined from current values in the compensating coils.

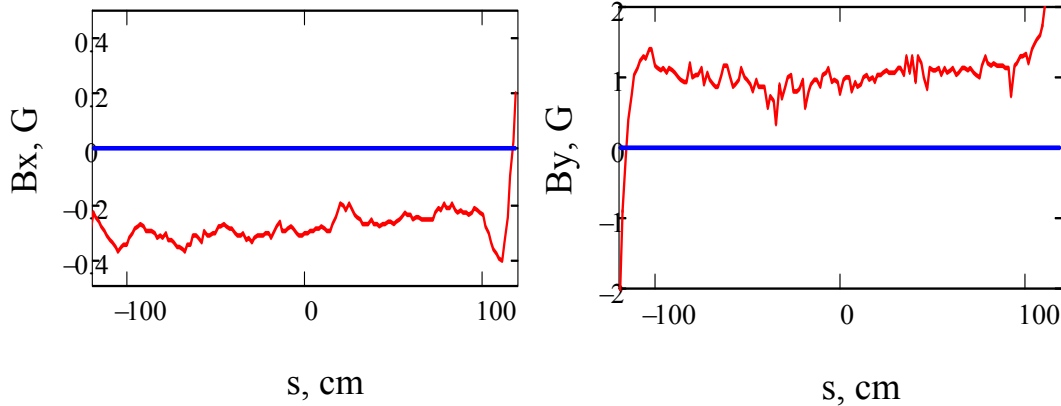


Figure 4: Results of the magnetic field measurements.

Some of the results obtained during the commissioning at COSY are presented in Fig.4. Transverse components of the magnetic field were measured in the cooling solenoid during the machine maintenance period in summer 2014. After performing the tuning procedures the rms noise of the horizontal component of the magnetic field amounted to $B_x/B=3\cdot 10^{-5}$ at the length of 200 cm and the noise of the vertical component to $B_y/B=10^{-4}$. The magnetic field in the cooling section was set to 1364 G at 241 A. The noise of the vertical component measurements is higher most likely due to different sensitivity of the compass to vertical and horizontal mechanical oscillations. The constant angle of the magnetic field in the cooling section is removed by means of long transverse correctors in the cooling section.

2.8.3 Diagnostics and Commissioning

The beam line is equipped with several types of beam diagnostics devices. The electron beam trajectory is measured by 12 BPMs. The two BPMs installed in the cooling section are also capable of measuring the proton beam position. The effective cooling demands minimization of the electron angles and envelope oscillation of the beam. For this purpose the electron gun is equipped with a 4-sector control electrode (see Fig. 3). An AC modulation signal can be applied to each sector of the control electrode. So, the position of one quadrant sector of the electron beam can be measured by the BPM system. Comparing the positions of each sector BPM by BPM or the sector positions in a single BPM for different corrector coils settings it is possible to analyze the optics of the electron beam transport channel.

Fig. 5 demonstrates the performance of the four-sector BPM system. The size of the electron beam changes depending on the DC voltage applied to the control electrode. The negative voltage decreases the radius of the electron beam. Fig. 6 shows the ability

of this system to measure the rotation of the electron beam induced by the space charge. One can see that the rotation angle accumulates from the first to last BPM and there is a dependence of rotation angle upon the electron current.

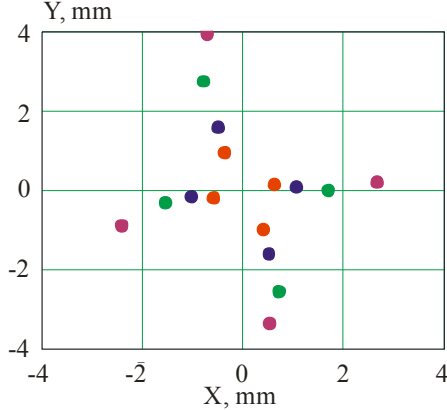


Figure 5: Beam size changing at the different DC voltage applied to the control electrode. The voltages of the control electrode are 0, -0.2, -0.4, -0.6 kV for points from outside to inside. The voltage of the anode is 1.4 kV.

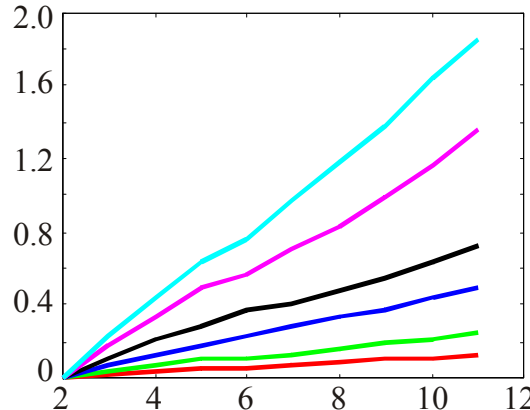


Figure 6: Rotation angle accumulating along the electron trajectory versus BPM number, Y-axis is radians. The electron current is changed from 50 to 400 mA (the curve from bottom to top).

The verification of the beam shape can be done independently by a set of Faraday cups located in 9 (see Fig. 1). The electron beam is guided by the correctors onto the diagnostics device. In order to minimize the load of the electrostatic generator the electron beam was pulse modulated (5 μ s pulse at 20 Hz repetition rate). So, the electrostatic generator is able to work in nominal regime because the average DC current to the ground is small enough. Fig.7 shows the measured profile with the parameters of the electron gun $U_{\text{grid}}=0$, $U_{\text{anode}}=1$ kV, $J_{\text{impulse}} \approx 30$ mA. This measurement agrees well with the calculations and previous measurement with a similar gun.

The electron beam should stay for hours at the nominal energy and currents. Continuous operation of the cooler with 200 mA electron beam at 1 MeV for six days showed an acceptable reliability level of the device.

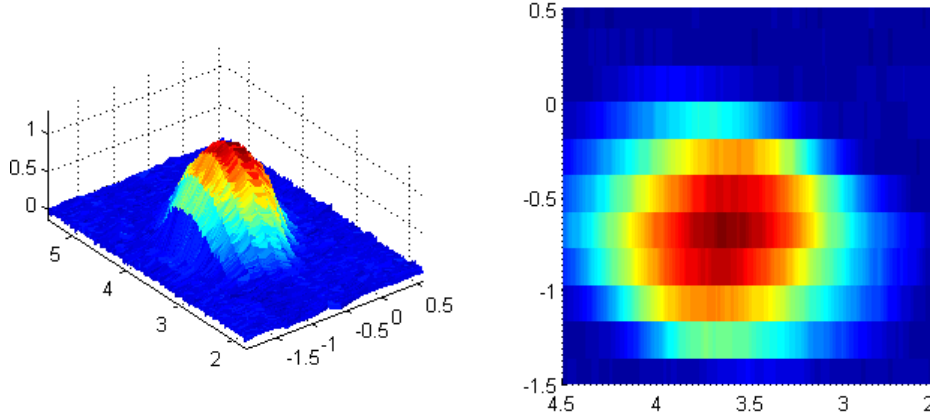


Figure 7: Profile of the electron beam measured with a set of Faraday cups.

2.8.4 First Experimental Results at COSY

Table 2 summarizes the electron and proton beam parameters during the recent cooling experiments [18]. The experimental results presented below are for a dc proton beam.

Table 2: Beam parameters used for cooling

Proton energy, MeV	Electron energy, keV	Max. electron current, mA
200	109	500
353	192	500
580	316	300
1670	908	340

2.8.4.1 Cooling at 200 MeV

At this energy the magnetic field in the cooling section was set to 480 G. Fig. 8 shows the result of transverse cooling of a dc proton beam using 200 mA electron beam at 109 keV. The number of protons in the ring was intentionally lowered to $1 \cdot 10^8$ to exclude intensity effects and to minimize the particle loss rate.

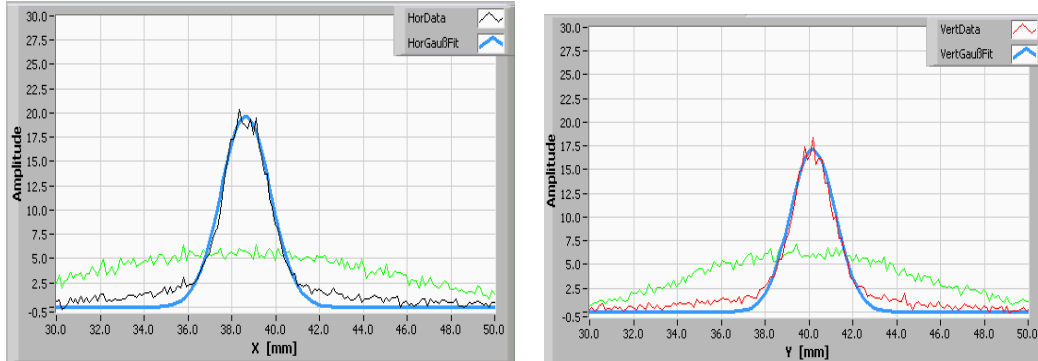


Figure 8: Horizontal and vertical profiles of the electron cooled proton beam. Profiles of an uncooled beam are shown in green, cooled beam profiles in black and red, the corresponding Gaussian fits in blue. Beam widths $\sigma_{\text{hor}} = 1.2$ mm and $\sigma_{\text{vert}} = 1.15$ mm were measured.

The Ionization Profile Monitor (IPM) was used to acquire beam profile data in real time [19]. Fig. 9 and Fig. 10 show transverse and longitudinal cooling in the same machine cycle. The cycle duration was set to 514 s. At $t = 30$ s in the cycle (flat top) the electron current was ramped up to 200 mA causing the beam to shrink transversally and longitudinally. At this energy cooling was also accompanied by significant beam losses.

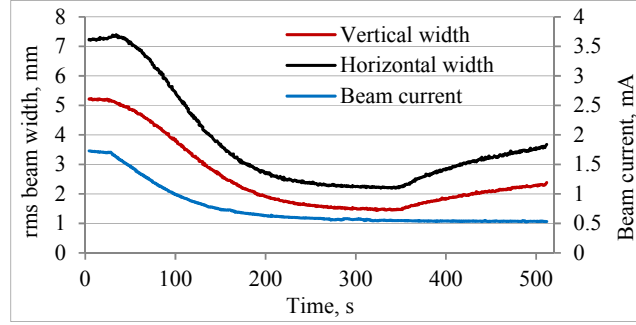


Figure 9: Evolution of horizontal and vertical beam width and beam current. The 200 mA electron beam was turned on at $t = 30$ s and turned off at $t = 350$ s.

In the middle of the machine cycle about $4 \cdot 10^9$ particles remained in the ring. After the e-beam was turned off at $t = 350$ s, the proton beam size as well as the width of the longitudinal spectra increased again due to intra-beam scattering. In contrast to the initial cooling the beam can be cooled again (not shown in Fig. 9 and 10) without losses. A standard COSY beam position monitor was used to measure the Schottky spectra [20].

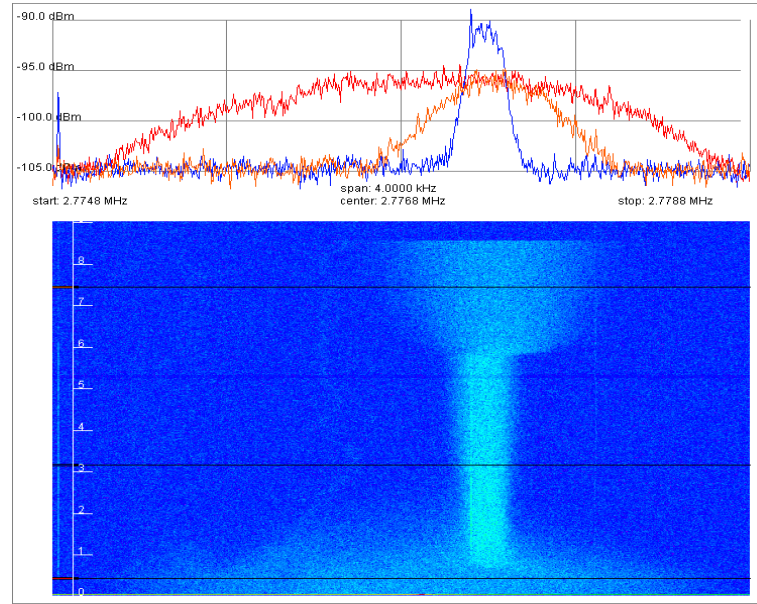


Figure 10: Evolution of the longitudinal Schottky spectra. The 200 mA electron beam was turned on at $t = 30$ s and turned off at $t = 350$ s. The upper plot shows the spectra of the uncooled (red) and cooled (blue) beam and a spectrum after the e-current was turned off (orange). Black lines represent the corresponding time markers in the spectrogram (lower plot). Time scale in minutes is shown on the left edge of the spectrogram.

2.8.4.2 Cooling at 1670 MeV

At 1670 MeV the magnetic field in the cooling section was set to 1.3 kG.

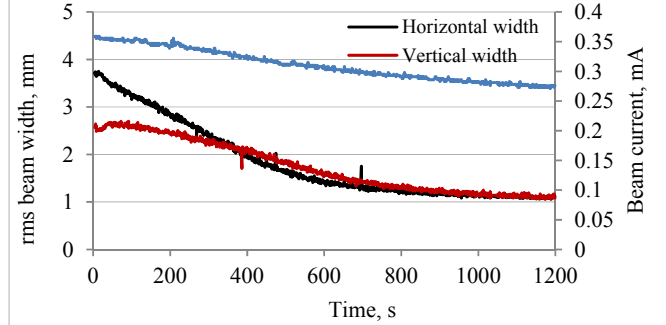


Figure 11: Evolution of the beam width and proton beam current during electron cooling with 320 mA.

In addition to Fig. 11 showing the effect of electron cooling on transverse beam size, the effect of precooling using the stochastic cooling system is shown in Fig. 12.

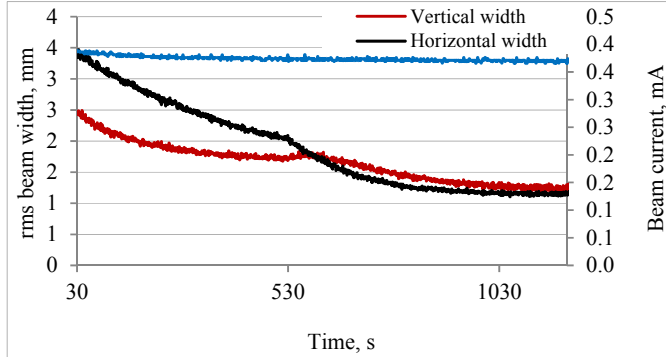


Figure 12: Evolution of the beam width and beam current during transverse stochastic (first half of the machine cycle) and electron cooling with 320 mA (second half).

Horizontal and vertical stochastic cooling was active in the first half of the machine cycle leading to a significant reduction of the transverse beam size without significant beam loss. The longitudinal behavior of the beam in the same machine cycle is shown in Fig. 13. One can see that the beam becomes wider due to the absence of longitudinal cooling in the beginning. Fast cooling of the beam core and somewhat slower cooling of the tails of the distribution has been observed after electron cooling was turned on at $t = 2$ min.

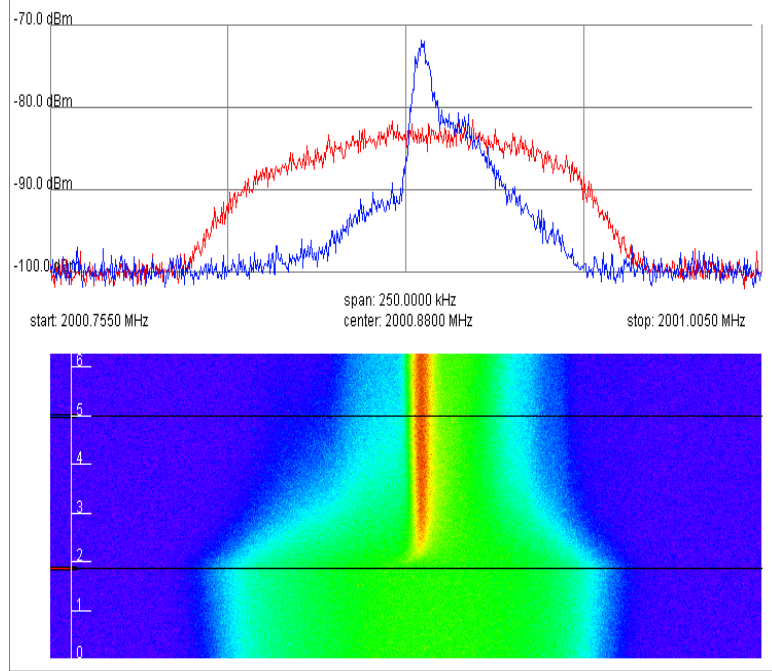


Figure 13: Longitudinal electron cooling of proton beam at 1670 MeV. A pickup of the stochastic cooling system was used to measure the Schottky spectra [21]. Only a part of the machine cycle is shown. Transverse stochastic cooling was active until $t = 2$ min, after that electron cooling was turned on. In the upper plot the red curve corresponds to the longitudinally uncooled beam while the blue one shows the spectrum of the cooled beam.

2.8.5 Conclusion

The 2 MeV electron cooler is being put into operation at COSY. The first series of experiments were carried out by the joint BINP-COSY team. Electron cooling of a proton beam up to 1670 MeV corresponding to 908 keV electron energy was demonstrated. The maximum electron beam energy achieved so far was 1.25 MeV. A high voltage up to 1.6 MV was obtained. Cooling of a deuteron beam at low energy was successful. Cooling into a barrier bucket as well as simultaneous electron and stochastic cooling was successfully demonstrated. The first impression is that the overall cooling time becomes shorter; the two systems however, need to be carefully matched. The emphasis of the recent experiments was put on the cooler hardware. The interaction of the cooler with the machine, in particular the cooling rates will be studied in detail during the upcoming dedicated beam time. The data obtained so far suggests a more favorable scaling of the cooling time with energy as compared to the $\beta^4 \gamma^5$ scaling [11]. At low energy a significant beam loss was observed during the cooling process, similar to the losses typically observed using the 100 kV cooler [22]. At higher energies the losses are much less pronounced. The loss mechanism has to be investigated in more detail. During the machine maintenance period in summer 2014 the straightness of the magnetic field in the cooling section was significantly improved. This is expected to improve the cooling performance at high energies. The recently developed software includes an automated correction of uncompensated transverse kicks, the electron beam experiences when passing the bent sections of the transport line. This is the first step towards a model based operation of the cooler.

2.8.6 Outlook

Further hardware and software upgrades of the cooler are being considered. The installation of a data logger in the high voltage terminal is scheduled for the end of 2014. This device is intended to continuously record the status of the equipment inside the HVT to allow offline analysis after an unexpected event occurred (e.g. interlock trip). Adaptive oil flow control depending on the operational mode of the cooler will further minimize the risks of oil leakage inside the HV-System. Additional software incorporating a higher degree of automation is close to completion and is scheduled for commissioning by the end of 2014. Further joint (BINP-COSY) electron cooling beam studies are scheduled in 2014 and 2015.

Experiments at the High Energy Storage Ring (HESR) require magnetized electron cooling at proton beam energies up to 15 GeV. The next step is to develop electron cooling systems with electron energies 4-8 MeV and beam currents up to 3 A. One of the challenges in the future HESR electron cooler is the powering of HV-solenoids. The development of prototypes is underway now [23].

2.8.7 References

1. A.N. Skrinsky, V.V. Parkhomchuk, "Physics of elementary particle and atomic nucleus", v.12 (1981), N.3, p. 557-613.
2. I.N. Meshkov, "Physics and technique of electron cooling", RIKEN-AF-AC-2, 1997.
3. Ya. S. Derbenev and A. N. Skrinsky, Particle Accelerators, 1978, Vol. 8, p. 235-243.
4. N.S. Dikansky, V.I. Kudelainwn, V.A. Lebedev et al., "Ultimate possibilities of electron cooling", BINP, Preprint 88-61.
5. V.V. Parkhomchuk, Nucl. Instr. Meth. A 441 (2000), p. 9-17.
6. A. Fedotov, D. Bruhwiler, A. Sidorin et al., Physical Review Special Topics Accelerators and Beams 9, 074401 (2006).
7. P. Beller, K. Beckert, B. Franzke et al, Nuclear Instruments and Methods in Physics Research A 532 (2004) p.427–432.
8. V.V. Parkhomchuk, "Review of cooling investigation at the Novosibirsk INP", Proc. of the 31st Workshop of INF Eloisotron Project, Crystaline beams and related issues, Erice, Italy, Nov.1995/, p.409-419.
9. T. Shirai, S. Fujimoto, M. Ikegami et al, Proceedings of COOL 2007, Bad Kreuznach, Germany THM1I02.
10. FAIR Conceptual Design Report (CDR), GSI 2004, <https://www-alt.gsi.de/documents/DOC-2004-Mar-201.html>.
11. M. Bryzgunov et al., "Conceptual project relativistic electron cooler for FAIR/HESR", Proc. of IPAC2014, Dresden, MOPRI074, p.774-776.
12. Th. Stöhlker et al., "SPARC experiments at the HESR: a feasibility study"; https://www.gsi.de/fileadmin/SPARC/documents/SPARC@HESR_FS_V26.pdf.
13. T. Katayama et al., "Electron cooling of heavy ions interacting with internal target at HESR of FAIR", MOPEA017, IPAC2013.
14. "Electron cooling for COSY", report, Novosibirsk, September 2005.
15. "2 MeV electron cooler for COSY", conceptual design report, Novosibirsk, November 2009.
16. V.B. Reva et al., "COSY 2 MeV cooler: design, diagnostic and commissioning", Proc. of IPAC2014, Dresden, MOPRI075, p. 777-779.
17. V. Bocharov, A. Bubley, S. Konstantinov, V. Panasyuk, V. Parkhomchuk, "Precision measurements and compensation for the transverse components of the solenoids

- magnetic field”, Instruments and Experimental Techniques, Vol. 48, Number 6, 2005, p. 772.
18. N. Alinovskiy et al., “2 MeV electron cooler for COSY and HESR- first results”, Proc. of IPAC2014, Dresden, MOPRI070, p. 765-767.
 19. C. Böhme et al., “Beam test of the FAIR IPM prototype in COSY”, TUPB12, DIPAC2009.
 20. J. Bojowald et al., “Diagnostic tools for the COSY-Juelich Synchrotron” EPAC1994.
 21. P. Brittner et al., “The stochastic cooling system of COSY”, EPAC1992.
 22. H.J. Stein et al., “Present performance of electron cooling at COSY - Juelich”; <http://arxiv.org/ftp/arxiv/papers/1101/1101.5963.pdf>
 23. A. Hofmann et al., ”Turbo generators for powering the HV-solenoids at the HESR electron cooler”, Proc. of IPAC2014, Dresden, MOPME051, p.492-494.

2.9 Beam Cooling at GSI

F. Nolden, M. Steck
 GSI Helmholtzzentrum, Planckstr.1 D-64291 Darmstadt, Germany
 Mail to: M.Steck@gsi.de

2.9.1 Introduction

Beam cooling activities at the GSI Helmholtz Centre started with the SIS/ESR project around 1985. The availability of cooled heavy ion beams was expected to offer unique opportunities for experiments with stored beams. Therefore already in the design phase the installation of both stochastic and electron cooling in the storage ring ESR was foreseen. The electron cooling system was installed from the beginning and was available during the commissioning in 1990, whereas the stochastic cooling system was installed and commissioned in 1995. Since then these systems have been continuously improved and employed in physics experiments.

In order to overcome a lack of intensity for beams of the heaviest species and of rare isotopes an electron cooling system was installed in the synchrotron SIS in 1998. It cools the heavy ion beam at injection energy and allows stacking of the beam by an accumulation method which is based on multiple multiturn injection in combination with fast transverse cooling.

2.9.2 Beam Cooling in the ESR Storage Ring

2.9.2.1 *ESR Electron Cooling*

Electron cooling in the ESR serves various purposes. The main application is cooling for experiments with stored ion or rare isotope beams. These beams are accelerated in the heavy ion synchrotron SIS to the required energy. The ESR electron cooling system presently covers the energy range from 3 to 430 MeV/u, corresponding to electron energies from 2 to 240 keV. In experiments with the internal gas jet target electron cooling compensates the energy loss and longitudinal and transverse scattering of the stored ions. The electron beam serves also the purpose of a target of free electrons either at zero relative velocity or with finite adjustable relative longitudinal velocity, which is achieved by detuning of the electron energy.

In various operational modes the electron cooling system supports the preparation of the beam or is essential part of internal experiments. During deceleration of highly charged ions electron cooling counteracts the increase of momentum spread and emittance. The bunching of ions is supported by forcing them into the bucket which is generated by the rf system and the momentum spread and consequently the bunch length is reduced. Beam accumulation is possible due to the fact that phase space compression provides space for the injection of more particles into a phase space volume which was previously occupied by already stored particles. In all these procedures electron cooling is applied in the ESR and has significantly improved the overall performance.

The ESR electron cooling system [1] has a rather traditional design with a cathode installed in a longitudinal magnetic field which is constant along the electron beam path. This way a cold electron beam with a diameter of 2 inches is produced which interacts in a cooling section of 2.5 m length with the ion beam. The magnetic field strength is typically 0.1 T for beams of energy higher than 200 MeV/u and has to be reduced at lower beam energies, as the closed orbit distortion for beams with lower magnetic rigidity increases to values which do not allow the achievement of a stable ion beam orbit. In the electron gun with a perveance of 1.9 μ P the anode voltage defines the electron beam current which is subsequently transported to the cooling section in the constant magnetic field, thus maintaining the electron beam diameter. The electron beam collector uses an electrostatic repeller potential and a decreasing magnetic field to suppress the emission of reflected electrons and their backstreaming into the cooling section. Thus relative loss currents in the low 10^{-4} range are achieved routinely. The whole electron beam section is operated with a vacuum in the low 10^{-11} mbar range which is mandatory for the storage of heavy ions over extended periods.

The main application of the electron cooling system in the ESR is associated with experiments with stored heavy ion beams. The parameters of the stored beams under the influence of electron cooling were studied in great detail [2]. The transverse emittance and the longitudinal momentum spread values which can be achieved with electron cooling are mainly determined by the equilibrium between electron cooling and intrabeam scattering. This is even true, if the internal target is operated with moderate thickness (less than 10^{13} particles/cm²). Only for rather high target thickness or a target that consists of heavy particles an influence of the target on the equilibrium values was observed [3]. In the intrabeam scattering dominated regime the equilibrium values for the transverse emittances increase typically with the square root of the number of stored ions $\varepsilon \propto N^{1/2}$, the momentum spread increases approximately with a power scaling law $\delta p/p \propto N^{0.3}$. This dependence is the result of the compensation of the intrabeam scattering growth rate by the cooling rate. As a consequence the best conditions for precision experiments are achieved for lower beam intensities.

Extreme beam parameters were demonstrated for very small numbers of stored particles. In experiments with very low intensity ion beams a suppression of intrabeam scattering was evidenced [4]. In the first experiments it was observed that the momentum spread drops suddenly by up to one order of magnitude when the number of ions is reduced below approximately one thousand, almost independent of the ion species. This indicated that the intrabeam scattering rate for such small particle numbers is lower than the cooling rate, in agreement with the observation of a dependence of the effect on the electron current, i.e. the cooling rate. In subsequent dedicated experiments it could also be confirmed that a corresponding discontinuous reduction of the

transverse emittance occurs [5]. In accordance with computer simulations, it was concluded from these experiments that for low intensities the beam enters a state of linear ordering with the particles forming a linear chain with tiny transverse beam size. The small momentum spread of the low intensity beam with a value $\delta p/p \leq 1 \times 10^{-6}$ was favorably used in experiments. Particularly, mass measurements of rare isotopes with the Schottky Mass Spectrometry [6] method greatly benefitted from the small momentum spread, which allows mass measurements with a mass resolving power $m/\Delta m$ on the order 10^6 .

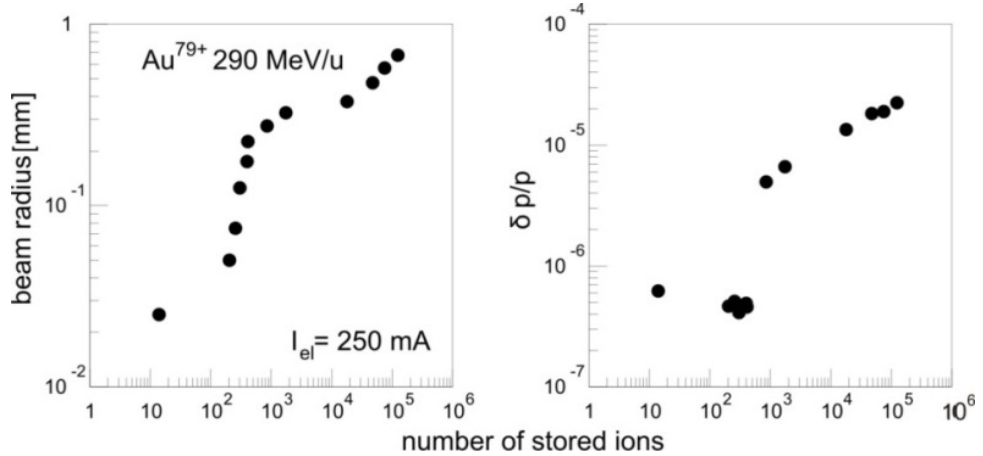


Figure 1: Discontinuous reduction of momentum spread and beam radius for small particle number of a Au^{79+} beam at 290 MeV/u cooled with an electron current of 0.25 A.

In the design of the ESR the operation as a decelerator for highly charged ions was incorporated, allowing experiments to profit from the reduction of Doppler effects due to the low velocity of the stored ions. The deceleration is supported by electron cooling which is typically used at certain energies during the deceleration process. At injection energy, typically in the range 300 – 400 MeV/u, either electron cooling or stochastic cooling is applied. As the energy of the electron beam can be easily changed by variation of the accelerating voltage of the electrons, cooling can be performed at lower energies as well. Depending on the required beam energy the cooling at the end of deceleration process is complemented by cooling at an intermediate energy, typically at 30 MeV/u when also the rf system switches from operation at the second harmonic to the fourth harmonic of the revolution frequency. To achieve a stable ion orbit the magnetic guiding field of the electron beam has to be reduced at lower energies in accordance with the reduced ion beam rigidity. Electron cooling when applied during the deceleration allows counteraction of unwanted emittance and momentum spread growth and improvement of the beam quality of the low energy beam. As an additional effect electron cooling helps to reduce beam losses during deceleration.

Another important aspect of the electron cooling of highly charged ions is the recombination between ions and electrons which has a rate which increases proportional to the square of the ion charge. Consequently it is in the first place an unwanted effect limiting the lifetime of the stored cooled beam. On the other hand, recombination is an important research subject, as it provides a wealth of information on the interaction between ions and electrons. These studies are not limited to the typical case of the cooling condition when ions and electrons have the same velocity. Experiments with

controlled changes of the relative velocity between ions and electrons were performed, particularly to study dielectronic recombination, when a bound electron is involved in the interaction and resonant excitation of the bound electron occurs. Such experiments are sensitive to the actual electron temperature. Thus a transverse temperature which is basically determined by the cathode temperature was derived from the recombination experiments to be 0.16 eV and a longitudinal electron temperature of 0.2 meV [7]. Even more detailed investigations on the electron beam parameters can be performed benefitting from the recombination effect.

2.9.2.2 ESR Stochastic Cooling

The stochastic cooling system of the ESR [8,9] was designed for the precooling of coasting secondary heavy ion beams. The final beam quality should be good enough for fast subsequent electron cooling. From the beginning the layout was such as to allow for rf stacking to an inner orbit, where the stacked beam is spatially displaced and practically neither visible to the pick-up electrodes nor disturbed by the cooling kicks. The cooling system works in a frequency band 0.9 - 1.7 GHz. A maximum cw rf power of 2.4 kW is installed, distributed equally between the three phase space subspaces. All pick-ups and kickers are installed at large dispersion (4 m for the longitudinal and vertical systems, 6.6 m for the horizontal system), because of the rf stacking option mentioned above. As a consequence longitudinal kicks always lead to horizontal blow-up, which must be compensated by horizontal cooling in order to prevent beam loss.

All the pick-up and kickers of the ESR stochastic cooling system are installed inside the vacuum chamber of magnets (both quadrupole and dipole) because of space restrictions. Meanwhile three different techniques of longitudinal cooling (Palmer, time of flight and notch filter) are available. The notch filter was added only recently and makes use of optical delay lines [10].

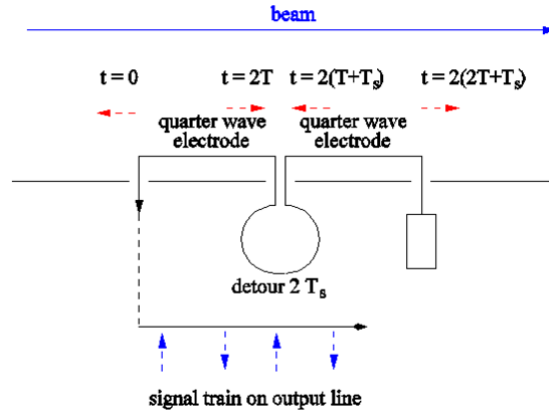


Figure 2: Schematic view of signals in a superelectrode.

The basic building block of the pick-ups and kickers are superelectrodes. A superelectrode consists of two quarter-wave or stripline electrodes in a row, with a half wave transmission line in between. The pick-up signal is extracted upstream. Ideally the signal from a single particle at the design energy would consist of four equally spaced spikes, two spikes of different sign from each quarter-wave plate. Whereas the power per unit installation length of a single quarter-wave plate is proportional to

$$\frac{P}{L} = \sin^2 \frac{f}{f_m} \frac{\pi}{2},$$

for a superelectrode it is

$$\frac{P}{L} = 2 \left[\sin \left(\frac{f}{f_m} \frac{\pi}{2} \right) \cos \left(\frac{f}{f_m} \pi \right) \right]^2$$

larger by 3 dB at mid frequency f_m at the cost of a somewhat reduced bandwidth, which however fits nicely to the one octave bandwidth of commercially available power amplifiers.

The system has always been operated at energies close to 400 MeV/u. The frequency slip factor is $\eta \approx 0.3$, which limits the momentum acceptance of the system due to undesired mixing. It is reasonable to define the momentum acceptance $\pm(\delta p/p)_{\max}$ of a stochastic cooling system by the requirement that the cooling force changes sign for these momenta at mid frequency f_m (1.3 GHz for the ESR system). Then $(\delta p/p)_{\max} = f / 2\eta f_m$, if the distance between pick-up and kicker is half the length of the closed orbit. At the ESR with a revolution frequency of roughly 2 MHz at 400 MeV/u, this leads to a momentum acceptance of just 2.5×10^{-3} .

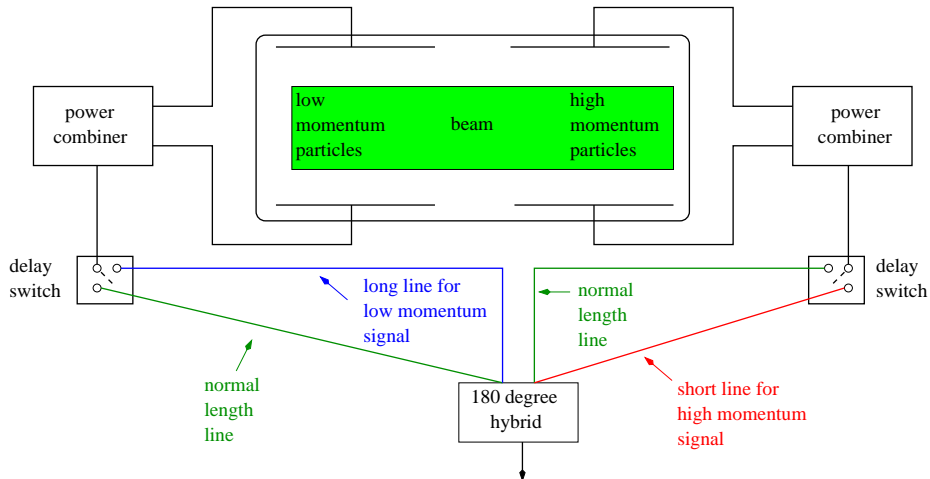


Figure 3: Signal paths with variable delays.

In order to enhance the momentum acceptance, we make use of a special scheme originally proposed by L. Thorndahl. In a normal Palmer pick-up, the momentum signal is derived from different electrodes or electrode arrays at large dispersion. In the ESR system, the electrical length between pick-up and kicker is made different for the low and high momentum parts of the signal in the beginning of cooling. These additional lengths can be made as large as $T_d = 200$ ps. This reduces the undesired mixing for the extreme parts of the momentum distribution. Therefore a much wider momentum distribution can be cooled:

$$\left(\frac{\delta p}{p} \right)_{\max} = \frac{2f}{\eta} \left[\frac{1}{4f_m} + T_d \right]$$

The initial momentum acceptance of the cooling system is doubled using these delays, fitting nicely the dynamical injection acceptance of the ESR. The difference between the two signal path lengths is gradually reduced to zero towards the end of the cooling cycle, until one gets a normal Palmer cooling system, when the momentum width reaches equilibrium. In the future it is planned to switch to filter cooling as soon as the beam momentum width is small enough.

The measured cooling rates [9] are close to the expectations [11]. The system is mostly used for the precooling of secondary ion beams followed by fast electron cooling. Typical experiments were precision Schottky mass spectrometry and nuclear lifetime experiments [6]. Typical overall stochastic precooling times are about 4 s, followed by another 2 s for electron cooling until a very well-cooled beam is ready for experiments. Very often, only a very small number of secondary particles (≈ 10) is prepared for such experiments.

A more recent development was the successful accumulation of secondary $^{56}\text{Ni}^{28+}$ ions for the measurement of nuclear properties using the internal gas jet target of the ESR [12]. About 8×10^4 secondary ions were injected in a single shot. At the end of the accumulation cycle roughly 4.8×10^6 ions were available to the experiment.

2.9.2.3 *Latest Achievements of the ESR Cooling Systems*

In recent years the ESR cooling systems were employed in studies of cooling concepts which are proposed for the Facility for Antiproton and Ion Research (FAIR) which is under construction as an extension of the existing GSI facility [13]. The ESR cooling systems were used for a comparison of realistic cooling conditions and simulation tools. The most important new concepts, which were experimentally verified at the ESR, are longitudinal accumulation methods for secondary beams, which employ both electron and stochastic cooling in combination with advanced rf systems [14,15]. From these experiments the predictive power of simulation tools can be benchmarked and the technical challenges of hardware components will be concluded.

2.9.3 **Electron Cooling in the Heavy Ion Synchrotron SIS**

The electron cooling system of the heavy ion synchrotron SIS is a dedicated cooling system for the accumulation of heavy ion beams at the injection energy 11.4 MeV/u of the synchrotron [16]. It was designed and manufactured in cooperation with the Budker Institute, Novosibirsk. In addition to the standard concept of an electron beam which is immersed in a longitudinal magnetic field, it allows a moderate transverse expansion (maximum expansion factor 8) by adiabatic reduction of the longitudinal magnetic field in the transport region between gun and cooling section. The main purpose of the expansion is the possibility to optimize the cooling time which is the figure of merit for this cooling system. On the other hand the cooling process is limited by the lifetime of the ions, which can be determined by interaction with the residual gas or by recombination of ions and free electrons. Most of the ions at the injection energy are incompletely stripped, therefore ionization to a higher charge state competes with recombination. Both processes can cause a beam lifetime in the order of seconds. The recombination with the electrons of the electron beam is due to radiative recombination or resonant recombination processes like dielectronic recombination. Consequently the lifetime due to such recombination processes can hardly be predicted.

Systematic measurements have been performed to study recombination and to choose the most favorable charge state with respect to recombination. This unfavorable situation is relieved by the fact that for heavy ions several neighboring charge states are produced in the stripper foil with comparable yield. Therefore it is possible to find for a given ion a charge state which allows accumulation with a sufficiently large gain factor.



Figure 4: Electron Cooling Device of the Heavy Ion Synchrotron SIS.

After accumulation at injection energy the ions are accelerated to the energy required by the experiment. Momentum spread and emittance of the cooled beam were measured both at injection energy and after acceleration. Measurements of the transverse emittance confirmed the expected cooling. The horizontal emittance after multturn injection of typically 100 mm mrad was reduced to a few mm mrad or even less. At the injection energy an emittance was found which for high intensity beams after accumulation increased linearly with the intensity. The linear emittance growth corresponded to a space charge driven heating according to a tune shift of about 0.1. It could be confirmed that the transverse emittance shrinks adiabatically during acceleration as expected. Measurement of the momentum spread at injection energy showed a weak dependence on the ion beam intensity with $\delta p/p \propto N^{0.37}$, similar to results at the ESR. Unlike the measured adiabatic reduction of the transverse emittance, the longitudinal momentum spread did not exhibit the expected reduction during acceleration. This is attributed to imperfections of the rf system and the absence of a phase stabilization system for the bunched beam during acceleration in the synchrotron.

The achievable gain factor of the accumulation depends on the cooling time and the lifetime of the ion beam. The cooling time is determined by the emittance after multturn injection and the longitudinal momentum spread, which can vary dependent on the tuning of the injector linac. Quantitative measurements require detailed measurements of the injection beam parameters. Even if such measurements are not routinely available, a general observation was that the cooling time for highly charged ions is on the order of a few hundred milliseconds. Consequently the cooling time allows an increase of the intensity at the injection energy of the synchrotron within a few seconds by an order of magnitude. Other processes, however, can limit the intensity. The lifetime of the ion beam in the residual gas can vary with the ion species and the charge state, therefore no general estimate of the gain factor due to residual gas interaction can be given. Intensity increases by one to two orders of magnitude for the beam accelerated in the SIS have been achieved for different ions compared to the intensity after a single multturn injection. Further intensity limitations are caused by transverse instabilities, as no transverse feedback system is presently available in SIS. In the condition of transverse instabilities it was even found that strong cooling by high

electron currents results in a faster loss rate, probably due to the higher phase space density of a strongly cooled beam. Transverse instabilities were the main limitation when the highest intensities of highly charged ions like uranium were accumulated. For U⁷²⁺ ions with the injection energy of 11.4 MeV/u the intensity maximum with electron cooling assisted accumulation was 3×10^9 ions with a total cooling time of 200-300 ms for the beam after multturn injection.

The largest benefit of the beam accumulation in SIS is achieved if the accelerated ion beam is transferred to the ESR storage ring as the storage time in the ESR is much longer than the time needed for accumulation in SIS. The efficiency of the beam transfer from the synchrotron to the storage ring is improved due the small emittance of the cooled beam which reduces losses in the beamline and during injection into the storage ring. Another application of the cooled synchrotron beams are plasma physics experiments which require a short intense bunch of highly charged ions focused onto a small spot.

In contrast to fast extraction, for operation of the synchrotron with slow extraction the average intensity is reduced by the fraction of time which is spent on accumulation. The horizontal beam emittance during slow extraction is determined by the extraction method and does not conserve the emittance of the cooled beam, only the reduction of the vertical emittance can in certain cases provide improved conditions for experiments.

In recent years primary heavy ion beam intensities have been increased for many species from the linear accelerator which injects into the SIS. Nevertheless, the SIS electron cooling system still offers valuable benefits, whenever small transverse beam emittance is required after the synchrotron or for the accumulation of species which can be produced in the ion source with small intensity.

2.9.4 References

1. N. Angert, W. Bourgeois, H. Emig, B. Franzke, B. Langenbeck, K.D. Leible, T. Odenweller, H. Poth, H. Schulte, P. Spädtke, B.H. Wolf, The 320 keV ESR Electron Cooler, Proc. EPAC'90 (1990) 1374-1376.
2. M. Steck, P. Beller, K. Beckert, B. Franzke, F. Nolden, Electron Cooling Experiments at the ESR, Nucl. Instr. Meth. In Phys. Res. A 532 (2004) 357-365.
3. V. Gostishchev, C. Dimopoulou, F. Nolden, M. Steck, A. Smirnov, Comparison of Measurements and Simulations of Internal Target Effects in the ESR Storage Ring, Nucl. Instr. Meth. in Phys. Res. A 461 (2011) 12-18.
4. M. Steck, K. Beckert, H. Eickhoff, B. Franzke, F. Nolden, H. Reich, B. Schlitt, T. Winkler, Anomalous Temperature Reduction of Cooled Heavy Ion Beams in the Storage Ring ESR, Phys. Rev. Lett. 77 (1996) 3803.
5. M. Steck, K. Beckert, P. Beller, B. Franzke, F. Nolden, Extremely Cooled Ion Beams in the ESR with Evidence of Ordering, Proc. PAC'01 (2001) 137-141.
6. B. Franzke, H. Geissel, G. Münzenberg, Mass and Lifetime Measurements of Exotic Nuclei in Storage Rings, Mass Spectrometry Reviews, 2008, 27, 428-469.
7. C. Brandau, C. Kozuharov, A. Müller, W. Shi, S. Schippers, T. Bartsch, S. Böhm, C. Böhme, A. Hoffknecht, H. Knopp, N. Grün, W. Scheid, T. Steih, F. Bosch, B. Franzke, P.H. Mokler, F. Nolden, M. Steck, T. Stöhlker, Z. Stachura, Precise Determination of the 2s_{1/2}-2p_{1/2} Splitting in Very Heavy Lithiumlike Ions Utilizing Dielectronic Recombination, Phys. Rev. Lett Vol. 91 No. 7 (2003) 073202-1.
8. F. Nolden, B. Franzke, A. Schwinn, F. Caspers, First Experiments on Stochastic Cooling of Heavy Ion Beams at the ESR, Proc. EPAC'98 (1998) 1052-1054.

9. F. Nolden, K. Beckert, P. Beller, B. Franczak, B. Franzke, A. Schwinn, M. Steck, F. Caspers, Fast Stochastic Cooling of Heavy Ions at the ESR Storage Ring, Proc. EPAC'00 (2000) 1262-1264.
10. W. Maier, C. Dimopoulou, R. Hettrich, F. Nolden, C. Peschke, P. Petri, M. Steck, The Novel Optical Notch Filter for Stochastic Cooling at the ESR, Proc. COOL2013 (2013) 142-145.
11. F. Nolden, Zur stochastischen Vorkühlung am ESR, PhD Thesis, Technical University of Munich 1996.
12. F. Nolden, C. Dimopoulou, R. Grisenti, C.M. Kleffner, S.A. Litvinov, W. Maier, C. Peschke, P. Petri, U. Popp, M. Steck, H. Weick, D.F.A. Winters, T. Ziglasch, Radioactive Beam Accumulation for a Storage Ring Experiment with Internal Target, Proc. IPAC'13 (2013), 91-93.
13. FAIR Baseline Technical Report, GSI, Darmstadt, 2006, <http://www.gsi.de/fair/reports/btr.html>.
14. C. Dimopoulou, B. Franzke, T. Katayama, F. Nolden, G. Schreiber, M. Steck, D. Möhl, Experimental Demonstration of Longitudinal Ion Beam Accumulation with Electron Cooling, Proc. EPAC'08 (2008) 3470-3472.
15. M. Steck, C. Dimopoulou, B. Franzke, O. Gorda, T. Katayama, F. Nolden, G. Schreiber, D. Möhl, R. Stassen, H. Stockhorst, I.N. Meshkov, A.O. Sidorin, G. Trubnikov, Demonstration of Longitudinal Stacking in the ESR with Barrier Buckets and Stochastic Cooling, Proc. COOL'11 (2011) 140-143.
16. M. Steck, L. Groening, K. Blasche, B. Franczak, B. Franzke, T. Winkler, V.V. Parkhomchuk, Beam Accumulation with the SIS Electron Cooler, Nucl. Instr. Meth. in Phys. Res. A 441 (2000) 175-182.

2.10 NICA Cooling Program

Igor Meshkov, Grigory Trubnikov*
 Joint Institute for Nuclear Research, Dubna, Russia
 Mail to: meshkov@jinr.ru, trubnikov@jinr.ru

Abstract:

Nuclotron-based Ion Collider fAcility (NICA) is the new experimental heavy-ion complex being constructed at Joint Institute for Nuclear Research, Dubna. Main purpose of the project is to provide experiment on colliding heavy ion beams (Au) for study of manifestation of hot and dense strongly interacting baryonic matter [1]. The construction of the accelerator complex is actively performed: production of elements of new 3.2 MeV/u heavy-ion linear accelerator (HILac) is now under completion, production of Booster synchrotron elements has been started. The New Test Facility for assembly and cold testing of superconducting magnets for NICA Booster, collider and SIS100 synchrotron (FAIR, Darmstadt) started to assemble and perform magnetic measurements of the first of series magnets [2].

Beam cooling systems are suggested for application at NICA. The Booster equipped with 35 keV electron cooling system is intended for the storage of $^{197}\text{Au}^{31+}$ ions to an intensity of about 4×10^9 particles and the formation of the necessary beam emittance using the electron cooling system. Two beam cooling systems: stochastic and electron, are supposed to be used in the collider. Parameters of cooling systems, proposed scenario of collider operation, their design intended to achieve required average luminosity of the order of $10^{27} \text{cm}^{-2}\text{s}^{-1}$ at high energies are presented. Recent

experimental results in stochastic cooling experiments achieved at Nuclotron which are of great practical interest for NICA collider operation are presented here and discussed.

2.10.1 Introduction

The detailed scheme of the NICA complex is described in Ref. [2,3], main parameters are presented in Table 1.

Table 1: Parameters of NICA accelerator complex

	Booster (project)	Nuclotron		Collider (project)
		Project	Status 2014	
Circumference, m	211.2		251.5	503.0
Maximum magnetic field, T	1.8	2.0	2.0	1.8
Magnetic rigidity, T·m	25.0	45	45	45
Cycle duration, s	4.02	4.02	7 - 1000.0	≥ 2000
B field ramp rate, T/s	1.2	2.0	0.8	< 0.5
Accelerated/stored particles	p- ¹⁹⁷ Au ⁷⁹⁺ , p↑, d↑		p-Xe, d↑	p- ¹⁹⁷ Au ⁷⁹⁺ , p↑, d↑
Maximum energy, GeV/u				
Protons	–	12.6	–	12.6
Deuterons	–	5.87	5.2/5.8(C ⁶⁺)	5.87
Ions, GeV/u	¹⁹⁷ Au ³¹⁺ , 0.6	¹⁹⁷ Au ⁷⁹⁺ , 4.5	¹²⁴ Xe ⁴²⁺ , 1.5	¹⁹⁷ Au ⁷⁹⁺ , 4.5
Intensity, ion number per cycle (bunch)				
protons	1·10 ¹¹	2·10 ¹¹	1·10 ¹⁰	2·10 ¹¹
deuterons	1·10 ¹¹	1·10 ¹¹	4·10 ¹⁰	1·10 ¹¹
¹⁹⁷ Au ⁷⁹⁺	1·5·10 ⁹	1·10 ⁹	1·10 ⁴ (¹²⁴ Xe ⁴²⁺)	1·10 ⁹

The collider design has to provide the project luminosity and its maintenance during a long time necessary for an experiment performance. That requires formation of ion beams of high intensity with sufficiently low emittance and long ion beam life time. To reach the required parameters a beam cooling is proposed both in the Booster and in the collider rings.

2.10.2 Operation of the Booster with Electron Cooling System Goals and Objectives

The maximum design ion energy of 4.5 GeV/u can be achieved at Nuclotron with fully stripped ions only. To provide high efficiency of the ion stripping one has to accelerate them up to the energy of a few hundreds of MeV/u. For this purpose a new synchrotron ring – the Booster is planned to use [4]. The Booster will have maximum magnetic rigidity of 25 T·m that corresponds to about 660 MeV/u of the ion energy, and the stripping efficiency is not less than 80%. The operation diagram of the Booster is shown in Fig.1.

The Booster is planned to be equipped with electron cooling system that allows to provide efficient cooling of the ions in the energy range from injection energy up to 65 MeV/u. Electron cooling at injection energy 3.2 MeV/u is required to accumulate intense beam especially if multiple injection is used. Such mode will be required also for storing highly charged ion states (e. g. Au⁶⁵⁺ ions) or polarized ions (e. g. ¹H⁻ atoms) with high intensity. Beam cooling at energy 60-70 MeV/u could be useful to

achieve special beam parameters required by fixed target experiments on the extracted beam from the Booster.

Another goal of the cooling of heavy ion beam at 60-70 MeV/u energy could be decreasing its longitudinal emittance to the value required for effective injection and acceleration in the Nuclotron before injection into the collider. Transverse beam emittance has to be stabilized at relatively large value to avoid space charge limitations in the Nuclotron and collider rings. Simulations of such a regime of the cooler operation performed with Betacool code showed that during 1 second of the cooling one can decrease the longitudinal beam emittance by about 3 times at practically constant transverse emittance [6].

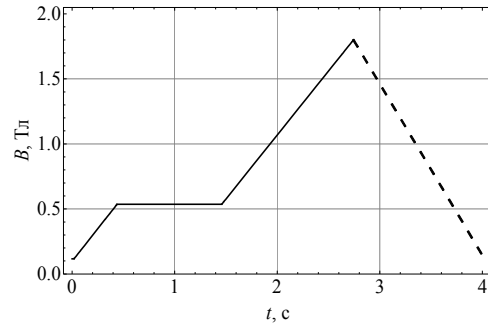
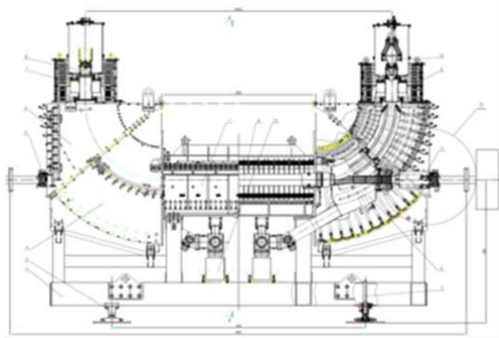


Figure 1: Booster cycle diagram (plateau at $B=0.55$ T corresponds to ion energy $E=65$ MeV/u)

The magnetic system of the Booster is superconducting. Its design is based on the experience of construction of the Nuclotron SC magnetic system. The electron cooling system for the Booster is supposed to be made using conventional solenoid. For this reason, special warm-to-cold transition sections are built into the magnet-cryostat system of a straight section in the Booster ring. Considering these geometrical limitations and other requirements main parameters of the electron cooler are formulated in the Table in Fig. 3. The system is quite typical: an electron beam current of 1A corresponds to the maximum electron energy, when cooling is required at the injection energy the current is limited by space charge effects and does not exceed 50–100 mA. The conceptual design of the system has been made in collaboration of JINR and Budker INP (Fig. 2), its construction is performed now at Budker INP [5].



Energy of electrons, keV	1,5 ÷ 35
Energy controlling, $\Delta E/E$	$\leq 1 \cdot 10^{-5}$
Electron beam current, A	$0,2 \div 1,0$
e-beam current stability, $\Delta I/I$	$\leq 1 \cdot 10^{-4}$
Straight solenoid length, mm	2522
Total length, mm	5715
Long. magnetic field, T	$0,1 \div 0,2$
B field homogeneity, $\Delta B/B$	$< 10^{-4}$
Vacuum conditions, Torr	$< 10^{-10}$

Figure 2: Electron cooling system for Booster. 1 – electron gun, 2 – magnetic coils and electrostatic plates, 3 – toroidal solenoids, 4 – straight solenoid, 5 – magnetic shield, 6 – collector of electrons, 7 – correcting coils for ion beam, 8 – ion beam chamber

One of the most serious problems in the electron cooling of heavy ion beams is the recombination of ions on electrons of the cooling electron beam which leads to a change in the charge state and the loss of an ion due to the change in the position of its orbit. Evaluations [7] of the recombination rate of Au31+ and Au51+ ions upon cooling at the energy of 100 MeV/u which were based on the experimental data from the electron cooled storage rings at CERN (Switzerland), GSI (Darmstadt, Germany), and MPI (Heidelberg, Germany), show that the ion loss within one second of cooling will be no larger than 2%. The correct choice of the ion charge state should be made to avoid the “resonant” recombination. Nevertheless, it is possible to increase the temperature of the transverse degree of freedom of electrons using modulation by the transverse electric field in the electron gun.

2.10.3 Low Energy Heavy Ion Collider: Requirements and Challenges for Luminosity, Region of Operation

Two superconducting rings of collider will have maximum magnetic rigidity of 45 T·m each. The rings are vertically separated by 320 mm locating in the same cryo-vacuum volume: so-called “double-aperture” magnet, operating at 4.5 K. The maximum field in the bending magnets is chosen to be 1.8 T. The rings are symmetrical and each consists of two arcs and two long straight sections with circumference of 503 m [8]. The arc optics based on FODO elementary cell at 12 cells per each arc is chosen for the ring lattice. The collider operation at luminosity of between 10^{26} and $10^{27} \text{ cm}^{-2} \cdot \text{s}^{-1}$ allows to perform experiments which should measure all hadrons comprising multi-strange hyperons, their phase-space distributions and collective flows, including also event-by-event observables. The scheme of the collider, ring composition and choice of the beam parameters to achieve design luminosity are discussed in [3,6]. Chosen beam parameters and estimated luminosity are shown in Table 2.

When the bunch phase volume is determined, the particles number per bunch is restricted by the total acceptable betatron tune shift $\Delta Q = \Delta Q_{\text{Las}} + 2\xi$ (Lasslet tune shift plus doubled beam-beam parameters corresponding to 2 IP's). For chosen working point ($Q_{x/z} = 9.43/9.44$) of the collider the limiting value is about $\Delta Q \leq 0.05$. This strategy of the parameter optimization allows to have the luminosity above $1 \cdot 10^{27} \text{ cm}^{-2} \cdot \text{s}^{-1}$ in the energy range from about 3 up to 4.5 GeV/u. In this energy range the tune shift can be even less than the limiting value of 0.05. Below 3 GeV/u maximum luminosity is reached at maximum tune shift due to dominated effect of the Lasslet tune shift. Expressing the luminosity via the tune shift we have the following estimation:

$$L = \beta^5 \gamma^2 \Delta Q_{\text{total}}^2 \frac{A^2}{Z^4} \cdot \frac{4\pi\varepsilon_{\text{unnorm}} c}{r_p^2 \beta^*} \cdot \left(\frac{k_{\text{punch}}}{\gamma^2} + n_{\text{IP}}(1 + \beta^2) \right)^{-2} \cdot \frac{n_{\text{bunch}}}{C_{\text{Ring}}} \cdot f_{HG},$$

$$k_{\text{punch}} = \frac{C_{\text{Ring}}}{\sqrt{2\pi}\sigma_s}, \quad n_{\text{IP}} = 2. \quad (1)$$

That shows that in the IBS dominated regime the luminosity scales with the beam energy approximately as $\beta^5 \gamma^6$ if $\xi \ll \Delta Q_{\text{Las}}$. The Keil-Schnell criteria for longitudinal microwave instability is satisfied for the bunch intensity in whole energy range.

Table 2: Collider beam parameters and luminosity

Ring circumference, m	503,04		
Number of bunches	23		
Rms bunch length, m	0.6		
β -function in the IP, m	0.35		
FF lenses acceptance	$40\pi \cdot \text{mm} \cdot \text{mrad}$		
Long. acceptance, $\Delta p/p$	± 0.010		
Gamma-transition, γ_{tr}	7.091		
Ion energy, GeV/u	1.0	3.0	4.5
Ion number per bunch	$2.75 \cdot 10^8$	$2.4 \cdot 10^9$	$2.2 \cdot 10^9$
Rms momentum spread, 10^{-3}	0.62	1.25	1.65
Rms beam emittance, h/v , (unnorm), $\pi \cdot \text{mm} \cdot \text{mrad}$	1.1 / 1.01	1.1 / 0.89	1.1 / 0.76
Luminosity, $10^{27} \text{ cm}^{-2} \cdot \text{s}^{-1}$	0.011	1	1
IBS growth time, sec	186	702	2540

The beam cooling application in the collider rings has two goals:

- beam accumulation using cooling-stacking procedure;
- luminosity preservation during experiment.

The first goal can be achieved with electron and stochastic cooling system of reasonable technical parameters, because in this case the beam has rather low linear particle density. It is discussed in chapter below and in [9]. The second goal is more important. Dedicated scenario of using stochastic and electron cooling systems to cover whole energy range with maximal achievable luminosity at low energies and to have luminosity of the order of $1 \cdot 10^{27} \text{ cm}^{-2} \text{ s}^{-1}$ at maximal energies is discussed below.

In equilibrium between IBS and the cooling the luminosity life-time is limited mainly by the ion interaction with the residual gas atoms. The vacuum conditions in the collider rings are chosen to provide the beam life time of a few hours. The beam preparation time is designed to be between 2 and 3 minutes. Therefore, the mean luminosity value is closed to the peak one. To realize this regime the cooling times have to be equal to the expected IBS heating times for all degrees of freedom. The way to increase the luminosity at low energy is to provide powerful cooling with cooling times sufficiently shorter than the IBS times. In such a regime (so called “*Space charge dominated*” regime) the bunch emittance is limited by achievable tune shift value but the momentum spread and the bunch length are determined by synchrotron tune suppression. Stochastic and electron cooling technique at the collider are proposed to have required luminosity with possibility of energy scan. Stochastic cooling application looks very attractive because it does not lead to additional particle loss and keeps the shape of ion distribution close to Gaussian one. However it cannot provide short cooling time at low energies.

Simulation showed that for the energy from 3 GeV/u and higher a cooling system has to provide the cooling times of about 500 seconds and more – that will be achieved by stochastic cooling system at bandwidth of 3 GHz. At low energies starting from $E = 1 \text{ GeV/u}$ cooling has to be of the order of ten seconds (that will be provided by electron cooling system) [3, 6].

Proposed cooling scenario for NICA collider is the following (Fig. 3): in the ion energy range from 1 to 3 GeV/u the electron cooling can provide rather short cooling times to keep *Space charge dominated regime* and increase luminosity in comparison

with IBS dominated one. HV electron cooling system with energy up to 1.5 MeV looks realistic. In the energy range from 3 to 4.5 GeV/u the usage of the stochastic cooling system is more preferable. Here the luminosity is equal to $1 \cdot 10^{27} \text{ cm}^{-2} \cdot \text{s}^{-1}$ and the collider can operate in *IBS dominated regime*.

Numerical simulations of the beam dynamics in the collider under stochastic and electron cooling are in progress.

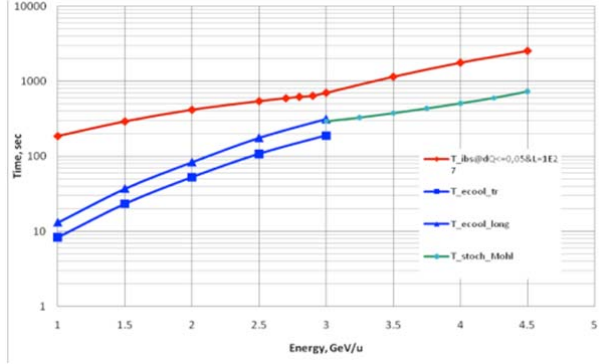


Figure 3: IBS growth times in the IBS dominated regime (red curve), electron cooling times – blue curves (below 3 GeV/u) and stochastic cooling time – green curve (above 3 GeV/u)

2.10.4 Beam Stacking in Longitudinal Phase Space

The beam accumulation in the collider in longitudinal phase space is planned with application of RF barrier bucket (BB) technique. This provides independent optimization of the bunch intensity, bunch number as well as controlling of the beam emittance and momentum spread during the bunch formation. The comparison of the beam stacking in the longitudinal phase space with stationary and moving under action of electron cooling or without cooling are presented in [10].

Simulation of the particle accumulation for NICA collider with the stationary barrier buckets and the electron cooling system [10, 11] showed that efficiency of accumulation is good at low ion energies and is not sufficient at higher energies. We found the serious disadvantage of using stationary barriers. Particles are injected into unstable region (potential “top”), period of their phase motion is longer in comparison to that one in stack. The cooling rate when particles are in injected region is slower because of large initial dp/p [12]. In addition (if particle energy is below transition one) while travelling through barriers from injection zone into stack, particles experience positive energy kick if their energy is above synchronous one and negative - if below. As result cooling time increases.

The simple scheme of stacking [3] with moving barriers can be proposed using special conditions at injection [10]. The pulse of the injection kicker is designed to be no less than 800 ns i.e. it occupies 1/2 of the collider's circumference in phase space. So the injection zone can not exceed 1/2 of the ring. But this difficulty can be circumvented when moving barriers are used, because phase space occupied by barrier pulses can be used for the leading and trailing edges of the kicker pulse.

The presented stacking scheme is not 100% adiabatic that leads to the additional emittance growth in comparison to the ideal stacking process. The key element for the

adiabaticity of the accumulation process is the "correct merging technique" of newly injected and stacked beam:

- Momentum spread of the injected particles should be as close as possible to momentum spread of stack ones before the merging.
- The barrier width and height between the injected and stacking beam should be adiabatically decreased precisely in proper way.

The using of the electron cooling with moving barriers can significantly decrease the particle losses as well as final momentum spread (Fig.4). As it was mentioned above the electron cooling time exceeds the time interval between injections for the energy of ions above 2.5 GeV/u if the scheme with 2 stationary barriers is implemented. The proposed stacking scheme with four moving barriers permits to apply the cooling method to all particles during whole accumulation procedure without particle losses in the injection region.

The ring optics of the NICA collider was optimized for the stochastic cooling at high energies (from 3 to 4.5 GeV/u). The barrier height (in units of momentum spread) has the maximum value for the maximum ion energy 4.5 GeV/u and smaller values for low energies. On the other hand the electron cooling is faster for lower energies. Simulations of the stacking efficiency for the different energies for the same parameters of barrier bucket system without and with electron cooling are presented in Table 3.

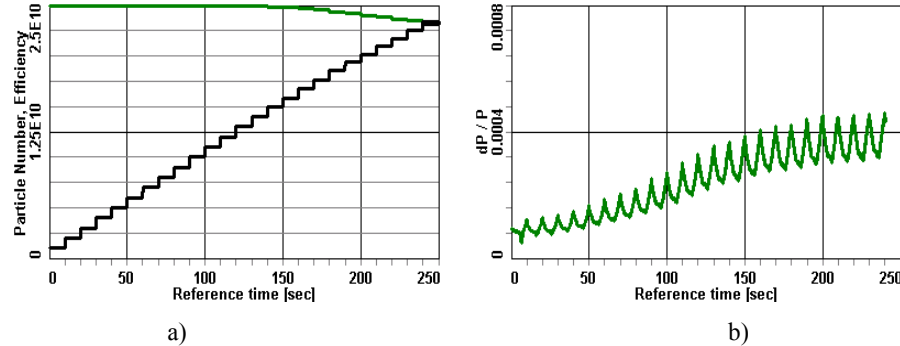


Figure 4: Accumulation with electron cooling and IBS: a) particle number (black) and accumulation efficiency (green), b) momentum spread. Ion energy E = 4.5 GeV/u.

Table 3: Stacking efficiency (%) with moving barriers

Ion energy, GeV/u	1.5	2.5	4.5
Barrier height, $(\Delta p/p) \times 10^{-3}$	0.87	1.08	2
Electron cooling rates, s^{-1}	1.0	0.25	0.03
Without cooling, %	68	70	74
With electron cooling, %	93	91	93

The presented simulation with moving barrier buckets shows that the beam stacking in the longitudinal phase space has a good efficiency for the expected parameters of injected beam even without cooling. However implementation of cooling methods is mandatory for the colliding.

2.10.5 Stochastic Cooling

The stochastic cooling (SC) is proposed for the collider to preserve the required luminosity at higher energies. For this goal the SC has to provide equilibrium with the

expected IBS heating. In our case for cooling of the longitudinal degree of freedom more preferable is to use Palmer method because of wider dynamical range of momentum deviation in comparison with other methods. At the optimum gain and neglecting the amplifier noise the stochastic cooling rate can be estimated for all degrees of freedom by the following formula [13]:

$$\frac{1}{\tau} = \frac{W}{N_{eq}} \frac{(1 - 1/M_{pk}^2)^2}{M_{kp}} \quad (2)$$

The “wanted” mixing from kicker to pick up is given by M_{kp} and in ideal case it has to be close to unity if ring slip-factor is fixed. Here η_{pk} , η_{kp} , T_{pk} , T_{kp} – are the partial slip-factor and time-of-flight from pickup to kicker and from kicker to pickup correspondingly.

The chosen lattice of the collider permits to optimize the pickup and kicker positions to provide small partial slip factor from the pickup to kicker (to avoid unwanted mixing) in the total required energy range [6]. For the Palmer method (longitudinal cooling) the pickup is located at the entrance into arc section near maximum of the dispersion function. The kicker is located in the long straight section at 132 m downstream from the pickup. The kicker position is chosen to have negative η_{pk} at maximum energy and positive at minimum energy. In this case we exclude practically the unwanted mixing in the all energy range and sufficiently increase the wanted one. At such position of the kicker one could have for the acceptable upper frequency of the band the value of about 20 GHz (at the momentum spread equal to the ring dynamic aperture $\Delta p/p = \pm 0.01$). It means that the system bandwidth is limited mainly by technical reasons. The luminosity of $1 \cdot 10^{27} \text{ cm}^{-2} \cdot \text{s}^{-1}$ corresponds to about $2.3 \cdot 10^9$ ions per bunch, the effective ion number is about $8 \cdot 10^{11}$. Simulations using D.Mohl’s formulae [13] showed that to provide the cooling time two-three times shorter than the IBS ones (to have a technical reserve) the cooling bandwidth can be chosen from 3 to 6 GHz.

The same pick-up can be used for cooling of both longitudinal and vertical degrees of freedom. The kicker for vertical degree of freedom is located in the long straight section in the position providing required phase advance. Pickup for horizontal degree of freedom is located in the straight section upstream the arc in the zero dispersion point, the horizontal kicker – in the straight section downstream the arc in the position providing required phase advance.

2.10.6 Electron Cooling

The electron cooling is aimed to suppress completely IBS heating at low energy and provide the collider operation in the *Space charge dominated regime*. In this case at small momentum spread the transverse emittance can be sufficiently larger, than determined by equi-partitioning condition. Therefore the luminosity at small energy can be sufficiently increased in comparison with *IBS dominated regime*.

For the cooling section at reasonable technical parameters (Table 4) the cooling times were estimated for the total ion energy range [6]. At small energies (below 3 GeV/u) the cooling times are about 20 times shorter than IBS heating times and the electron cooling is strong enough to provide space charge dominated regime of the collider operation.

Table 4: Main parameters of the collider electron cooler

Maximum electron energy, MeV	0.5-2.5
Cooling section length, m	6.0
Electron beam current, A	0.1-1.0
Electron beam radius, cm	0.5
Magnetic field in cooling section, T	0.1-0.2
Magnetic field imperfection	2×10^{-5}
Beta functions in cooling section, m	20
Collector PS, kW	2x2
HV PS stability, dU/U	1e-4

General problem which has to be solved for effective application of the electron cooling is the ion recombination with the cooling electrons. At typical temperature of electron transverse degree of freedom below 1 eV the beam life-time due to recombination is about a few hundreds of seconds. There are two ways to increase the life-time: either to increase artificially the electron transverse temperature or to introduce energy shift between electrons and ions.

The main peculiarity of the electron cooler for the NICA collider is use of two cooling electron beams (one electron beam per each ring of the collider) that never has been done. Two versions of design of the cooling system are under consideration presently Fig. 6 [14]. Design of the collider electron cooling system is performed in co-operation with All-Russian Electrotechnical Institute (AEI, Moscow) and Budker INP on the basis of cascade-type high voltage generator [14]. In JINR-AEI scheme the acceleration and deceleration of the electron beams is produced by common high voltage (HV) generator. The cooler consists of three tanks. Two of them contain acceleration/deceleration tubes and are immersed in common superconducting solenoids. The third one contains HV generator. The second scheme (BINP) has two coolers (one per each ring of the collider). The coolers have own high voltage systems. The electron cooler consists of two tanks. One tank contains acceleration/deceleration tubes which immersed in own magnetic field created by separated coils accommodated inside the tank [14].

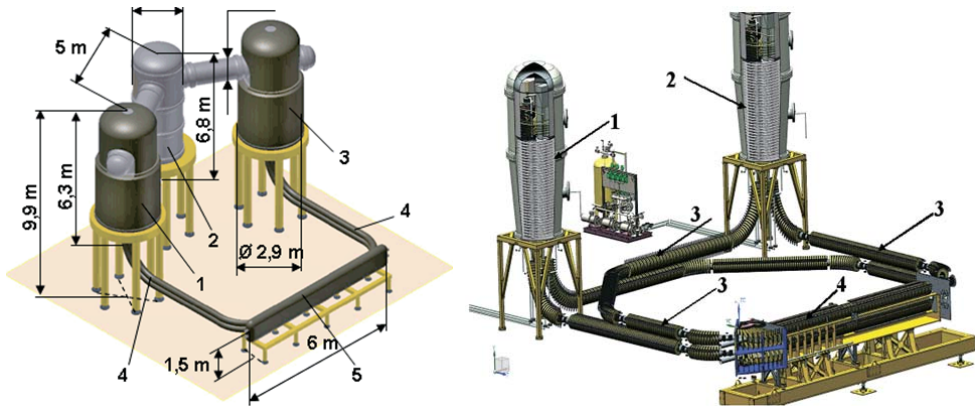


Figure 5: Two versions of HV electron cooler for NICA Collider: a) version JINR-AEI: 1, 3 – the tanks with electron gun and acceleration tube and deceleration tube + collector for electron beams of opposite direction , 2 – tank with HV generator, 4 – beam transportation solenoids, 5 – electron cooling section; b) version BINP: 1, 2 – tanks with electron gun and acceleration tube and deceleration tube + collector, 3 – beam transportation solenoids, 4 – electron cooling section

In both cooler versions magnetized electron beams are planned to be used. The longitudinal magnetic field is formed with superconducting solenoids – straight and toroidal ones. In the “a” version (JINR-AEI) the superconducting solenoids form the magnetic field along all electron trajectories – from the gun up to collector. These solenoids in acceleration/deceleration area are placed inside the tanks. In the “b” version (BINP) the solenoids in high-voltage part are located inside the tanks and are “warm” (normal conducting). Other part of the system is superconducting. Both solenoid systems have straight and toroidal sections of different diameter. Magnetic field formation at solenoids’ connection is done with magnetic shields.

2.10.7 R&D for Collider Stochastic Cooling System, Results at Nuclotron Complex

The Nuclotron having the same magnetic rigidity as the future NICA collider and based on the same type of the magnetic system is the best facility for testing of the collider equipment and operational regimes [2]. Application of the beam cooling in the collider rings has the goal of beam accumulation using cooling-stacking procedure and luminosity preservation during experiments.

It was proposed to install the prototype of the stochastic cooling system for collider at operating Nuclotron synchrotron. The pick-up and kicker stations of the stochastic cooling system prototype elaborated in cooperation with FZJ are similar to that one designed for the HESR of the FAIR project [15]. Simulations of the stochastic cooling process at Nuclotron have been performed for different types of particles: protons and carbon ions C(6+): for proton beam the required power for beam cooling expected to be of order of 30-40W with gain at 140 dB. For the carbon beam C⁶⁺ the power requirements correspondingly decreases to 10W and 130dB gain. During 2011-2013 the elements of the stochastic cooling system for Nuclotron were designed, constructed and installed in the ring. Main parameters of the system are the following: bandwidth 2-4 GHz, optimal beam kinetic energy 3.5 GeV/u, system (and notch filter) delay accuracy 1 ps, $N_{ion} \sim 10^9$. This work performed in close collaboration with the Forschungszentrum Jülich (FZJ) is also important for testing elements of the stochastic cooling system designed for the High-Energy Storage Ring (HESR, FAIR) [15].

Simulation of the collider magnetic system operational conditions had been performed at Nuclotron in 2012-2013 with long plateau (up to 1000 seconds) of the magnetic field at 1.5 T was demonstrated. In March 2013 the effect of the longitudinal stochastic cooling using filter method had been demonstrated at the Nuclotron for the first time. Cooling time experimentally obtained for deuteron beam is in good agreement with simulation results. The next experiment for the stochastic cooling effect had been successfully demonstrated in December 2013 both for coasting and bunched carbon beams (Fig.6) [2,16]. Transverse Schottky signals of the beam were also measured. Due to small charge of ions (D+) and short pick-up structure the betatron side-bands are almost at noise level, but signals were discernible.

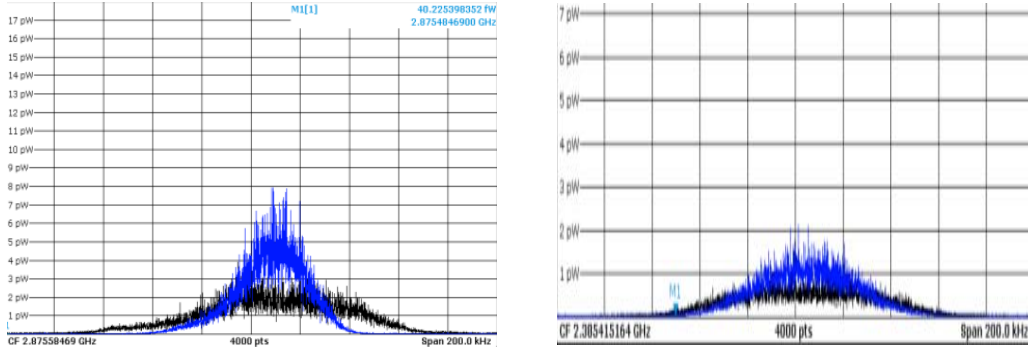


Figure 6: Experimental results of beam stochastic cooling of coasting $^{12}\text{C}^{6+}$ and bunched $^{12}\text{C}^{6+}$. Schottky beam spectra: black – initial beam, blue – cooled beam. Left: coasting beam, $I \sim 2\text{e}9$ ions, $E = 2.5 \text{ Gev/u}$, $\Delta p/p_{\text{initial}} = 0.15\text{e}-3$, $\Delta p/p_{\text{final}} = 0.07\text{e}-3$, $\tau_{\text{cool}} \sim 27 \text{ sec}$. Right: bunched beam, $I \sim 2\text{e}9$ ions, $E = 2.5 \text{ Gev/u}$, $dp/p_{\text{initial}} = 0.2\text{e}-3$, $dp/p_{\text{final}} = 0.13\text{e}-3$, $\tau_{\text{cool}} \sim 64 \text{ sec}$

New scheme of beam cooling system, which includes FZJ ring-slot couplers as pick-up and kicker, unique optical notch-filter and a full remote-controlled automation of measurements and adjustments, has been successfully commissioned in 2013. New optical comb filter was developed and commissioned. The device has a compact size, low insertion loss and dispersion. Comb filter adjustment was automated with developed special software, which sufficiently reduces adjustment time and increases accuracy up to a few Hz. This filter has new optimized parameters in comparison to standard coaxial and optical filters: in average the attenuation of minimal signal amplitudes increased by 5 dB, dispersion is decreased from 25 Hz to 5-7 Hz. The progress in development of such automated comb filter has great importance for stochastic cooling in NICA collider, where it is planned to use for damping of synchrotron signals excited in bunched beam.

We also started experimental study of the potential band-overlapping process in the energy range $E=2.5\text{--}4 \text{ GeV/u}$ at Nuclotron, that is extremely important for collider. Here it is possible carefully study of stochastic cooling time dependence for the bunched beam when increasing RF amplitude one measures beam momentum spread ($\Delta p/p$) which gives direct estimation of the efficient mixing factor.

The concept of start-up configuration of the stochastic cooling system for the collider has become a result of simulations using dedicated program code [16] (benchmarked with experimental results from Nuclotron). It is considered as follows at this moment: 32 rings each is 8-electrodes slot-coupler RF structure (FZJ design), bandwidth of 2–4 GHz. For the ion energy $E=3.5 \text{ GeV/u}$, $I_{\text{ions}}=2.7\times 10^{10}$, $\Delta p/p=6\times 10^{-4}$, proposed to use filter method for longitudinal cooling and standard betatron method for transverse cooling, the expected optimal gain of the system is to be at 75 dB, output power at kicker is at 765 W, “longitudinal” cooling time is around 730 seconds.

Estimations for the stochastic cooling system operated in the energy range 3–4.5 GeV/u show expected output power of the system equal to 1200 W for longitudinal and 500 W for transverse degrees of freedom correspondingly. The table with initial parameters for stochastic cooling simulations shown below (Table 5).

Table 5: Parameters and requirements for the collider stochastic cooling system

W, GHz	Init.rms dp/p, 10^3	Energy GeV/u	Number of ions	Palmer or filter	η full turn	η , PU- kicker	H	Cooling time lower than:
2-4	0.62	1	6×10^9	Both	0.215	0.199	22	200s
	1.	2	1×10^{10}		0.082	0.067		350s
	1.25	3	5.3×10^{10}		0.037	0.021		700s
	1.65	4	4.8×10^{10}		0.016	0.00061		1500s
	1.65	4.5	4.8×10^{10}		0.0099	-0.0057		2000s

Palmer method for longitudinal cooling looks as preferable. The collider optics is self-consistent from point of view of beam stability and tunability, unfortunately it is not perfect for the Palmer method because dispersion in the pick-up position is comparatively small (about 2.5 meters). On the other hand filter method could be successfully applied in our case only in the narrow energy range (high momenta) due to expected band overlapping. That is why we investigate now possibilities to optimize geometry of pick-up, requirements for beam misalignment, etc in order to find solution for effective stochastic cooling in all energy range from 3 to 4.5 GeV/u.

Simulations made by L.Thorndall [17], showed that beam misalignment on the PU center and high betatron amplitudes could lead to the degradation of longitudinal cooling performance. The common mode problem for a pickup dispersion of 2.7 m remains a major worry for the Palmer cooling. This should be foreseen in pickup geometry precision, beam position and microwave echo reasons. The following requirements are formulated: the r.m.s. initial betatron amplitudes should not be larger than 1mm, the same has to be applied to the beam misalignment (with respect to the pickup centre). In other case each additional mm in misalignments will lead to reduction by ~20% in cooling efficiency.

It is shown also that for higher intensities and same gains the betatron cooling overtakes the momentum cooling. The betatron cooling has more effective bandwidth: 2 side bands per revolution frequency interval instead of only one.

As a further possible development we consider design upgrade of the slot coupler aimed reducing the aperture from 90 to 70 mm that could give advantage in achieving more powerful useful beam signal when intensity is not high (few per cent of designed value) and beam r.m.s. size is around 1–2 mm. Simulations for comparison of the optimal bandwidth in the total energy range (2–4 GHz or 3–6 GHz) are now in progress.

Another important result of our experimental measurement at Nuclotron is that we expect to be safe with using slot-coupler structures and filter method for the bunched beam with low bunching factor. At Nuclotron it is equal to 5, in collider will be 22. Basing on our experience we can preliminary expect that with decreasing of particle intensity (and "power" of Schottky signal as a consequence) at the same system gain, the cooling time will also decrease. It means those structures will efficiently cool the bunched beam in NICA collider at its start-up configuration: bunch intensity $3-5 \times 10^8$, $\Delta p/p \sim 4 \times 10^{-4}$, energy 3–4.5 GeV/u, bunch length, $\sigma=1.2$ m, 22-nd harmonics. We need further experimental investigations.

2.10.8 NICA Start-up Configuration

Start-up configuration of the NICA collider has been proposed. Energy range for first experiments chosen from 3.5 to 4.5 GeV/u, factor 1/4 of the design intensity (5×10^8 instead of 2×10^9 ions per bunch). Advantage is that at low beam intensity one can

neglect with parasitic collisions in the straight sections. Expected luminosity in the start-up configuration is $1\div 7 \times 10^{25} \text{ cm}^{-2}\cdot\text{s}^{-1}$.

As soon as collider will start to operate at fixed energy (comparatively high) – we do not need electron cooling system at the first stage of operation. One can restrict ourselves with reduced (initial) version of stochastic cooling system: filter method for longitudinal degree of freedom and betatron cooling method for the transverse one. Both methods are tested at Nuclotron. We plan also to start with “reduced version” of collider RF system consisting of Barrier Bucket (BB) RF system and RF-2 – for beam bunching at harmonics $h=22$. Operation scenario will be the following: stacking with BB RF system + longitudinal stochastic cooling, then bunching forming 22 bunches with length about 1.2 m instead of 0.6m, momentum spread of 4.2×10^{-4} instead of 1×10^{-3} . It allows us to reach the “start-up luminosity”.

2.10.9 Acknowledgement

Authors are grateful to their colleagues: T.Katayama, V.Parkhomchuk, N.Shurkhno, A.Sidorin, A.Smirnov, R.Stassen and L.Thorndall for fruitful discussions, productive scientific collaboration and valuable contributions to this article.

2.10.10 Reference

1. http://theor.jinr.ru/twiki/pub/NICA/WebHome/WhitePaper_5.03.pdf.
2. G.Trubnikov et al., Proc. IPAC2014 (Dresden, Germany), TUPRO005.
3. Meshkov et al., Physics of Particles and Nuclei Letters, V.9, No. 4–5, 2012, 313.
4. A.Butenko et al., Proc. RUPAC2012, Saint-Petersburg, TUPPB003.
5. A. Bubley et al., ibid., TUPPB034
6. G. Trubnikov et al., Proc. of COOL2011, MOIO07.
7. Kuznetsov A. B., Meshkov I. N. and Philippov A. V., ibid., THCOB01.
8. O.Kozlov et al., Proc. RUPAC2012, Saint-Petersburg, MOPPA017.
9. T.Katayama, Proc. COOL2013, Murren, Switzerland,THAM2HA01.
10. A.Smirnov et al, ibid., WEPP002.
11. T. Katayama, I. Meshkov, A. Sidorin and G. Trubnikov, Proc. RuPAC2012, TUYCH02.
12. I.Meshkov, PEPAN, v.45, No.2, 2014, p.769
13. Mohl D. et al., Phys. Rep. V. 58, No. 2, 1980, 75.
14. E.V. Ahmanova et al., Proc. COOL2013, Murren, Switzerland WEPP008
15. R. Stassen, et al., Proc. COOL2007, THAP13.
16. N.Shurkhno et. al., Proc. of COOL2013, TUPM1HA01.
17. L.Thorndall, JINR Internal report “2–4 GHz Stoch. Cooling in NICA at various Energies”, May 2014.

2.11 Stochastic Cooling for FAIR

C. Dimopoulou

On behalf of the contributing colleagues D. Barker, R. Böhm, O. Dolinskii, R. Hettrich, J. Krieg, W. Maier, F. Nolden, C. Peschke, J. Roßbach, M. Steck, A. Stuhl (GSI), L. Thorndahl (CERN), R. Stassen, H. Stockhorst (FZ Jülich) and others.

GSI Helmholtzzentrum, Planckstr.1, D-64291 Darmstadt, Germany

Mail to: C.Dimopoulou@gsi.de

2.11.1 Introduction

Efficient and versatile beam cooling is an indispensable ingredient for beam preparation and physics experiments both in the existing GSI accelerator complex as well as in the new FAIR facility (Fig. 1). A review of beam cooling activities in the operating GSI machines SIS18 and ESR is given in [1] of this Newsletter. Beam cooling systems will be implemented in the FAIR machines, as follows (Fig. 1).

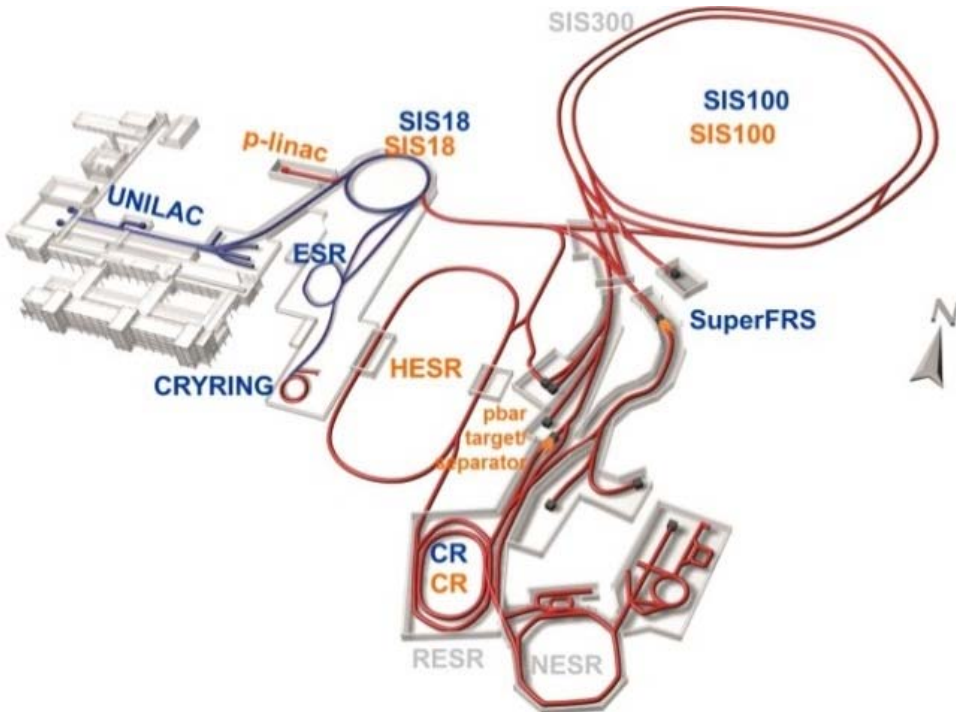


Figure 1: Overview of the GSI and FAIR accelerator complex. SIS300, RESR and NESR will be added to the FAIR project later. Orange paths: primary proton/secondary antiproton beam; blue paths: primary stable heavy ion/secondary rare isotope beams (RIBs).

CR (13 Tm, stochastic cooling): collection, pre-cooling of antiprotons/stable ions/RIBs.

HESR (50 Tm, stochastic and electron cooling, internal target): accumulation, storage, acceleration/deceleration, experiments with antiprotons (also stable ions/RIBs).

RESR (13 Tm, stochastic cooling) [2]: accumulation of up to 10^{11} antiprotons.

NESR (13 Tm, electron cooling, internal target) [3]: accumulation, storage, experiments with stable ions/RIBs deceleration of antiprotons/stable ions/RIBs.

The stochastic cooling systems for the CR and HESR storage rings are being planned, and developed and realised during the last decade. This paper reviews the CR stochastic cooling system and introduces the HESR system, which is further described in [4] of this Newsletter. Information about the beam cooling systems of RESR or NESR, which are beyond the scope of the first phase of the FAIR project, can be found in the references above.

2.11.2 The Stochastic Cooling System of the Collector Ring (CR)

2.11.2.1 Overview

The main purpose of the CR within the FAIR project is the fast reduction of the phase space occupied by the hot secondary beams i.e. antiprotons and rare isotope beams (RIBs) coming from the production targets in a very short (~ 50 ns) bunch. At injection into the CR, the secondary beams have the largest momentum spread and fill the transverse aperture. After bunch rotation and adiabatic debunching their momentum spread is reduced, whereas the transverse emittances remain unchanged. This reduced momentum spread is a prerequisite for stochastic cooling at all. Otherwise the effect of unwanted mixing would exclude particles in the momentum tails from being cooled.

The stochastic cooling system has to cool antiproton beams (at fixed velocity of $v=0.97c$, 3 GeV kinetic energy) and RIBs (at fixed velocity of $v=0.83c$, 740 MeV/u kinetic energy).

Table 1 lists the momentum spread and emittance parameters of the beams before cooling i.e. after the bunch rotation and adiabatic debunching and after stochastic cooling. In order to meet the requirements of maximum production rate the CR stochastic cooling system has to strongly reduce all 3 phase subspaces, within 9 s for the antiprotons and 1 s for the highly charged RIBs.

Table 1: Required stochastic cooling performance in the CR [5].

	Antiprotons 3 GeV, 10^8 ions		Rare isotopes/stable heavy ions 740 MeV/u, 10^8 ions	
	$\delta p/p$ (rms)	$\varepsilon_{h,v}$ (rms) [π mm mrad]	$\delta p/p$ (rms)	$\varepsilon_{h,v}$ (rms) [π mm mrad]
Before/after cooling	0.35 % / 0.05 %	40 / 1.25	0.2 % / 0.025 %	35 / 0.125
Phase space reduction	7×10^3		6×10^5	
Cooling down/cycle time	≤ 9 s / 10 s		≤ 1 s / 1.5 s	

In the first stage of FAIR, in the absence of RESR and NESR, experiments in the HESR are the only users of pre-cooled antiproton and stable heavy ions/RIBs from the CR. For the RIBs, originally, the phase space reduction in Table 1 was dictated by the need for fast electron cooling in the NESR. For the antiprotons, it was dictated by the need for fast accumulation in the RESR. At present, taking into account the rebunching of the antiproton/RIBs beams for transfer to the HESR as well as the small momentum acceptance of the HESR and its stochastic cooling systems, up to 30% lower final momentum spread would be needed after cooling in the CR. On the other hand, higher emittances can be accepted in the HESR. For the demanding case of the antiprotons, the momentum spread budget should be within reach by optimizing the interplay among the longitudinal and transverse cooling in the CR, the rebunching/debunching procedures of the transfer as well as the longitudinal cooling in the HESR. The primary beams of stable heavy ions come into the CR after acceleration in the synchrotrons, i.e. with much smaller phase space than the hot RIBs; what is more, they can be pre-cooled over many seconds in the CR in case high beam quality is needed for precision experiments in the HESR.

Antiproton cooling is limited by the poor ratio of beam noise signal to thermal noise. To cope with that it is foreseen in the CR:

- to keep the pick-up electrodes inside the vacuum at cryogenic temperatures (20-30K), using on the pick-up tanks cryoheads cooled by Helium.
- to strive for the largest possible electrode sensitivity during cooling by synchronously moving (plunging) the pick-up electrodes by means of linear motor drives on the pick-up tanks, following the shrinking beam size.
- to choose the notch filter technique for longitudinal cooling, which advantageously filters out the thermal noise at all harmonics of the revolution frequency in the bandwidth. To reach sufficient momentum acceptance (and well-separated Schottky bands) for notch filter cooling, very small values of $|\eta|=0.011$ ($\eta=\gamma^2-\gamma_{tr}^2$) for the antiproton ion optical lattice must be chosen. The drawback is that the transverse cooling suffers from the increasingly high value of the desired mixing $M(t)\sim[|\eta|\delta p(t)/p]^{-1}$ during the simultaneous longitudinal cooling.
- to simultaneously optimize both longitudinal and transverse cooling processes, by distributing the available installed power accordingly. For a fixed lattice $\eta=-0.011$, this essentially means to reduce the performance of the longitudinal cooling at the profit of the transverse cooling until a reasonable compromise is found. A better remedy comes from the flexibility of the CR lattice in setting different γ_{tr} values. Thus, as $\delta p/p$ shrinks during the cooling cycle, the ring $|\eta|$ can be slightly increased by a factor 2-3, by small tuning of the quadrupole strength, so as to control $M(t)$.

For RIBs, the limitation comes from the undesired mixing between pick-up and kicker, so that only the Palmer method can be applied in the beginning of cooling. For the chosen RIB ion optical lattice $\eta=0.18$.

Along these lines, the concept is as follows (Fig. 2).

- The stochastic cooling system will operate in the frequency bandwidth 1-2 GHz.
- It consists of 2 pick-up (HL, VL) and 2 kicker tanks (HL, VL), all in straight sections with zero dispersion, and one special pick-up tank based on the Palmer method (Palmer pick-up) at high dispersion. The pick-up tank HL(VL) and kicker tank HL(VL) is used for horizontal (vertical) and longitudinal cooling. For antiproton cooling the pick-ups HL and VL are used as well as the notch filter technique. In the latter, to improve the signal to noise ratio, signals from both pick-ups HL and VL are taken in sum mode.

For RIBs only the Palmer pick-up is useful in the first stage (pre-cooling), in all 3 phase space planes. After some time (i.e. after the rms $\delta p/p$ has decreased below 0.1%) it is possible to switch off the signals from the Palmer pick-up and turn to cooling from the pick-ups HL and VL combined with the notch filter down to the final beam quality.

- The foreseen installed cw output power at the kickers of the 1-2 GHz system is 8 kW. It has to be sufficient for cooling of antiprotons or RIBs in all 3 phase space planes simultaneously.
- As a future upgrade, for the antiprotons, an additional longitudinal cooling system in the band 2-4 GHz by means of a notch filter is foreseen. It consists of a pick-up tank (probably with plunging electrodes) and a kicker tank, both in dispersion-free straight sections. The design $\eta=-0.011$ ($\gamma_{tr}=3.85$) of the

antiproton ion optical lattice guarantees optimum momentum acceptance for both bands.

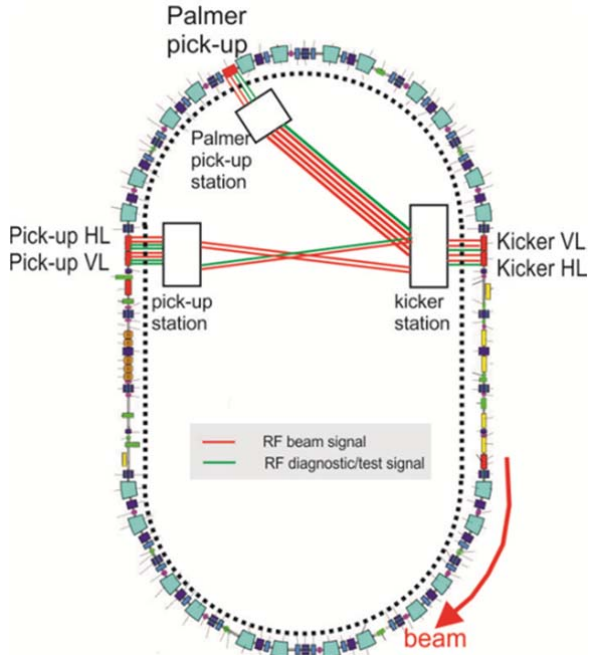


Figure 2: Layout of the CR storage ring with the stochastic cooling system. Inside the storage ring vacuum of UHV grade (pressure in the 10^{-9} mbar range) is present. The bending dipole magnets (light blue), focussing quadrupole magnets (dark blue) and other ring components are schematically shown. The dotted line indicates the separation between the ring tunnel and the supply area in the middle of the building. The pick-up stations are directly connected to the kicker station via several rigid RF coaxial transmission lines suspended through the supply area.

In summary, the stochastic cooling paths and their purpose in the CR are:

- Pick-ups HL,VL → Kickers HL,VL: Antiprotons 3D cooling, longitudinal cooling with notch filter method
- Palmer pick-up → Kickers HL,VL: RIBs 3D cooling, first stage, longitudinal cooling with Palmer method
- Pick-ups HL, VL → Kickers HL,VL: RIBs 3D cooling, final stage, longitudinal cooling with notch filter method.

The lattice of the CR is dictated by the demands from the stochastic cooling system:

- (i) flexibility in setting different transition energy values for antiprotons and RIBs to reach an optimal compromise for the mixing parameters of the stochastic cooling,
- (ii) accommodation of pick-ups and kickers in regions of appropriate dispersion,
- (iii) control of the horizontal and vertical betatron phase advance between pick-ups and kickers of the transverse stochastic cooling systems,
- (iv) reducing chromaticity over the whole momentum range.

2.11.2.2 Hardware Design and Developments

The hardware components of the CR stochastic cooling system are very challenging. During the last 5 years, intensive in-house developments, engineering and prototyping have been going on. Procurement of critical system components has started.

2.11.2.2.1 Electrodes, Pick-ups and Kicker tanks

Slotline electrodes shown in Fig. 3 have been developed [6] for the pick-ups HL and VL because of their following properties: high coupling impedance to the beam both for antiprotons ($v=0.97c$) and RIBs ($v=0.83c$), broadband characteristics within the system bandwidth of 1-2 GHz, good properties with respect to electrode movement (flexibility, robustness), possibility of UHV-compatible production using ceramic substrate. First ceramic electrode plates have been delivered, their metallisation is underway. Dummy electrode modules with equivalent RF properties are used for tests.

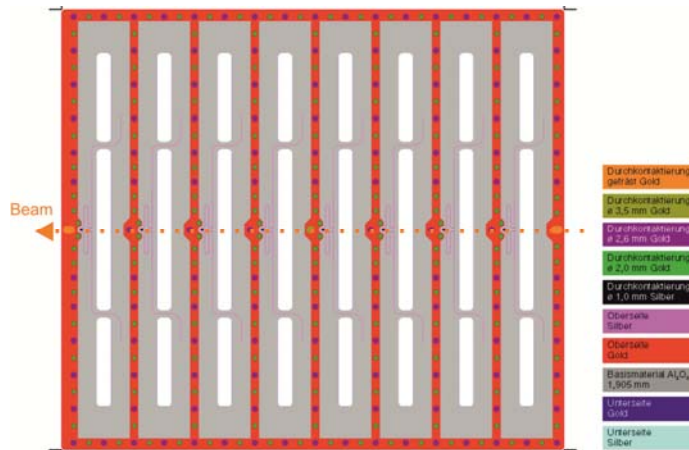


Figure 3: Design of the slotline electrodes on the Al_2O_3 ceramic substrate.

Each pick-up and kicker tank (HL or VL) consists of two plates (up/down for vertical, left/right for horizontal). Each plate consists of 8 arrays (modules) of 8 identical slotline electrodes, i.e. 64 electrodes. Fig. 4 shows schematically the main components inside the pick-up tank VL. Four double-modules i.e. 4 pairs of arrays of slotline electrodes at each side of the tank are movable (plungeable) by means of synchronous linear motor drives.

The water-cooled linear motor drive units (Fig. 5, 6) have been tested synchronously at room temperature. As specified they can be plunged in the range from ± 80 mm from the beam axis at the beginning of cooling down to ± 10 mm at the end of cooling, and (ii) at the end of the cycle, they move back out to their maximum aperture within 200 ms, before a new beam is injected.

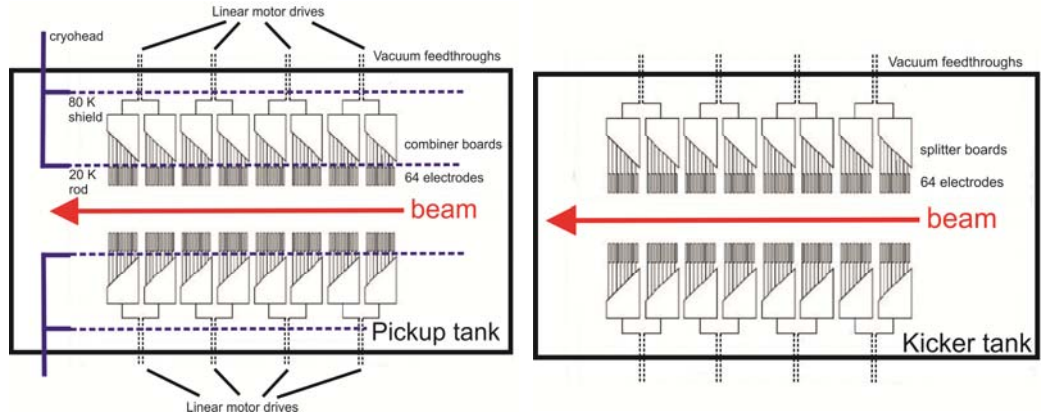


Figure 4: Schematic picture of the pick-up tank VL and the kicker tank.

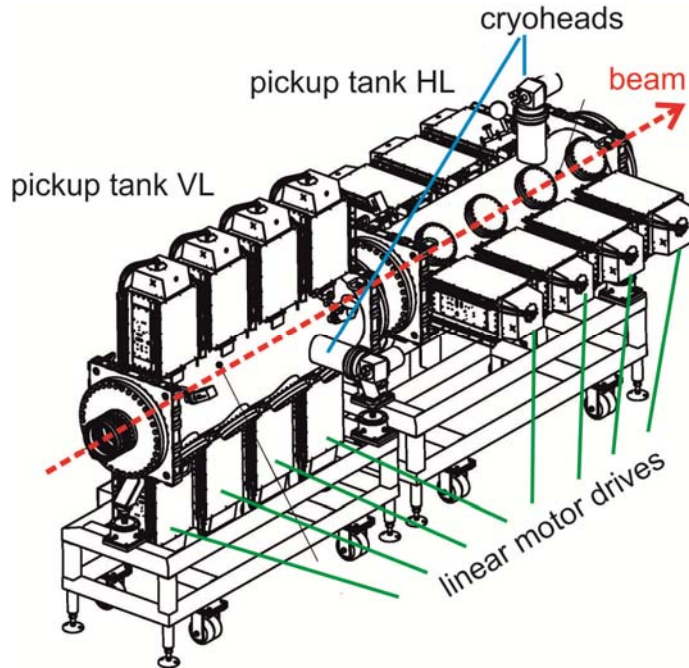


Figure 5: Drawing of the pick-up tanks HL and VL (the total installation length for the 2 tanks is 4.7 m), including cryoheads and linear motor drives. The cryoheads are cooled by Helium, the linear motors are water-cooled.

Two cryoheads are connected to the tank. The cryoheads cool (i) the movable double-module bodies directly at 20-30 K by contact with special flexible silver-plated BeCu sheets and (ii) an intermediate cryoshield at 80 K (Fig. 4, 6).

The intermediate cryoshield is ready and was inserted into the tank at room temperature (Fig. 6). It consists of 4 half-shells, each 1 m long, and bears holes for the motor drives and for assembling, it is made of oxygen-free copper. Afterwards, its pieces were galvanically gold plated, so as to reach very low thermal emissivity.

In a preliminary design the kicker tank in Fig. 4 is identical to the pick-up tank, using also identical slotline electrodes, with two important differences: First, no electrode movement is foreseen and second, the kicker electrodes are held at 300 K by

water cooling. The HL pick-up or kicker tank is identical to the VL pick-up or kicker tank by rotating its components by 90^0 (Fig. 5).

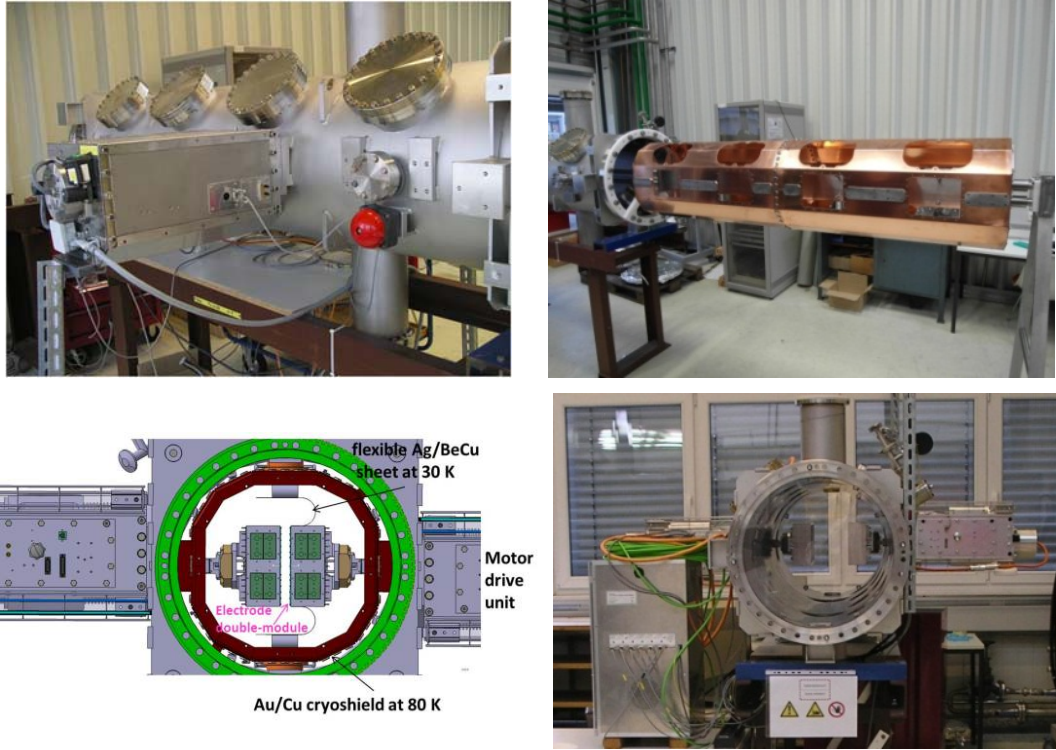


Figure 6: Up, left: The 2 m long prototype pick-up tank, where the challenging mechanical and thermal concepts are being tested. Up, right: Copper cryoshield before mounting in the tank.

Down, left: Cryocooling and plunging concept in the pick-up tank. Down, right: The synchronously movable electrode modules fixed on the linear motor drive units..

The Palmer pick-up is being designed for operation at room temperature. Simulations with the HFSS (High Frequency Structure Simulator) code have led to possible designs of its Faltin-type travelling wave electrodes, optimized for maximum pick-up impedance coupled to the beam and linear output signal phase with respect to the particle pulse [7]. Electrode plunging is not needed for pre-cooling of RIBs, but the sensitivity of the pick-up is limited because of their large vertical aperture (± 66 mm with respect to the beam axis), so as not to intercept the injected beams.

2.11.2.2.2 RF Signal Processing

All microwave signal processing components of the system have to fulfill very stringent specifications for amplitude flatness and phase linearity within the system bandwidth [8]. Saving electrical length is also an issue, since the flight time of the quasi-relativistic particles from pick-up to kicker is very short.

The stringently specified water cooled 1-2 GHz power amplifiers at the kickers, which are a major cost factor, have been ordered. The very demanding antiproton cooling calls for a total cw microwave power of 8 kW (32x250 W units).

The development of the optical notch filters in which the RF signal is temporarily converted into the optical infrared region is now completed, as specified i.e. with notch depth below -30 dB within 1-2 GHz.

2.11.2.3 Simulations of Cooling Performance

The stochastic cooling performance in the CR is being studied in the frequency domain, using the Fokker-Planck equation (CERN code). In a first conservative assumption, no plunging of the pick-up electrodes is included in the simulations.

Cooling of $N=10^8$ antiprotons is the most demanding case. As shown in [9], for notch filter cooling with the slotline electrodes, the requirements can be best met with $G_{\parallel}=150$ dB during 10 s, resulting in a final $\sigma_p/p=3 \cdot 10^{-4}$, within acceptable power. However, there seems to be no safety margin. The option of time of flight (TOF) cooling [10] has been studied, too [11]. The momentum acceptance of the TOF method is 3 times higher than that of the notch filter method ($\pm 1.2 \cdot 10^{-2}$). The best case is with $G_{\parallel} \approx 140$ dB during 10-15 s, leading down to $\sigma_p/p=1.2 \cdot 10^{-3}$. At higher gain, not only the power is unacceptable, but also the TOF cooling loop becomes rapidly unstable.

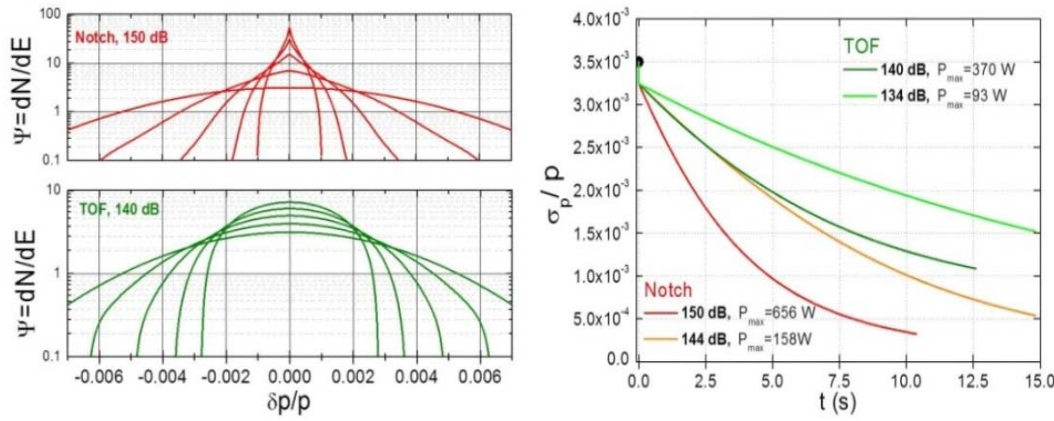


Figure 7: Simulations of TOF and notch filter cooling of 10^8 antiprotons in the CR. Left: Evolution of the particle density Ψ during cooling. Plots at $t=0, 2.5$ s, 5 s, 7.5 s and 10 s. Gaussian initial distribution with $\sigma_p/p = 3.5 \cdot 10^{-3}$. Right: Evolution of the beam rms momentum spread during cooling as well as the maximum cw power. The installed power should be by rule of thumb 4 times higher in order to account for statistical fluctuations.

Characteristic results are given in Fig. 7. As expected, since it suppresses both Schottky and thermal noise in the center of the distribution, the notch filter cools the beam core much more efficiently and ultimately leads to lower momentum spreads than the TOF cooling. The TOF method cools the tails faster.

The results confirm that the notch filter method is the choice par excellence for the noise-limited antiproton cooling in the CR. As $\delta p/p$ shrinks, the ring $|\eta|$ can be slightly increased (decrease γ_{tr}), so as to control $M(t) \sim [|\eta| \delta p(t)/p]^{-1}$, as required for the simultaneously operating transverse cooling [9]. An alternative would be to apply first the TOF and then the notch filter method. The TOF method is slower and because of its larger momentum acceptance it can be easily envisaged to operate at slightly higher $|\eta|$ (lower γ_{tr}), e.g. $\eta \approx -0.02$, thus reducing the initial desired mixing for the transversally hot beam and tune to the design $\eta = -0.011$ when notch filter cooling takes over.

As a next step, plunging of pick-up electrodes can be included to study the ultimate performance of the cooling system. It is expected to reduce the diffusion, especially in the transverse planes.

The longitudinal cooling performance for stable heavy ions in the CR with the notch filter and TOF methods was investigated in the same way with the Fokker-Planck

equation and also in a time-domain approach [12]. Since the thermal noise was negligible with respect to the particle noise and the latter scales with Q^2 , it was sufficient to take a costing beam of U^{92+} as a reference, with an initial rms momentum spread within the notch filter/TOF momentum acceptance (for the RIB lattice $5 \cdot 10^{-4} / 1.5 \cdot 10^{-3}$, respectively.) The expected response of the slotline electrodes is included as in [9]. An example is shown in Fig.8.

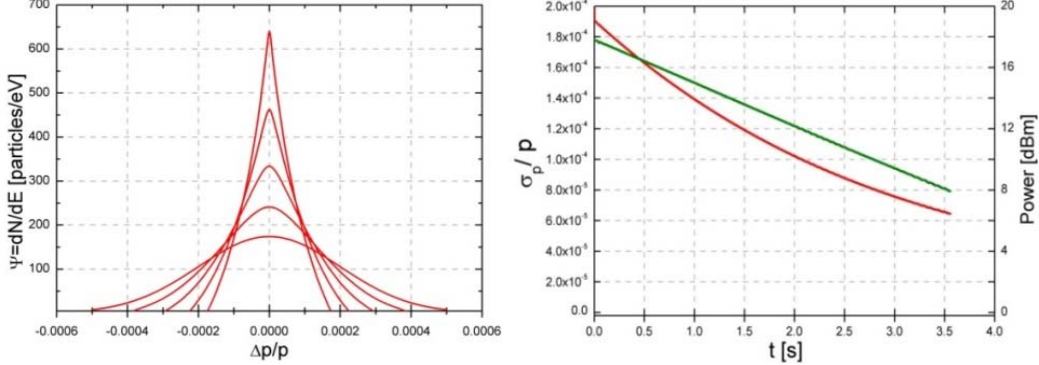


Figure 8: Notch filter cooling of $10^8 U^{92+}$ ions in the CR. Up: Evolution of the particle density, plots at $t=0$, 0.9 s, 1.8 s, 2.6 s and 3.5 s. Bottom: Evolution of the rms momentum spread (red line) and of the total cw power in the bandwidth (green line).

In conclusion, the option of TOF cooling of antiprotons or ions is useful alone for moderate cooling requirements on the final $\delta p/p$ or on the cooling time (e.g. lower particle number) or, due to its larger momentum acceptance, as pre-cooling of the beam tails before the notch filter takes over.

Longitudinal cooling of hot RIBs with the Palmer method is being simulated with the CERN code taking into account the response of the Faltin structures currently being designed. In [13], simulations of Palmer cooling of RIBs as well as its handover to notch filter/TOF cooling are presented, assuming loop couplers for all pick-up and kicker electrodes.

2.11.3 The Stochastic Cooling System of the HESR

Stochastic cooling in the HESR is necessary not only during the experiments to fulfill the beam requirements, but also during the accumulation process due to the postponed RESR. The stochastic cooling will consist in two systems: one main system working in the frequency range 2-4 GHz and one system for longitudinal cooling only, working in the range 4-6 GHz. Extensive simulations and prototype measurements have been carried out to optimize the HESR stochastic cooling system with new slot-ring couplers. These slot-ring couplers surround the whole beam and thus cover the total image current.

The coupling structure for the main 2-4 GHz system (Fig. 9) is a ring structure with octagonal arrangement of inductive electrodes and an aperture of 89 mm equal to the normal beam-pipe diameter of the HESR [14]. The round cell is somewhat like a classical iris-loaded linac cell which is heavily loaded by the eight 50 Ohm microstrip lines to obtain the octave bandwidth. Simulations with HFSS give more than two times higher longitudinal coupling impedances per unit length than comparable lambda/4

structures, while the field uniformity is constant over a wide range. This round structure offers the most compact solution for the HESR stochastic cooling system. With less than 2 m total active length at the pick-up side it satisfies the initial specification of the HESR longitudinal and transverse cooling. The modular design of this system allows an easy increase of the number of rings in a self-supporting structure.



Figure 9: Stack of 16 slot ring couplers.

Two consecutive octagonal rings are centred by circumferential steps of 3 mm length. They guarantee that the diameters fit within a margin of 0.05 mm. These structures have the great advantage that they can be simultaneously used in all three cooling planes. Another advantage in the case of the HESR, where already pre-cooled beams from the CR are injected, is the fact that no movable parts (plunging) inside the vacuum are needed to obtain a good signal to noise ratio.

In a small test tank these structures were successfully operated at the synchrotron COSY [15] as pick-up only. Extensive measurements at COSY with proton beams in 2008 and 2009 have shown that the vertical and horizontal betatron sidebands can be separated, although the structure has a continuous slot around the beam [16]. No unwanted coupling between the horizontal and vertical plane has been found (Fig. 10).

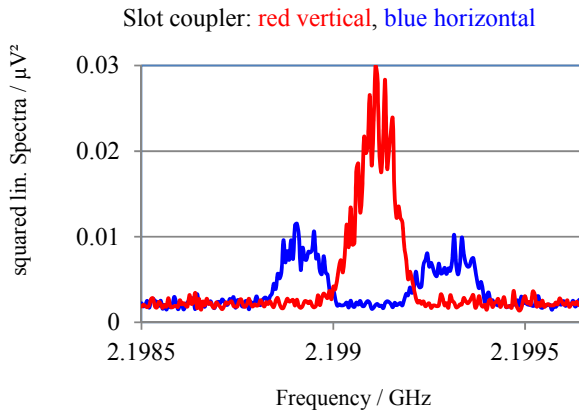


Figure 10: Vertical and horizontal betatron sidebands measured with the same structure. The vertical sidebands merge together because the tune Q_y was close to 3.5.

In a small version of 16 rings, these structures have been tested as pick-up and kicker in the Nuclotron in Dubna, where, in March 2013, the first stochastic cooling was demonstrated (Fig. 11). This small cooling system acts as test bench for the NICA project [17].

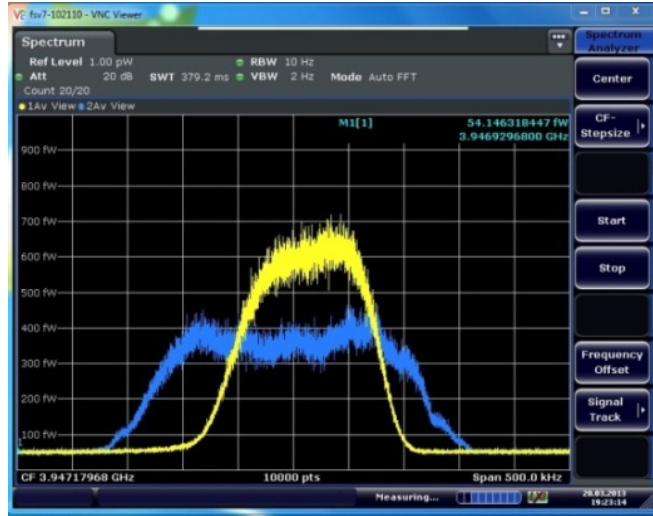


Figure 11: Demonstration of stochastic cooling at Nuclotron with HESR cooling structures.

Besides the main 2-4 GHz system, a second 4-6 GHz system is needed to fulfill the requirements of the HESR operation in the high-resolution mode [4]. This 4-6 GHz system will be used for additional longitudinal cooling only and will have a similar design. Due to the higher frequency range all dimensions except the aperture have been scaled. At least 12 electrodes are needed to suppress unwanted modes. Since 12 combiner boards are no longer mountable along the structure, always 2 electrodes will be combined already in the structure with an impedance matching network (Fig. 12).



Figure 12: Two slot coupler rings with combined electrodes for the 4-6 GHz longitudinal cooling system.

2.11.3.1 Stochastic Cooling Tanks

The system design is now finished including additional simulations [18] and system extensions to fulfill the requirements during the accumulation process. In total, 5 stochastic cooling tanks will be installed, each tank housing 64 slot coupler rings. Two tanks will be used as pick-ups, each cryogenically cooled by two cryoheads on top of the tank (Fig. 13). The mechanical layout of the cooling structure has been optimized. Support bars and rings connect the combiner boards with the second stages of the cryopumps. Thus, the lowest temperature of about 20 K will be achieved at the Wilkinson resistors, which are the main noise sources.

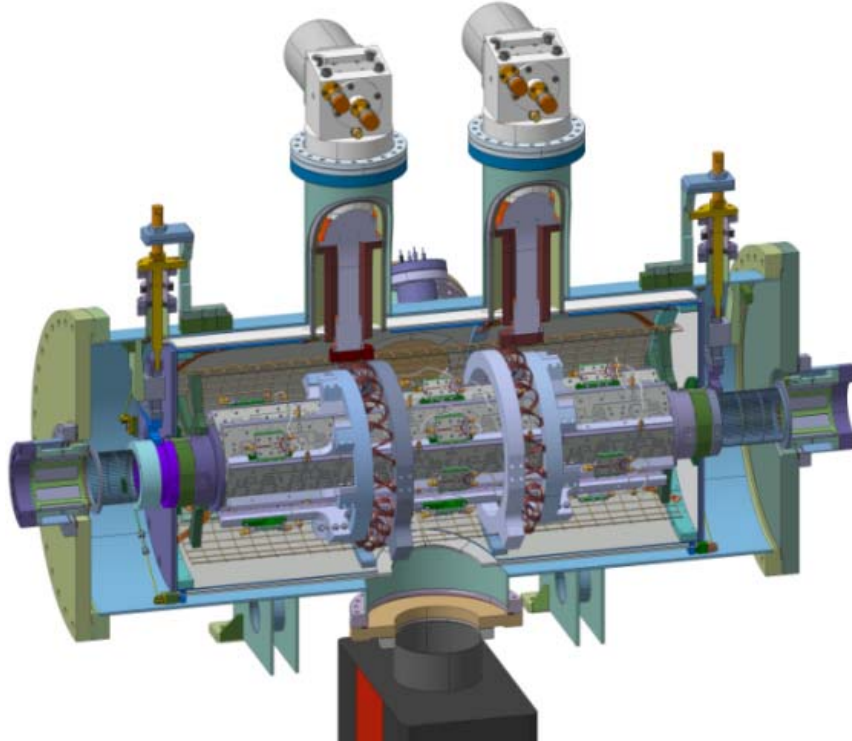


Figure 13: Completed design of the pick-up tanks.

Each pick-up will be used to detect the signals of all three cooling planes at the same time. The kicker tank layout will be similar to those of the pick-up tank except that no cryogenic cooling system will be installed and the electrode combination within the tank and thus the number of feedthroughs will be adjusted according to the RF power needed for the new accumulation scheme [19]. Here, three tanks will be installed, one for each cooling plane. Nevertheless, all tanks will be fully equipped with power amplifiers to ensure that each tank can be used for any cooling plane. This gives a good compromise to meet the necessary phase advance at the different optics. During the accumulation, all tanks will be used for longitudinal cooling, where higher RF power is needed. A switch matrix will be used to change between the different operation modes. This concept provides an installed RF power of about 300 W for each transverse cooling direction at each tank, or 600 W per tank when used for longitudinal cooling.

The tanks for the 4-6 GHz system will look like the same, except that 88 rings will be installed in one tank because of reduced size in beam direction. Only one pick-up and one kicker are needed.

Two longitudinal cooling methods will be used at the HESR: TOF as pre-cooling and when a sufficiently low beam momentum spread is reached, the powerful notch filter cooling [20]. Both signal paths of the notch filter will operate in the optical range. This eliminates phase noise and amplitude variation from the laser. The fluctuations of each notch over the time must be within 0.5 Hz. A temperature control in the order of 0.1K would be necessary taking into account the high temperature sensitivity of the optic fibre delay lines (30 ps/km/K). A much better solution has been found by an active control of the notch frequency. Besides the signal from the pick-up, a fixed frequency pilot signal will be added and transmitted through both optical paths. Directional couplers after the photodetectors take band-pass filtered parts of the transmitted signals to a phase detector. Any differences between the lengths of the two signal paths and thus any change of the notch frequencies will be detected by the phase detector. The controller closes this active loop by driving a fibre delay unit.

2.11.3.2 *Signal Combination*

Sixteen to one (16:1) combiners, optimized for the best signal combination at injection energy ($\beta = 0.96$), join the electrodes in the beam direction and built the smallest group without an active change of signal delay. The combiner losses at the lowest HESR energy and hereby the degradation of the signal to noise ratio are in the order of 2.5 dB, which is still tolerable.

Two to one (2:1) combiners join neighboring electrode rows to get the upper, lower, right and left signals for the transverse cooling. These combiners are designed as heat traps for the heat flow coming from the RF lines. Outside the tank the preamplified signals will be combined in 3 further layers (Fig. 14). Hereby, switchable delay lines are required to compensate for the energy-dependent drift time of the beam. The delay lines will be switched in steps of 10 mm of electrical length at the first layer (PV1) and 20 mm at the further layers (PV2, PV4).

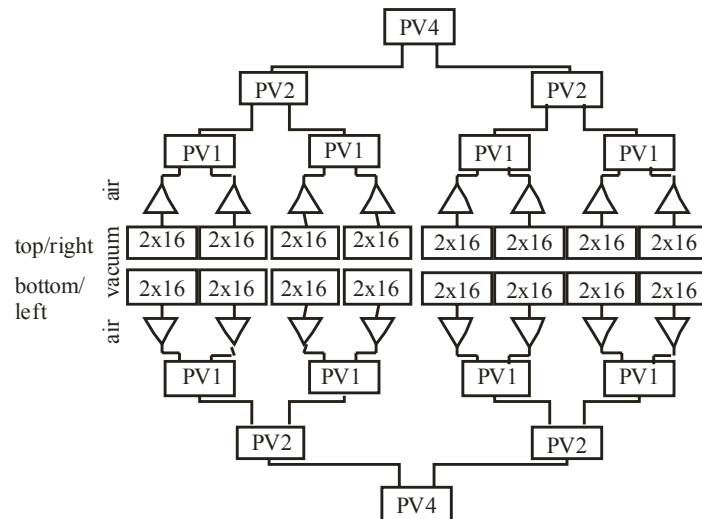


Figure 14: Pick-up section of the main system with programmable delay lines (PV) to provide stochastic cooling in the whole energy range of the HESR (lengths are not to scale).

Each programmable delay line includes a Wilkinson coupler which combines the two input signals after the switching stage. A deviation of 10 mm from the ideal length leads to a phase difference between the Wilkinson inputs that causes at 4 GHz an additional attenuation of nearly 0.8 dB. The last Wilkinson layer adds the power of both adjoining tanks. This allows stochastic cooling in the whole energy range of the HESR (0.8 - 14 GeV antiprotons). To minimize the number of switches, the reference plane is shifted at different energies, but this can be easily compensated by adjusting the delay line between pick-up and kicker. Furthermore, each signal path of the delay lines contains the same number of switches, and has therefore a similar amplitude-frequency characteristic. This reduces the expense of its compensation. All delay lines were built, tested and fulfill all RF requirements.

2.11.4 References

1. M. Steck, F. Nolden ‘Beam Cooling at GSI, this Newsletter.
2. M. Steck al., Proc. IPAC'10, Kyoto, Japan, THPEC038 (2010).
3. C. Dimopoulou et al., Proc. COOL'09, Lanzhou, China, THM2MCIO02 (2009).
4. H. Stockhorst, R. Stassen, T. Katayama ‘Stochastic Beam Cooling in the Storage Rings COSY and the future HESR with Internal Target Operation’, this Newsletter.
5. CR Technical Design Report 2014 (Doc TDR-CR-V15_27_02_2014.pdf
GSI EDMS Doc. 1367254/1).
6. C. Peschke et al., Proc. COOL'09, Lanzhou, China, MOA1MCIO03 (2009).
7. D. Barker et al., Proc. COOL'13, Mürren, Switzerland, WEPP021 (2013).
8. C. Peschke et al., Proc. COOL'13, Mürren, Switzerland, WEPP020 (2013).
9. C. Dimopoulou et al., Proc. COOL'11, Alushta, Ukraine, TUOB02 (2011).
10. W. Kells, in: Proc. of 11th Int. Conf. on High Energy Accelerators, Geneva, p.777 (1980).
11. C. Dimopoulou et al., Proc. IPAC'12, New Orleans, USA, MOPPD005 (2012).
12. C. Dimopoulou et al., Proc. COOL'13, Mürren, Switzerland, TUAM1HA01 (2013).
13. T. Katayama et al., Proc. COOL'13, Mürren, Switzerland, TUAM1HA04 (2013).
14. L. Thorndahl, 90mm Full-Aperture Structures with TM01-Mode propagation for 2-4 GHz Stochastic Momentum Cooling in HESR, internal report, (2010).
15. R. Maier, Cooler Synchrotron COSY – performance and perspectives, NIM A 390 (1997) 1-8.
16. R. Stassen, F.J. Etzkorn, R. Maier, D. Prasuhn, H. Stockhorst, L. Thorndahl, COSY as ideal Test Facility for HESR RF and Stochastic Cooling Hardware, Proc. PAC'09, Vancouver, Canada, (2009).
17. G. Trubnikov et al., Project of the Nuclotron-based ion collider facility (NICA) at JINR, Proc. EPAC'08, Genoa, Italy, (2008).
18. H. Stockhorst, R. Maier, D. Prasuhn, R. Stassen, T. Katayama, Status of stochastic cooling predictions at the HESR, Proc. IPAC'11, San Sebastian, Spain, (2011).
19. T. Katayama, T. Kikuchi, R. Maier, I. Meshkov, D. Prasuhn, R. Stassen, M. Steck, H. Stockhorst, Beam accumulation with barrier voltage and stochastic cooling, Proc. IPAC'10, Kyoto, Japan, (2010).
20. H. Stockhorst, R. Stassen, D. Prasuhn, R. Maier, T. Katayama, L. Thorndahl, Compensation of mean Energy Loss due to an internal Target by Application of a Barrier Bucket and Stochastic Momentum Cooling at COSY, Proc. COOL'09, Lanzhou, China, (2009).

2.12 Stochastic Beam Cooling in the Storage Rings COSY and the future HESR with Internal Target Operation

H. Stockhorst¹, T. Katayama², B. Lorentz¹, R. Maier¹, D. Prasuhn¹, R. Stassen¹

¹Forschungszentrum Juelich GmbH, Postfach 1913, D-52425 Juelich, Germany

²Nihon University, Narashino, Chiba, Japan

Mail to: h.stockhorst@fz-juelich.de

2.12.1 Introduction

The High-Energy Storage Ring (HESR) [1] of the future International Facility for Antiproton and Ion Research (FAIR, see C. Dimopoulou this ICFA issue) at GSI in Darmstadt has been originally designed for storage and acceleration of up to 10^{11} antiprotons for internal target experiments with high momentum resolution up to $\approx 1 \cdot 10^{-5}$ in the momentum range $1.5 \text{ GeV}/c$ to $15 \text{ GeV}/c$. Since in the modularized start version the storage rings RESR and NESR are postponed the accumulation of the beam delivered by the collector ring CR has to be accomplished in the HESR itself. The well-established stochastic stacking method [2] is however not applicable. Instead a different method using moving barriers and stochastic filter momentum cooling is proposed [3] to accumulate 10^{10} antiprotons within 1000 s . Recently, proposals were tabled to also prove the feasibility of the HESR storage ring for the application of cooled heavy ion beams with the special emphasis on the experimental program of the SPARC collaboration at FAIR.

In a series of experiments a Fokker-Planck and a particle tracking code developed for the investigation of the HESR cooling system properties to cool an antiproton or ion beam subject to the beam-target interaction have been experimentally verified at the cooler synchrotron COSY. The Time-Of-Flight momentum cooling technique (TOF cooling) [4] invented in 1980 has been verified experimentally at COSY for the first time in 2009. This technique offers the feature of a large momentum cooling acceptance and is easily established when filter cooling equipment is already available. Therefore, TOF cooling will be applied also in the HESR internal target experiments when a large initial momentum spread of the beam prevents the application of fast filter cooling. After a sufficient pre-cooling the beam with the TOF cooling mode the cooling system can be easily switched to fast filter cooling without any beam losses.

2.12.2 Brief Outline of Stochastic Momentum Cooling

The stochastic cooling method [5] is well established in many laboratories over the world [6]. In this contribution we restrict the description to an illustration of the main difference between the filter and the TOF momentum cooling technique. A detailed description of the theoretical cooling model for the HESR and COSY is presented in [7]. In the Fokker-Planck model of momentum cooling the main quantities are the drift (“cooling force”), describing the coherent energy change per second a particle receives at the kicker due to its own energy error at the pickup, and the diffusion heating terms which originate from thermal electronic noise in the cooling system and particle Schottky noise in the beam. Both contributions are illustrated for filter and TOF cooling in figure 1. The HESR cooling system, see C. Dimopoulou this ICFA issue, with a bandwidth ($2 - 4$) GHz is considered for a 3 GeV antiproton beam with $N = 10^{10}$

particles. The beam target interaction [8] contributes a diffusion due to energy loss straggling in the target and an additional drift originated by the mean energy loss. It is assumed here that the strong mean energy loss contributing to the drift term is compensated by a barrier bucket cavity as discussed below. The figure demonstrates the larger cooling acceptance for TOF cooling as compared to filter cooling. The arrow in the figure indicates the cooling acceptance of filter cooling. Outlying particles are heated. The figure suggests that, as compared to the TOF method, with the filter technique the beam core is cooled much faster due to the suppressed Schottky and thermal contributions. On contrary, the TOF technique cools the tails of the distribution faster. To avoid too much heating the electronic gain for TOF cooling is chosen to be smaller than for filter cooling. Consequently filter cooling is faster.

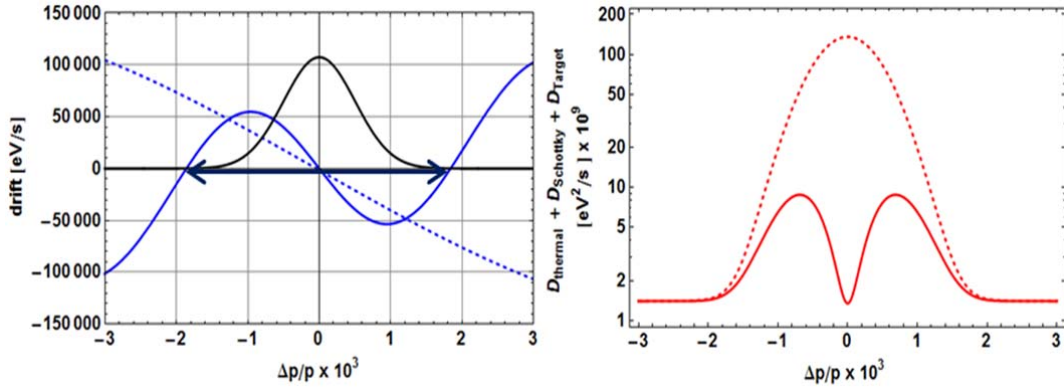


Figure 1: Left, the drift (cooling) term for TOF (dotted) and filter cooling. The mean energy loss is assumed to be compensated. Right, the diffusion contributions due to thermal noise, Schottky particle noise and beam-target interaction at the beginning of cooling. Thermal and Schottky noise contributions are suppressed in the center of the distribution due to the Notch filter in the signal path. The electronic gain is 110 dB. The cooling acceptance for filter cooling is indicated as an arrow. The drift for TOF cooling shows up a wider linear range and the larger cooling acceptance is visible. The initial momentum distribution is drawn in black.

Since in the one-dimensional Fokker-Planck equation the synchrotron motion is not included a numerical two-dimensional particle tracking code [9] is applied when rf-cavity fields are used to compensate the mean energy loss. The tracking model includes the synchrotron motion caused by the electro-magnetic fields of a barrier bucket cavity or a $h=1$ cavity. Cooling is described by the drift term used in the Fokker-Planck approach. Random energy changes from time step to time step are included that take into account the diffusion caused by Schottky particle and thermal electronic noise. A random energy change of a particle due to intrabeam scattering is included as well. The tracking code accounts for the coherent energy change a particle receives due to the mean energy loss and a random energy change caused by energy loss straggling in the presence of an internal target.

2.12.3 Model Predictions and Experimental Results at COSY

The first experiment at COSY that benefit from stochastic cooling was the COSY-11 experiment [10]. The COSY-11 collaboration concentrated on the threshold region for the production of mesons and meson-pairs using a COSY dipole as a zero degree

spectrometer and a hydrogen cluster target. Since the target in front of the dipole was located in a dispersive region strong particle losses occurred and consequently the experiment suffered from fast decreasing detector counting rates. An impressive improvement of the luminosity was achieved with stochastic cooling in all planes. The mean energy loss was compensated by cooling alone and the emittance blow up could be reduced. The target thickness was in the order of $N_T=3\times 10^{14}$ atoms/cm².

2.12.3.1 Internal Target Experiments with Stochastic Cooling assisted by a Barrier Bucket Cavity

The successfully tested Fokker-Planck model predicts that the mean energy loss can only be compensated by stochastic cooling alone if the target is sufficiently thin. The simulations indicate that a mean energy loss compensation by stochastic cooling alone is not possible for the target thickness envisaged in the HESR. In addition to cooling a barrier bucket (BB) cavity [11,12] will be used to accomplish this goal. The expected advantage of a barrier cavity for stochastic cooling is that the beam remains nearly coasting except a small gap.

Experimental tests for beam cooling with the barrier cavity at COSY [13] have been carried out with a beam containing $N=2\times 10^9$ protons at $2.6\text{ GeV}/c$. Figure 2 shows the barrier voltage pattern. The barrier frequency is 7 MHz and the peak voltage amounts 175 V . Two half sine waves spaced apart from one another by the revolution period $T_0=65\text{ }\mu\text{s}$ constitute the barriers.

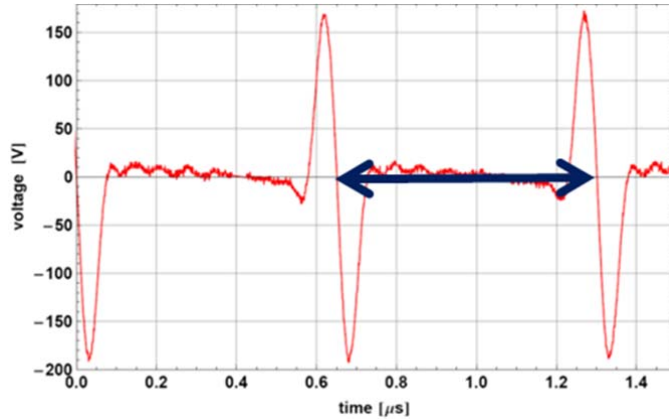


Figure 2: Barrier bucket cavity voltage. The revolution period is indicated by the arrow.

The DC beam is initially heated to increase the beam momentum spread such that almost 70% of the beam lie outside the barrier bucket area. Stochastic momentum cooling with the band II ($1.8 - 3\text{ GHz}$) system is then applied to cool the beam into the bucket. The results are depicted in figure 3. A phase probe monitor is used to measure the beam distribution along the ring. Initially when the beam is DC no signal is observed. The measured phase probe monitor signals increase during cooling indicating that more and more particles are trapped in the barrier until equilibrium is attained. It is visible that the beam remains almost DC during cooling except a small gap. During cooling ripple emerges in the beam distribution along the ring. This is due to the slight asymmetric voltage pattern and the ripple visible in figure 2. Figure 3 shows also that the beam momentum spread is effectively reduced during cooling.

The experimental results and the simulations suggest that this technique to cool beam particles into the barrier bucket potential can be successfully applied in internal target experiments for the case when the initial beam has a too large momentum spread that exceeds the barrier height, see also figure 10. Inserting a target into the beam would then result in particle losses. This can be avoided if the beam particles are cooled into the bucket before the internal target experiment starts.

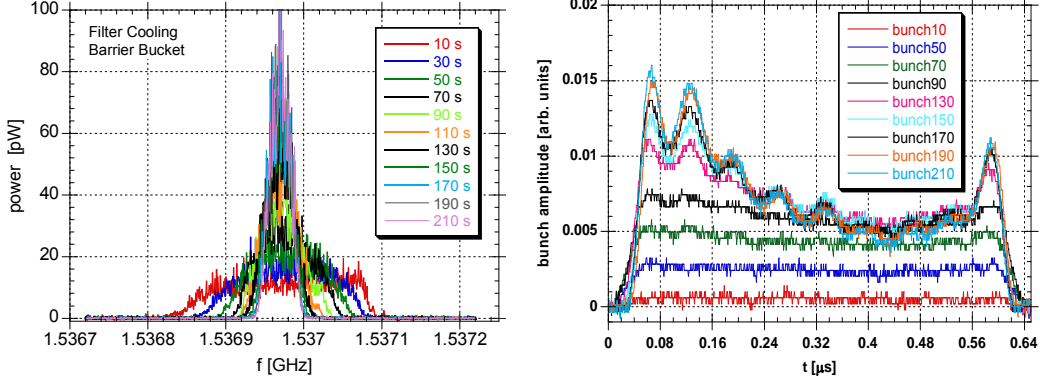


Figure 3: Left: Momentum distributions during cooling. Right: Beam distribution along the ring.

Stochastic beam cooling experiments with a thick internal target and barrier bucket operation have been carried out at $2.6 \text{ GeV}/c$ with $N = 2 \cdot 10^9$ protons. The WASA pellet target [14] located in one straight section of COSY with zero dispersion was used. It is capable to deliver a target thickness $N_T \approx 3 \cdot 10^{15}$ atoms / cm^2 which is an order of magnitude larger than that of the ANKE cluster target and has a similar thickness as will be used in the PANDA experiment in the HESR.

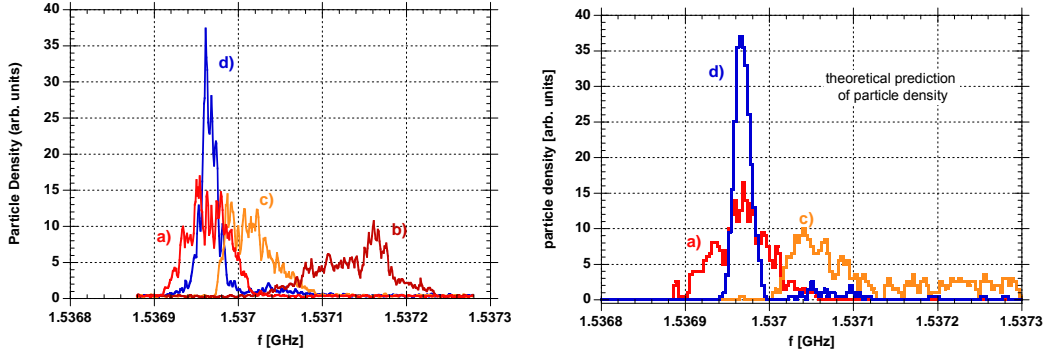


Figure 4: Measured Schottky spectra (left figure) of a COSY proton beam measured at the 1000th harmonic: a) initial distribution; b) distribution after 180 sec only pellet target, the energy loss led to a shift to higher frequencies since $\eta < 0$; c) only pellet-target and cooling; d) after 180 sec with cooling and barrier bucket as well as target. The right figure shows the simulation results.

Only stochastic momentum cooling is applied in the frequency range (1.8 – 3) GHz. The experimental results are shown in figure 4, left. The initial distribution is drawn in red. The beam frequency distribution without cooling and barrier cavity operation is

shown after 180 s (b). Due to the mean energy loss it is shifted towards a larger frequency since the machine is operated above transition energy ($\eta < 0$). With stochastic cooling and target ON the distribution marked with c) is observed after 180 s indicating that the effect of the mean energy loss is reduced. The distribution labeled with d) is observed when additionally the barrier bucket cavity was switched ON. The measured beam distribution shows that the mean energy loss is compensated and the resulting beam distribution is symmetric w.r.t. the nominal frequency or beam momentum. The distributions right-hand in figure 4 describe the theoretical predictions [9] according to the numerical particle tracking code. The results are marked with the same labels. A remarkable agreement between the experimental results and the model prediction is found.

2.12.3.2 Time-Of-Flight and Filter Cooling

The Time-Of-Flight cooling technique is easily realized in COSY by opening the filter delay path and reversing the electronic gain. To test the larger cooling acceptance with TOF cooling as predicted by the cooling model experiments with a 2.6 GeV/c proton beam have been carried out. The initial momentum spread of the beam was increased by applying band-limited white noise at harmonic number one with a momentum kicker. In figure 5, left, the initial momentum is shown which has an almost rectangular shape due to the heating. Frequency distributions during TOF cooling have been measured which clearly show the cooling effect by this method. The steepness of the distribution at 900 s confirms the model prediction that with the TOF cooling method the tails are more effectively cooled. The distribution at 900 s is slightly offset. This can be corrected by a minor change of the delay length in the cooling chain. If the delay length is increased by 7.5 mm the beam will slightly be accelerated. This is illustrated in figure 5, right. Since the machine was operated above transition energy a downwards shift of the frequency distribution was observed. After 900 s an equilibrium is attained.

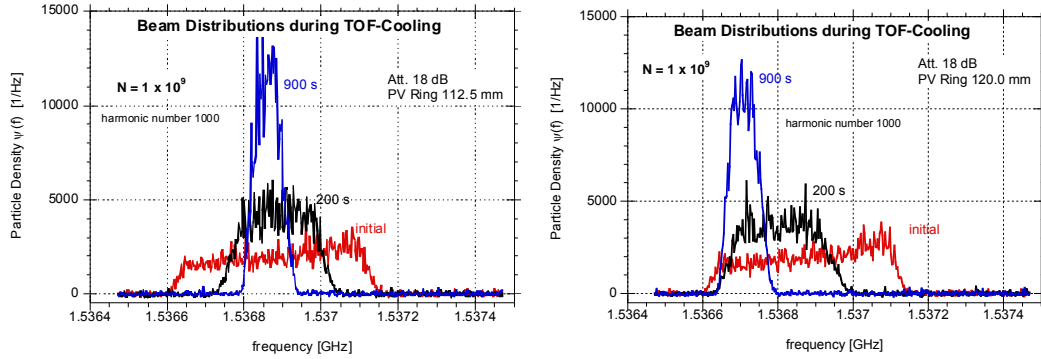


Figure 5: Time evolution of the frequency distribution during TOF momentum cooling for two different delay line lengths.

To explore the prediction of the larger cooling momentum acceptance of TOF cooling as compared to filter cooling the initial beam distribution was further heated by applying band-limited white noise. In figure 6 the result of only filter cooling is displayed. After 200 s the distribution is cooled but it exhibits still tails towards lower and higher frequencies. This indicates that filter cooling is more effective in the center. Particles with lower or higher frequencies in the tails which are outside the filter cooling

acceptance see a wrong sign in the cooling force (see figure 1) and are driven further out of the center. As a result a part (28 %) of the beam particles in the tails is heated by the cooling system and is lost at the momentum acceptance of the machine. At 1.53734 GHz a small peak (see arrow in figure 6) is visible which is due to a vanishing local frequency slip factor. The available particle frequency attains here a maximum value. Particles which loose energy due to the heating cannot have frequencies beyond that value. They enhance the density in the vicinity of this value leading to asymmetric distributions. As seen in figure 6 the tails are reduced by cooling as time proceeds. However particles close to the peak are almost not cooled indicating that these particles exceed the filter cooling acceptance.

In order to avoid initial particles losses the beam was pre-cooled with the TOF method for 200 s. After pre-cooling the cooling system was switched to filter cooling: The filter part that contains the delay by one revolution was closed and the gain was inverted. One observes that the tails are reduced by TOF cooling. Particles are moved to the center during pre-cooling ($t=210\text{ s}$). Note also that the particle enhancement at the small peak in the distributions at 1.53734 GHz indicated with the arrow is reduced noticeably with TOF cooling indicating the larger cooling acceptance of TOF cooling and a stronger tail cooling. In this case no particle losses were observed. The final relative momentum spread after 900 s of cooling was $1 \cdot 10^{-4}$ (FWHM).

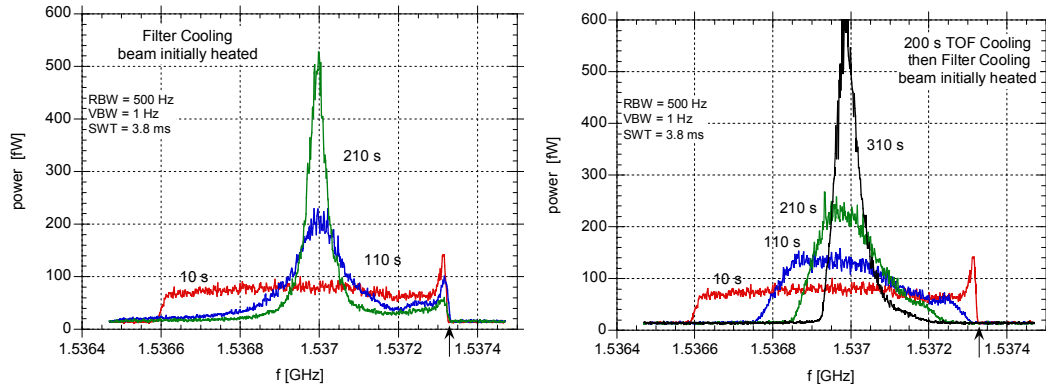


Figure 6: Power spectra at $n = 1000$ during cooling. Left only filter cooling. Right, pre-cooling with TOF for 200 s. Then switch to the filter cooling method.

In conclusion, the measurements confirmed the cooling model predictions that TOF cooling can easily be established when a filter cooling system is already installed and that this method obeys the larger cooling acceptance. Applying TOF cooling to an initially broad beam is an easy and effective technique to reduce the momentum spread so that it fits into the acceptance of the faster filter cooling method. The TOF cooling technique has therefore been adopted for momentum pre-cooling in the HESR.

It is important to point out the following remarks. The electronic cooling chain forms a feedback loop via the beam [5]. Thus, depending on the system gain the cooling loop may become stable or unstable. The analysis reveals [7, 15] specifically for TOF cooling that feedback via the beam enhances the cooling force at the edge of the distributions while it reduces cooling in the core. The cooling loop may become unstable if the particle momentum or energy distribution becomes too stiff at the edges as shown in figure 5. To avoid instabilities the gain should be reduced accordingly during cooling which however leads to a slower cooling and a larger equilibrium value.

With target operation the cooling loop is less vulnerable to instabilities due to the additional heating which smooth the edges of the beam distributions. Filter cooling with smooth tails, see figure 6, is thus less affected especially with target operation.

2.12.4 Stochastic Momentum Cooling Investigation for the HESR

2.12.4.1 *The Antiproton Beam Mode in the HESR*

The proposed way of antiproton beam accumulation for the HESR uses the already designed stochastic cooling system and the BB cavity of the HESR. The BB cavity is used to separate the circumference of the HESR ring into two regions, one reserved for the injected beam and the other one for the accumulated beam. The fixed and moving barrier cases have been studied in detail with a particle tracking code [3]. Considerably better results of antiproton beam accumulation were achieved when the moving barrier method is applied. The results are illustrated in figure 7 for the first injection cycle. A beam bunch of 10^8 antiprotons delivered by the CR is kicked injected every 10 seconds into the central part of the two full wave barrier pulses (figure 7, 0 s.). Just after beam injection the barrier voltages are switched off and the beam becomes coasting (9.2 s). Fast filter stochastic cooling is continuously applied during the whole accumulation process. In the well cooled coasting beam again two full-wave barrier voltages are excited adiabatically and the right hand voltage moves (figure 7 at 9.6 s) to the injection position (figure 7, 10 s) within the period of 0.5 sec. A new particle free gap for the injection of the next bunch is available. This procedure is repeated 100 times (1000 s) until 10^{10} antiprotons are accumulated.

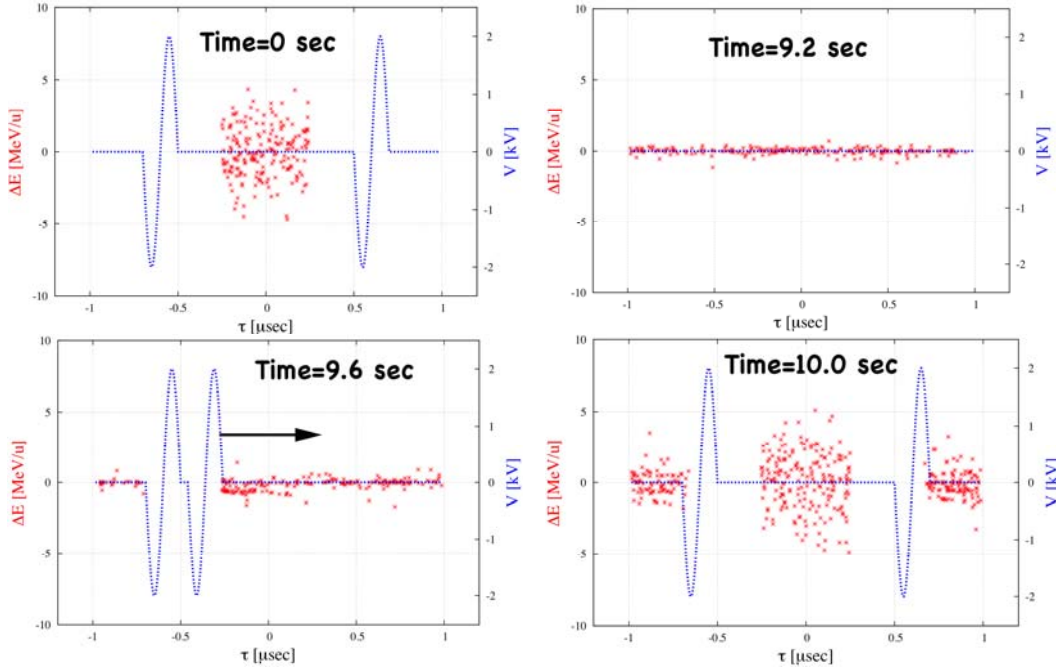


Figure 7: Moving barrier accumulation scheme. Details see the text.

The accumulation efficiency reaches 97 %, figure 8. The relative momentum spread is reduced from the start value $5 \cdot 10^{-4}$ to $5 \cdot 10^{-5}$ at the end of accumulation. It is essential

for an efficient accumulation to reduce the electronic gain of the cooling system from initially 130 dB to 115 dB during accumulation, figure 8 right. This is suggested by the fact that Schottky noise heating being proportional to the amplifier voltage gain squared increases with an increasing antiproton density in the HESR. The final relative momentum spread that is attained is $\Delta p/p = 5 \cdot 10^{-5}$ (rms).

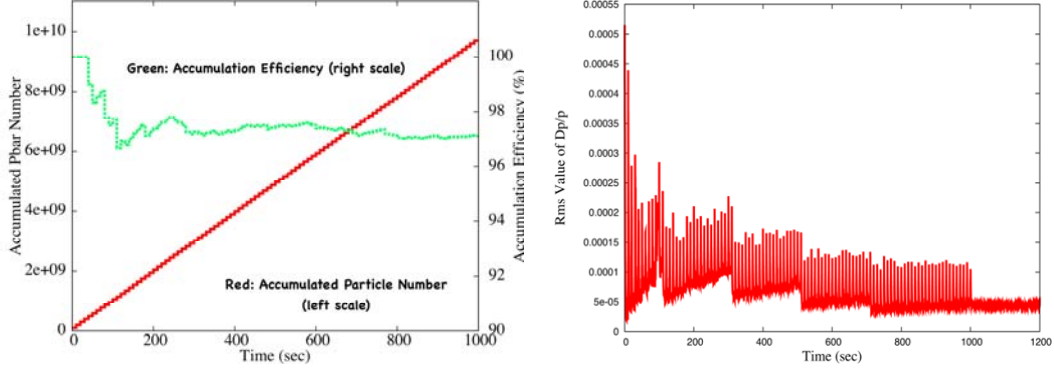


Figure 8: Left, Number of accumulated antiprotons (red) versus time and accumulation efficiency (green). Right, relative momentum spread during the accumulation process. The electronic gain is reduced in four steps during accumulation from 130 dB to 115 dB .

The initial microwave power amounts 70 W for the highest gain 130 dB . As a rule of thumb, the total electronic power that has to be installed should be a factor 3 to 5 larger to account for the statistical fluctuations of the signals. The total power does not exceed the envisaged 500 W for the HESR stochastic cooling system.

Recently, an international collaboration consisting of members from GSI, Japan, Russia, CERN and FZJ Juelich could successfully demonstrate at the GSI the possibility of beam stacking with a BB system assisted by electron and stochastic cooling. The results are in close agreement with the accumulation simulations [16].

Figure 9 shows the result of filter momentum cooling for 10^{10} antiprotons at $T=3\text{ GeV}$ subject to an internal hydrogen target with thickness $N_T=4 \cdot 10^{15}\text{ cm}^{-2}$.

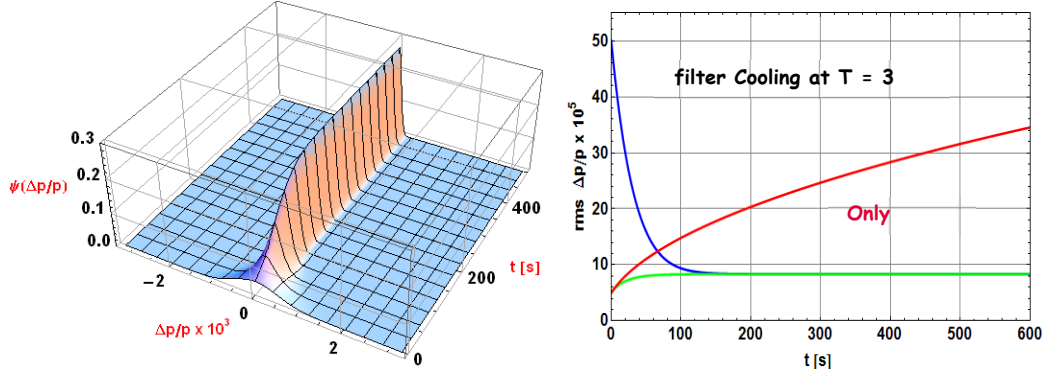


Figure 9: Left: Time evolution of the beam momentum distribution. Right: Time development of the relative momentum spread of a beam with 10^{10} antiprotons at 3 GeV interacting with an internal target. The red curve shows the beam heating when cooling is off.

The Fokker-Planck equation with the drift and initial diffusion term shown in figure 1 has been solved numerically to determine the cooling property for two initial

momentum spreads. The mean energy loss induced by the target-beam interaction has been assumed to be compensated with a BB cavity.

The blue curve shows the reduction of the rms relative momentum spread for the initial value $5 \cdot 10^{-4}$ while the green curve starts with the initial value $5 \cdot 10^{-5}$ resulting at the end of the accumulation process. The simulations predict that in both cases the same equilibrium value is attained approximately after 200 s is $(\Delta p/p)_{rms}=8 \cdot 10^{-5}$. The red curve shows the increase in momentum spread when cooling is switched off and only the energy loss straggling due to the beam-target interaction is present.

The expected momentum cooling performance at three energies is summarized in table 1. In all cases an equilibrium value is attained at $(\Delta p/p)_{rms} \approx 8 \cdot 10^{-5}$. The time (cooling down time) needed to approach this value depends on the initial value. The simulation results are found for an optics lattice with $\gamma_{tr}=6.2$. The Schottky particle power is below 25 W. The thermal noise power is negligible. Again, the total electronic power that has to be installed should be a factor 3 to 5 larger.

Table 1: Expected momentum cooling performance at three different kinetic energies of an antiproton beam and major system parameters.

<i>T [GeV]:</i>	<i>3</i>	<i>8</i>	<i>15</i>
Initial rms rel. momentum spread δ_{rms} :	$5 \cdot 10^{-4}$	$5 \cdot 10^{-4}$	$5 \cdot 10^{-4}$
Final rms rel. momentum spread δ_{rms} :	$8 \cdot 10^{-5}$	$8 \cdot 10^{-5}$	$6 \cdot 10^{-5}$
cooling down time [s]:	≈ 200	≈ 300	≈ 300
Voltage gain [dB]:	110	118	120
Schottky power [W]:	5	7	24
Thermal Noise [W]:	0.06	0.4	0.6
Cooling acceptance $\times 10^3$:	± 1.8	± 2.6	± 1.9

2.12.4.2 *The Heavy Ion Beam Mode in the HESR*

Heavy ion stochastic momentum cooling is investigated under the constraint of the present concept of the HESR [17]. The magnetic rigidity range $5Tm \leq B\rho \leq 50Tm$ allows the storage of $^{238}U^{92+}$ ions in the kinetic energy range 740 MeV/u up to ≈ 5 GeV/u. For an internal target experiment at 740 MeV/u the CR beam with 10^8 ions is kicked injected into the stable area of two full wave barriers 1.1 μ s apart with the maximum available barrier peak voltage 2 kV as shown in the longitudinal phase space figure 10. The momentum spread of the incoming beam bunch (red points) significantly exceeds the bucket height for the available BB cavity operating at a frequency $f_{bb}=5$ MHz. After injection the barriers are moved adiabatically within 500 ms in the direction as indicated in the figure by arrows. The revolution period is $T_0=2.31$ μ s. The final position of the barriers after 500 ms is shown in figure 10, right-hand. It can be seen that the momentum spread of the ions inside the separatrix is adiabatically reduced while those outside the separatrix only debunch and stay outside the separatrix. They are not lost since the momentum acceptance of the HESR is larger than $\pm 2.5 \cdot 10^{-3}$. Stochastic TOF momentum cooling with a gain set to 85 dB and a cooling acceptance of $\Delta p/p = \pm 7 \cdot 10^{-4}$ is now invoked for 2.5 s to cool the ions into the separatrix. The hydrogen internal target with a thickness $N_T=4 \cdot 10^{15}$ cm⁻² is switched on 3 s after injection. The tracking simulations predict an equilibrium after 6 s and that almost all of the particles outside the separatrix are well cooled into it. The equilibrium momentum distribution (blue) is depicted in figure 11. It is clearly apparent that the mean energy loss due to the

thick hydrogen target is effectively compensated with cooling assisted by the barrier cavity. More than 70 % of the uranium ions inside the stable area of the separatrix have a fractional momentum spread less than $5 \cdot 10^{-5}$ during the internal target experiment. Those particles which are initially outside the cooling acceptance will be lost (3 %).

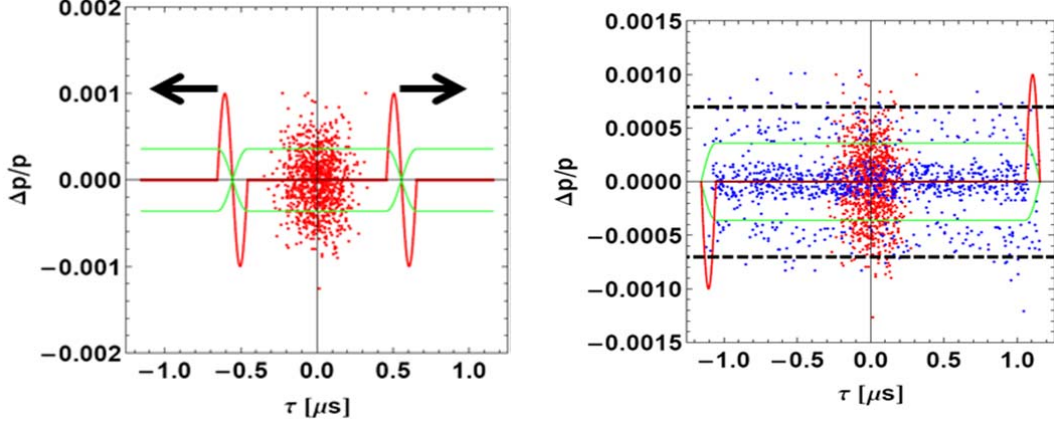


Figure 10: Left: Phase space portrait of the injected beam bunch (red points). The separatrix of the BB is drawn in green. After injection the barriers are moved as indicated with arrows. Right: Phase space portrait of the beam (blue points) after 500 ms. For comparison the injected beam (red points) is shown. The dotted lines indicate the TOF cooling acceptance.

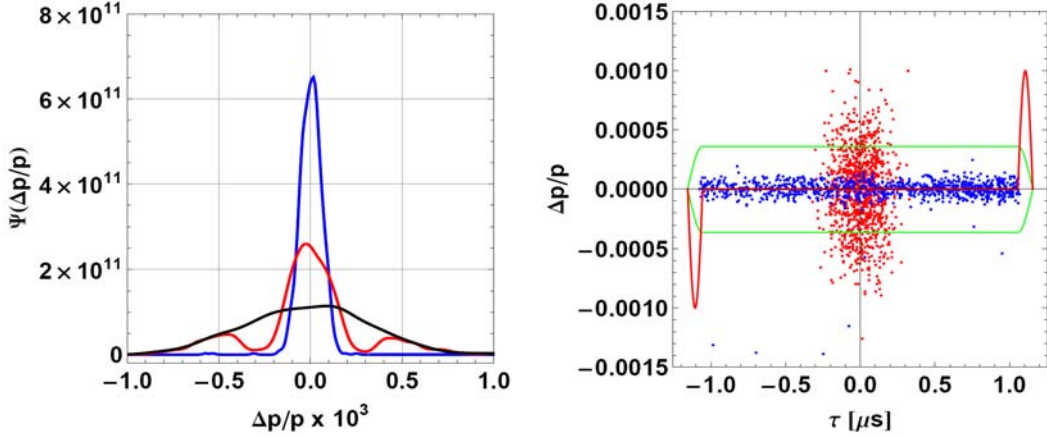


Figure 11: Left: The initial beam distribution is shown in black. The beam distribution at $t=0.5\text{ s}$ (red) exhibits two bumps at $\pm 0.5 \cdot 10^{-3}$ corresponding to the particles outside the separatrix in figure 10. Cooling moves these particles into the stable area of the separatrix, blue curve. The corresponding phase space (blue dots) is shown in the right figure. The beam is almost DC with a gap of 10%.

For heavy ion beam acceleration a bunch with 10^8 ions from the CR is kicked injected into the standing bucket of the $h=1$ cavity with the maximum peak voltage 2 kV . The maximum achievable energy gain per nucleon per turn of an bare uranium ion is $dT=0.165\text{ keV/u/turn}$ since the magnetic field ramp rate in the HESR is limited to $dB/dt=25\text{ mT/s}$. The acceleration ramp to 4.5 GeV/u possesses an intermediate flat top at 3 GeV/u where after an adiabatic reduction of the cavity voltage to zero and de-bunching to a DC beam the standard lattice optics with $\gamma_{tr}=6.2$ is changed to $\gamma_{tr}=14.6$

in order to avoid a too small ring frequency slip factor. After an adiabatic re-capture acceleration is continued and reaches after 50 s the top final energy. The voltage is adiabatically switched off thereby reducing the momentum spread so far that it well fits into the cooling acceptance for fast filter cooling. The standard lattice optics is then used for an internal target experiment. The simulations predict an equilibrium after 10 s with an rms fractional rms momentum spread $2 \cdot 10^{-5}$. In the simulation an electronic gain 108 dB has been chosen. The microwave power amounts initially 60 W.

2.12.5 Summary and Conclusions

During the past extensive theoretical model investigations and numerical simulations of the stochastic cooling process of antiproton beams in the HESR have been carried out with the aim to achieve the required challenging beam quality and the requested beam intensities in internal target experiments. The moving barrier bucket accumulation scheme with stochastic cooling has been introduced since the RESR as accumulator ring for the HESR is postponed in the modularized start version of FAIR. In a proof-of-principle experiment it could be successfully demonstrated that this method will be a reliable solution for the HESR. The barrier bucket cavity of the HESR will also be employed to compensate the mean energy loss introduced by the beam-target interaction during internal target experiments. The theoretical studies predict that the present design of the HESR is capable to store and accelerate uranium ions as well. Ion beam experiments with internal target and stochastic cooling assisted by a barrier bucket cavity operation for mean energy loss compensation are expected to be feasible.

The beam target interaction with various target densities has been explored at COSY with stochastically cooled proton beams assisted by a $h=1$ cavity, or in comparison, with a barrier bucket cavity. While for thin targets filter cooling is capable to compensate the mean energy loss alone a BB cavity is mandatory for thick targets. The experimental results were found in good agreement with model predictions. Therefore it is expected that these models will provide reliable results for the HESR as well.

A valuable momentum cooling technique is the proposed TOF cooling method. No additional cooling system equipment is necessary if the filter momentum cooling method is already installed. In COSY experiments the proposed method was successfully tested and it could be proven that the method in comparison with the filter momentum method processes the larger cooling acceptance as was theoretically predicted. It was also shown that only one cooling system could be efficiently applied to a beam with an initially broad momentum distribution by first sufficient TOF cooling and then switching to the faster filter cooling.

2.12.6 Acknowledgement

Thanks are due to F. Caspers, C. Dimopoulou, F. Nolden and L. Thorndahl for many stimulating discussions and valuable advice.

2.12.7 References

1. HESR, “Baseline Technical Report”, <http://www.fz-juelich.de/ikp/hesr/2-11-HESR.pdf>, update Apr. 2008
2. F. Caspers and D. Möhl, “Stacking with Stochastic Cooling”,

- CERN-AB-2004-028 RF
3. T. Katayama, M. Steck, R. Maier, D. Prasuhn, R. Stassen, H. Stockhorst, I. Meshkov and T. Kikuchi, "Beam Accumulation with Barrier Voltage and Stochastic Cooling", Proc. of IPAC 2010, 23 – 28 May 2010, Kyoto, Japan
See also: T. Katayama, M. Steck, H. Stockhorst, I. Meshkov and T. Kikuchi, "Beam Accumulation and Bunching with Cooling", Proc. of COOL 13, 10-14 June 2013, Muren, Switzerland
 4. W. Kells, "Filterless Fast Momentum Cooling", Proc. of the 11th Int. Conf. on High-Energy Accelerators, Geneva, Switzerland, July 7-11, 1980, p. 777, and ref. therein
 5. D. Möhl, Stochastic Cooling of Particle Beams, Lecture Notes in Physics 866, Springer Verlag, 2013, ISBN 978-3-642-34978-2
 6. F. Caspers and D. Möhl, Eur. Phys. J. H, 36,4, 2012, 601-632
 7. H. Stockhorst, T. Katayama, R. Maier, "Beam Cooling at COSY and HESR, - Theory and Simulation -", to be published
 8. F. Hinterberger, "Beam-Target Interaction and Intrabeam Scattering in the HESR Ring", 2006, JüL-4206, ISSN 0944-2952
 9. H. Stockhorst, R. Maier, D. Prasuhn, R. Stassen and T. Katayama, "Stochastic Momentum Cooling Experiments with a Barrier Bucket Cavity and Internal Targets at COSY-Juelich in Preparation for HESR at FAIR", Proc. of IPAC 2010, 23 – 28 May 2010, Kyoto, Japan
 10. A. Kupść, P. Moskal, M. Wolke, editors, "Meson Physics at COSY-11 and WASA-at-COSY", An International Symposium, Krakók, Poland, 17 - 22 June 2007
 11. J.E. Griffin, C. Ankenbrandt, J.A. MacLachlan and A. Moretti, IEEE Transactions on Nuclear Science, Vol. NS-30, No. 4, August 1983
 12. S.Y. Lee, Accelerator Physics, World Scientific Publishing Co. Pte. Ltd, 1999
 13. P. Brittner, H.U. Hacker, R. Maier, U. Pfister, D. Prasuhn, H. Singer, W. Spiess, R. Stassen, H. Stockhorst, A. Zumloh, "The Stochastic Cooling System for COSY", Proc. of EPAC92, 24 -28 March, 1992, Berlin, Germany
 14. H.-H. Adam et al., e-Print: nucl-ex/0411038
 15. C. Dimopoulou, A. Dolinskii, T. Katayama, F. Nolden, C. Peschke, M. Steck, D. Möhl, L. Thorndahl, "Simulations of Stochastic Cooling of Antiprotons in the Collector Ring CR", Proc. of COOL 11, September 12-16, 2011, Alushta, Ukraine
 16. M. Steck, C. Dimopoulou, B. Franzke, O. Gorda, T. Katayama, F. Nolden, G. Schreiber, D. Möhl, R. Stassen, H. Stockhorst, I. N. Meshkov, A. O. Sidorin, G. Trubnikov, "Demonstration of Longitudinal Stacking in the ESR with Barrier Buckets and Stochastic Cooling", ibidem
 17. H. Stockhorst, R. Maier, D. Prasuhn, R. Stassen and T. Katayama, "Simulation Study of Heavy Ion Beam Injection and Acceleration in the HESR for Internal Target Experiments with Cooling", Proc. of IPAC 14, June 15 – 20, 2014, Dresden, Germany

3 Activity Reports

3.1 The Advanced Superconducting Test Accelerator at Fermilab

Elvin Harms, Jerry Leibfritz, Sergei Nagaitsev, Philippe Piot¹, Jinhao Ruan,
 Vladimir Shiltsev, Giulio Stancari, Alexander Valishev

Fermi National Accelerator Laboratory, Batavia IL 60510

Mail to: piot@fnal.gov

3.1.1 Introduction

The Advanced Superconducting Test Accelerator (ASTA) facility (<http://asta.fnal.gov>) currently under construction and commissioning at Fermilab will enable a broad range of beam-based experiments to study fundamental limitations to beam intensity and to develop transformative approaches to particle-beam generation, acceleration and manipulation [1]. Three main elements of the ASTA facility include the Integrable Optics Test Accelerator (IOTA) ring capable of storing electrons or protons; b) 150-300 MeV electron injector based on existing ASTA SRF electron linac; c) 2.5 MeV proton injector based on existing HINS proton source. ASTA is intended to be operated as a test facility for advanced accelerator research and developments (AARD) towards intensity frontier proton accelerators. It is anticipated that experimental studies at ASTA's IOTA ring with protons and electrons, augmented with corresponding modelling and design efforts should pave the way for a proposal that will allow substantial increase of the proton flux available for high-energy Physics research with Fermilab accelerators at a lower cost. ASTA will be the only accelerator R&D facility in the worldwide. ASTA will support the development of new ideas towards the next generation high-intensity proton facilities and allows a broad range of intensity-frontier-motivated experiments, such as *integrable optics* with non-linear magnets and with electron lenses, and *space-charge compensation* with electron lenses and electron columns.

At the same time, ASTA will establish a unique resource for R&D towards Energy-Frontier facilities and a test-bed for SRF accelerators and high-brightness-beam applications. The unique features of ASTA include: (1) a high repetition-rate, (2) one of the highest peak and average brightness within the U.S., (3) a GeV-scale beam energy, (4) an extremely stable beam, (5) the availability of SRF and high-quality beams together, and, of course, (6) the IOTA storage ring capable of supporting a very broad range of ring-based advanced beam dynamics experiments. These unique features have a potential to foster a broad program in advanced accelerator R&D that cannot be explored at other facilities.

Besides these high priority tests, which are to be supported by Fermilab's Accelerator Science program, a number of studies can be performed by the broader user community at the IOTA ring and its injectors utilizing the facility's unique beam capabilities. The facility is foreseen to be able to serve a broad community intensity-frontier and energy-frontier-motivated researchers from many institutions (FNAL, CERN, ORNL, LBNL, JLab, NIU, CSU, University of Maryland, JINR/Dubna and

¹ also Department of Physics and Northern Illinois Center for Accelerator & Detector Development (NICADD), Northern Illinois University, DeKalb IL 60115, USA

BINP/Novosibirsk are already among the collaborating institutions). The ASTA team welcomes interested users without regard to national or institutional affiliation and researchers from national- and international universities and groups, the Department of Energy's National Laboratories; small business and industrial companies. ASTA users' meetings are held annually, the first two took place in July 2013 and in June 2014 [2].

3.1.2 Facility Overview & Capabilities

The construction of the ASTA facility is staged. The first stage enables a low-energy AARD program based on the photoinjector (~ 50 MeV) and a 300 MeV program based on a single SRF cryomodule, with associated beam transport lines and beam dumps; see Fig. 1.

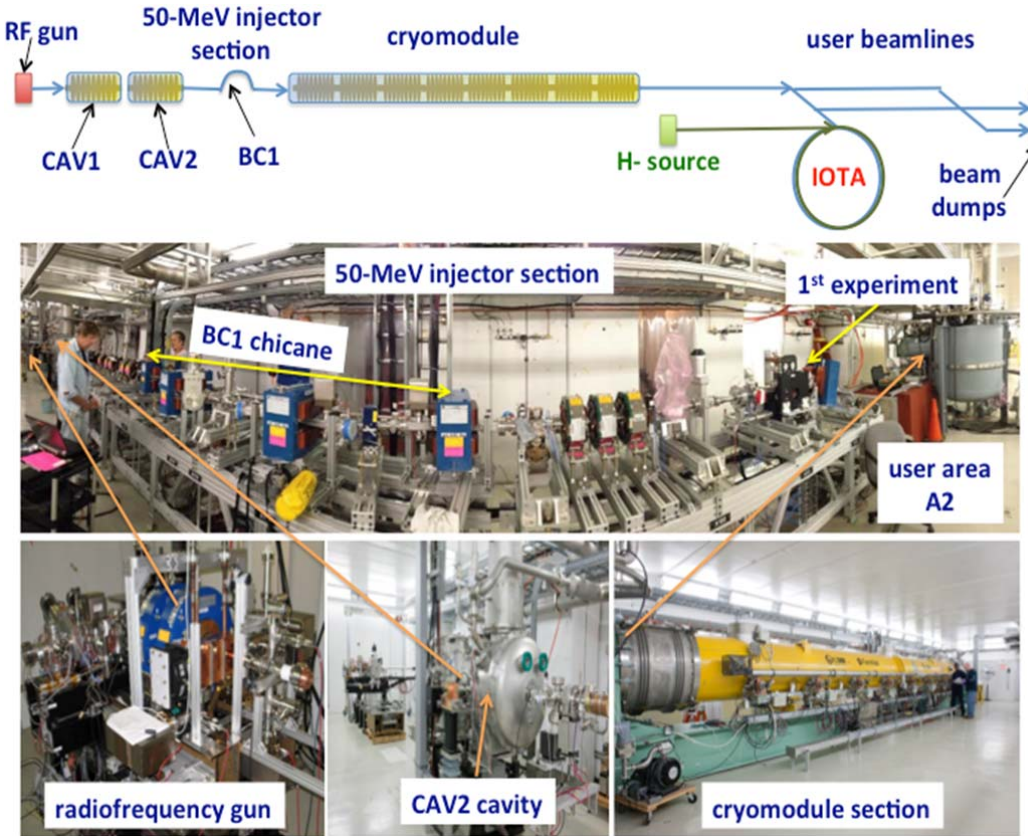


Figure 1: Overview of ASTA (top row) and photographs of the beamline sections (middle and lower rows). The labels "CAV1" and "CAV2" correspond to superconducting TESLA-type cavities, "BC1" is a magnetic-chicane bunch compressor, and "IOTA" stands for integrable-optics test accelerator. The total length of the facility is approximately 130 m.

The first stage also enables one of the transformative beam dynamics experiments: exploration of novel, non-linear accelerator lattices in the Integrable Optics Test Accelerator (IOTA). An overview diagram of the foreseen facility in its first phase appears in Fig. 1 along with photographs of key subsystems already installed or in operation at the facility. Longer-term plans for expansion of ASTA are discussed at the end of this report.

Several experimental areas will be available to users for installation of experiments. A low-energy area situated within the photoinjector (eventually including an off-axis beamline), will provide electron bunches, possibly compressed, with energies up to ~ 50 MeV. A high-energy experimental area located downstream of the cryomodule section incorporates two (possibly three) parallel beamlines and the IOTA ring. Beam can in principle be delivered to the various user beamlines and IOTA quasi simultaneously as switching the beam from one beamline to the other would only require minor optical-lattice adjustment. Finally, the eventual availability of a H^- source would allow IOTA to be operated independently from the ASTA electron-beam users.

3.1.2.1 *Injector and Superconducting Radiofrequency (SRF) Linac*

The backbone of the ASTA facility is a normal-conducting radiofrequency (RF) photoinjector coupled with 1.3-GHz superconducting accelerating cryomodules (CMs); see Fig. 1. The electron source consists of a 1-1/2 cell 1.3-GHz cylindrical-symmetric RF gun [3] comprised of a Cs_2Te photocathode illuminated by an ultraviolet (UV, $\lambda = 263.5$ nm) laser pulse. The photocathode drive laser is capable of producing a train of bunches repeated at 3-MHz within a 1-ms-duration macropulse [4]. The train are repeated at a 5-Hz frequency; see Fig. 2 (right). The laser system consists of a commercial fiber-based seed laser followed by a free-space chain of amplifiers; see Fig. 2 (left schematics). The seed laser was designed and built by Calmar Laser Inc.TM. It is an active mode-locked Yb-fiber system centered at $\lambda = 1054$ nm in the infrared (IR). The laser cavity consists of Yb-doped fiber amplifier, output coupler, electro-optics modulator, tunable filter, and fibers linking each component. A piezo stage is used to adjust the cavity length and achieve stable mode locking. The output-pulse duration is typically measured to be ~ 4 ps (rms). The laser is locked to a 1.3-GHz master oscillator. The modulator DC bias voltage requires constant adjustment to ensure proper mode locking as it typically drifts over time. This adjustment is typically made automatically through a feedback system. The output from the seed laser then passes through a pulse picker, which yields a ~ 1 -ms long train consisting of bunches repeated at a frequency 3 MHz. The pulses are then amplified by a chain of free-space single-pass amplifiers yielding a single-pulse energy of $\sim 9 \mu J$. These amplifiers are based on end-pumped Nd:YLF crystals pumped with 100QCW or 200QCW diodes from Dilas Inc.TM. The final amplification is accomplished with a high-power amplifier pumped by Northrop-GrummanTM diodes and yield a pulse energy of $\sim 180 \mu J$. Finally, the IR pulses are frequency converted to UV via two second-harmonic-generation stages before being transported to the accelerator vault in an evacuated transport line including a relay-imaging optics.

The 5-MeV electron bunches exiting the RF gun are then accelerated with two SRF TESLA-type cavities (CAV1 and CAV2) to approximately 50 MeV; see Fig. 1. Downstream of this accelerating section the beamline includes quadrupole and steering dipole magnets, along with a four-bend magnetic compression chicane (BC1) [5]. The beamline also incorporates a round-to-flat-beam transformer (RTFB) capable of manipulating the beam to generate a high transverse-emittance ratio [6]. In the early stages of operation, the electron bunches will be compressed in BC1. In this scenario the longitudinal phase space is strongly distorted and the achievable peak current limited to less than 6 kA. Eventually, a longitudinal phase-space linearizer will be added thereby enabling the generation of bunches with 10-kA peak currents. An active linearizer, based on a 3.9-GHz cavity, and a passive linearizer, based on a high-

impedance structure [7,8], are being considered as possible option for the linearizer structure. In addition the linearizer could also be used to tailor the current profile of the electron bunch [9,10]. The photoinjector was extensively simulated and optimized [11]. At a later phase the photoinjector will eventually include an off-axis experimental beamline branching off at the second dipole of BC1 in support to low-energy (<50-MeV) beam-physics experiments and diagnostics R&D.

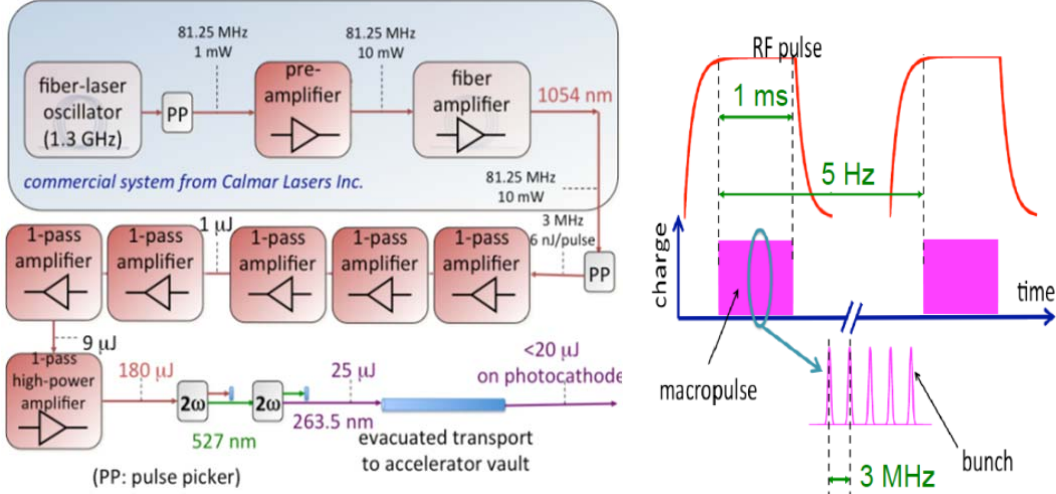


Figure 2: Block diagram of the photocathode drive-laser system (**left**) and schematics of the nominal beam temporal format (**right**). The macropulse format is adjustable within the range summarized in Table. 1

The 50-MeV beam is then injected into the SRF linac, which could eventually consist of three, 12-m long, TESLA/ILC-type CMs. Each CM includes eight 1.3-GHz nine-cell cavities. The first two CMs are foreseen to be of TESLA Type-III+ design, whereas the third (CM3) will be an ILC Type-IV design [12]. Together, these three CM's would constitute a complete ILC RF Unit. The SRF linac will be capable of providing an energy gain of ~750-MeV. The installation of the CM will be staged pending the completion of their construction.

Downstream of the linac is the high-energy test beam line section, which includes an array of multiple high-energy beam lines that transport the electron beam from the accelerating cryomodules to one of two beam dumps. The expected beam parameters are summarized in Table 1.

The beamline is instrumented with a comprehensive suite of diagnostics including electromagnetic beam position monitors, beam-current monitors, scintillating (Ce:YAG) at low energies and optical transition radiation (OTR) screens for measurements of the beam's transverse density. A sub-ps resolution streak camera is also available along with other bunch-length diagnostics based on frequency analysis of the coherent THz radiation (either synchrotron or transition) produced by the electron bunch. Precise beam-arrival monitor based on electro-optical sampling are being developed.

Table 1: Anticipated electron-beam parameters for the ASTA linac. The ranges are values expected for lower/larger bunch charge. Higher peak current are realized to the detriment of transverse emittance. After bunch compression in BC1, the horizontal and vertical beam emittances are different.

Parameter	Nominal value	Range	Unit
Beam energy	300 (1 CM) 800 (3 CMS)	50-800	MeV
Bunch charge	3.2	0.02-20	nC
Bunch spacing	333	10-∞	ns
Bunch train duration	1	0-1	ms
Train frequency	5	0.1-5	Hz
RMS normalized emittance	~5 (uncompressed)	< 1, > 100	μm
RMS bunch duration	1	0.01-10	ps
Peak current	5	0.05-10	kA

3.1.2.2 *Integrable-Optics Test Accelerator (IOTA) Ring*

ASTA layout includes a small storage ring to enable a ring-based AARD program in advanced beam dynamics of relevance to both Intensity and Energy Frontier accelerators. The Integrable Optics Test Accelerator (IOTA) ring is ~40 meters in circumference and will be capable of storing electrons from 50 to 150 MeV in energy [13]. Figure 3 shows the placement of the ring in the ASTA facility layout. It is planned to further expand capabilities for AARD in ASTA by installing of a 2.5-MeV proton/ H^- RFQ accelerator that was previously used for High Intensity Neutrino Source (HINS) research at Fermilab's Meson Detector Building facility [14].

The IOTA lattice is required to be periodic, with the element of periodicity comprised of a drift space with equal beta-functions, and a focusing and bending block with the betatron phase advance in both planes equal to π [a block dubbed “T-insert” in Figure 4 (a)]. The drift space must be long enough (> 2 m) to accommodate practical nonlinear magnets. The T-insert must be tunable to support a wide range of phase advances (and beta-functions) in the drift space in order to study different betatron tune working points. The focusing block is achromatic in order to avoid strong coupling between the transverse and longitudinal degrees of freedom. The ring must have one long (~5 m) straight section to accommodate a planned proof-of-principle experiment on optical stochastic cooling (OSC). Finally, IOTA has to fit within the footprint of the experimental hall and be properly oriented with respect to the injection line.

In its current design the ring is made of four cells. The cells are mirror-symmetric in pairs, and each consists of eight quadrupoles and two dipole magnets bending by 30 and 60 degrees. Given the betatron phase advance per cell of 0.8, a total betatron tune of 3.2 is achieved. Hence, in the extreme case the maximum tune shift generated by the nonlinear magnets may reach 1.6, leading some particles within the bunch to cross an integer resonance.

The IOTA-lattice design provides 2-m insertions for the nonlinear magnets, two 1-m-long straight sections for RF and other systems, and two 5-m sections – one for injection/extraction and another to accommodate a proof-of-principle experiment on optical stochastic cooling. Five quadrupole magnets are at least required to implement

an axially symmetric lens in a straight section. The large number of quadrupoles used in the ring allow for a wide range of tuning for the betatron tune, which can be varied between 2.4 and 3.6, and dispersion and momentum compaction. Table 2 lists the main parameters of the IOTA ring when operated with an electron beam.

Table 2: Anticipated IOTA-ring parameters.

Parameter	Value	Unit
e^- beam nominal kinetic energy	150	MeV
e^- beam nominal intensity	1×10^9	e^-
e^- transverse rms emittance	0.1	μm
p^+ beam nominal kinetic energy	2.5	MeV
p^+ beam nominal intensity	8×10^{10}	p^+
p^+ transverse rms emittance	1-2	μm
Circumference	~40	M
Bending field	0.7	T
Beam pipe diameter	50	mm
Maximum beta function β_x, β_y	12, 5	m
Momentum compaction	[0.02 ÷ 0.1]	—
Betatron tune	[3 ÷ 5]	—
Natural chromaticity	[−10 ÷ −5]	—
e^- synchrotron radiation damping time	0.6	S
RF voltage, frequency, harm. Number	30, 30, 4	kV, MHz, —
e^- synchrotron tune	[0.002 ÷ 0.005]	—
e^- bunch length	[1 ÷ 2]	Cm
e^- momentum spread	1.4×10^{-4}	—

Figure 3 depicts the proposed location of HINS within the ASTA facility. The HINS accelerator starts with a 50-kV, 40-mA proton (or H^- ion) source followed by a two-solenoid low energy beam transport (LEBT) line. The protons/ions are then accelerated by the pulsed 325-MHz RFQ to 2.5 MeV (with ~1 ms pulse duration) before injection into IOTA. The source will be located near the end of the electron beam line and will incorporate a debunching cavity necessary to reduce the relative energy spread to below 10^{-3} . A bending magnet will steer the proton beam into the injection line to IOTA. The injection line is also used to inject electron beams from the ASTA linac in IOTA.

The IOTA ring will be equipped with 16 button-type beam-position monitors necessary to allow for a precise measurement of the betatron function in the drift upstream of the T -insert. In addition, optical windows located in the dipole-magnet vacuum chambers will permit extraction of synchrotron radiation for non-interceptive diagnostics. Finally, quadrupole pickups capable of non-interceptive measurement of the quadrupole moment of the transverse beam distribution are under consideration.

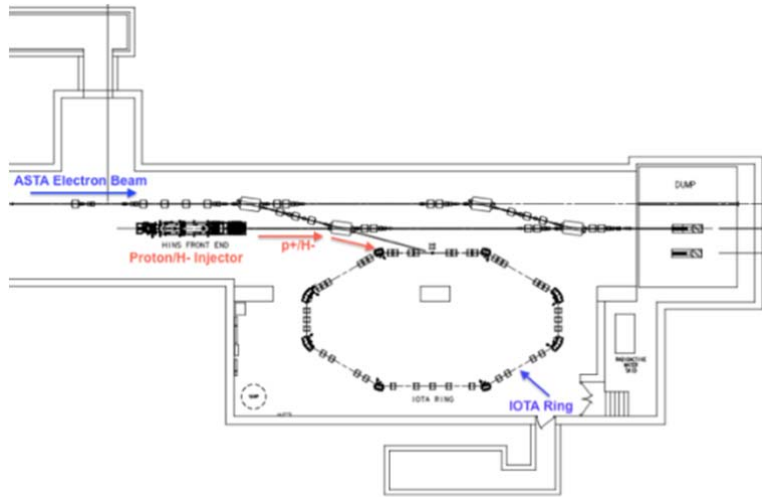


Figure 3: Layout of the IOTA ring within the ASTA facility.

3.1.2.3 *Superconducting Radiofrequency (SRF) Infrastructure*

The SRF infrastructure at ASTA was originally designed as an ILC test area in support of operating one ILC RF unit (a string of three cryomodules). It has since been repurposed to support the ASTA user facility. In this scheme, the main SRF devices are two single-cavity cryomodules dubbed cavity 1 and 2 (CAV1, CAV2 in Fig. 1) and one eight-cavity TESLA-style cryomodule. All of these systems are designed to operate with a 1.6-ms long pulse and a 5-Hz repetition rate. Regardless, the necessary RF, cryogenics, controls interlocks and diagnostics systems exist and have been made operational for this SRF facility. The main subsystems include (1) a cryogenics system capable of providing up to 120 Watts of 2K cooling, (2) a 5-MW klystron and associated high voltage supply and modulator for the 8-cavity cryomodule. A 10-MW multi-band klystron is on hand should more cryomodules be installed at ASTA, (3) two 300-kW klystrons and high-voltage sources for each of the two cavities (CAV1 and 2 in Fig. 1), (4) low-level RF drive systems for each klystron/RF module, an adaptive Lorentz force detuning compensation system for each, (5) interlock systems for each unit, which can provide fast response/shut down in case of a fault, (6) digitized readouts of diagnostics, and (7) interface and user control via Fermilab's accelerator controls network (ACNET) [15]. Further details on these subsystems can be found in Ref. [16,17].

In Ref. [18] operation of the first SRF device to be installed at ASTA is described. CAV2 is a single cavity 9-cell device of TESLA design. Its original operation of CAV2 at ASTA was to provide a heat load for commissioning of the cryogenics system as well as to provide installation and operating experience with an SRF system prior to the arrival of the first ILC-style cryomodule. Since 2010 CAV2 has been operated in two periods with warm-up to room temperature necessary to accommodate cryomodules installation. A peak gradient of 24.5 MV/m has been achieved although recent operation has been limited to 21 MV/m due to coupler vacuum activity and excessive field-emission probe activity in the RF input coupler. An additional single cavity cryomodule, CAV1, is currently being upgraded with a higher-gradient cavity, tested to 29 MV/m at Fermilab's horizontal test stand. Installation is expected in late 2014. CM1 was the first 8-cavity ILC/TESLA-type cryomodule to be operated at ASTA. During its

stay between 2010 and March 2012 it was cooled down and operated at 2K with its eight cavities achieving peak gradients between 20.2 and 28.2 MV/m. CM1 has since been removed. In April 2013 a second eight-cavity cryomodule, CM2 was installed at ASTA. CM2's history and performances to date are documented below. Reference [19] extensively summarizes SRF activities at ASTA to date.

3.1.3 Planned Experiments & Opportunities

The combination of a state-of-the-art superconducting linear accelerator and a flexible storage ring enables a broad research program directed at the particle physics accelerators of the future. Synopses of *some* of the enabled opportunities are discussed below.

3.1.3.1 IOTA-based Experiments

The proposed research program includes at IOTA has expanded well beyond its initial goal to test non-linear, integrable, accelerator lattices, which have the potential to shift the paradigm of future circular accelerator design [20, 13]. IOTA will also enable the exploration of a range of topics supporting the high-intensity frontier. The electron beam is expected to enable a proof-of-principle experiment on optical-stochastic cooling [21]. The addition of a H^- source will also enable the investigation of integrable optics in presence of significant space charge effects. The H^- beam will also open the path to the study of space-charge compensation schemes in high-intensity circular accelerators [22]. IOTA will also support some fundamental Physics studies such as the measurement of the wave function associated to a single electron using a method similar to an experiment previously attempted [23].

3.1.3.1.1 Integrable-Optics

Achieving high-intensity in circular accelerator is often limited by machine resonances, tune shifts and spreads, and collective instabilities. These three phenomena are interdependent in all present accelerators, which employ a “linear” focusing optics. A path towards the potential mitigation of these limiting factors consists in designing accelerators that operates in a nonlinear beam-dynamics regime [24,25]. Practical implementations of such ideas proved elusive until recently when a solution for nonlinear integrable accelerator lattice that can be implemented with tailored magnets was discovered [20].

The ASTA facility will offer a unique opportunity to carry out the proposed research toward demonstration of the feasibility of the integrable optics technique. That research requires the construction and operation of a dedicated storage ring (IOTA) and cannot be carried out at the existing storage rings as it involves very special insertions (highly nonlinear magnets), which extend over a significant fraction of the ring circumference, special arrangements of the optics lattice and precise control of the elements (strength, positions, etc.).

In a first stage nonlinear magnets [see Fig. 4 (b)] will be used and the single-particle (nonlinear) dynamics of the ring will be investigated using pencil electron beams produced by the ASTA linac. Subsequently, the influence of space charge effects would be explored using H^- beams produced from the HINS source. Eventually, the inclusion of an electron lens formerly used for halo-collimation and tune-shift control in the Tevatron could also serve as a nonlinear element.

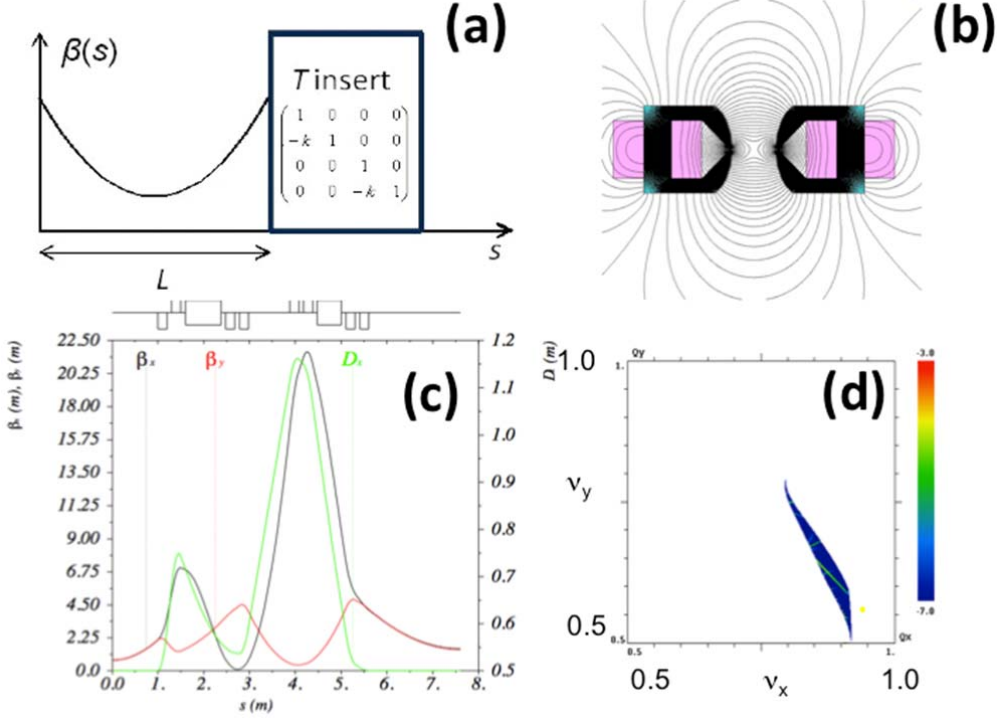


Figure 4: Configuration of one lattice cell: a drift space with equal beta-functions followed by a “ T -insert” (a), cross section of a nonlinear insert (b), betatron (red and black traces) and horizontal dispersion (green trace) functions over two lattice cells (c), example of fractional tune footprint obtained from frequency-map analysis (d).

3.1.3.1.2 Optical-Stochastic Cooling

Besides the experiments on highly non-linear integrable optics, the 150-MeV electron storage ring IOTA at ASTA will be used to carry out proof-of-principle experiment on optical stochastic cooling (OSC). The concept of OSC was proposed in the early 90’s [26] and remains untested despite its significant advantage of allowing an increase of the stochastic-cooling bandwidth by ~ 3 to 4 orders of magnitude compared to microwave-based stochastic cooling. OSC therefore results in a significant decrease of damping time in high luminosity hadron colliders from thousands of hours to below an hour. Consequently, a successful demonstration of OSC would allow for effective luminosity control during a store and has potential serious implications for a range of heavier (than electron) particle accelerators, ranging from LHC and Muon Collider to other rings.

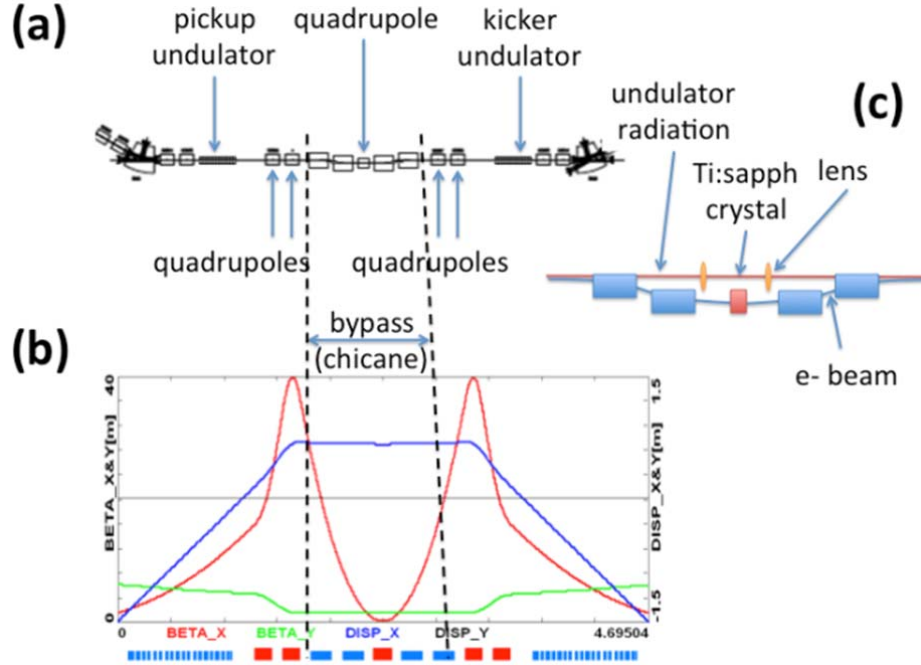


Figure 5: Configuration of the optical-stochastic cooling in a 5-m long straight section of IOTA (a), associated design lattice functions (b), and close up of the bypass chicane showing the optical transport (red path) for the undulator radiation (c). Figure adapted from Ref. [21].

The experiment will consist of two stages. In a first stage the cooling will be attempted without the inclusion of an optical amplifier: the radiation pulse produced by the pickup undulator will be directly refocused in the kicker undulator. Calculations indicate that undulator radiation without amplification should still provide a damping rate higher than the cooling rate due to synchrotron radiation. In the second stage, higher damping rates will be attempted by amplifying the pickup undulator-radiation pulse before coupling it back to the beam in the kicker undulator. One of the main challenges is to achieve significant amplification within a short footprint to insure the optical pulse can still be overlapped in the kicker with the electron bunch slice that originated the radiation pulse in the pickup undulator. Another critical factor is the requirement for optical amplification with minimal distortion over the full spectrum of the radiation. These two requirements call for the design of a high-gain single-pass optical amplifier (OA). The OA will be based on a Titanium-Sapphire (Ti:sapph) medium capable of supporting amplification over large optical bandwidth and a prototype Ti:sapph laser is currently being developed at Fermilab.

The IOTA ring will offer unique opportunity to carry out the proposed research toward demonstration of the feasibility of the optical stochastic cooling technique. The 100-150 MeV electrons beam combined with ~6-cm-period undulator will produce optical pulses with wavelength centered around 800 nm suitable for amplification with Ti:sapph. Figure 5 shows the configuration of the OSC in IOTA and the simulated lattice functions. The radiation from the pickup undulator will be focused on the Ti:sapph crystal and imaged back in the kicker undulator. Further details can be found in Ref. [21]. It should finally be pointed out that one of the capability to be demonstrated – the amplification of radiation fields produced by electron bunches –

could have far-reaching applications well beyond OSC to, e.g., electron-beam diagnostics and manipulations or accelerator-based radiation sources.

3.1.3.1.3 Space-Charge Compensation for High-Intensity Circular Accelerators

Through its past success in electron cooling of high-energy antiprotons [27], beam-beam compensation using electron lenses [28], and controlled halo removal by hollow electron beams [29], Fermilab has gained extensive experience and resources in manipulating high-energy particle beams by means of well-controlled electrons. As the mission of US high-energy physics program is pushing the Intensity Frontier, it is of great technical and scientific merit for the community if these techniques could be applied to overcome the beam intensity limit in the present accelerator technology. Consequently, IOTA is also foreseen to support investigation on novel methods of space-charge-compensation methods to achieve very intense and stable beams in circular accelerators through trapping and controlling of the electrons generated from beam-induced residual gas ionization. The method has a great potential to improve performance of leading high-current proton accelerator facilities and experiments, such as the Long-Baseline Neutrino Experiment (LBNE), Mu2e and $g-2$ after the intensity upgrades, and in compressor and accumulation rings envisioned in the Neutrino Factory and Muon Collider projects. The method may also offer a transformational technology for the next generation of high-intensity proton sources, e.g., such as those needed for the Accelerator Driven Systems.

The main idea of this compensation method is based on the long-known fact that the negative effect of Coulomb repulsion can be mitigated if beams are made to pass through a plasma column of opposite charge. This idea has been successfully applied to transport high-current low-energy proton and H^- beams into the RFQ in many linacs. In circular machines, partial neutralization by ionized electrons was attempted with notable improvements in beam intensity, namely one order of magnitude higher than the space-charge limit. However, the beam-plasma system was subject to strong transverse electron-proton ($e-p$) instability. In principle, this difficulty can be overcome if protons and electrons are immersed in a longitudinal magnetic field which is a) strong enough to freeze the electron density distribution; b) strong enough to suppress the $e-p$ instability; c) weak enough to allow positive ions to escape transversely, in addition to longitudinal draining; and d) uniform enough to avoid beta-beat excitations. In addition, we note that significant improvements have been made on the physics of non-neutral plasmas and on the stability of beam-plasma systems in the plasma physics community over the past decade, some of which could be readily adopted for the present project.

The existing components from the HINS program to be reused as an injector for the IOTA ring will facilitate researches on space-charge-compensation scheme. Additionally, the Tevatron electron lens system, a nonlinear element to be installed in IOTA ring, can be used to trap electrons for the initial space-charge compensation experiments. The experimental program will include the studies of the physics of electron column formation [30] and the stability of beam-plasma system, the measurements of electron accumulation and beam-plasma stability at HINS beamline, the design and construction of charge-exchange injection system for IOTA ring, and the measurements of electron accumulation and beam-plasma stability at IOTA ring using the electron lens system [22].

3.1.3.2 *Linac-based Experiments*

3.1.3.2.1 Accelerator R&D at the Energy and Intensity Frontiers

The availability of advanced phase space manipulations (flat beam generation [6] and eventually transverse-to-longitudinal phase space exchanger [31]) will support the development and test of beam-driven acceleration methods, which would greatly benefit from shaped current profiles to significantly increase the transformer ratio - the energy gain of the accelerated bunch over the energy loss of the driving bunch. When combined with the aforementioned round-to-flat beam transformation, transverse-to-longitudinal exchanger could enable the production of electron bunch suitable for acceleration in asymmetric structures [32] or provide a tool for arbitrary emittance repartitioning within the three degrees of freedom. Other acceleration methods to be tested at ASTA include beam-driven acceleration in crystalline media [33].

Finally, the high-power beam produced by the SRF linac will provide opportunities for high-energy Physics detector R&D. These include the high-power tests of target required for the LBNE [34] and the generation of tagged-photon beams necessary to test components associated high-energy-physics detectors [35].

3.1.3.2.2 Accelerator R&D for Future SRF Accelerators

High gradient, high-power SRF systems are critical for many accelerator facilities under planning for the needs of high-energy physics, basic energy sciences and other applications. ASTA offers a unique opportunity to explore most critical issues related to the SRF technology and beam dynamics in SRF cryomodules. The low injection energy ~50 MeV combined with achievable low emittance beams is well suited to explore beam dynamics effects and especially beam degradation due to the time-dependent field asymmetries introduced by the input and higher-order mode (HOM) couplers. The pulsed operation of SRF cavities at high-gradient while accelerating mA beam currents over a long macropulse is also relevant to the International Linear Collider (ILC) program. Furthermore, the SRF linac will provide an experimental platform necessary to develop the required low-level RF controls for the PiP-II pulsed linac [35]. Additionally, comprehensive beam-based measurements of long-range wakefield in SRF CMs are being planned using an upgraded version of the photocathode laser that would enable the production of charge-modulated bunch trains. Scanning the charge-modulation frequency and recording the HOM-induced beam displacements downstream of the cryomodule under test would enable the characterization of HOMs over a continuous range of frequencies [36]. Finally, a precise characterization of the jitter and beam-based stabilization of the SRF cryomodule has been proposed. It relies on the measurement of the bunch relative time of flight downstream of a bunch compressor, bunch energy and on the detection of coherent synchrotron radiation. These measurements are fed to an algorithm and used to control the phase and amplitude of the SRF cryomodules.

It was also pointed out that with appropriate changes in the RF system, the ILC-type cryomodule installed at ASTA could in principle be operated in CW mode and support tests relevant to the proposed next-generation CW light sources such as LCLS-II [37]. The cryogenic system and HOM couplers would limit the maximum gradient attainable by the cavities when operated in CW mode. Cryogenic considerations indicate that the maximum gradient would be limited to ~ 5-7 MV/m. Likewise, the ILC-type input

coupler design nominally used at ASTA would limit the average beam current to <1 mA [38].

3.1.3.2.3 Accelerator R&D for Novel Radiation Sources

High energy, high-peak and high-average brightness electron beams are essential to the generation of high-brilliance high-flux light sources with photo energies ranging from keVs to MeVs. The high average power and brightness of the ASTA electron beam has unmatched potential for development of several novel radiation-source concepts.

Head-on collision of the electron bunch with an intense laser produces radiation with maximum upshifted frequency $\omega \simeq 4\gamma_L^2\omega_L$ where γ_L is the bunch's Lorentz factor and ω_L the laser frequency. At ASTA, colliding the bunch with a 800-nm laser would provide γ rays with energies ranging from ~1 to ~20 MeV; see typical spectrum in Fig 6 (left). If the laser repetition frequency matches the electron bunch frequency, an unprecedented γ -ray brilliance in excess of $\sim 10^{24}$ phot.mm⁻².mrad⁻².s⁻¹/(0.1%BW) could be attained [39]. The main technical challenge will be to develop a laser capable of producing Joule-level pulse energy with MHz repetition rate and will rely on a recirculating optical cavity [40]. Such high-flux γ -ray source is foreseen to be extremely beneficial to the measurement of the cross section associated to the $^{12}C(\alpha,\gamma)^{16}O$ reaction which is crucial in nuclear astrophysics as it enters in the synthesis of many elements. Due to its low cross section, a precise measurement of this reaction using a nucleation process in a bubble chamber remains elusive with presently available γ -ray sources (as only a handful of events per year are expected). The potential availability of a high-flux γ -ray source at ASTA could result in significantly higher statistics (up to 200,000 events per year) [41].

In the photoinjector area, it is foreseen to test a concept enabling the production of high-brilliance x rays by combining the low-emittance beam produced out of the photoinjector with channeling radiation (CR) [42,43]. The production of CR will occur downstream of the bunch compressor (BC1) [44]. Several crystal materials will be tested. Simulations using a 140- μ m-thick diamond crystal indicate the production of x rays with energies in the [10-150]-keV range given the electron-beam energies available in the ASTA photoinjector (~15 to ~50 MeV); see Fig. 6 (right). The expected photon yield was estimated to $\sim 5 \times 10^8$ phot.mm⁻².mrad⁻².s⁻¹/(0.1%BW) [43].

Additionally, it was suggested that the available long stable bunch train could serve for a proof-of-principle experiment of an extreme-ultraviolet (EUV) radiation source. An FEL oscillator operating at 13.4-nm wavelength was investigated and preliminary simulations indicate that saturation of the FEL process occurs after ~300 passes [42]. Initial experiments could be conducted at low energy (250-300 MeV) and provide 120-nm FEL radiation. An alternative configuration for the generation of EUV radiation consisting of a single-pass high-efficiency FEL is also being explored. FEL-based EUV sources driven by SRF linacs are expected to benefit to EUV lithography [43].

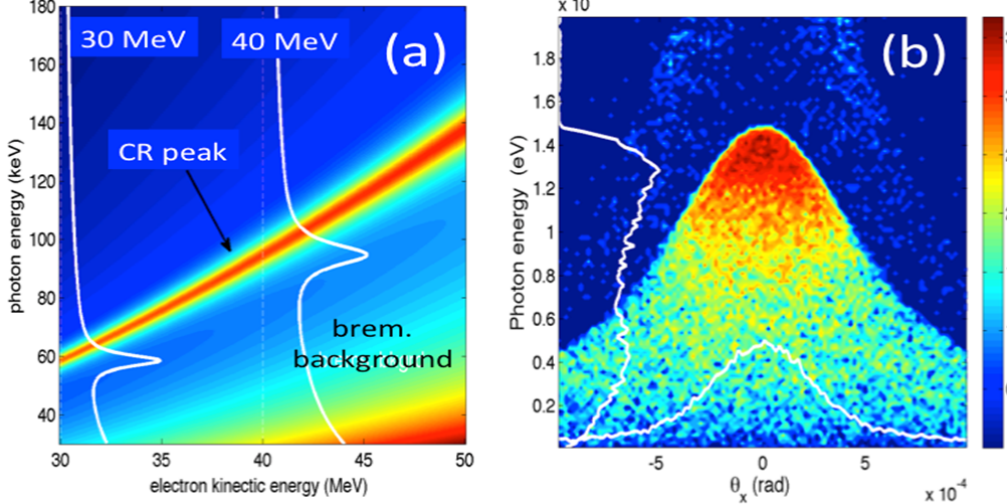


Figure 6: X rays spectral yield as function of electron beam energy (available in the ASTA photoinjector) and photon energy for the $1 \rightarrow 0$ transition along the (110) plane of diamond. Both CR and bremsstrahlung are considered in these calculations. The white traces are expected photon-energy spectrum for 30 and 40-MeV electrons (a). Spectral-angular distribution of γ rays produced by a 800-nm laser pulse backscattered on the ASTA 800-MeV beam (ultimately available with three cryomodules installed) (b).

Finally, the combination of flat beams with long bunch train could support the test of micro-undulators [47]. These micro-undulators, made of laser-micro-machined bulk rare-earth magnetic materials (SmCo and NdFeB), have magnetic fields with spatial period on the order of a few 100 μm . The associated undulator parameter is on the order of $K \sim \mathcal{O}(10^{-2})$ which results in a low photon yield $N \sim \alpha K^2$ (where α is the fine-structure constant). Therefore the test and characterization of the associated undulator radiation would greatly benefit from the long bunch train available at ASTA.

3.1.3.2.4 Accelerator R&D for Stewardship and Applications

With its high energy, high brightness, high repetition rate, and the capability of emittance manipulations built-in to the facility design, ASTA is an ideal platform for exploring novel accelerator techniques of interest for very broad scientific community beyond high-energy physics.

Some of the experiments include the development and test of subsystems and beam-manipulation schemes to improve the performance and decrease the cost of next-generation accelerator-based light sources. An example include the combination of the aforementioned phase-space manipulations to tailor the emittance partition within the three degrees of freedom to produce ultra-low emittance beams for future hard X-ray free-electron lasers.

Several low-cost ideas to ``dechirp'' the beam, i.e. to remove the residual correlated energy spread that generally subsists downstream of the final bunch compression stage in FEL drivers, were formulated and tested the past few years. The proposed dechirping methods include (*i*) the use of short-range wakefields impressed on the bunch as it passes in a dielectric [48] or corrugated [49] passive structure, or (*ii*) the judicious arrangement of three transverse-deflecting cavities to produce a transfer matrix with a non-vanishing longitudinal dispersion R_{56} [50]. In addition using these passive structures to further control the longitudinal-phase-space nonlinearities could also be

tested at ASTA [51]. Demonstrating the compatibility of these techniques with high-repetition rate beam available at ASTA could lead to their inclusions in planned accelerator-based light sources drive by SRF linacs.

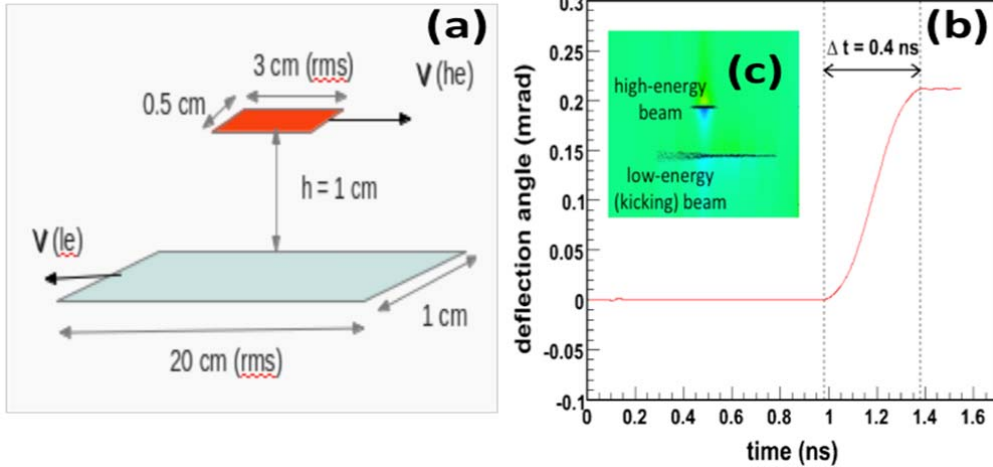


Figure 7: Overview of the beam-beam kicker configuration (a): A low-energy (“le”) high-charge beam is counter propagated to the high-energy (“he”) beam being kicked. Particle-in-cell simulations of a flat-beam kicker showing a rise time of ~400 ps (b). The inset (c) shows a side view (z, x) of the beam distributions (shown as dark dots) and associated (velocity) field E_x (appearing as a contour plot) [Courtesy of D. Mihalcea, Northern Illinois University].

The flat-beam transformation available at ASTA could also support tests relevant to nuclear-physics accelerator R&D, e.g., to validate the concept of a fast beam-beam kicker [52] or investigate beam dynamics challenges associated to the transport and manipulation of magnetized beams [53]. Preliminary simulations using ASTA beam parameters with a 1-MeV 5-nC kicker beam indicate that rise time of ~400 ps could be achieved with kick strength in excess of ~20 mrad as depicted in Fig. 7. These researches could have important implications on, e.g., the Medium-energy Electron-Ion Collider (MEIC) [54] being explored at Jefferson Laboratory.

Finally, the beam available at ASTA will foster the development and tests of advanced beam diagnostics relevant to, e.g., CW FELs or energy-recovery linacs. Some of these diagnostics especially those capable of measuring single-bunch parameters within the RF macropulse, will be crucial for optimizing the feedback system needed to stably operate the ASTA SRF cryomodule(s).

3.1.4 Commissioning Status

Commissioning of the subsystems comprising ASTA has been ongoing since 2010 in parallel with installation and construction activities. Similarly commissioning of these components has also been largely in parallel. In the coming months it is expected that bringing them into operation as an accelerator will be realized. Electrons with energies up to 50-MeV are foreseen in 2014. This will be achieved by operation of the RF gun at 5 MeV and two single-cavity cryomodules (CAV1 and CAV2) each capable of boosting the beam energy by 25 MeV. Beam will be delivered to a low energy absorber at the end of the injector section. Activities relating to these main components – laser, gun, beamline, and SRF components – are described below.

3.1.4.1 Photocathode Laser System

Construction of the laser room at the ASTA facility in NML was completed in August 2012 and the commissioning of laser system was completed at the end of CY2012. The final UV bunch energy ranges from 0.1 to 3 μ J and the corresponding laser-pulse duration is approximately 3.8 ps (rms). Figure 8 provides snapshots of the evolution of a 100-pulse train throughout the IR amplifying chain, and downstream of the first (green) and second (UV) stages of the fourth-harmonic generation conversion. The pulse-intensity fluctuations within the bunch are maintained to less 5% throughout the laser system as shown in Fig. 8 (lower-right histogram).

In its present design, the photocathode laser system support a maximal bunch frequency of 3 MHz within a train. A next stage upgrade plan is to improve the operation of laser system. This limitation to 3 MHz came from a multi-pass amplifier that was recently substituted by three single-pass amplifiers. There is therefore no technical limitation toward increasing the intra-train operation frequency from 3 to 81.25 MHz. Although such a frequency increase would come at the expense of single-pulse energy (i.e. single bunch charge), it would extend the range of bunch-train format available to users and could, for instance, support experiments on higher-order mode investigation using charge-modulated bunch trains [36] or permit the generation of high-brilliance x-ray radiation via inverse Compton scattering.

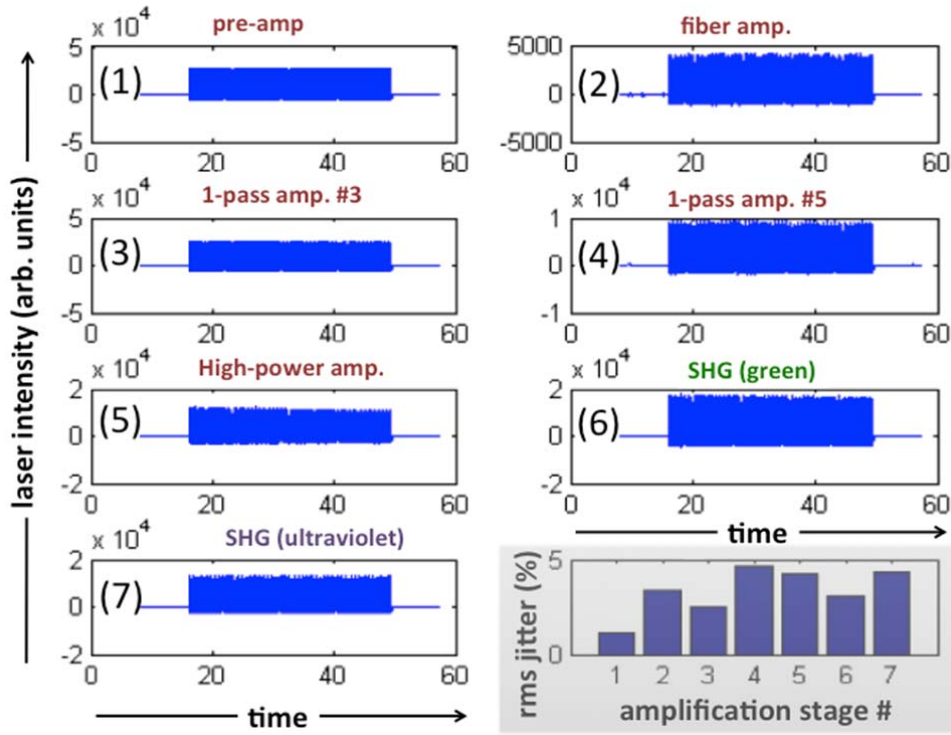


Figure 8: A single capture of 100 bunches on the VME-based digitizer from each of seven photodiodes installed throughout the laser system shown in Fig. 2 (left). The lower-right histogram provides the laser intensity fluctuation downstream of the amplification-stage number (corresponding to the numeric labels on the other plots)

3.1.4.2 *Radiofrequency Gun Characterization*

The gun system consists of three parts: gun-cavity, coaxial coupler with a “doorknob” transition and RF vacuum window. In 2011, the rf vacuum window (manufactured by ThalesTM) was first conditioned to ~ 4 MW [in two modes: fully reflected mode (20- μ s pulse length) and fully transmitted mode (1-ms pulse length)]. The power was limited by the klystron and arcing in an isolator. The conditioning of the assembled RF-gun system started in December 2012, and was completed in the middle of CY2013 given the limited availability of klystron(s) and on-going installation activities. The RF gun system was first conditioned up to 1.2 MW (1-ms pulse width, 5-Hz repetition rate) with a molybdenum cathode using a 4-MW klystron designated for cryomodule test. It was subsequently conditioned to 3.7 - 4.1 MW (1-ms pulse width, 1-Hz repetition rate) with a molybdenum cathode using a new klystron dedicated to the gun system. Finally, the molybdenum cathode was replaced with Cs₂Te-coated cathode and the system was reconditioned up to 3.7 - 4.1 MW (1-ms pulse width, 1-Hz repetition rate). This power level exceeded the required 3.5-MW power for a peak accelerating field of 45 MV/m at the cathode surface. During conditioning, the resonant frequency of the RF gun was controlled via the cooling-water temperature. However the water temperature response time is intrinsically slow and the control system is designed for normal operation (stable power level). At higher average power levels (longer pulse width) a power change (either planned or unplanned due to events such as sparking) can cause rapid change of resonant frequency of the cavity, which would be out of our water-cooling control. To circumvent this issue, the klystron’s operating frequency was manually adjusted to follow each sudden change of the cavity’s resonant frequency.

ASTA successfully produced its first photoelectron beam from the gun to a Faraday cup on June 20th, 2013. The initial beam was produced using the bare molybdenum cathode, about 8-15 laser pulses at 1-Hz and electrons were observed on three of the primary diagnostics immediately downstream of the gun: loss monitor, resistive wall current monitor, and Cerium-doped yttrium aluminum garnet (Ce:YAG) screen. Due to the limited quantum efficiency of the bare-molybdenum photocathode the charge produced was very low (\sim pC). Subsequently a Cs₂Te-coated cathode was inserted into the gun in March 2014 and enabled the formation of 4-nC bunches downstream of the RF gun. After extensive conditioning of the RF gun and optimization of the laser system 1-ms bunch train were generated and measure with the Faraday cup; see Fig. 9. The pulse train is strikingly flat except for some transient fluctuations at the beginning of the pulse.

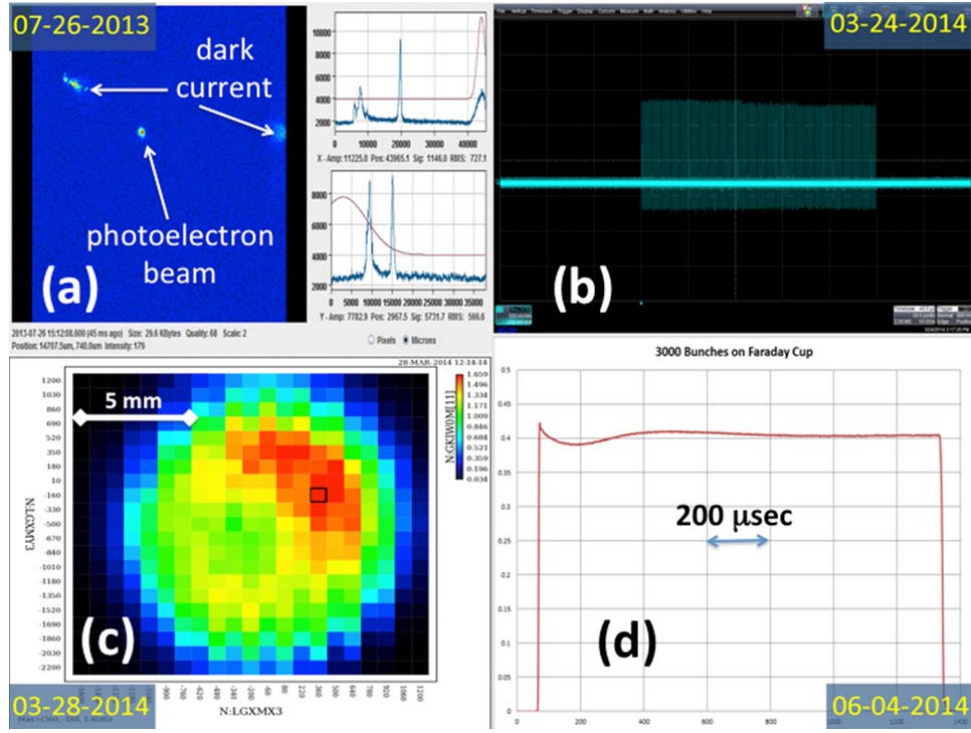


Figure 9: Milestone pertaining to the gun commissioning: first electron image on the Ce:YAG screen located downstream of the gun (a), first electron-bunch train produced with Cs₂Te cathode (b), quantum-efficiency map of the Cs₂Te cathode (c), and demonstrating of the production of 1-ms bunch train with 3000 pulses (d).

3.1.4.3 Electron Beam Measurements

The first characterization of the electron beam properties included beam intensity, beam energy, a beam-based calibration of the RF gradient, and emittance measurements at low charge. Preliminary results were presented in Ref. [55].

Measurements were based on the instrumentation available between the RF gun and the diagnostic table, placed about 1.1-m downstream of the photocathode. The main components were the bucking and main solenoids surrounding the gun cavity, horizontal and vertical trim dipole magnets, a Ce:YAG screen, and a Faraday cup. The maximum bunch intensity achieved is ~3 nC for a laser pulse energy of approximately 2 μ J, corresponding to a quantum efficiency of the cathode of 1.5%. The laser spot on the cathode was aligned with the electrical axis of the cavity by turning off the solenoids and by observing the displacement of the beam spot on the Ce:YAG screen as the phase of the RF gun was changed [56]. With this method, the accuracy of the laser-cavity alignment was about 0.1 mm.

A direct calibration of the beam energy, accurate to about 10%, was obtained by observing the deflection of the focused beam on the YAG screen as a function of the horizontal or vertical trim dipole settings. The RF gun power and phase were typically set to achieve a kinetic energy of 4.5 MeV.

Several properties of the RF gun and of the electron beam could be inferred from solenoid scans at low charge (less than 2 pC/bunch) with the nominal laser-pulse duration. The beam spot at the Ce:YAG screen was measured as a function of the solenoid settings. The main and bucking solenoids were kept at a fixed field ratio so that

the magnetic field at the cathode was negligible. Under these conditions, transport between the cathode and the screen was emittance dominated. Therefore the beam dynamics could be modeled by transfer matrices that include the effects of cavity fields with superimposed solenoids. To evaluate systematic uncertainties, these transfer matrices were calculated with two models: the ASTRA tracking code [57] and a longitudinal slicing of the gun [58,59]. The peak field in the RF cavity, its phase, and the initial beam emittance were independent free parameters and they were inferred from a least-squares fit of the models to the data.

The peak fields had a statistical uncertainty of less than 1% and provided a beam-based calibration of the RF gradient. This method, based on gun and solenoid field maps, also provided a calibration of the final electron energy (derived from gradient and phase) independent from the direct deflection measurement with the trim dipoles.

Emittance values at low charge were in agreement with the expected intrinsic emittance of cesium telluride cathodes. For instance, for a typical rms laser spot size of 0.6 mm, we measured an rms-normalized emittance of $0.6 \mu\text{m}$. The drift of the beam spot on the screen as a function of solenoid current will be used to check the alignment of the magnetic axis of the solenoid. The space-charge model of the injector will be verified with solenoid scans at high charge (up to 3 nC/bunch).

In the coming weeks, we plan to accelerate electrons up to 20 MeV with CAV2 (see Fig. 1). The 20-MeV beam will enable the commissioning of the beamline connecting the photoinjector to the cryomodule as far as the low-energy beam absorber located upstream of the cryomodule.

3.1.4.4 *SRF Cavities Achieve ILC Specifications*

Upon arrival in ASTA in April 2013 and after cool down to 2 Kelvin (23 Torr) in November 2013, cryomodule 2 (CM2) individual cavity characterization was carried out with seven of the eight cavities achieving a peak gradient of 31.5 MV/m as shown in Fig. 10 (left). The outlier was limited to 30.5 MV/m by quenching. The 31.5-MV/m gradient is an administrative limit consistent with the ILC gradient specification. Reference [60] describes the performance of the cavities prior to assembly into a complete module. The steps required to fully characterize each cavity: on-resonance coupler conditioning, tuning to resonance, signal calibration, peak gradient determination, measurement of dark current and X-ray field emission, and dynamic heat load (DHL) measurement to determine the Q_0 required on average one week to complete. Reference [61] describes early performance results. In recent weeks CM2 operation as a unit has been initiated: all cavities powered simultaneously, except cavity #8 which has a warm-coupler vacuum issue. This issue will be addressed in the future when an opportunity to warm the cryomodule to room temperature avails itself. Transitioning to the mode of unit powering required the installation of a waveguide distribution system fabricated by SLAC to allow the output of a single RF source (klystron) to power all cavities simultaneously. Variable tap offs to each of four pairs of cavities were adjusted to control what fraction of the total RF output is provided to each cavity pair. As of this writing the average accelerating gradient achieved per cavity is 30 MV/m with the system operating at the nominal pulse width of 1.6 milliseconds and 5-Hz repetition rate; see Fig. 10 (right). Adaptive Lorentz-force detuning compensation (LDFC) was active in order to maintain a relatively flat peak field within the macropulse.

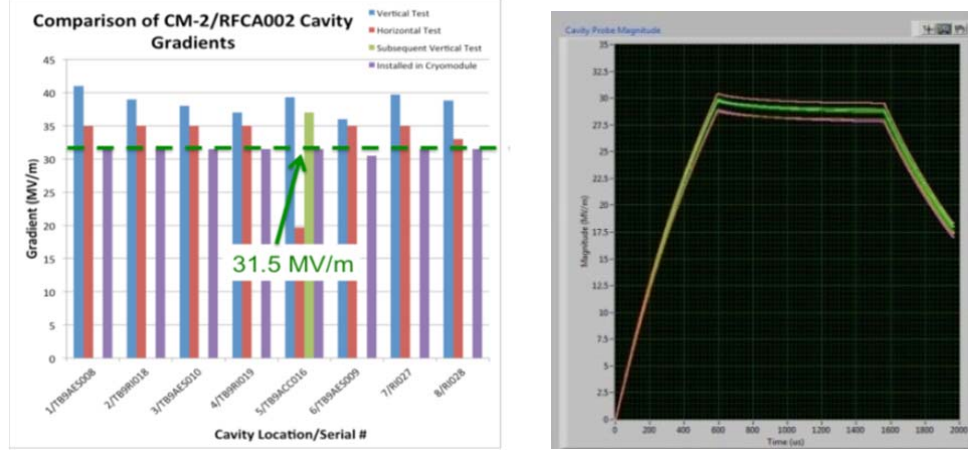


Figure 10: Comparison of CM-2/RFCA002 cavity gradients: vertical test (blue), horizontal (red), and in CM-2 (purple). An administrative limit of 31.5 MV/m was set for CM-2 testing (**left**). CM2 peak gradients achieved as of August 2014 in operation as a unit (**right**). The goal is operate all cavities within the cryomodule to at least 31.5 MV/m simultaneously.

A full suite of testing including raising the gradient to at least 31.5 MV/m, operating the low level RF system in closed loop, optimizing adaptive LFDC, and repeating DHL to measure the cumulative Q_0 will follow shortly. Plans call to operate CM2 with beam by end of CY2015.

3.1.5 Upgrade Path

ASTA will evolve over time to address the demands of the accelerator R&D program. In its first stage the main subsystems of ASTA include a 50-MeV photoinjector source with auxiliary lasers systems, a linear accelerator based on a single SRF cryomodule, an electron-storage ring (IOTA) and several experimental areas for research with low-energy and high-energy beams. Possibilities exist to further expand the capabilities of the R&D program including the installation of a H^- source to expand the IOTA program to protons and the addition of SRF cryomodules to increase the linac beam energy. Depending on user demand, a staged bunch-compression system could also be incorporated and would rely on the addition of a linearizing cavity (a 3.9-GHz SRF cavity located downstream of CAV2).

We therefore envision a multi-staged approach to ASTA completion as illustrated in Fig. 11. The first stage enables a low-energy AARD program based on the photoinjector and a 300 MeV program based on a single superconducting cryomodule, with associated beam transport lines and beam dumps. The first stage also enables one of the transformative beam dynamics experiments: exploration of novel, non-linear accelerator lattices in the Integrable Optics Test Accelerator (IOTA). The subsequent stages will ultimately be guided by user demands.

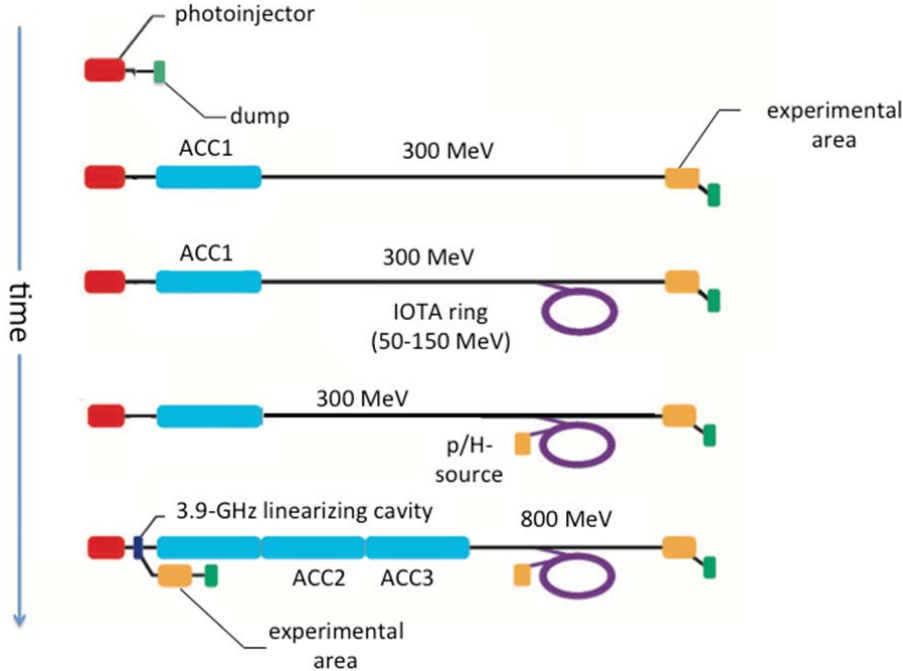


Figure 11: A possible path for staged construction of ASTA. Currently only the configurations shown in the top four rows are being pursued. Subsequent upgrade stage(s) will be guided by user demands.

3.1.6 Acknowledgements

The ASTA scientific program was developed in partnership with many national laboratories, Universities, and companies; see list in Ref. [1]. The successful initial commissioning of ASTA would not have been possible without a team of dedicated scientific and technical staffs.

Fermilab is operated by Fermi Research Alliance, LLC under Contract No. DE-AC02-07CH11359 with the United States Department of Energy.

3.1.7 References

1. P. H. Garbincius, S. Henderson, J. Leibfritz, P. Piot, V. Shiltsev (Editors), “Proposal for an Accelerator R&D User Facility at Fermilab’s Advanced Superconducting Test Accelerator (ASTA),” Fermilab TM-2568 (2013).
2. Information on ASTA can be found at <http://asta.fnal.gov>
3. B. Dwersteg, et al., “RF gun design for the TESLA VUV Free Electron Laser,” Nucl. Instr. Meth. A **393**, 93 (1997).
4. J. Ruan, et al., “Commission of the Drive Laser System for Advanced Superconducting Test Accelerator,” in Proc. of IPAC13, p. 3061 (2013).
5. C. R. Prokop, et al., “Beam dynamics performances and applications of a low-energy electron-beam magnetic bunch compressor,” Nucl. Instr. Meth. A **719**, p. 17 (2013).
6. J. Zhu, et al., “Formation of compressed electron beams with high transverse-emittance ratio,” Phys. Rev. ST Accel. Beams **17**, 084401 (2014).
7. P. Craievich, “Passive longitudinal phase space linearizer,” Phys. Rev. ST Accel. Beams **13**, 034401 (2010).
8. M. Venturini, “Passive linearizer,” presented at the 2nd Advanced Superconducting

- Test Accelerator Users Meeting, Fermilab, June 9-10, 2014,
<https://indico.fnal.gov/event/8409>
9. P. Piot, et al., "Generation and characterization of electron bunches with ramped current profiles in a dual-frequency superconducting linear accelerator," Phys. Rev. Lett. **108**, 034801 (2012).
 10. F. Lemery and P. Piot, "Ballistic bunching of photo-injected electron bunches with dielectric-lined waveguides," preprint arXiv:1407.1005 [physics.acc-ph] (2014).
 11. P. Piot, et al., "Beam dynamics simulations of the NML photoinjector at Fermilab," Proc. of IPAC10, Kyoto, Japan, p. 4316 (2010).
 12. T. Arkan, et al., "Superconducting RF cryomodule production & testing at Fermilab," Proc. of Linac10, Tsukuba, Japan, p. 599 (2010).
 13. S. Nagaitsev, "Design and Simulation of IOTA - a Novel Concept of Integrable Optics Test Accelerator," Proc. of IPAC12, New Orleans, LA, p. 16 (2012).
 14. R. C. Webber, et al., "Overview of the high-intensity neutrino source linac R&D at Fermilab," Proc. LINAC08, Victoria, BC, 36 (2008).
 15. ACNET user guide is available at <http://www-ppd.fnal.gov/fibf/acnet.html>.
 16. E. Harms, et al., "Test Results of Tesla-style Cryomodules at Fermilab," MOPB054, Proc. of LINAC2012, Tel Aviv, p 297 (2012).
 17. W. Schappert and Y. Pischnikov, "Adaptive Compensation for Lorentz Force Detuning in Superconducting RF Cavities," Proc. of SRF2011, Chicago, p 940 (2011).
 18. E. Harms, et al, "Operating Experience with CC2 at Fermilab's SRF Beam Test Facility," Proc. of LINAC2010, Tsukuba, p. 818 (2010).
 19. E. Harms, et al, "SRF Systems for ASTA at Fermilab," Proc. of IPAC2014, Dresden, p. 2601 (2014).
 20. V. Danilov, S. Nagaitsev, "Nonlinear accelerator lattices with one and two analytic invariants," Phys. Rev. ST Accel. Beams **13**, 084002 (2010).
 21. V. Lebedev, et al., "Test of Optical Stochastic Cooling in the IOTA Ring," Proc. of NAPAC13, p. 422 (2013).
 22. M. Chung, et al., "Space-charge Compensation for High-intensity Linear and Circular Accelerators at Fermilab," Proc. of NAPAC13, Pasadena, CA, p. 402 (2013).
 23. V.V. Danilov, et al., "Possible Experiments on Wave Function Localization Due to Compton Scattering," Proc. of NAPAC13, Pasadena, CA, p. 919 (2013).
 24. E. M. McMillan, in Topics in Modern Physics. A Tribute to E. U. Condon, edited by E. Britton and H. Odabasi (Colorado University Press, Boulder, 1971), p. 219.
 25. V. V. Vecheslavov and Yu. F. Orlov, "Fundamental properties of non-linear focusing," *J. Nucl. Energy, Part C Plasma Phys.* **8**, 717 (1966).
 26. A. A. Mikhailichenko, M. S. Zolotorev, "Optical Stochastic Cooling," Phys. Rev. Lett. **71**, 4146 (1993).
 27. S. Nagaitsev et al., "Experimental demonstration of relativistic electron cooling," Phys. Rev. Lett. **96**, 044801 (2006).
 28. V. Shiltsev et al., "Experimental demonstration of compensation of beam-beam effects by electron lenses," Phys. Rev. Lett. **99**, 244801 (2007).
 29. G. Stancari et al., "Collimation with Hollow Electron Beams," Phys. Rev. Lett. **107**, 084802 (2011).
 30. V. D. Shiltsev, "New possibilities for beam-beam and space-charge compensation: MCP gun and electron columns," in Proc. of PAC2007, p. 1159 (2007).
 31. P. Piot, et al. "Generation of relativistic electron bunches with arbitrary current distribution via transverse-to-longitudinal phase space exchange," Phys. Rev. ST Accel. Beams **14**, 022801 (2011).
 32. D. Mihalcea, et al., "Three-Dimensional Analysis of Wakefields Generated by Flat Electron Beams in Planar Dielectric-Loaded Structures," Phys. Rev. ST Accel. Beams **15**, 081304 (2012).
 33. Y.-M. Shin, et al., "Ultra-high gradient beam-driven channeling acceleration in hollow

- crystalline media,” in Proc. of IPAC14, Dresden, Germany, p. 1512 (2014).
34. RaDIATE (Radiation Damage in Accelerator Target Environments) Collaboration, <http://www-radiate.fnal.gov/index.html>.
 35. S. Henderson, S. Holmes, A. Kronfeld, R. Tschirhart, (Editors) “Project X: Accelerator Reference Design, Physics Opportunities, Broader Impacts,” FERMILAB-TM-2557 (2013).
 36. S. Fartoukh, “A new method to detect the high impedance dipole modes of TESLA cavities,” report CEA/DAPNIA/SEA-98-18, Saclay, France (1998).
 37. J. Galayda, “The Linac Coherent Light Source-II Project,” Proc. of IPAC2014, Dresden, Germany, p. 935 (2014).
 38. N. Solyak (Fermilab), private communication (2013).
 39. A. Murokh (Radiabeam LLC), private communication (2013).
 40. R. Tikhoplav, et al., “High-power pulse recirculation in a stable pseudo-confocal geometry,” Opt. Lett. **37**, 4717 (2012).
 41. C. Ugalde, et al., “First determination of an astrophysical cross section with a bubble chamber,” Phys.Lett. B **719**, 74 (2013).
 42. C. A. Brau, et al., “Channeling radiation as a source of hard x-rays with high spectral brilliance,” Sync. Rad. News **25** (1), 20 (2012).
 43. T. Sen, et al., “Spectral Brilliance of Channeling Radiation at the ASTA photoinjector,” preprint arXiv:1407.6053v1 [physics.acc-ph] (2014).
 44. B. Blomberg, et al., “Channeling radiation with low-energy electron beams: experimental plans & status at Fermilab,” Proc. of FEL13, New-York NY, p. 38 (2013).
 45. A. Lumpkin, et al., “Feasibility of an XUV FEL Oscillator at ASTA,” Proc. of FEL13, New-York NY, p. 88 (2013).
 46. A. Murokh and A. Tremaine (Organizers), “Collaboration meeting on FEL sources for EUV lithography: part II”, Santa Monica, CA, April 23-24, 2014.
 47. B. A. Peterson, et al., “Technology Development for Short-period Magnetic Undulators,” Physics Procedia, **52**, 36 (2014).
 48. S. Antipov, et al., “Experimental demonstration of energy-chirp compensation by a tunable dielectric-based structure,” Phys Rev Lett. **112**, 114801 (2014).
 49. P. Emma, et al., “Experimental demonstration of energy-chirp control in relativistic electron bunches using a corrugated pipe,” Phys Rev Lett. **112**, 034801 (2014).
 50. N. Yampolsky, et al., “Imposing Strong Energy Slews with Transverse Deflecting Cavities,” talk at NAPAC13, Pasadena, CA, 2013 (unpublished).
 51. P. Craievich, “Passive longitudinal phase space linearizer,” Phys. Rev. ST Accel. Beams **13**, 034401 (2010).
 52. V. Shiltsev, “Beam-beam kicker for superfast bunch handling,” Nucl. Instr. Meth. Sec. A **374**, 137 (1996).
 53. P. Piot, Y.-E Sun, “Generation and dynamics of magnetized electron beams for high-energy electron cooling,” to appear in Proc. of the 2014 workshop on electron-ion collider, Newport News, VA, March 21-24, 2014 (in press).
 54. S. Abeyratne, et al. [MEIC collaboration], “Science Requirements and Conceptual Design for a Polarized Medium Energy Electron-Ion Collider at Jefferson Lab,” arXiv:1209.0757 [physics.acc-ph] (2012).
 55. J. Ruan et al., “Commissioning status of the Advanced Superconducting Test Accelerator at Fermilab,” Proc. of IPAC2014, Dresden, Germany, p. 2615 (2014).
 56. F. Stephan et al., “Detailed characterization of electron sources yielding first demonstration of European X-ray Free-Electron Laser beam quality,” Phys. Rev. ST Accel. Beams **13**, 020704 (2010).
 57. K. Flöttmann, “ASTRA: A Space Charge Tracking Algorithm,” <http://www.desy.de/~mpyflo> (April 2014).
 58. C. Gulliford and I. Bazarov, “New method for generating linear transfer matrices through combined RF and solenoid fields,” Phys. Rev. ST Accel. Beams **15**, 024002

- (2012).
59. G. Stancari, “Electron beam measurements in the ASTA rf gun,” presented at the 2nd Advanced Superconducting Test Accelerator Users Meeting, Fermilab, June 9-10, 2014, <https://indico.fnal.gov/event/8409>.
 60. A. Hocker, et al, “Individual RF Test Results if the Cavities Used in the First US-built ILC-type Cryomodule,” Proc. of IPAC2012, New Orleans, p 2321, (2012).
 61. A. Hocker, et al, “Results from RF Tests of the First US-built High-gradient Superconducting Cryomodule,” Proc. of IPAC2014, Dresden, p 2598 (2014).

4 Workshop and Conference Reports

4.1 ICFA Mini-Workshop “Electromagnetic Wake Fields and Impedances in Particle Accelerators”

E. Métral (CERN, Geneva) and V.G. Vaccaro (INFN, Naples)

Mail to: Elias.Metral@cern.ch, vittorio.vaccaro@na.infn.it

An ICFA Mini-Workshop on “Electromagnetic Wake Fields and Impedances in Particle Accelerators” was held in Erice (Sicily) from April 24th to April 28th, 2014. It was hosted by the Ettore Majorana Foundation and Centre for Scientific Culture and sponsored by the CERN LIU and HL-LHC projects, INFN, EUCARD-2 and XBEAM. The workshop was attended by 52 accelerator physicists from all around the world and all the relevant information can be found on the web site:

<http://indico.cern.ch/event/287930/>.

The program was grouped in eleven sessions with invited and contributed talks, spread over four days:

- Session 1: Impedance theory and related effects
- Session 2: Impedance numerical simulations
- Session 3: Impedance bench and beam-based measurements
- Session 4: Extensions of the impedance concept
- Session 5: Impedance challenges for new projects
- Session 6: Building the impedance model of a machine
- Session 7: Space charge and resistive-wall impedances
- Session 8: Geometrical impedance
- Session 9: Impedance of diagnostics structures (followed by a poster session)
- Session 10: Impedance of collimators and kickers
- Session 11: Summaries

This workshop is dedicated to A.M. Sessler, who passed away just before the workshop on 17/04/2014.

Together with V.G. Vaccaro, A.M. Sessler introduced the concept of impedance in particle accelerators. The first mention of this concept appeared on November 1966 in the CERN internal report “Longitudinal Instability of a Coasting Beam above Transition, due to the Action of Lumped Discontinuities” by V.G. Vaccaro. A more general treatment of it appeared in 1967 in the CERN yellow report “Longitudinal Instabilities of Azimuthally Uniform Beams in Circular Vacuum Chambers of Arbitrary Electrical Properties” by A.M. Sessler and V.G. Vaccaro. The concept of wake fields came two years later, in 1969, in a paper from A.G. Ruggiero and V.G. Vaccaro (The

Wake Field of an Oscillating Particle in the Presence of Conducting Plates with Resistive Terminations at Both Ends). This was the beginning of many studies, which took place over the last four decades, and today, impedances and wake fields continue to be an important field of activity, as concerns theory, simulation, bench and beam-based measurements. The recent/current main challenges concern the computation, simulation and measurement of the (resistive) wall effect for cylindrical and non cylindrical structures, any number of layers, any frequency, any beam velocity and any material property (conductivity, permittivity and permeability); the electromagnetic characterization of materials; the effect of the finite length of a structure; the computation and simulation of geometrical impedances for any frequency; the computation and simulation (in time and frequency domains) of all the transverse impedances needed to correctly describe the beam dynamics (i.e. the usual driving or dipolar wake, the detuning or quadrupolar wake, the angular wake, the constant and nonlinear terms, etc.); the issue of the wake function needed (inverse Fourier transform of the impedance, response to a delta-function) vs. the wake potential obtained from electromagnetic codes (i.e. response to a usually Gaussian pulse); the simulation of all the complexity of equipment like kickers, collimators and diagnostics structures; etc. All this is needed to ultimately build a reliable impedance model of a machine, which will be used to understand better the performance limitations (from beam-induced RF heating and/or collective effects such as coherent instabilities, emittance growths and beam losses), reduce the impedance of the main contributors, study the interplay with other mechanisms such as beam-beam (in a collider), space charge, electron cloud, transverse damper, etc.

The Workshop was very interesting and well appreciated by many participants thanks to the participation of the many experts, all representative of the worldwide best research Centers and thanks to the excellent progress made over the last decade(s). We have also the pleasure to acknowledge the high quality of the presentations. As a witness of the current significance and of the vitality of this field of activity, a remarkable number of young speakers gave contributions. We would like therefore to thank all the participants, the administrative staff of the Ettore Majorana Centre and all the sponsors.

5 Recent Doctorial Theses Abstracts

5.1 Optics Designs of Final-Focus Systems for Future LHC Upgrades

José Luis Abelleira Fernández
Mail to: jose.abelleira@cern.ch

Graduation date: February 2014

Institutions: CERN, École Polytechnique Fédérale de Lausanne (Switzerland)

Thesis jury members: Prof. R. Houdré (president), Prof. Leonid Rivkin, Dr. Frank Zimmermann, Dr J.-P. Koutchouk, Dr T. Pieloni, Prof. A.F.Wrulich

Abstract:

The main topic of the thesis is the study of a novel option for the high-luminosity upgrade of the Large Hadron Collider (LHC) comprising a large Piwinski angle, flat beams, and crab waists. Flat beams and crab waists are not only pre-requisites for a crab-waist scheme, but, even by themselves; each of these two elements alone could boost the luminosity of the existing collider as built.

The new optics involves an upgrade of the interaction region of the two high-luminosity experiments, ATLAS and CMS, in order to provide them with a substantially higher luminosity. To this end, a flat-beam optics scenario has been explored for the High Luminosity LHC (HL-LHC), with a much reduced vertical beta function at the interaction point (IP), β_y^* . In addition, a large Piwinski angle is considered. Advantages of a large Piwinski angle include a reduction in the hourglass effect over the length of the collision area, which allows for the significant β_y^* decrease. In addition there is a reduction of the beam-beam effect so that the same beam-beam tune shift is reached only for much brighter beams, with a consequent luminosity increase. Flat beams and large Piwinski angle can boost the luminosity of the existing LHC as built, but they also open up the possibility to implement a crab-waist collisions scheme. The challenge here was to apply the collision concept, which so far has been employed only in the DA ϕ NE $e^+e^- \varphi$ factory, to a much bigger collider with pp collisions, which do not easily allow for a symmetric optics.

The second important concept implemented in this version of the LHC upgrade is a (partially) local chromatic correction scheme, by installing chromatic sextupoles near the IP. For this purpose, the interaction region had to be redesigned. As the optics for the crab-waist scheme must be symmetric, the polarities of the final quadrupoles must change with respect to the present configuration. This includes the region where the two beams share the same aperture. In this case, a novel magnetic element called “double-half quadrupole” (DHQ) is proposed, which would provide quadrupolar fields of opposite sign at opposite locations from the centre. The element then acts as a horizontally defocusing element for either beam, and helps focusing the vertical beta-function to the small value required at the IP.

Finally, this thesis includes some considerations on applying the same optics and collision concepts to the High Energy LHC (HE-LHC) and to a design of the final-focus system for the LHeC electron line, which is also equally based on a local chromatic correction scheme.

Published in the editorial series on Accelerator Science and Technology (“EuCARD Monograph”), vol. 24, Warsaw University of Technology, 2014.

5.2 Electron Cloud Studies for the LHC and Future Proton Colliders

César Octavio Dominguez Sanchez de la Blanca
 Mail to: codomiguez@gmail.com

Graduation Date: 28 October 2013
 Institution: École Polytechnique Fédérale de Lausanne (EPFL)
 Supervisors: Leonid Rivkin (EPFL), Frank Zimmermann (CERN)

Thesis jury members: N. Grandjean (président), L. Rivkin, F. Zimmermann, O. Brüning, K. Oide, T. Nakada

Abstract

The Large Hadron Collider (LHC) is the world's largest and most powerful particle collider. Its main objectives are to explore the validity of the standard model of particle physics and to look for new physics beyond it, at unprecedented collision energies and rates. A good luminosity performance is imperative to attain these goals. In the last stage of the LHC commissioning (2011-2012), the limiting factor to achieving the design bunch spacing of 25 ns has been the electron cloud effects. The electron cloud is also expected to be the most important luminosity limitation after the first Long Shutdown of the LHC (LS1), when the machine should be operated at higher energy and with 25-ns spacing, as well as for the planned luminosity upgrade (HL-LHC) and future high energy proton colliders (HE-LHC and VHE-LHC). This thesis contributes to the understanding of the electron cloud observations. This thesis contributes to the understanding of the electron cloud observations during the first run of the LHC (2010-2012), presents the first beam dynamics analysis for the next generation of high energy hadron colliders, and assists in the prediction of how electron clouds will impact the performance of the future high-luminosity and high-energy machines. In particular, the thesis discusses a method to benchmark pressure measurements at the LHC against electron cloud build-up simulations for identifying the most relevant surface parameters. This method allowed monitoring the effectiveness of LHC "scrubbing runs", revealing that in the warm regions, the maximum Secondary Electron Yield, δ_{max} , decreased from an initial value of about 1.9 down to about 1.2 (with a low-energy electron reflectivity $R \approx 0.3$), thanks to surface conditioning. In addition, the "map formalism", a good approximation to quickly explain and predict electron cloud effects, has been further developed and applied, for the first time, to optimize the scrubbing process at the LHC. For the HL-LHC, several novel filling schemes have been analyzed in terms of luminosity performance and electron cloud activity. Only a few of them are compatible with an electron cloud activity lower than for the baseline scenario. We highlight a promising option which could be a good fallback scenario in case the electron cloud effects prevent the injection of the baseline beam. This option could also be considered for the nominal LHC after the LS1 if electron cloud turns out to be a serious obstacle. Regarding the future high-energy proton colliders (HE- and VHE-LHC), in the frame of this thesis a performance model was developed to predict the luminosity as a function of time and to optimize the beam parameters, carrying out the first ever performance analysis for these machines. Several scenarios have been considered, including round and flat beams as well as different bunch spacings. The parameters presented in this thesis have been submitted as an input for the most recent update of the European Strategy for Particle Physics. Finally, we also report the electron cloud studies performed for both high energy machines. The large amount of primary photoelectrons generated by synchrotron radiation at these high energies motivates the consideration of high efficiency photon stops as well as other mitigation techniques (e.g. a-C coatings and clearing electrodes). Although for both machines (HE- and VHE-LHC) a tentative bunch spacing of 25 ns has been considered as baseline assumption, the results of this thesis suggest the possibility of going down to 5 ns, since such a beam would present several advantages.

Published in the editorial series on Accelerator Science and Technology (“EuCARD Monograph”), vol. 23, Warsaw University of Technology, 2014.

6 Forthcoming Beam Dynamics Events

6.1 4th Low Emittance Rings Workshop

We are pleased to announce that the 4th Low Emittance Rings Workshop (LOWeRING 2014) will be organized by the INFN at LNF, Frascati from the 17th to the 19th of September 2014.

The goal of the workshop is to bring together experts from the scientific communities working on low emittance lepton rings. This community, represented in the LOWeRING network and the Ultimate Storage Ring workshops collaboration, includes light source storage rings, linear collider damping rings and future e+/e- circular collider projects.

The workshop is supported by the EuCARD-2 project. It is the forth in a series of workshops initiated in 2010:

[LER2010](#)
[Lowering2011](#)
[Lowemittance2013](#)

The workshop theme will be beam dynamics and technology challenges for producing and controlling ultra-low emittance beams and the participants will benefit from the experience of colleagues who have designed, commissioned and operated such rings.

Workshop sessions will include:

- Low Emittance optics design and tuning
- Collective Effects and beam instabilities
- Low Emittance Ring Technology

Students are encouraged to participate and present posters. A prize will be awarded to the best student poster to allow for participating in a major conference presenting work related to Low Emittance Rings.

Relevant information about the workshop organization and scientific programme will be communicated shortly in the workshop web site:

<http://agenda.infn.it/event/ler2014>

Proposals for contributions to the workshop should be addressed to:

Riccardo Bartolini, riccardo.bartolini@diamond.ac.uk, JAI and Diamond Light Source

Yannis Papaphilippou, ioannis.papaphilippou@cern.ch, CERN

Susanna Guiducci, susanna.guiducci@lnf.infn.it, INFN-LNF

6.2 International Workshop on Beam Cooling and Related Topics COOL'15

We are pleased to announce that the next “International Workshop on Beam Cooling and Related Topics, COOL'15”, will take place at Thomas Jefferson

Accelerator Facility (Jefferson Lab), Newport News, Virginia, USA, from September 28 to October 3, 2015. This is the 10th workshop in the series which was first held at Karlsruhe, Germany in 1984 and has been a bi-annual event since 1999. The workshop will highlight the latest developments in the field of particle beam cooling and will provide a perfect opportunity for accelerator physicists, engineers and students to meet and interact in a quiet and relaxed environment. The oral (invited and contributed) and poster sessions will be organized for the workshop. The proceedings will be published electronically at the JACoW site.

Workshop co-chairs: Yaroslav Derbenev (derbenev@jlab.org)
Yuhong Zhang (yzhang@jlab.org)

6.3 ICFA Mini-Workshop on Beam Commissioning for High Intensity Accelerators

There will be an ICFA mini-workshop on the subject of "Beam Commissioning for High Intensity Accelerators" from April 27 to 29, 2015. The mini-workshop will take place at CSNS site, Dongguan city, Guangdong province, China. It will discuss a broad range of topics associated with commissioning of high intensity accelerators, for both high power hadron accelerators and high luminosity colliders, e.g., the commissioning preparation of the new projects, the experiences of commissioning in the existing projects, the advanced beam diagnostics methods used in the beam commissioning, beam loss control and etc.

This workshop is sponsored by Dongguan branch, Institute of Higher Energy Physics, CAS. For more information, please contact:

Sheng Wang, workshop co-chairman,
Dongguan branch, IHEP,
wangs@ihep.ac.cn,
Tel: 86-0769-89156403

For administrative information, please contact:

Weiling Huang, workshop secretary,
Dongguan branch, IHEP,
huangwei@ihep.ac.cn,
Tel: 86-0769-89156408

7 Announcements of the Beam Dynamics Panel

7.1 ICFA Beam Dynamics Newsletter

7.1.1 Aim of the Newsletter

The ICFA Beam Dynamics Newsletter is intended as a channel for describing unsolved problems and highlighting important ongoing works, and not as a substitute for journal articles and conference proceedings that usually describe completed work. It is published by the ICFA Beam Dynamics Panel, one of whose missions is to encourage international collaboration in beam dynamics.

Normally it is published every April, August and December. The deadlines are 15 March, 15 July and 15 November, respectively.

7.1.2 Categories of Articles

The categories of articles in the newsletter are the following:

1. Announcements from the panel.
2. Reports of beam dynamics activity of a group.
3. Reports on workshops, meetings and other events related to beam dynamics.
4. Announcements of future beam dynamics-related international workshops and meetings.
5. Those who want to use newsletter to announce their workshops are welcome to do so. Articles should typically fit within half a page and include descriptions of the subject, date, place, Web site and other contact information.
6. Review of beam dynamics problems: This is a place to bring attention to unsolved problems and should not be used to report completed work. Clear and short highlights on the problem are encouraged.
7. Letters to the editor: a forum open to everyone. Anybody can express his/her opinion on the beam dynamics and related activities, by sending it to one of the editors. The editors reserve the right to reject contributions they judge to be inappropriate, although they have rarely had cause to do so.

The editors may request an article following a recommendation by panel members. However anyone who wishes to submit an article is strongly encouraged to contact any Beam Dynamics Panel member before starting to write.

7.1.3 How to Prepare a Manuscript

Before starting to write, authors should download the template in Microsoft Word format from the Beam Dynamics Panel web site:

<http://www-bd.fnal.gov/icfabd/news.html>

It will be much easier to guarantee acceptance of the article if the template is used and the instructions included in it are respected. The template and instructions are expected to evolve with time so please make sure always to use the latest versions.

The final Microsoft Word file should be sent to one of the editors, preferably the issue editor, by email.

The editors regret that LaTeX files can no longer be accepted: a majority of contributors now prefer Word and we simply do not have the resources to make the conversions that would be needed. Contributions received in LaTeX will now be returned to the authors for re-formatting.

In cases where an article is composed entirely of straightforward prose (no equations, figures, tables, special symbols, etc.) contributions received in the form of plain text files may be accepted at the discretion of the issue editor.

Each article should include the title, authors' names, affiliations and e-mail addresses.

7.1.4 Distribution

A complete archive of issues of this newsletter from 1995 to the latest issue is

available at

<http://icfa-usa.jlab.org/archive/newsletter.shtml>.

This is now intended as the primary method of distribution of the newsletter.

Readers are encouraged to sign-up for electronic mailing list to ensure that they will hear immediately when a new issue is published.

The Panel's Web site provides access to the Newsletters, information about future and past workshops, and other information useful to accelerator physicists. There are links to pages of information of local interest for each of the three ICFA areas.

Printed copies of the ICFA Beam Dynamics Newsletters are also distributed (generally some time after the Web edition appears) through the following distributors:

Weiren Chou	<u>chou@fnal.gov</u>	North and South Americas
Rainer Wanzenberg	<u>rainer.wanzenberg@desy.de</u>	Europe ⁺⁺ and Africa
Toshiyuki Okugi	<u>toshiyuki.okugi@kek.jp</u>	Asia ^{**} and Pacific

⁺⁺ Including former Soviet Union.

^{**} For Mainland China, Jiu-Qing Wang (wangjq@mail.ihep.ac.cn) takes care of the distribution with Ms. Su Ping, Secretariat of PASC, P.O. Box 918, Beijing 100039, China.

To keep costs down (remember that the Panel has no budget of its own) readers are encouraged to use the Web as much as possible. In particular, if you receive a paper copy that you no longer require, please inform the appropriate distributor.

7.1.5 Regular Correspondents

The Beam Dynamics Newsletter particularly encourages contributions from smaller institutions and countries where the accelerator physics community is small. Since it is impossible for the editors and panel members to survey all beam dynamics activity worldwide, we have some Regular Correspondents. They are expected to find interesting activities and appropriate persons to report them and/or report them by themselves. We hope that we will have a "compact and complete" list covering all over the world eventually. The present Regular Correspondents are as follows:

Liu Lin	<u>Liu@ns.lnls.br</u>	LNLS Brazil
Sameen Ahmed Khan	<u>Rohelakan@yahoo.com</u>	SCOT, Oman
Jacob Rodnizki	<u>Jacob.Rodnizki@gmail.com</u>	Soreq NRC, Israel
Rohan Dowd	<u>Rohan.Dowd@synchrotron.org.au</u>	Australian Synchrotron

We are calling for more volunteers as Regular Correspondents.

7.2 ICFA Beam Dynamics Panel Members

Name	eMail	Institution
Rick Baartman	baartman@lin12.triumf.ca	TRIUMF, 4004 Wesbrook Mall, Vancouver, BC, V6T 2A3, Canada
Marica Biagini	marica.biagini@lnf.infn.it	INFN-LNF, Via E. Fermi 40, C.P. 13, Frascati, Italy
John Byrd	jmbyrd@lbl.gov	Center for Beam Physics, LBL, 1 Cyclotron Road, Berkeley, CA 94720-8211, U.S.A.
Yunhai Cai	yunhai@slac.stanford.edu	SLAC, 2575 Sand Hill Road, MS 26 Menlo Park, CA 94025, U.S.A.
Swapan Chattopadhyay	swapan@cockcroft.ac.uk	The Cockcroft Institute, Daresbury, Warrington WA4 4AD, U.K.
Weiren Chou (Chair)	chou@fnal.gov	Fermilab, MS 220, P.O. Box 500, Batavia, IL 60510, U.S.A.
Wolfram Fischer	wfischer@bnl.gov	Brookhaven National Laboratory, Bldg. 911B, Upton, NY 11973, U.S.A.
Yoshihiro Funakoshi	yoshihiro.funakoshi@kek.jp	KEK, 1-1 Oho, Tsukuba-shi, Ibaraki-ken, 305-0801, Japan
Jie Gao	gaoj@ihep.ac.cn	Institute for High Energy Physics, P.O. Box 918, Beijing 100039, China
Ajay Ghodke	ghodke@cat.ernet.in	RRCAT, ADL Bldg. Indore, Madhya Pradesh, 452 013, India
Ingo Hofmann	i.hofmann@gsi.de	High Current Beam Physics, GSI Darmstadt, Planckstr. 1, 64291 Darmstadt, Germany
Sergei Ivanov	sergey.ivanov@ihep.ru	Institute for High Energy Physics, Protvino, Moscow Region, 142281 Russia
In Soo Ko	isko@postech.ac.kr	Pohang Accelerator Lab, San 31, Hyoja-Dong, Pohang 790-784, South Korea
Elias Metral	elias.metral@cern.ch	CERN, CH-1211, Geneva 23, Switzerland
Yoshiharu Mori	mori@rri.kyoto-u.ac.jp	Research Reactor Inst., Kyoto Univ. Kumatori, Osaka, 590-0494, Japan
George Neil	neil@jlab.org	TJNAF, 12000 Jefferson Ave., Suite 21, Newport News, VA 23606, U.S.A.
Toshiyuki Okugi	toshiyuki.okugi@kek.jp	KEK, 1-1 Oho, Tsukuba-shi, Ibaraki-ken, 305-0801, Japan
Mark Palmer	mapalmer@fnal.gov	Fermilab, MS 221, P.O. Box 500, Batavia, IL 60510, U.S.A.
Chris Prior	chris.prior@stfc.ac.uk	ASTeC Intense Beams Group, STFC RAL, Chilton, Didcot, Oxon OX11 0QX, U.K.
Yuri Shatunov	Yu.M.Shatunov@inp.nsk.su	Acad. Lavrentiev, Prospect 11, 630090 Novosibirsk, Russia
Jiu-Qing Wang	wangjq@ihep.ac.cn	Institute for High Energy Physics, P.O. Box 918, 9-1, Beijing 100039, China
Rainer Wanzenberg	rainer.wanzenberg@desy.de	DESY, Notkestrasse 85, 22603 Hamburg, Germany

The views expressed in this newsletter do not necessarily coincide with those of the editors.

The individual authors are responsible for their text.